MIMO Techniques in UTRA Long Term Evolution

Wei, Na

Publication date:
2007

Document Version
Publisher's PDF, also known as Version of record

MIMO Techniques for UTRA Long Term Evolution

by

NA WEI

A Dissertation submitted to
the Faculty of Engineering and Science of Aalborg University
in partial fulfilment of the requirements for the degree of
DOCTOR OF PHILOSOPHY,
September 2007, Aalborg, Denmark.

Supervisors
Associate Professor Troels B. Sørensen, Ph.D.,
Aalborg University, Denmark.
Professor Preben E. Mogensen, Ph.D.,
Aalborg University, Denmark.
Wireless Network Specialist Troels E. Kolding, Ph.D.,
Nokia Siemens Networks, Aalborg R&D, Denmark.

Defence Chairman
Associate Professor Flemming B. Frederiksen, Ph.D.,
Aalborg University, Denmark.

Opponents
Associate Professor Patrick C. F. Eggers, Ph.D.,
Aalborg University, Denmark.
Senior Specialist, Bo Hagerman, Ph.D.,
Ericsson Research, Sweden.
Professor Olav Tirkkonen, Ph.D.,
Helsinki University of Technology, Finland.

ISSN 0908-1224
ISBN 87-92078-05-2

天道酬勤

God helps those who help themselves.

Abstract

To meet the ambitious peak data rate and spectral efficiency target for the UTRA Long Term Evolution (LTE), Multiple-Input Multiple-Output (MIMO) is identified to be one of the most essential technologies for LTE. While MIMO is a widely researched topic, most studies disregard the interaction of MIMO with other essential enhancement mechanisms in the system including Link adaptation (LA), Hybrid ARQ (HARQ) L1 retransmission, packet scheduling, etc. Therefore, this PhD study focuses on the efficient integration of MIMO in the LTE system by making a careful design and analysis of the interoperation of different gain mechanisms at different layers, rather than an evaluation of their individual performance potential only. More specifically, the investigation exploits new algorithms for MIMO, which jointly optimize the LTE system with reasonable complexity and low signalling requirements. An important consideration for the optimum interoperation/integration is the overall throughput performance at both link and system level, where the associated issues like the range of available SINRs, the signaling overhead, and user fairness become important. The complexity of combining those realistic factors and multiple gain mechanisms often require Monte Carlo simulations. However, theoretical analysis under ideal assumptions is also useful to gain insight on upper bounds and to support and verify the Monte Carlo simulation work. Thus both approaches are utilized in this Ph.D. study.

First of all, in order to gain an analytical insight into MIMO with the OFDM based system, a conceptual unified MIMO-OFDM framework has first been formulated based on the linear dispersion code. To include the impact from all gain mechanisms and practical issues in the physical layer on the LTE single-user performance, a detailed link level simulator was developed which features most of the LTE Physical Layer and some MAC layer functionalities. To benchmark the performance and complexity of more advanced enhancements, baseline MIMO schemes are evaluated in terms of spectral efficiency. After that, more advanced MIMO solutions are investigated. Among them, the Closed-Loop Transmit Diversity (CLTD) is of special interest to us. The emphasis is given on designing efficient methods to reduce the required weights feedback for CLTD. We further considered the adaptive MIMO concept by which the MIMO schemes are chosen instantaneously according to the channel condition. Useful insight into the principles of adaptive MIMO through theoretical analysis is provided by using a unified SINR concept. Besides, we propose the practical channel quality metric design for

LA algorithms including MIMO adaptation.

The multi-user diversity gain with opportunistic Frequency Domain Packet Scheduling (FDPS) is further explored in spatial domain by combining with MIMO in spatial division multiplexing mode (SDM-FDPS). A theoretical analysis of post-scheduling SINR distribution with some simplified assumptions is first performed to give insight into the different SDM-FDPS concepts, namely single-user (SU-) and multi-user (MU-) MIMO. For MU-MIMO, multiple users can be scheduled on different streams on the same time-frequency resource, while SU-MIMO restricts one time-frequency resource to a single user. After that, the MIMO aware proportional fair FDPS algorithms with moderate complexity are proposed. The performance of SDM-FDPS is then assessed with a quasi-static network simulator which provides traffic modelling, multi-user scheduling, and LA including HARQ, etc. Results reveal that in the micro-cell scenario a gain in cell throughput of around 22% and 30% is obtainable with SU- and MU- MIMO schemes, respectively, with precoding assuming 10 active users in the cell. As the signalling overhead with SDM-FDPS is shown to be greatly increased compared to 1x2 FDPS, various methods are further proposed to bring down the signalling overhead (88% in uplink and 30% in downlink) without affecting the performance significantly (loss within 7-10%).

Dansk Resumé [1]

For at imødekomme de ambitiøse top data rater og spektrum effektivitets målsætninger fra UTRA Long Term Evolution (LTE), er Multiple-Input Multiple-Output (MIMO) blevet identificeret til at være en af de mest essentielle teknologier for LTE. Selvom meget forskning har haft fokus på emnet MIMO, har de fleste studier set bort fra interaktionen mellem MIMO og andre essentielle forbedrings mekanismer i systemet, såsom Link Adaptation(LA), Hybrid ARQ (HARQ) L1 retransmission, pakke planlægning osv. Derfor fokuserer dette Ph.D. studium på en effektiv integration af MIMO i et LTE system ved at lave et omhyggeligt design og analyse af interaktionen af de forskellige forbedringsmekanismer ved de forskellige fysiske lag, i stedet for kun en evaluering af deres individuelle funktionelle præstations potentiale. Mere specifikt, så baserer denne undersøgelse sig på nye algoritmer for MIMO, som tilsammen optimerer LTE systemet med et acceptabelt kompleksitets niveau og lave signaleringskrav. En vigtig betragtning for den optimale interaktion/integration er det samlede bit gennemløb ved både link og system niveau, hvor effekter såsom SINR rækkevidden, signalerings- omkostninger, og bruger "fairness" bliver vigtige. Kompleksiteten ved at kombinere disse realistiske faktorer og multiple forbedrings mekanismer kræver ofte Monte Carlo simuleringer. En teoretisk analyse under ideelle antagelser er også brugbar for at opnå indsigt i øvre grænser og for at supportere Monte Carlo simuleringerne. Derfor er begge tilgangsmetoder anvendt i dette Ph.D. studium.

Først og fremmest er en begrebsmæssig samlet MIMO-OFDM ramme formuleret, baseret på lineære sprednings koder, med det formål at opnå en analytisk indsigt i MIMO med et OFDM baseret system. For at inkludere virkningen fra alle forbedringsmekanismer og praktiske aspekter i det fysiske lag af LTE enkelt-bruger præstations potentiale, er en detaljeret link niveau simulator blevet udviklet. Denne simulator inkluderer de fleste egenskaber af det fysiske lag fra LTE og også nogle egenskaber fra MAC laget. For at måle præstationen og kompleksiteten af mere avancerede forbedringer, er nogle grundlinie MIMO algoritmer blevet evalueret ved hjælp af spektrum effektivitet. Derefter er mere avancerede MIMO løsninger undersøgt. Blandt disse er Closed-Loop Transmit Diversity (CLTD) af speciel interesse. Hovedvægten er lagt på at designe effektive metoder til at reducere den

[1] Translation by Chrisitian Rom, Department of Electronic Systems, Aalborg University, Denmark.

nødvendige vægtede tilbagemelding for CLTD. Derefter betragtede vi det adaptive MIMO koncept, i hvilket MIMO algoritmerne er valgt øjeblikkeligt afhængigt af kanal tilstanden. Værdifuld indsigt i adaptiv MIMO principperne ved at bruge et samlet SINR koncept er givet via teoretisk analyse. Derudover forslår vi et praktisk kanal kvalitetsmål design for LA algoritmer, som også tager MIMO tilpasning i betragtning.

Multi-bruger diversitets gevinsten med opportunistisk Frequency Domain Packet Shceduling (FDPS) er yderligere udforsket i det rumlige domæne ved at kombinere den med MIMO i spatial division multiplexing mode (SDM-FDPS). En teoretisk analyse af post-planlægning af SINR distribution med nogle simplificerede antagelser er først udfærdiget for at give indsigt i de forskellige SDM-FDPS koncepter som er: single-user (SU-) og multi-user (MU) MIMO. For MU-MIMO kan forskellige brugere blive planlagt på forskellige data strømme i den samme tid-frekvens ressource, men for SU-MIMO kan en tid-frekvens ressource kun anvendes af 1 bruger. Derefter er den MIMO bevidste proportional fair FDPS algoritme foreslået med moderat kompleksitet. SDM-FDPS præstationen er derefter studeret med en kvasi-statisk netværkssimulator, som giver os trafik modellering, multi-bruger planlægning og LA, som inkluderer HARQ, osv. Resultater afslører, at i et micro-celle scenario kan man vinde 22% til 30% præstation med SU- og MU-MIMO algoritmer, med prekodning og antagelse af 10 aktive brugere i en celle. Da det viser sig, at signaleringsomkostningerne med SDM-FDPS er stærkt forøget i forhold til 1x2 FDPS, forslår vi flere metoder til at reducere disse signaleringsomkostninger (88% i uplink og 30% i downlink) uden at nedbringe præstationen betydeligt (tab på under 7 til 10%).

Preface and Acknowledgments

This dissertation is the result of a three-years project carried out at the section of Radio Access Technology (RATE), Department of Electronic Systems, Aalborg University, Denmark. This Ph.D. is under supervision and guidance from Associate Professor Troels B. Sørensen (Aalborg University, Denmark), Professor Preben E. Mogensen (Aalborg University, Denmark), and Dr. Troels E. Kolding (Nokia Siemens Networks, Aalborg R&D, Denmark). The dissertation has been completed in parallel with the mandatory coursework, teaching, and project work obligations in order to obtain the Ph.D. degree. The research has been co-financed by Aalborg University and Nokia Siemens Networks Aalborg R&D. On the 22^{th} August 2007 the work has been successfully defended against questions from the assessment committee and from the public audience. The committee consisted of Senior Specialist Bo Hagerman (Ericsson Research, Sweden), Professor Olav Tirkkonen (Helsinki University of Technology, Finland), and Associate Professor Patrick C. F. Eggers (Aalborg University, Denmark, Chairman of the committee). The defence was chaired by Associate Professor Flemming B. Frederiksen (Aalborg University, Denmark).

First of all I would like to express my strong gratitude to my supervisors for their guidance, advice and patience. Every one of them has contributed significantly to this work, each in a very individual way.

Further, I would like to thank the members of the assessment committee who through their detailed reading and constructive feedback have helped to correct and clarify individual points throughout this dissertation.

Clearly the presented work would not have been possible without being part of an inspiring network of colleagues, enabling interesting discussions and collaboration. In this respect I would like to particularly point out the good collaboration with Lars Berger (now with the company DS2, Spain), Akhilesh Pokhariyal, Christian Rom and Basuki E. Priyanto from Department of Electronic Systems, Aalborg University, and Frank Frederiksen and Claudio Rosa from Nokia Siemens Networks, Aalborg R&D, which have led to common publications. Further, I would like to specifically thank Klaus. I. Pedersen, Istvan Kovacs from Nokia Siemens Networks for their valuable input.

The proofreading for paper and thesis writing from the secretary Jytte Larsen is highly appreciated. Besides, I am very grateful for the constant friendly support from secretary Lisbeth Schiønning Larsen, especially for the hundreds of phone

calls she made to help me get danish visa every year.

I am also very grateful to have had a very nice bunch of friends around me that made my stay here in Aalborg very enjoyable. Due to limited space, I will not be able to mention the name list, but I had it in my memory.

Finally, I would like to thank the constant love and affection of my parents. Of course my special thanks also go to my husband yaoda who have been very supportive for this work. And I have to say thanks to the by-product of this Ph.D. study, my three-year old “little angel” vivi, who always has the magic power to light up my days.

Na Wei, Sep. 2007

Notation

Acronyms and mathematical conventions are listed below for quick reference. They are additionally defined at their first occurrence.

Acronyms

2G	Second Generation
3G	Third Generation
ACK	Acknowledgement
AMC	Adaptive Modulation and Coding
CLTD	Closed-Loop Transmit Diversity
CC	Chase Combining
CP	Cyclic Prefix
CQI	Channel Quality Indication
CSI	Channel State Information
DFT	discrete Fourier Transform
D-TxAA	dual-stream TxAA
EESM	Exponential Effective SIR Mapping
FDLA	Frequency Domain Link Adaptation
FDPS	Frequency Domain Packet Scheduling
FFT	fast Fourier Transform
HARQ	Hybrid Automatic Repeat reQuest
HSDPA	High-Speed Downlink Packet Access
HSUPA	High-Speed Uplink Packet Access
HSPA	High-Speed Packet Access
IR	Incremental Redundancy
ICI	Inter Carrier Interference
IDFT	inverse discrete Fourier Transform

IFFT	inverse fast Fourier Transform
IR	Incremental Redundancy
ISI	Inter Symbol Interference
JC	Joint Coding
LA	Link Adaptation
LDC	Linear Dispersion Coding
LLR	Log-Likelihood Ratio
LTE	Long Term Evolution
MCS	Modulation and Coding Scheme
MU-	Multi-user
MIMO	Multiple-Input Multiple-Output
MISO	Multiple-Input Single-Output
MMSE	Minimum Mean Square Error
MRC	Maximal Ratio Combining
NACK	Negative Acknowledgement
OFDM	Orthogonal Frequency Division Multiplexing
OFDMA	Orthogonal Frequency Division Multiple Access
PAC	per Antenna Coding
PARC	per Antenna Rate Control
PF	Proportional Fair
PRB	physical resource block
RLC	Run Length Coding
SAW	Stop-And-Wait
SDM	Spatial Division Multiplexing
SFC	Space Frequency Coding
SIC	Successive Interference Cancellation
SIMO	Single-Input Multiple-Output
SU-	Single-user
SVD	Singular Value Decomposition
STBC	Space-Time Block Coding
STTD	Space-Time Transmit Diversity
TxAA	Transmit Antenna Array
UDO	User Diversity Order
UE	User Equipment
ZF	Zero-forcing

Mathematical Conventions

Although some parameters and values will be presented in dB, calculations are always displayed using linear values. Further, following conventions are used throughout.

$\mathbf{A}$	Bold upper case indicates a matrix.
$\mathbf{a}$	Bold lower case indicates a vector.
A, a	Non-bold indicates scalar.
$a \times b$ or (a, b)	Matrix dimension indication, *i.e.* a rows times b columns.
$\mathbf{I}_a$	An $a \times a$ identity matrix.
$(\cdot)^*$	Complex conjugate.
$(\cdot)^T$	Transpose.
$(\cdot)^H$	Hermitian, *i.e.* complex conjugate transpose.
$(a)^x$	a to the power of x.
$\lvert \cdot \rvert$	Absolute.
$\lvert\lvert \cdot \rvert\rvert$	2-Norm.
$\mathrm{E}_x \{f(x)\}$	Expectation with respect to x.
$Pr(a)$	Probability of a
$Pr(a\lvert b)$	Conditional Probability of a conditioned on b
$\min(a)$	minimum value of a
$\max(a)$	maximum value of a
$\mathrm{Var}\{x\}$	Variance of random variable x, $\mathrm{Var}\{x\} = \mathrm{E}\left\{(x - \mathrm{E}\{x\})^2\right\}$.
$\mathrm{Std}\{x\}$	Standard deviation of random variable x, $\mathrm{Std}\{x\} = \sqrt{\mathrm{Var}\{x\}}$.
$\mathrm{E}_x \langle f(x) \rangle_a$	Ensemble average over a realisations of x, $\mathrm{E}_x \langle f(x) \rangle_a = \frac{1}{a} \cdot \sum_{i=1}^{a} f(x_i)$
$\mathrm{Var}_x \langle f(x) \rangle_a$	Variance estimate taken from a realisations of x, $\mathrm{Var}_x \langle f(x) \rangle_a = \frac{1}{a-1} \cdot \sum_{i=1}^{a} \left(f(x_i) - \mathrm{E}_x \langle f(x) \rangle_a\right)^2$
	Standard deviation estimate taken from a realisations of x, $\mathrm{Std}_x \langle f(x) \rangle_a = \sqrt{\mathrm{Var}_x \langle f(x) \rangle_a}$
$\widetilde{\sigma}_x$	Short notation for the estimate of the relative standard deviation of x, $\widetilde{\sigma}_x = \frac{\mathrm{Std}_x \langle f(x) \rangle_a}{\mathrm{E}_x \langle f(x) \rangle_a}$. The number of realisations a will be clear from the context.
$\mathrm{p}(x)$	Probability density function of x.
$F(x)$	Cumulative probability density function of x.
$\overline{x}$	Short notation for the mean of x.
$\widehat{x}$	Short notation for the estimate of x.
$\angle(x)$	angle of x

Contents

Chapter 1

Introduction

The Second Generation (2G) mobile networks made it possible for people to communicate effectively with voice service while being on the move. With the Third Generation (3G) system's coming into our daily life, new services like multimedia messaging, web browsing, online gaming, streaming, etc. are also available. As a member of the 3G family, WCDMA systems are providing service for more than 100 million users by January of 2007 [1]. The new 3G updates, High-Speed Downlink Packet Access (HSDPA) for downlink and High-Speed Uplink Packet Access (HSUPA) for uplink together are called High-Speed Packet Access (HSPA). With these enhancements, the 3G radio access technology will be highly competitive for several years to come [Holm06]. However, to ensure competitiveness in an even longer time frame, i.e. for the next 10 years and beyond, the Long Term Evolution (LTE) of the 3GPP radio access technology is already initiated within the 3GPP framework [3GPP06b]. The comparison of 3G, 3G enhancements, LTE and 4G in terms of main benchmarking parameters are listed in Figure 1.1. in principle the LTE is equipped with the 4G technology, but is using/sharing 3G spectrum and platform. Once the new spectrum for 4G is released (expected to be around 100MHz bandwidth [ITU 03]), LTE can offer a smooth migration path towards 4G [Moge07a]. The roadmap of this evolution and time frame plan is illustrated in Figure 1.2.

To achieve the target data rate of LTE and eventually 4G, many new techniques are necessary. Multiple-Input Multiple-Output (MIMO) is one key technique among them because of its ability to enhance the radio channel capacity of cellular systems at no extra cost of spectrum. The pioneering work by Foschini [Fosc96] and Telatar [Tela95] showed that the capacity of MIMO can be up to $min(N_t, N_r)$ times larger than the single-antenna capacity where N_t and N_r is the number of antenna elements at transmitter and receiver respectively. In

[1] see http://www.3gtoday.com/wps/portal/subscribers

	3G(WCDMA)	HSPA	LTE	4G
Standard	R99 WCDMA	R5&6 HSPA	UTRAN LTE	??
Spectrum	850/900/1700/1800 /1900/2000/2500	850/900/1700/1800 /1900/2000/2500	as HSPA + 450	Higher frequency bands ?
RF Bandwidth	5 MHz	5 MHz	1.25-20 MHz	20-100 MHz
Latency user plane	100-200 ms	<50 ms	<10 ms	?
Latency control plane	500-800 ms	300-500 ms	<100 ms	?
Peak bit rate DL	0.384 Mbps	14.4 Mbps	Up to 100 Mbps	Up to 1000* Mbps
Peak bit rate UL	0.384 Mbps	5.76 Mbps	Up to 50 Mbps	Up to 1000* Mbps
Spectral efficiency DL	0.16 bps/Hz	1.0 bps/Hz	~2.0 bps/Hz	? bps/Hz
Spectral efficiency UL	0.16 bps/Hz	0.25 bps/Hz	~1.0 bps/Hz	? bps/Hz

Figure 1.1: Comparison of different systems and benchmarking parameters [Moge07a]

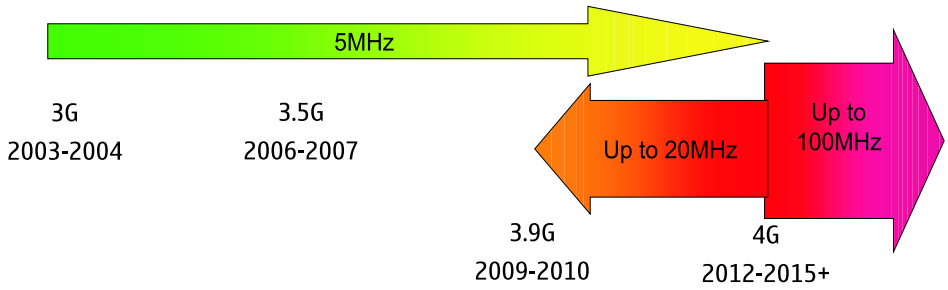

Figure 1.2: Roadmap of cellular system evolution [Moge07a]

this context, the expression MIMO includes both traditional beamforming and diversity techniques [Wint87], as well as spatial multiplexing techniques [Tela95]. The diversity format of MIMO was included in 3G and 3G enhancements already, like Space-Time Transmit Diversity (STTD) [Daba99], Closed-Loop Transmit Diversity (CLTD) [Hama00], mainly targeting at increasing the link quality. To reach the ambitious target peak data rate of LTE, MIMO in terms of spatial multiplexing also needs to be exploited to increase the peak data rate of users. This Ph.D. thesis focuses on the performance of MIMO as a capacity enhancing technique for future cellular systems. Application to the FDD mode of LTE downlink is the primary motivation, but the considered techniques are general, and the analysis in this thesis can also be extended. The rest of this chapter is organized as follows. Since the UTRA LTE is taken as a case study for this Ph.D. thesis, a short description of this system and its main principles are given in Section 1.1. A survey of state of art concerning MIMO is presented in Section 1.2. The motivation and objectives of this Ph.D. study are introduced in Section 1.3. Further, the methodology of the study is briefly addressed in Section 1.4. Finally, an outline of the dissertation and contributions is given in Section 1.5 and The list of publications produced during

the Ph.D. study is provided in Section 1.6.

1.1 UTRA Long Term Evolution - MIMO is essential

The related Study Item (SI) for UTRA LTE started in December 2004 [3GPP00b]. At the starting point of thesis writing, LTE was still in the Work Item (WI) phase in 3GPP. The estimated finish time of the WI is around June 2007. Since most of the study is carried out during the Study Item phase, the parameter assumptions might deviate from the final WI outcome.

The objective of LTE is to develop a framework for the evolution of the 3GPP radio access technology towards a *high-data-rate*, *low-latency*, and *packet-optimized* radio access technology [3GPP06b]. The key issue is to increase spectral efficiency and coverage while maintaining acceptable complexity and cost. From the radio interface point of view, the current 3GPP Release 5 and 6 solutions can achieve up to 14.4 Mbps downlink and 5.7 Mbps uplink peak data rates (without channel coding) using HSPA. Thus for the long term evolution, clearly more ambitious goals were set up. Among others, the main targets are presented below [3GPP06b]:

- Significantly increased peak data rate e.g. 100 Mbps (downlink) and 50 Mbps (uplink).
- Significantly improved spectrum efficiency (e.g. 2-4 times that of Release 6 HSPA system)
- Radio Network user plane latency below 10 ms *Round Trip Time* (RTT) with 5 MHz or higher spectrum allocation.
- Scalable bandwidth up to 20 MHz (lowest possible bandwidth: 1.25 MHz).
- Support for inter-working with existing 3G systems and non-3GPP specified systems.
- Support for packet switched domain only (voice is carried by e.g. VoIP).
- Optimized for low mobile speed, but also with support for high mobile speed.

The *Transmission Time Interval* (TTI) is made as short as 1 ms in order to improve the *Round Trip Time* (RTT) performance. The downlink transmission scheme is based on conventional OFDM using a cyclic prefix [3GPP06a]. The system has a scalable bandwidth up to 20 MHz, with smaller bandwidths covering 1.25 MHz, 2.5 MHz, 5 MHz, 10 MHz and 15 MHz to allow for operation in differently sized spectrum allocations. The transmission bandwidth is varied by varying

the number of OFDM sub-carriers while keeping the sub-carrier spacing constant. The throughput enhancing mechanisms in LTE downlink are explained in details as follows, namely the Orthogonal Frequency Division Multiplexing (OFDM), Link Adaptation (LA), fast Frequency Domain Packet Scheduling (FDPS), Hybrid Automatic Repeat reQuest (HARQ) and Multiple-Input Multiple-Output (MIMO).

1.1.1 OFDM

After finding its way in many standardizations, such as digital audio broadcasting (DAB) [DMB], digital video broadcasting (DVB-T) [DVB], the IEEE 802.11 local area network (LAN) standard [IEEE99] and the IEEE 802.16 metropolitan area network (MAN) standard [IEEE01], OFDM has been selected as the modulation scheme for UTRA LTE downlink in 3GPP as well.

OFDM is based on the principle of Multi-Carrier Modulation (MCM), or Frequency Division Multiplexing (FDM). This technique is designed to split a high-rate data stream into several interleaved streams and use these to modulate a large number of frequency multiplexed narrowband sub-carriers, which are transmitted simultaneously. Spectral overlap could be avoided by putting enough guard space between adjacent sub-carriers. In this way, the Inter Carrier Interference (ICI) can be eliminated. This method, however, leads to a very inefficient use of spectrum. A more efficient use of bandwidth can be obtained with parallel transmissions if the spectra of the sub-channels are permitted to partly overlap. *Orthogonal* FDM succeeds in this aim by transmitting orthogonal sub-carriers. In this system rectangular pulses are transmitted, and thus each sub-carrier presents a non-limited bandwidth sinc shape, which can be overlapped in the transmitter and recovered in the receiver [Bing90]. As shown in the frequency domain representation of OFDM in Figure 1.3, the individual peaks of each sub-carrier line up with the zero crossing of all other sub-carriers. With this nice property, the receiver can correlate the received signal with the known set of sinusoids to recover the signal. The effects of the multipath channel can be mitigated within the transmitted symbol by means of the inclusion of a guard time in the beginning of each symbol. If the duration of the guard is larger than the maximal delay spread of the channel, all the multipath components would arrive within this guard, and the useful symbol would not be affected. One particular realization of the guard time concept is the Cyclic Prefix (CP). In this case the last part of the useful OFDM symbol is copied to the beginning of the same symbol, as shown in time domain representation of OFDM in Figure 1.3. This strategy manages to maintain its orthogonality properties, the negative effects like Inter Symbol Interference (ISI) and ICI can be mitigated, and no equalization for multipath (*e.g.* RAKE receiver) is required, simplifying the design of the receiver [Nort03].

Further, since the OFDM sub-carriers are constructed as parallel narrowband

channels, the fading process experienced by each sub-carrier is close to frequency flat, and can be modelled as a single constant complex gain. This characteristic may simplify the implementation of advanced gain mechanism such as MIMO, frequency domain packet scheduling. The task of pulse forming and modulation can be performed efficiently by using the discrete Fourier Transform (DFT) and its counterpart, the inverse discrete Fourier Transform (IDFT). In practice, OFDM systems are implemented by using a combination of fast Fourier Transform (FFT) and inverse fast Fourier Transform (IFFT) blocks that are mathematically equivalent versions of the DFT and IDFT [Edfo96].

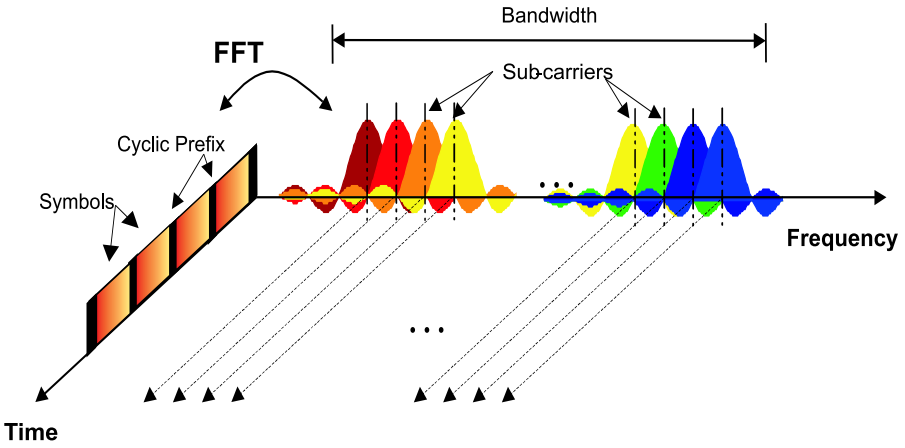

Figure 1.3: Frequency-Time Representation of an OFDM Signal. [3GPP04]

However, OFDM is very sensitive to the non-linear distortion due to the natural high peak-to-average power ratio (PAPR) of a typical OFDM signal [Behr02]. Another major drawback of OFDM is sensitivity to frequency synchronization errors where the orthogonality is lost [Stam02].

1.1.2 AMC based Link Adaptation (LA)

Similar to HSDPA, Adaptive Modulation and Coding (AMC) is utilized to adapt to a wide dynamic range of channel quality variations experienced at the UE (including fast as well as distance-dependent variations, etc.). The LTE downlink encoding scheme is based on the UTRA Release 6 Turbo coding with a basic rate of 1/3, but adds rate matching with puncturing and repetition to obtain a high resolution on the effective code rate (approximately from 1/6 to 1/1) [Kold03]. Potential usage of additional polynomial for lower rates is still under discussion [3GPP06a]. To facilitate very high peak data rates, the LTE concept adds 64QAM on top of the existing QPSK and 16QAM modulation available in HSDPA. Including the 64QAM imposes high challenges for manufactures, especially the RF modules. The com-

bination of modulation order and coding rate is called Modulation and Coding Schemes (MCS). The instantaneous SINR versus attainable spectral efficiency in AWGN channel with some example MCS are plotted in Figure 1.4. Compared to the Shannon capacity curve, there is a distance of approximately 2-3dB from QPSK spectral efficiency curves to ideal Shannon, while the difference is increased to 5-6dB for 64QAM spectral efficiency curves. The difference comes from the effect of realistic modulation and coding. With the information of instantaneous channel condition, the transmitter can adapt its transmission format accordingly with the MCS that maximizes the spectral efficiency.

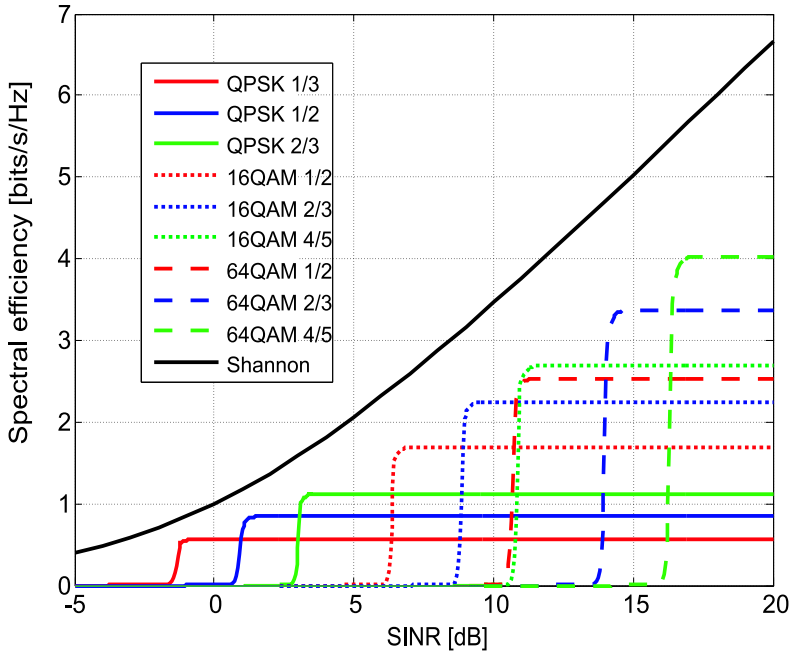

Figure 1.4: SINR vs attainable spectral efficiency for MCS examples in AWGN channel.

1.1.3 Fast Frequency Domain Packet Scheduling (FDPS)

Fast channel aware FDPS can be facilitated by the Orthogonal Frequency Division Multiple Access (OFDMA) which is a multi-user version of the OFDM digital modulation scheme. A scheduling node (eNode-B) can dynamically control which time/frequency resources are allocated to a User Equipment (UE) at a given time. The smallest granularity of resource allocation is referred to as a physical resource block (PRB) consisting of a number of consecutive sub-carriers over a number of consecutive OFDM symbols. The working assumption for this study is that the PRB equals 25 sub-carriers over frequency and 7 OFDM symbols over time. To support FDPS, the UE should give feedback of the Channel Quality Indication (CQI) to the eNode-B, and the eNode-B should inform UE via down-

link control signaling what resources and corresponding transmission formats have been allocated to each scheduled UE.

The scheduler can instantaneously choose the best multiplexing strategy based on the channel condition of each UE. As illustrated in Figure 1.5, the users are only given the PRBs where the channel condition is good. This leads to multiuser diversity gain at a cost of increased signaling requirements.

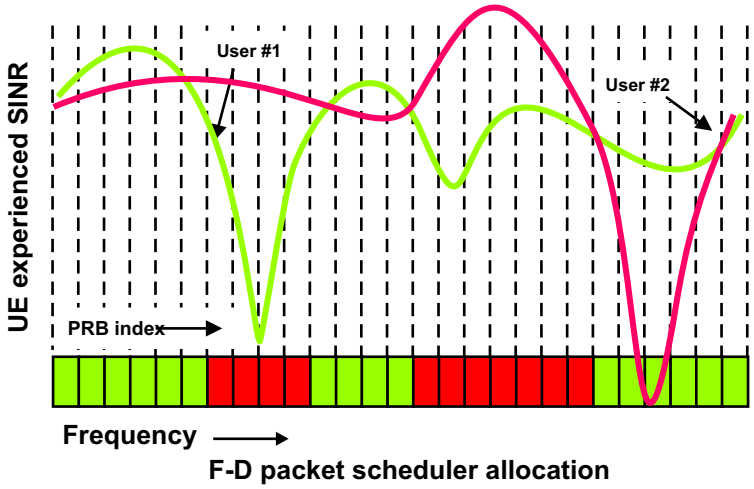

Figure 1.5: Multiuser diversity gain can be achieved by channel aware FDPS.

1.1.4 HARQ based on fast L1 retransmissions

The main principle of HARQ is as follows: In case a data packet is not correctly decodable, then the eNode-B performs fast layer one retransmission of that data packet, thus the receiver can achieve SNR gain by combining soft information for all transmissions (The working procedure is further explained in Subsection 1.1.6). The downlink of LTE supports both the Incremental Redundancy (IR) and Chase Combining (CC) retransmission strategies. The basic idea of the CC scheme is to transmit an identical version of an erroneously detected data packet. With the IR scheme, additional redundant information is incrementally transmitted. When the coding rate is quite high, the IR outperforms the CC since it can lower the effective code rate. The Stop-And-Wait (SAW) protocol supporting several parallel logic channels is used for downlink HARQ.

1.1.5 Multiple-Input Multiple-Output (MIMO)

The definition of Multiple-Input Multiple-Output (MIMO) is quite straightforward. Wireless communication systems with multiple antenna elements at transmitter end and multiple antenna elements at the receiver end are called MIMO system. And for simplicity, the Multiple-Input Single-Output (MISO) and Single-Input Multiple-Output (SIMO) with multiple antenna elements at one end are also taken as a special case of MIMO in this thesis. Basically, MIMO can be split into two groups: either increase the link quality (*diversity* MIMO) or data rate (*spatial multiplexing* MIMO). The diversity MIMO idea can be traced several decades back to the so-called *smart antennas*. And the spatial multiplexing MIMO originates from the brilliant work of Telatar [Tela95], which is considered as one of the most significant technical breakthroughs in the wireless communication field. Comprehensive overviews about MIMO can, among others, also be found in [Gesb03], [Paul03]. The introduction of MIMO will be detailed in Chapter 2.

1.1.6 The working flow of UTRA LTE downlink

The gain mechanisms explained above are tightly integrated to work efficiently for UTRA LTE downlink. The working procedure is illustrated in Figure 1.6.

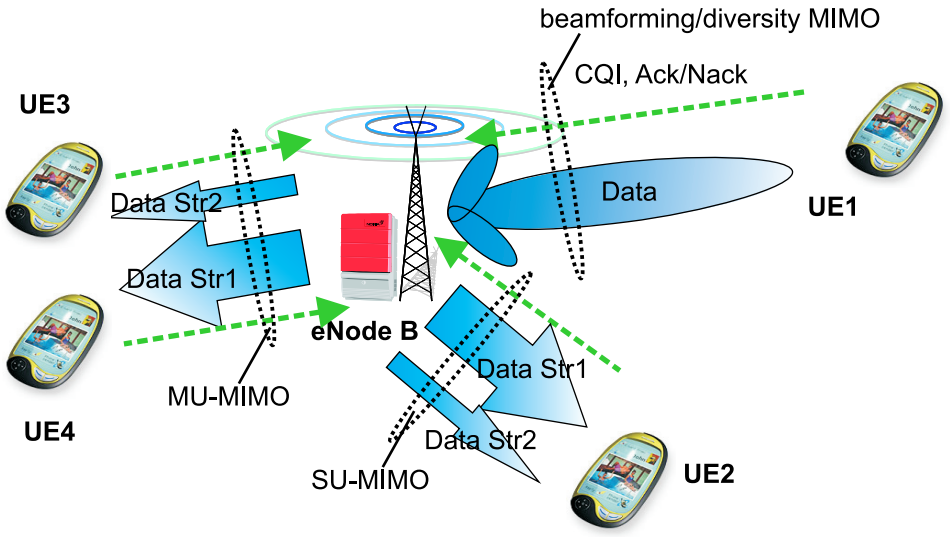

Figure 1.6: Illustration of the main principles of UTRA LTE downlink.

We consider the UTRAN LTE downlink consisting of a scheduling node (eNode-B) with FDPS functionality and several UEs capable of SDM reception. All UEs first measure the channel quality every TTI, and the CQI is sent to eNode-B via up-

link. Based on this, the eNode-B makes decisions on frequency-time resource allocation and corresponding data rate adaptation. Three options of MIMO processing are proposed in 3GPP for multi-user downlink transmission (Section 7.1.1.4.3 [3GPP06a]). The first option is to use the traditional beamforming and diversity MIMO schemes, as shown in Figure 1.6 for UE1 in the cell edge. This option is specially targeted at increasing the coverage for cell edge users. The other two options are meant for the users with a good channel condition, where multi-stream spatial multiplexing MIMO is applicable. All spatial streams can be sent to one UE, which is labeled as Single-user (SU-) MIMO for UE2 in Figure 1.6. Otherwise, the spatial streams could be sent to different UEs, labeled as Multi-user (MU-) MIMO for UE3 and UE4 in Figure 1.6. The MIMO scheme selection could be made either by short-term or long-term channel characteristics [Qual06b]. Once the transmission format is decided, the transmitter performs the space-time processing accordingly and the signal is sent by antennas. The allocation and data rate information is sent to the UEs via control channels. After receiving the packet, the UE performs MIMO space-time detection and recovers the data and performs CRC check to determine whether the data packet is error free. If so, the packet is passed on to higher layers for further processing, and an Acknowledgement (ACK) is signaled back to the eNode-B. If the packet is not correctly decodable, its bits remain in the UE buffer, and a Negative Acknowledgement (NACK) is signaled back to the eNode-B. Upon reception of a NACK the eNode-B performs fast layer one retransmission of the data packet. Should one packet still not be correctly decodable after maximum retransmissions, the data will be removed from the buffer, and a higher layer retransmission protocol is needed.

1.2 State of Art - A crowded MIMO community

Although MIMO has been intensively studied for many years, it remains one of the most hot topics today. A short survey of research activity in the MIMO technology field is presented below, and this review is restricted to the related work of this thesis only.

A good overview tutorial on the general MIMO can be found in [Gesb03]. For frequency selective channels, it is quite natural for people to think of the possibility of introducing MIMO together with OFDM, referred to as “MIMO-OFDM”. The marriage of MIMO and OFDM is natural and beneficial since OFDM enables support for more antenna elements and larger bandwidth without complex time domain equalization such as rake receiver and MIMO can increase the capacity at no cost in bandwidth. Quite a few general overview papers can be found in the literature for MIMO-OFDM, *e.g.* [Paul04], [Stub04], [Ogaw03], [Park05], [Blcs02]. Some field trials of the MIMO-OFDM concept have been carried out worldwide, see for example NTT Docomo in Japan [Kish03] and Iospan Wireless Inc. in USA

[Samp02].

Numerous MIMO schemes have been proposed in the past years with different design goals, for example, the space-time coding [Alam98], *Vertical Bell Laboratories Layered Space-Time Architecture* (V-BLAST) [Woln98] and per Antenna Rate Control (PARC) [Chun01] [Luce02], and matrix transmission [Hott03b], just to name a few. Generally speaking, MIMO could be utilized either to maximize the data rate using multi-stream transmission or maximize the link quality through space-time diversity processing. Besides, some hybrid schemes are proposed aiming to achieve both diversity and spatial multiplexing gain at the same time [Texa01]. But there is always a tradeoff between spatial multiplexing gain, diversity gain, and complexity. With MIMO-OFDM, the design of the so-called space-time-frequency (STF) coding also attracts a lot of attention [Liu04]. In [Bolc00], the maximum achievable diversity with the STF system is discussed, and the design guideline to maximize the diversity order is provided as well. This work is further extended to take into account the diversity-multiplexing trade-off consideration in the follow-up paper [Bolc03].

With the increasing number of MIMO proposals, a generalized expression of MIMO schemes becomes an interesting issue in this community. Hassibi etc. proposed the so-called Linear Dispersion Coding (LDC) [Hass02], and essentially identified a unified framework for many kinds of MIMO schemes in flat fading channels. Code design methods to optimize the mutual information are analyzed as well. Another paper with a similar target in mind is from [Sand01], in which a more general form of expression is presented, and the design criteria are extended to take into account both the error probability and the channel capacity. In [Barb04], the authors proposed the *Trace-Orthogonal Design* (TOD) such that a great flexibility in designing code can be achieved with the desired trade-off between bit error rate, transmission rate, and receiver complexity.

Another interesting topic in this field is the adaptive selection of MIMO schemes. This concept is proposed in [Catr02] where the system can adaptively choose among MIMO schemes with different diversity-multiplexing tradeoff capabilities based on instantaneous channel conditions to maximize the spectral efficiency. Following that, quite a number of important contributions concerning adaptive MIMO [Xia04] [Fore05] [Heat05] [Chae04] [Zhou02] [Tang05] [Vese06] have been published with different selection criteria design methods. In the frame-work of UTRA LTE, this means that the chosen MIMO scheme can be changed based on CQI as often as every TTI.

The signaling issue is also considered an important research topic. From an information theory point of view, the capacity of the MIMO system with Channel State Information (CSI) known to the transmitter is higher than the system with CSI unknown to the transmitter [Zels04] [Shar05]. Typically for the FDD system, the receiver can get the CSI via channel estimation, while the transmitter has no

knowledge of CSI unless the information is sent by the UE in uplink. There are two common ways of utilizing the CSI at the transmitter. (1) The transmitter uses CSI to perform the principal-eigenmode transmission, *i.e.* the traditional transmit antenna array (TxAA) techniques, where the link quality (received SNR) is maximized. In the 3GPP terminology, TxAA is also known as CLTD. Considering practical signaling issues, different TxAA beamforming weight quantization resolutions and corresponding achievable array gain numbers are identified in [Naru97] for flat Rayleigh channel. Later, Love etc. proposed a method such that the receiver only sends the label of the best beamforming vector in a predetermined codebook to the transmitter. And by using the distribution of the optimal beamforming vector in independent and identically distributed Rayleigh fading matrix channels, the codebook design problem is solved and related to the problem of Grassmannian line packing [Love03] for uncorrelated channels. This work is extended to correlated channels in [Love04]. Further, the column by column quantization approach is proposed for larger number of transmit antenna elements in [Inte06]. (2) Otherwise, the transmitter can perform eigen-beamforming transmission to maximize the achievable data rate, in which a MIMO channel is transformed into a bank of scalar channels with no crosstalk from one scalar channel to the others [Ande98]. One practical scheme following this concept, but with equal power allocation and quantized beamforming weight, is dual-stream TxAA (D-TxAA) [Moto06]. When transmit beamforming techniques are to be combined with OFDM, ideally we should send feedback weight for each sub-carriers due to frequency selectivity. This method however generates huge feedback requirements. Various approaches have been proposed in order to reduce the signaling while most of the gain is kept, *e.g.* [Choi05] [Thom05].

When multiple users are present at the system, opportunistic packet scheduling can explore the potential by multi-user diversity gain. When this concept is extended to frequency domain in OFDMA, the so called FDPS can bring significant gain to the system, by exploiting multi-user diversity gain on both time and frequency domains. Optimal and sub-optimal sub-carrier based adaptation has been widely studied in the literature, see [Sung03] [Rhee00] and the references therein. The concept is studied with more realistic assumptions under the LTE framework considering band adaptation and CQI issues in [Pokh06]. Concerning the multiuser MIMO system [Spen04], one important theoretical literature addressing the capacity of MIMO broadcast channels was published in [Vish02]. And the problem of exploiting multi-user diversity in MIMO systems with linear receivers have been discussed by Heath [Heat01a] where some sub-optimal solutions were proposed with much reduced complexity. When the multiuser MIMO is to be combined with OFDMA, the bit and power loading issues have to be jointed optimized with MIMO selection, which results in quite high complexity (see for example the exhaustive search algorithm in [Jung04] [Pan04] [Dupl05] [Hott03a] [Pasc04]).

Besides, measurement and modeling work for MIMO channels are still carried

on worldwide [3GPP03] [Baum05] [Elek03]. Another relevant research such as the radio frequency (RF) imperfections for multiple antennas [Woo06] is also a crucial topic for practical application of MIMO.

1.3 Motivation and Objective

Although huge potential is revealed in a capacity perspective for MIMO [Tela95], it is still a big challenge to map this huge potential into attainable cell throughput gain in a practical system. Therefore, the overall objective of this study is identified to answer this question "*How to enhance the spectrum efficiency in the OFDM systems with MIMO technology?*". As a case study, we will concentrate on UTRA LTE system downlink. More specifically, we identified the following open issues concerning the efficient application of MIMO in the LTE system.

As introduced in the Section 1.2, there are many MIMO schemes proposed with different complexity, signalling requirements and gain mechanisms. Therefore, the first issue we need to address is to choose MIMO schemes, depending on the system requirements and targets. Besides, there is always interactions of MIMO with other gain mechanisms in the system. For example, the Link Adaptation and HARQ are also trying to improve the performance by SNR combination gain and/or diversity gain, similar to many MIMO schemes. The gain from different functionalities can not be added upon each other as if they are addressed separately. All these interactions need to be investigated to make a more realistic overall evaluation of the system. Further, other effects such as realistic coding and modulation, CQI imperfections, the cell scenarios, etc., will also have a big impact on the performance of MIMO and need to be evaluated.

The second critical issue for the system design is the signalling and performance tradeoff. It is known that the performance of MIMO schemes can be improved at the cost of weight information feedback, as introduced in the Section 1.2. The feedback load and performance gain should be analyzed during system design. Besides, when spatial multiplexing schemes combined with channel coding, it is possible to either encode the streams jointly (single codeword) or separately (multiple codewords) [Noki06a]. The use of multiple codewords allows for adjusting the code-rates of the streams separately, and also gives the possibility to use serial interference cancelation receivers [Qual05]. However, the Single codeword approach results in less feedback and possibly to different type of receivers. In this context, the best signalling and performance compromise should be found for practical system design.

Another hot research topic concerning MIMO is about MIMO adaptation, as introduced in Section 1.2. In principle, if we can feedback the CQI information for all the MIMO mode supported, the eNode-B can make prediction on the throughput

for all MIMO schemes and make the choice of MIMO schemes accordingly on an instantaneous basis. But the associated issues need to be addressed like how to analyze the potential of MIMO adaptation and how fast should we make the adaptation. The extra signalling to support the MIMO adaptation certainly make those issues critical to consider.

When multiple-users are present in the cell, MIMO can be further combined with FDPS. Diversity MIMO with FDPS is quite straightforward extension of FDPS. But the utilization of the spatial multiplexing MIMO with FDPS is more complicated. Two possible options are called SU-MIMO and MU-MIMO, as illustrated in Figure 1.6, depending on the scheduling resolution. The SU-MIMO and MU-MIMO require different level of signalling and offer different performance gains. Besides, since spatial multiplexing MIMO schemes can only be used in good conditions, the fall back diversity MIMO schemes have to be used in bad conditions, that involves again the MIMO adaptation. Moreover, the functionalities in eNode-B such as Packet Scheduler, Link Adaptation, HARQ need work together efficiently to get the best out of the system. The practical scheduling algorithm to handle all these factors, but still with reasonable complexity is also critical for the system.

In summary, these detailed objectives boils down to two fundamental tasks. That is

- Performance enhancement with advanced MIMO solutions.
- Complexity and Signaling control for the system.

1.4 Assessment Methodology

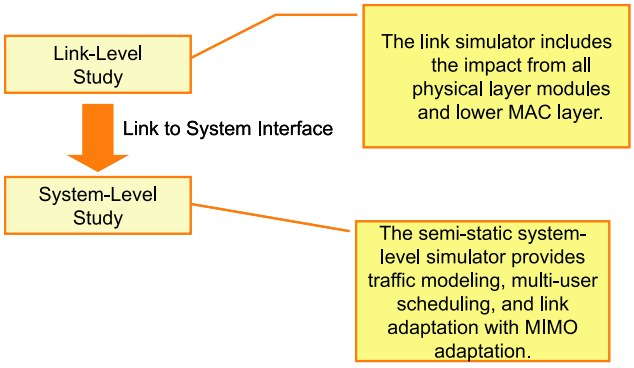

Figure 1.7: Two-phase Evaluation Methodology.

The evaluation of the study is conducted in two phases, as illustrated in Fig-

ure 1.7. First, to include the impact from all modules in physical layer such as MIMO channel, modulation order, HARQ, LA, turbo coding, practical CQI issues etc, the first step is the link-level performance evaluation of MIMO techniques in a UTRA LTE downlink scenario. The link-level performance is abstracted with the link to system interface. Based on that, the evaluation of cell throughput gain is conducted in a semi-static system-level simulator. The effect of traffic models, multi-user scheduling, MIMO adaptation etc will be studied.

1.5 Outline of the Dissertation and Contributions

The dissertation is divided into 9 chapters. With exception of introduction (chapter 1), conclusion (chapter 9) and the background (chapter 2), the chapters 3-5 focus on the link-level study and the chapters 6-8 summarize the system-level study. A general preview of all chapters is presented. Furthermore, the main contributions are emphasized with bullet points. The order of the content logically follows as background, link-level study, and system-level study. The work is usually conducted in two phases. Firstly it is analyzed through a theoretical approach to identify the potential and gain insight, then detailed simulation is performed to evaluate it by including more realistic factors under UTRA LTE framework.

In Chapter 2, the background information for reading this thesis is introduced with an emphasis on the MIMO-OFDM techniques. Since many tutorials and textbooks exist for MIMO and MIMO-OFDM, only essentially related background is discussed. To gain more insight into this promising combination of MIMO and OFDM, we formulate a unified framework of MIMO-OFDM based on the LDC code. The detailed formulation of framework is further introduced in Appendix A. Afterwards, the considered practical MIMO-OFDM schemes are explained in more details.

- Inspired by the authors in [Moli02] who point out basic equivalence between antenna elements and OFDM sub-carriers, we formulate a unified framework of MIMO-OFDM system based on the linear dispersion code [Hass02]. This provides a more general view and a practical tool for further optimization of this promising combination.

Chapter 3 summarizes our [2] contributions on baseline link-level evaluation for UTRA LTE downlink. Basic MIMO schemes are chosen as benchmarking results

[2] Phd students Akhilesh Pokhariyal, Christian Rom and Basuki E. Priyanto from the Department of Electronic Systems, Aalborg University, Denmark and Frank Frederiksen and Claudio Rosa from Nokia Siemens Networks, Aalborg R&D, Denmark.

for more advanced techniques later. Firstly, the main LTE system parameters assumptions are presented. Secondly, the link level simulator developed for UTRA LTE downlink is introduced in details. The validations of simulator implementation are presented in Appendix C. Thirdly, the spectral efficiency performance of different MIMO schemes with long-term or short-term LA is obtained. And the issue of CQI signaling is addressed as well. Further, the cell level throughput for various MIMO schemes considered are estimated under macro or micro cell scenarios for LTE downlink.

- To make an overall performance assessment of LTE, a detailed link level simulator which features main LTE L1 functionalities is developed for UTRA LTE downlink. My major contributions for this simulator are the implementation of turbo code/decoder module, multipath MIMO channel model and various MIMO schemes. Attainable spectral efficiency is evaluated with different gain mechanisms together (MIMO, Link Adaptation, HARQ etc.) under more realistic factors. The results help making the selection on MIMO schemes depending on cell scenarios, correlation, etc. This work was partly published in [Wei06b]. The simulator also provided SINR traces for the FDLA study in [Kold05].

The open-loop transmit diversity schemes like space-time coding can achieve full diversity without any feedback. On the other hand the CLTD can achieve transmit array gain on top of diversity gain at the cost of weight feedback requirements. Since the CLTD is considered an important candidate for UTRA LTE, the performance of CLTD is investigated in Chapter 4. The emphasis is given on designing efficient methods to reduce the required weights feedback. More specifically, we perform loss analysis with different quantization and grouping strategies. Then the attainable spectral efficiency and eventually the cell throughput estimate is evaluated with different antenna configurations, quantization resolution and grouping size, etc.

- The CLTD is addressed in the LTE scenarios with limited feedback. The performance is evaluated in terms of attainable spectral efficiency and cell throughput. The tradeoff between signalling requirements and performance gain is identified. The results were published in [Wei06d]. Some other way of feedback reduction using Run Length Coding (RLC) is also explored, and the related results are published in [Wei06a].

The adaptive MIMO principle is analyzed and evaluated in Chapter 5. We have two tasks in this chapter. Firstly, we provide useful insight into the principles of adaptive MIMO through theoretical analysis. This is achieved by using a unified SINR concept. Secondly, we propose the practical channel quality metric design

for LA algorithms including MIMO adaptation and evaluate the algorithms with detailed link simulator by including more imperfections.

- The adaptive MIMO capacity gain analysis is formulated from an instantaneous SINR perspective. A unified SINR concept is proposed to make a easy comparison of MIMO schemes with different number of spatial streams. With the analysis, we can identify whether the adaptive MIMO selection of certain MIMO schemes should be performed or not considering the signalling overhead and the achievable gain. Regarding the practical issues, advanced LA algorithm including MIMO adaptation was proposed and evaluated as well. And the results were accepted for publication in [Wei06c].

In Chapter 6, simulation methodology and assumptions for system-level evaluation simulations of Chapter 7 and Chapter 8 are summarized. Besides, the key performance indicators for system-level evaluation is briefly introduced as well.

In Chapter 7, the multiuser diversity gain with opportunistic FDPS is further explored in spatial domain by combining FDPS with MIMO in Spatial Division Multiplexing (SDM) mode (SDM-FDPS). The chapter starts with an introduction of system model and terminology definition. Following that, MIMO aware FDPS algorithms are proposed. Further, a theoretical analysis with some simplified assumptions are carried out to give insight into the different SDM-FDPS concepts. The performance results are then evaluated with a quasi-static network simulator which provides traffic modeling, multiuser scheduling, and link adaptation including HARQ, etc. The modeling and validation of the network simulator is provided in Appendix E.

- To include the effect from scheduler, a simplified theoretical analysis of post-scheduling SINR distribution is performed first to gain insight into the different SDM-FDPS schemes. Based on that, the theoretical cell level performance upper bounds are derived.

  For practical application of SDM-FDPS, to find a good compromise between complexity and gain, the suboptimal MIMO aware FDPS algorithms with moderate complexity are proposed. And the system level performance of SDM-FDPS is benchmarked without signaling constraints under LTE framework downlink. Finally, the theoretical bounds derived are compared with the simulation results. Quite good agreement are found. The results were accepted for publication in [Wei07b]. And part of the results were also provided as supporting material for a more general performance analysis of LTE with Shannon capacity formula [Moge07b].

As the signaling overhead with SDM-FDPS is shown to be greatly increased compared to SIMO FDPS, various methods are proposed in Chapter 8 to bring

down the signaling without affecting the performance significantly. The considered methods are first explained sequentially, namely semi-adaptive MIMO selection concept, single codeword for SU-MIMO transmission, and the threshold-based CQI schemes. The performance is then evaluated with all methods incrementally.

- In order to bring down the signaling to a practical level without sacrificing too much in the SDM-FDPS gain, several effective approaches are identified by considering the interaction of FDPS and other gain mechanisms. The results with reduced signaling is shown to be able to maintain most of the performance. The relevant results are accepted for publication in [Wei07a].

Finally, the concluding remarks are summarized in Chapter 9 and some potential future work are proposed as well.

1.6 Publications

The following articles have been published during the Ph.D. study:

[Wei06a] N. Wei, L. T. Berger, T. B. Sørensen, T. E. Kolding, and P. E. Mogensen. Tackling MIMO-OFDMA feedback load through feedback encoding. In The International Symposium on Wireless Communication System, Sep. 2006.

[Wei06b] N.Wei, A. Pokhariyal, C. Rom, B. E. Priyanto, F. Frederiksen, C. Rosa, T. B. Sørensen, T. E. Kolding, and P. E. Mogensen. Baseline E-UTRA downlink spectral efficiency evaluation. In The 64th IEEE Vehicular Technology Conference, Sep. 2006.

[Wei06c] N. Wei, T. B. Sørensen, T. E. Kolding, and P. E. Mogensen. Analysis and evaluation of link adaptation including MIMO adaptation. In The 64th IEEE Vehicular Technology Conference, Sep. 2006.

[Wei06d] N.Wei, B. Talha, T. B. Sørensen, T. E. Kolding, and P. E.Mogensen. Spectral efficiency of closed-loop transmit diversity with limited feedback for UTRA Long TermEvolution. In The 17th IEEE Personal, Indoor and Mobile Radio Communications, Sep. 2006.

[Wei07a] N. Wei, A. Pokhariyal, T. B. Sørensen, T. E. Kolding, and P. E. Mogensen. Mitigating signalling requirement for MIMO with frequency domain packet scheduling. In IEEE 65th Vehicular Technology Conference, Apr. 2007.

[Wei07b] N.Wei, A. Pokhariyal, T. B. Sørensen, T. E. Kolding, and P. E.Mogensen. Performance of MIMO with Frequency Domain Packet Scheduling in UTRAN LTE downlink. In IEEE 65th Vehicular Technology Conference, Apr. 2007.

In addition, the following articles were co-authored during the Ph.D. study:

[Kold05] T. E. Kolding, A. Pokhariyal, N. Wei, and P. E. Mogensen. Impact of Channel Quality Signaling on Frequency Domain Link Adaptation Performance. In Wireless Personal Mobile Communications, Sep. 2005.

[Moge07b] P. E.Mogensen, N.Wei, A. Pokhariyal, I. Kovacs, F. Frederiksen, K. Pedersen, K. Hugl, T. E. Kolding, and M. Kuusela. LTE capacity versus Shannon. In IEEE 65th Vehicular Technology Conference, Apr. 2007.

Chapter 2

Background and Framework for MIMO OFDM

2.1 Introduction

This chapter provides background information for MIMO-OFDM and summarizes the proposed MIMO-OFDM framework. An overview of essential background of MIMO techniques is provided in Section 2.2. After the introduction of a generic system model of MIMO, an eigenvalue interpretation of MIMO channel is presented. Depending on whether the CSI is made available at the transmitter or not, the corresponding systems are sometimes referred to as "open-loop" and "closed-loop" respectively. The capacity of open-loop and closed-loop MIMO are introduced and compared as well. Further, the MIMO gain mechanisms and MIMO categorization are explained. The combination of MIMO with OFDM is discussed in Section 2.3, in which a conceptual unified MIMO-OFDM framework is proposed. This provides a more general view and gives more insight into the promising combination of MIMO-OFDM. At last, although many MIMO-OFDM schemes have been proposed already, we only pick some of the most popular ones for further evaluation in this thesis. The choice is motivated by many factors, such as complexity, back compatibility, etc. The selected schemes are explained in detail in the Section 2.4.

2.2 Overview of MIMO

2.2.1 System Model and Eigenvalue Analysis

Consider a general MIMO system as shown in Figure 2.1. The time index is not included here for simplicity. Assuming N_t transmit antennas at eNode-B and N_r receive antennas at UE, the discrete signal model can be expressed as

$$\mathbf{y} = \mathbf{H}\mathbf{s} + \mathbf{n} \ , \tag{2.1}$$

where $\mathbf{y} \in C^{N_r \times 1}$ is the received signal vector, $\mathbf{s} \in C^{N_t \times 1}$ is the transmit signal vector with elements picked from a unit energy constellation, and $\mathbf{n} \in C^{N_r \times 1}$ is the complex additive white Gaussian noise vector with variance, $\sigma_n^2 \mathbf{I}_{N_r}$. The channel matrix $\mathbf{H} \in C^{N_r \times N_t}$ represents the links between transmitter and receiver as

$$\mathbf{H} = \begin{bmatrix} h_{11} & h_{12} & \cdots & h_{1N_t} \\ h_{21} & h_{22} & \cdots & h_{2N_t} \\ \vdots & \vdots & \ddots & \vdots \\ h_{N_r 1} & h_{N_r 2} & \cdots & h_{N_r N_t} \end{bmatrix} \ . \tag{2.2}$$

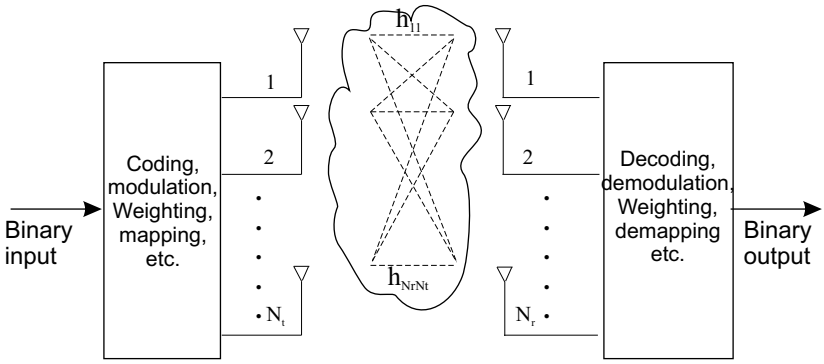

Figure 2.1: Generic MIMO system structure.

A nice and convenient way to visualize the impact of the MIMO channel on the capacity is based on Singular Value Decomposition (SVD) of given channel matrix [Golu96]. The SVD of $\mathbf{H}$ equals

$$\mathbf{H} = \mathbf{U}\mathbf{D}\mathbf{V}^H, \tag{2.3}$$

where $\mathbf{U} \in C^{N_r \times N_r}$ and $\mathbf{V} \in C^{N_t \times N_t}$ are unitary matrices. The diagonal matrix $\mathbf{D} \in C^{N_r \times N_t}$ having the singular values of $\mathbf{H}$ on its diagonal, *e.g.* $\mathbf{D} = \text{diag}(\lambda_1, \lambda_2, ...\lambda_K)$ where $K = \text{rank}(\mathbf{H}\mathbf{H}^H) \leq \min(N_t, N_r)$. With Equation 2.3, we can rewrite the Equation 2.1 as

$$\mathbf{y} = \mathbf{U}\mathbf{D}\mathbf{V}^H\mathbf{s} + \mathbf{n} \ . \tag{2.4}$$

Assuming that we have full knowledge at the transmitter already, we can set $\mathbf{V}$ as an eigenbeamforming filter at the transmitter and $\mathbf{U}^H$ as a matched filter at the receiver. As shown in Figure 2.2, the signal model results in

$$\mathbf{r} = \mathbf{U}^H\mathbf{y} = \mathbf{U}^H\mathbf{U}\mathbf{D}\mathbf{V}^H\mathbf{V}\mathbf{s} + \mathbf{U}^H\mathbf{n} = \mathbf{D}\mathbf{s} + \mathbf{n}' \quad . \tag{2.5}$$

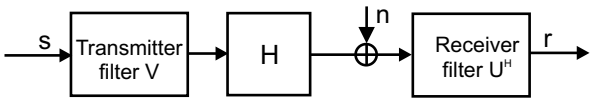

Figure 2.2: Illustration of MIMO eigenmode transmission.

A component wise notation of Equation 2.5 results in

$$r_k = \lambda_k s_k + n'_k \qquad k = 1...K \quad . \tag{2.6}$$

In this case, as shown in Figure 2.3, the equivalence of MIMO channel consists of K parallel spatial subchannels with different eigenvalues λ_k, where λ_k^2 represents the channel gain for subchannel k.

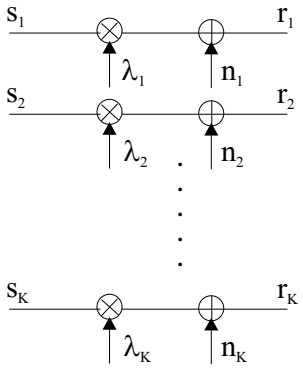

Figure 2.3: Equivalence of MIMO channel model.

The number of available spatial eigenmodes indicates the potential capacity that a MIMO channel can support. Then by using Shannon's capacity formula

[Shan48], the capacity of MIMO channel can be derived as

$$\begin{aligned} C &= \log_2 \det\left(\mathbf{I}_{N_r} + \frac{q_{kk}}{\sigma_n^2}\mathbf{H}\mathbf{H}^H\right) \\ &= \log_2 \det\left(\mathbf{I}_{N_r} + \frac{q_{kk}}{\sigma_n^2}\mathbf{U}\mathbf{D}\mathbf{V}^H(\mathbf{U}\mathbf{D}\mathbf{V}^H)^H\right) \\ &= \log_2 \det\left(\mathbf{I}_{N_r} + \frac{q_{kk}}{\sigma_n^2}\mathbf{U}\mathbf{D}\mathbf{D}^H\mathbf{U}^H\right) \\ &= \log_2 \det\left(\mathbf{I}_{N_r} + \frac{q_{kk}}{\sigma_n^2}\begin{bmatrix} \lambda_1^2 & 0 & 0 \\ 0 & \ddots & 0 \\ 0 & 0 & \lambda_K^2 \end{bmatrix}\mathbf{U}\mathbf{U}^H\right) \\ &= \sum_{k=1}^{K}\log_2\left(1 + \frac{\sigma_{s,k}^2}{\sigma_n^2}\right) \ , \end{aligned} \tag{2.7}$$

where $\sigma_{s,k}^2$ is the effective power on the kth subchannel, which is the product of the transmit power q_{kk} and the channel gain λ_k^2 for each subchannel.

Assuming Gaussian input signal and perfect CSI feedback with no delay, the optimal power allocation to maximize the capacity under the total power constraint P_t is solved via water-filling [Tela95] as follows,

$$q_{kk} = \left(\mu - \frac{\sigma_n^2}{\lambda_k^2}\right)^+ , \qquad k = 1...K \ , \tag{2.8}$$

where μ is chosen to satisfy $\sum_{k=1}^{K} q_{kk} = P_t$, and where

$$(x)^+ = \begin{cases} x, & \text{if } x \geq 0 \\ 0, & \text{if } x < 0 \end{cases} \ , \tag{2.9}$$

Thus the capacity with full CSI is given as

$$C = \sum_{k=1}^{K}\log_2(1 + \lambda_k^2\frac{q_{kk}}{\sigma_n^2}) \ . \tag{2.10}$$

Assuming no CSI at transmitter, the optimal strategy will be to distribute the power equally among the transmit antenna elements, and thus the capacity without CSI is given by

$$C = \sum_{k=1}^{K}\log_2(1 + \lambda_k^2\frac{P_t}{N_t\sigma_n^2}) \ . \tag{2.11}$$

Given the Equation 2.10 and Equation 2.11, the ergodic capacity is calculated for uncorrelated MIMO channels with different number of antenna elements as

shown in Figure 2.4. For those curves, 10,000 realizations of the flat rayleigh channel matrix is performed to determine the average capacity, *i.e.* , ergodic capacity. It is observed that the capacity with full CSI is superior to the capacity without CSI only when the average SNR is low or when $N_t > N_r$.

To include the effect of antenna correlation, we consider a simple double-coefficient spatial correlation model from [Zels04] where a transmit antenna correlation matrix $R_{tx} \in C^{N_t \times N_t}$ with a structure as

$$R_{tx} = \begin{bmatrix} 1 & r_{tx} & r_{tx}^2 & \dots & r_{tx}^{N_t-1} \\ r_{tx} & 1 & r_{tx} & \ddots & \vdots \\ r_{tx}^2 & r_{tx} & 1 & \ddots & r_{tx}^2 \\ \vdots & \ddots & \ddots & \ddots & r_{tx} \\ r_{tx}^{N_t-1} & \dots & r_{tx}^2 & r_{tx} & 1 \end{bmatrix}, \tag{2.12}$$

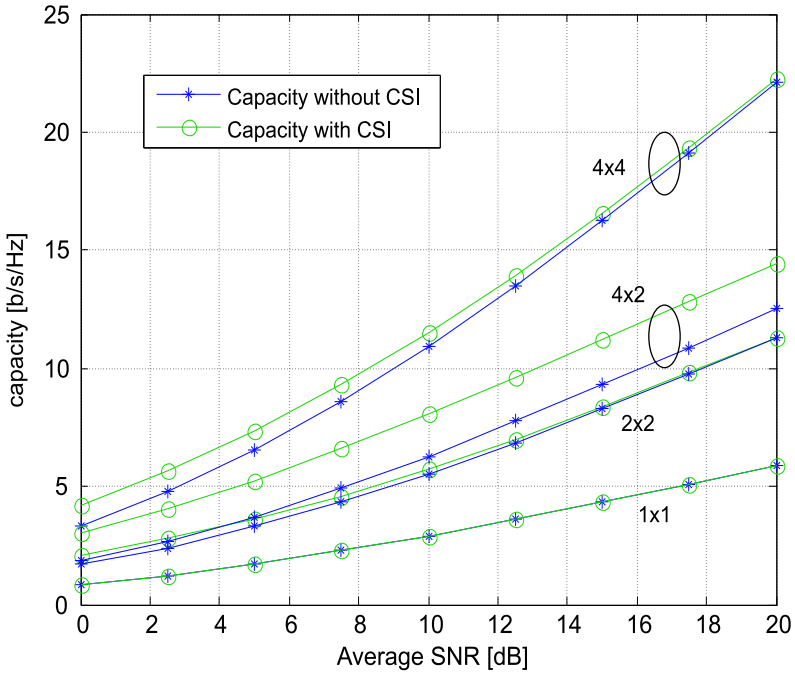

Figure 2.4: Ergodic channel capacity for MIMO with different antenna configurations in flat Rayleigh channel.

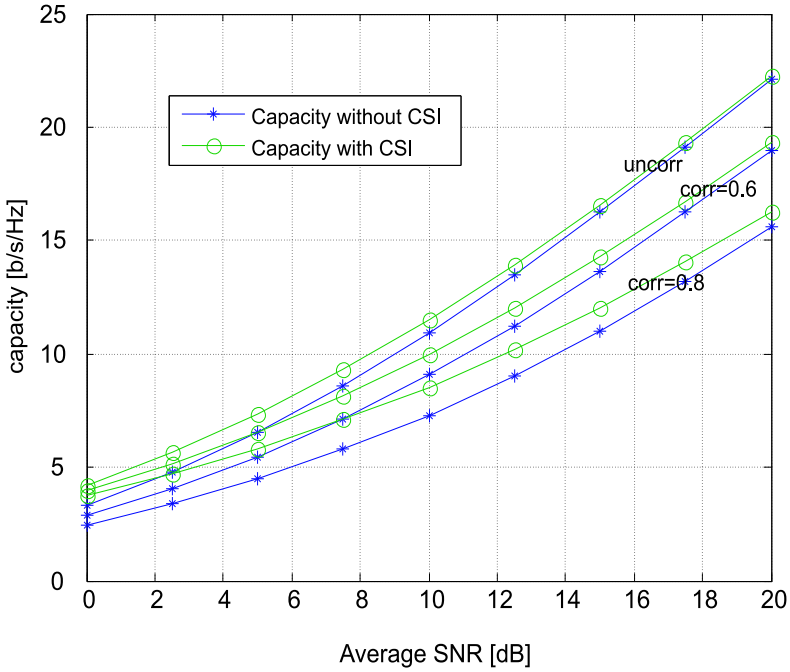

Figure 2.5: Ergodic channel capacity for 4x4 MIMO with different level of correlation at both ends in flat Rayleigh channel.

and a receive antenna correlation matrix $R_{rx} \in C^{N_r \times N_r}$ with a structure as

$$R_{rx} = \begin{bmatrix} 1 & r_{rx} & r_{rx}^2 & \dots & r_{rx}^{N_t-1} \\ r_{rx} & 1 & r_{rx} & \ddots & \vdots \\ r_{rx}^2 & r_{rx} & 1 & \ddots & r_{rx}^2 \\ \vdots & \ddots & \ddots & \ddots & r_{rx} \\ r_{rx}^{N_t-1} & \dots & r_{rx}^2 & r_{rx} & 1 \end{bmatrix} . \tag{2.13}$$

Based on this, the channel matrix with spatial correlation can be represented as [Zels04]

$$\mathbf{H} = R_{tx}^{\frac{1}{2}} \mathbf{H}_{iid} (R_{rx}^{\frac{1}{2}})^T \ , \tag{2.14}$$

where $\mathbf{H}_{iid} \in C^{N_r \times N_t}$ is with i.i.d. zero-mean unit variance elements. Under the assumption that the elements of $\mathbf{H}$ are zero mean and have a variance of one, the correlation matrices can be found as follows:

$$R_{tx} = E\left[(\mathbf{h}_q)^T (\mathbf{h}_q)^*\right], \quad \text{for all } q, \quad q = 1, ..., N_r \ , \tag{2.15}$$

$$R_{rx} = E\left[\mathbf{h}_p \mathbf{h}_p^H\right], \quad \text{for all } p, \quad p = 1, ..., N_t \ , \tag{2.16}$$

where $\mathbf{h}_q$ is the q-th row of $\mathbf{H}$, $\mathbf{h}_p$ is the p-th column of $\mathbf{H}$, and $(.)^*$ denotes the element wise conjugate of the corresponding vector or matrix.

Obviously the introduced spatial correlation model may not be the accurate model for some real-world scenarios, but it is a simple model that allows us to study the effect of correlation in an explicit way. With this model the capacity of MIMO in scenarios with correlation at both the transmitters and the receivers are compared in Figure 2.5. As shown the capacity with full CSI is higher than that without CSI for the whole range of average SNR. The reason is that for such non-orthongnal channels in correlated scenarios, the eigenmodes have quite unequal channel gains. To achieve higher capacity, the optimal transmitter solution of having full CSI will use more power on the stronger sub-channels to enhance the capacity, whereas the transmitter without CSI applies equal power on all sub-channels and wastes energy in the bad eigenmodes and thus loss in capacity.

2.2.2 MIMO Gain Mechanisms

Generally speaking, the gain of MIMO can be traced from four gain mechanisms, *i.e. , array gain, diversity gain, interference rejection gain, and spatial multiplexing gain.* The first three gain mechanisms can be obtained already with MISO or SIMO, while the last gain mechanism must have multiple antennas at both ends. These gains may sometimes be mutually conflicting, implying that the total spatial freedom of MIMO channel can be used in different ways.

2.2.2.1 Array Gain

Array gain is an increase in average received SNR by a coherent combining of signal from multiple antenna elements at transmitter and/or receiver. The array gain requires channel knowledge. Channel knowledge at the receiver is typically available via channel estimation, whereas channel information at the transmitter is in general more expensive to obtain. As a example we consider a $1 \times N_r$ SIMO system. Further we assume that there is no CSI at the transmitter, but full CSI at the receiver. Following the system model in Equation 2.1, the SIMO system can be expressed as

$$\mathbf{y} = \mathbf{H}s + \mathbf{n} = \begin{bmatrix} h_{11} \\ h_{21} \\ \vdots \\ h_{N_r 1} \end{bmatrix} s + \mathbf{n} \tag{2.17}$$

Since the maximum-gain receiver weights are the conjugate of the channel matrix, $\mathbf{H}^*$, the recovered signal is coherently combined as

$$\mathbf{H}^*\mathbf{y} = \mathbf{H}^*(\mathbf{H}s + \mathbf{n}) = (||h_{11}||^2 + ||h_{21}||^2 + ... + ||h_{N_r 1}||^2)s + \widehat{n} \tag{2.18}$$

Since the received signal power is the sum of the signal power from the N_r receiver elements, the array gain in this case is clearly N_r.

2.2.2.2 Diversity Gain

Diversity gain (time/frequency/space) is a result of the fact that the possibility that all signals fade at the same time is much lower. Provided there are several branches (time, frequency, and space) which exhibit independent fading, diversity exploits these branches to minimize the signal level variability. Extracting spatial diversity without CSI at the transmitter is possible with suitable signal processing techniques, for example with the space-time coding [Alam98]. Consider again the example in the above discussion in array gain subsection, if all the receive elements are uncorrelated, we get N_rth order diversity gain.

2.2.2.3 Interference Rejection

Co-channel interference arises due to frequency reuse in wireless channels, which causes serious performance degradation for cell edge users. When multiple antennas are used, the different spatial signatures of desired signal and interference signal can be exploited to reduce or cancel the interference. In a multipath rich environment this leads to a situation where at the receiver the different streams exhibit different spatial signatures that have been imposed by the scattering medium. The receiver can then use spatial interference suppression to discriminate the different streams on the basis of their signatures. Transmitter interference avoidance and receive interference cancelation can be performed depending on where the CSI is available. Now consider a simple example with one desired signal s_1 and one interference signal s_2 from a different transmitter as

$$\mathbf{y} = \mathbf{H}\mathbf{s} + \mathbf{n} = \begin{bmatrix} h_{11} & h_{12} \\ h_{21} & h_{22} \end{bmatrix} \cdot \begin{bmatrix} s_1 \\ s_2 \end{bmatrix} + \mathbf{n}. \tag{2.19}$$

The simplest receiver to null out the interference signal is the Zero-forcing (ZF) receiver whose weights are $(\mathbf{H}^H\mathbf{H})^{-1}\mathbf{H}^H$. The signal and interference recovered can be expressed as

$$\begin{bmatrix} \widehat{s_1} \\ \widehat{s_2} \end{bmatrix} = (\mathbf{H}^H\mathbf{H})^{-1}\mathbf{H}^H\mathbf{y} = \begin{bmatrix} s_1 \\ s_2 \end{bmatrix} + (\mathbf{H}^H\mathbf{H})^{-1}\mathbf{H}^H\mathbf{n}. \tag{2.20}$$

As shown, the spatial freedom from multiple antennas are utilized to null the interference signal out at the cost of noise enhancement. Up to $[\min(N_r, N_t) - 1]$ interferers can be cancelled.

2.2.2.4 Spatial Multiplexing Gain

The idea of spatial division multiplexing (SDM), sparked by the information theory from [Tela95], is based on transmitter and/or receiver interference suppression. A

spatial multiplexing system transmits multiple data streams and reuses all other resources, e.g. frequency, time and codes, etc. Different data streams are, however, transmitted from different antenna elements or through different transmit antenna weights. Consider again the example in the above discussion in the interference cancellation subsection, where the only difference is that both data streams are the desired signal now. In this way the spectral efficiency can be increased without increasing the bandwidth. Besides, with CSI at transmitter, the system can perform advanced power allocation to further increase the spectral efficiency, as addressed in the eigenmode analysis in the previous section.

2.2.3 MIMO Categories

2.2.3.1 Diversity MIMO vs Multiplexing MIMO

The spatial freedom introduced by a MIMO system can be used in two distinct ways [Zhen03] [Catr02], *i.e.* , either to improve link quality (diversity MIMO) or to enhance throughput (multiplexing MIMO). Diversity MIMO schemes in general can increase the performance by exploit array gain and/or diversity gain, but it will have the same data rate as the SISO system, *e.g.* Space-time coding. On the other hand, multiplexing MIMO can increase the symbol data rate at no cost of extra spectrum, *e.g.* BLAST. A hybrid combination of the two is also possible, but with a total spatial freedom constraint [Texa01].

2.2.3.2 Closed-Loop MIMO vs Open-Loop MIMO

As mentioned earlier, the channel information at the receiver usually can be obtained with channel estimation, but the channel information at the transmitter is quite expensive to have in FDD mode systems. Depending on whether the CSI is available at the transmitter, MIMO schemes can be divided into Closed-Loop and Open-Loop schemes. That is, when there is no channel information at the transmitter, it is considered an Open-Loop scheme, *e.g.* Space-time coding. And it is called a Closed-Loop scheme if the opposite is the case. Moreover, the amount of required CSI for Closed-Loop schemes differs a lot, some require full CSI [Tela95], while more schemes aim at getting most of the gain with only partial CSI [Naru98].

2.3 Unified MIMO-OFDM Framework

When MIMO is to be combined with OFDM, many options are available [Paul04]. In order to gain insights into this, we propose a unified framework for MIMO-

OFDM systems in this section. This can be envisioned as a good starting point for further optimization of scheme design. Since the manipulation of three dimensions (frequency/time/space) is not very convenient, we reduced it back to two dimensions by the equivalence concept view of antenna elements and sub-carriers from Molisch etc. [Moli02] as introduced in Subsection 2.3.1. Following that, the unified framework is explained in Subsection 2.3.2. As the scope of this thesis is the interaction of MIMO with other gain mechanisms in the LTE systems, we identified a simplified version of MIMO-OFDM framework which is more suitable for practical application, and that is discussed in Subsection 2.3.3.

2.3.1 Equivalence of Antenna Elements and Sub-carriers

As the basis for the framework, we consider the concept of unified view of antenna elements and sub-carriers from Molisch etc. [Moli02]. The authors point out that there is a basic equivalence between antenna elements and OFDM sub-carriers. In short, if there is no crosstalk between the antenna elements and between the sub-carriers, all the $N_t \times N_c$ isolated links are equivalent. Here we assume that N_t is equal to the number of transmit antenna elements, and N_c is the number of useful sub-carriers. This analogy is further extended by two considerations with relaxed requirements [Moli02].

(1) Viewing the antennas as additional sub-carriers: If the channel is known, a singular value decomposition of the channel matrix transforms it into isolated (but not identically distributed) channels. This recovers the analogy to the isolated sub-carriers. For this very special case, the MIMO-OFDM system decomposed to a parallel of isolated SISO channels.

(2) Viewing the sub-carriers as additional antennas: In this case, the "additional antennas" just exhibit a special type of crosstalk description (namely, zero crosstalk). Note that the crosstalk might be beneficial for diversity purposes. However, crosstalk between sub-carriers could be enforced, e.g., by using multicarrier-CDMA instead of conventional OFDM. For this more general case, the links with crosstalk could be separated in the receiver with interference cancellation algorithms.

2.3.2 MIMO-OFDM Framework Representation

To incorporate most of the MIMO-OFDM schemes, we consider a general structure (*i.e.* consideration (2)) as shown in Figure 2.6. Note that the channel coding, modulation is performed beforehand and is not involved with space-time-frequency processing here, thus this framework does not support some schemes, *e.g.* space time trellis codes. And for simplicity, we consider the equivalent representation

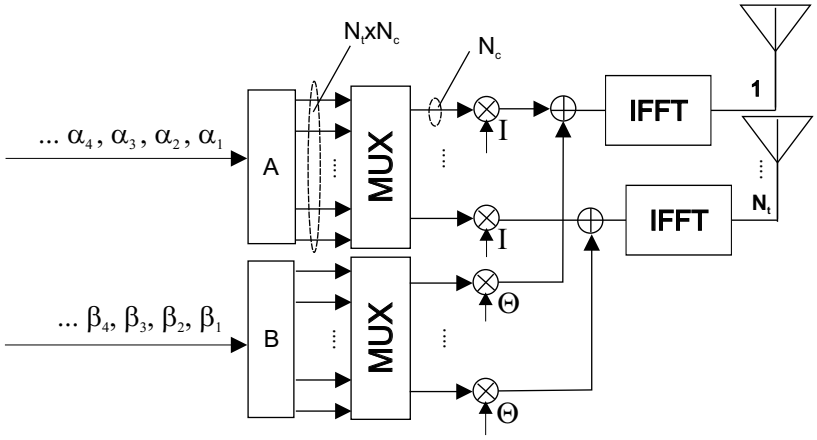

Figure 2.6: Illustration of unified framework for MIMO-OFDM.

of LDC with a separate real and imaginary part as Equation A.3. Therefore, the real and imaginary part of the input modulated symbols are coded with dispersion blocks $\mathbf{A}$ and $\mathbf{B}$, respectively. The output is then fed into a multiplexer and mapped to corresponding sub-carriers and antenna elements. As a consequence, each input symbol could be dispersed to any space-time-frequency resources. With the general space-frequency-time linear dispersion coding structure above, we could potentially optimize the code under certain constraints such as in [Bolc00] and [Bolc03]. The formulation of the framework is further introduced in detail in Appendix A. Since this framework is extended from the LDC concept [Hass02], the background information of LDC is provided in Appendix A as well.

2.3.3 Simplified MIMO-OFDM Framework Representation

Although the above framework provides a very good insight into the MIMO-OFDM system, the optimization of such a complex system is not a trivial task. On the other hand, we argue that the potential benefits are rather small under the LTE scenario as follows:

The potential benefit from the introduction of the frequency domain into the space-time processing is the extra frequency diversity gain. However, in the cases where a reasonably large diversity is already available in the system through transmit, receive, time diversity etc., the potential gain from frequency diversity is rather small [Zels04]. Moreover, in the cases where multiuser diversity over frequency is to be exploited, *e.g.* FDPS, block wise transmission (localized) [3GPP06a] is actually more desired. Even in the cases where the frequency diversity is crucial, a more structured frequency processing like transmission on non-consecutive (scattered, distributed) sub-carriers [3GPP06a] or frequency spreading can achieve most of the frequency diversity with much less complexity.

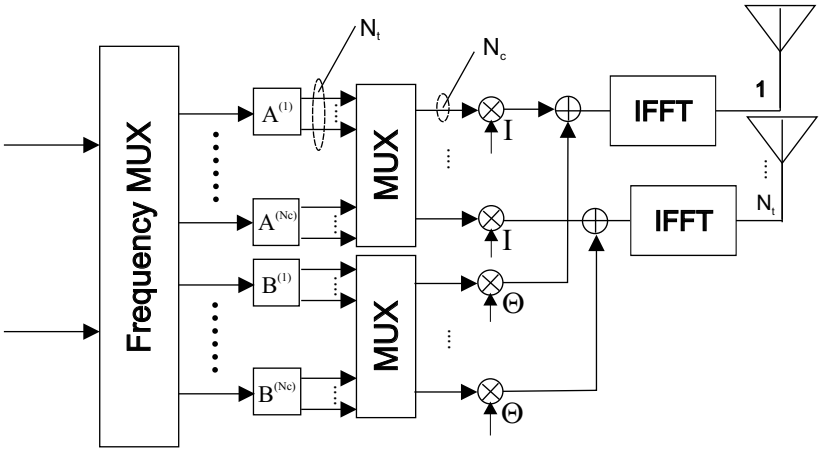

Figure 2.7: Simplified MIMO-OFDM schemes with detached frequency and space-time processing.

Based on the above arguments, we find an alternative, simplified code structure with a detached frequency and space-time processing more attractive, as illustrated in Figure 2.7. As shown, a frequency MUX is deployed before time and space only dispersion on each sub-carrier. Through a careful design of frequency MUX, most of the frequency diversity could be maximized with much less complexity. Thus this simplified framework is considered for further study here. It is important to note that with such a simplified configuration, we still have the potential to deploy different LD codes over time and frequency depending on the SNR and condition (practical rank) of channel variation.

2.4 Considered MIMO-OFDM Schemes

The MIMO-OFDM schemes considered in this thesis are introduced in this section. Since the baseline antenna configuration proposed in [3GPP06a] is two transmit antennas at the cell site (eNode-B) and two receive antennas at the UE, we have chosen to consider the following popular MIMO-OFDM schemes, namely SIMO, Space Frequency Coding (SFC)[Paul04], Transmit Antenna Array (TxAA) [Lo99](or equivalently CLTD in 3GPP terminology), Joint Coding (JC) [Qual06a], PARC [Chun01] and dual-stream TxAA (D-TxAA) [Moto06]. The SIMO is the default setting for LTE, with one transmit antenna and two receive antennas operating in Maximal Ratio Combining (MRC) mode. The summary of main features of all schemes considered are listed in Table 2.1.

Table 2.1: Overview of the considered MIMO schemes

MIMO scheme	Tx Ant.	Rx Ant.	Diversity order	Array gain (dB)	Spatial streams	Precoding
SISO	1	1	1	0dB	1	No
SIMO	1	2	2	3dB	1	No
SFC	2	2	4	3dB	1	No
CLTD	2	2	4	4.86dB [a]	1	Yes
JC/PARC	2	2	1	-3dB [b]	2	No
D-TxAA	2	2	1	-3dB	2	Yes

[a] The 4.86dB array gain is for uncorrelated scenario with 2 bits quantization in phase (see Equation 4.7 in Chapter 4), and the gain is up to 6dB in full correlated case where the transmit diversity is lost.

[b] The -3dB is to describe the equal power allocation on transmit antennas. There is no receiver array gain with linear receivers, and the receiver array gain can be up to 3dB for nonlinear receivers.

2.4.1 Diversity MIMO

As mentioned earlier, diversity MIMO can increase the link quality through diversity and array gain, but there is no data rate improvement compared to SISO. Practical schemes like SIMO, SFC and CLTD fall into this category.

2.4.1.1 SFC

The Space-Time Block Coding (STBC) [Alam98] by Alamouti is a classic modulation scheme discovered for the two transmit elements wireless systems. It has an elegant mathematical solution for providing full space diversity over the coherent, flat-fading channel without any feedback from the receiver to the transmitter. In addition, they require extremely simple encoding and decoding.

The SFC considered here is a variant of Alamouti STBC which is applied on neighboring sub-carriers instead of adjacent time symbols [Paul04]. The assumption behind this is that the channel is constant on neighboring N_t sub-carriers. Note that SFC defined here exploits all available space diversity without any frequency diversity. Similar to other STBC, the SFC utilizes all the spatial freedom on diversity and array gain. The transmit mapping of SFC is sketched in Figure 2.8. The input symbols and their complex conjugates are mapped to neighboring sub-carriers. With a two antenna elements transmitter, every two neighboring sub-carriers are considered as a code block.

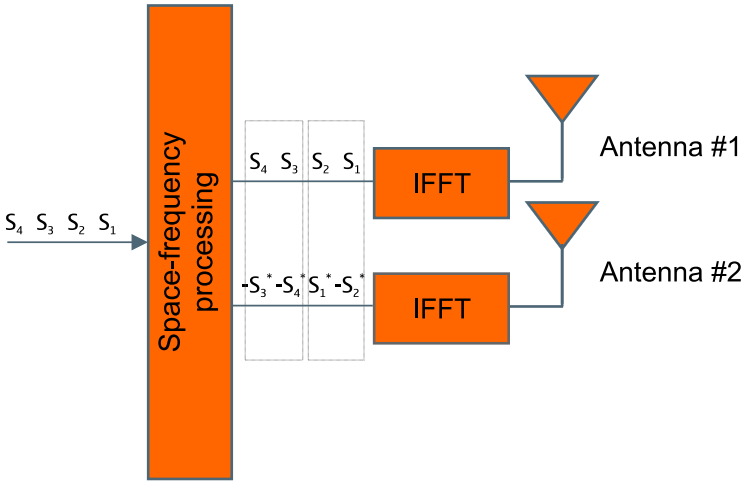

Figure 2.8: Illustration of space-frequency coding.

If we only take the first code block with sub-carrier index 1 and 2 as example, assuming that the neighboring two sub-carriers are experiencing identical channel, the system model can be expressed as

$$\mathbf{y} = \mathbf{H}\mathbf{s} + \mathbf{n} \ . \tag{2.21}$$

The transmit signal can be shown to be

$$\mathbf{s} = \begin{bmatrix} s_1 & s_2 \\ -s_2^* & s_1^* \end{bmatrix} \ . \tag{2.22}$$

With arbitrary N_r receive antennas, the received signal with dimension of space (antennas) as well as frequency (two sub-carriers) can be expressed as

$$\mathbf{y} = \begin{bmatrix} y_{11} & y_{12} \\ y_{21} & y_{22} \\ \vdots & \vdots \\ y_{N_r1} & y_{N_r2} \end{bmatrix} \ . \tag{2.23}$$

The noise matrix is similarly defined as

$$\mathbf{n} = \begin{bmatrix} n_{11} & n_{12} \\ n_{21} & n_{22} \\ \vdots & \vdots \\ n_{N_r1} & n_{N_r2} \end{bmatrix} \ , \tag{2.24}$$

and channel matrix with dimension (N_r, N_t) is defined as

$$\mathbf{H} = \begin{bmatrix} h_{11} & h_{12} \\ h_{21} & h_{22} \\ \vdots & \vdots \\ h_{N_r1} & h_{N_r2} \end{bmatrix} \ . \tag{2.25}$$

For i^{th} receive antenna, the signal model can be expressed as

$$\begin{bmatrix} y_{i1} \\ y_{i2} \end{bmatrix} = \begin{bmatrix} s_1 & s_2 \\ -s_2^* & s_1^* \end{bmatrix} \cdot \begin{bmatrix} h_{i1} \\ h_{i2} \end{bmatrix} + \begin{bmatrix} n_{i1} \\ n_{i2} \end{bmatrix} \quad . \tag{2.26}$$

Equivalently, the signal can be given as a function of an equivalent orthogonal channel matrix.

$$\begin{bmatrix} y_{i1} \\ y_{i2}^* \end{bmatrix} = \begin{bmatrix} h_{i1} & h_{i2} \\ h_{i2}^* & -h_{i1}^* \end{bmatrix} \cdot \begin{bmatrix} s_1 \\ s_2 \end{bmatrix} + \begin{bmatrix} n_{i1} \\ n_{i2}^* \end{bmatrix} \quad . \tag{2.27}$$

Multiply the (Equation 2.27) by the Hermitian transpose of the equivalent orthogonal channel, and the estimated signal is recovered as

$$\begin{bmatrix} \widehat{s_1} \\ \widehat{s_2} \end{bmatrix} = \begin{bmatrix} h_{i1}^* & h_{i2} \\ h_{i2}^* & -h_{i1} \end{bmatrix} \cdot \begin{bmatrix} y_{i1} \\ y_{i2}^* \end{bmatrix} = (|h_{i1}|^2 + |h_{i2}|^2) \cdot \begin{bmatrix} s_1 \\ s_2 \end{bmatrix} + \begin{bmatrix} \widetilde{n_{i1}} \\ \widetilde{n_{i2}^*} \end{bmatrix} \quad . \tag{2.28}$$

If the receiver only has one branch, the signal can be obtained by a straightforward scaling. Otherwise, the signals from different receive branches are coherently added with the MRC principle. Through this processing, the Alamouti scheme can achieve a diversity order of $2N_r$.

2.4.1.2 CLTD

In cases where instantaneous downlink channel information can be made available to the Node-B via uplink signalling, TxAA presents the possibility to exploit the array gain also at the transmitter side [Lo99]. In 3GPP terminology, the TxAA is also called CLTD [3GPP00a]. The equivalent channel on the k^{th} subcarrier with CLTD is illustrated in Figure 2.9.

At the eNode-B, the k^{th} subcarrier symbol $s(k)$ is weighted by the beamforming vector $\mathbf{w}(k) = [w_1(k), w_2(k), ..., w_{N_t}(k)]^T$ before transmission. The UE is assumed to have full channel information with ideal channel estimation in this thesis. After processing with the combining vector $\mathbf{z}(k) = [z_1(k), z_2(k), ..., z_{N_r}(k)]^T$, the combined signal at subcarrier k can be expressed as

$$y(k) = \mathbf{z}^H(k)\{\mathbf{H}(k)\mathbf{w}(k)s(k) + \mathbf{n}(k)\} \quad , \tag{2.29}$$

where $1 \leq k \leq N_c$, and $\mathbf{n}(k)$ is the N_r-dimensional noise column vector.

We assume $||\mathbf{w}(k)|| = 1$, where $||(.)||$ means the 2-norm of $(.)$, to maintain the overall power constraint. Without loss of generality we can fix $||\mathbf{z}(k)|| = 1$. Then, the received combined SNR for subcarrier k can be written as

$$\gamma(k) = \frac{\varepsilon_s |\mathbf{z}^H(k)\mathbf{H}(k)\mathbf{w}(k)|}{N_0} \quad . \tag{2.30}$$

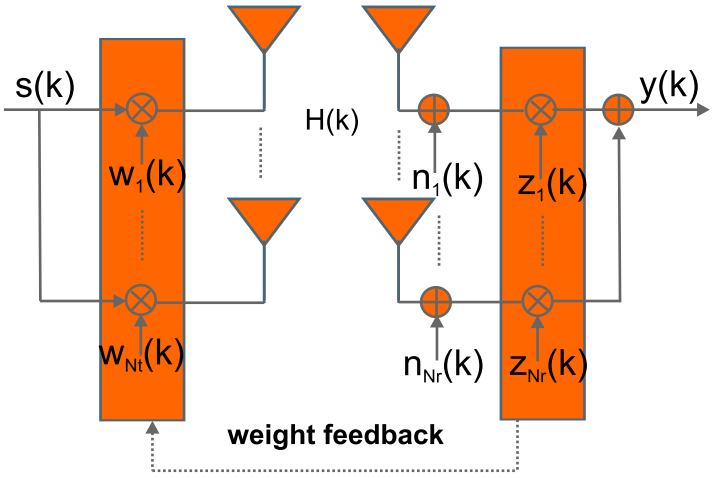

Figure 2.9: Illustration of Closed Loop Transmit Diversity on k^{th} subcarrier.

The optimum weight $\widetilde{\mathbf{w}}(k)$ to maximize the received SNR at the receiver equals the eigenvector corresponding to the largest eigenvalue of $\mathbf{H}^H(k)\mathbf{H}(k)$ [Lo99]. Depending on how much CSI is available, the eNode-B may choose a different weight $\hat{\mathbf{w}}(k)$ due to quantization, grouping, delay, and errors. These imperfections will be further discussed in Chapter 4. Under the unit norm constraint on $\mathbf{z}(k)$, it can be shown that the SNR is maximized by using MRC at the receiver

$$\mathbf{z}(k) = \frac{\mathbf{H}(k)\hat{\mathbf{w}}(k)}{||\mathbf{H}(k)\hat{\mathbf{w}}(k)||} \quad . \tag{2.31}$$

2.4.2 Spatial Multiplexing MIMO

Inspired by the information theoretical work of [Tela95], a number of spatial multiplexing MIMO schemes are proposed [Fosc96], [Woln98], [Zels04], [Chun01] and [Moto06]. The fundamental diagonally layered space-time architecture from Foschini [Fosc96] is among the first proposals, now known as *diagonal* BLAST or D-BLAST. The D-BLAST is an elegant diagonally layered coding structure in which code blocks are dispersed across diagonals in space and time. This structure, however, imposed quite high complexity in real implementation. Thus a simplified version of BLAST known as *Vertical* BLAST or V-BLAST is proposed [Woln98]. The V-BLAST we consider is with equal power allocation across transmit antennas with MMSE receiver. When V-BLAST is to be combined with channel coding, Li etc. [Li00] compared three possible options, namely Vertical coding, Horizontal coding and Vertical-and-Horizontal coding. Following the terminology in [Zels04], we denote the combination of Vertical channel coding with V-BLAST as JC, and the combination of Horizontal channel coding with V-BLAST as per Antenna Coding (PAC). If PAC is further combined with per antenna rate control,

it is called PARC [Chun01]. In this thesis we consider JC and PARC when no precoding is used. Once PARC is further employed with precoding, the scheme called D-TxAA [Moto06] is considered.

2.4.2.1 JC

As illustrated in Figure 2.10 for Joint coding (JC), the information bits are coded together and then converted into N_t parallel streams of which each data stream is modulated with same modulation order and mapped on to the transmit antennas. After propagate through the wireless channel, the receiver will demodulate the data separately before gathering all bits and performing MMSE detection on each subcarrier. For k^{th} subcarrier, the signal model can be seen as

$$\mathbf{y}(k) = \mathbf{H}(k)\mathbf{s}(k) + \mathbf{n}(k) \ , \tag{2.32}$$

where

$$\mathbf{s}(k) = [s_1(k) \quad s_2(k) \quad ... \quad s_{N_t}(k)]^T \ . \tag{2.33}$$

To recover the signal, the straightforward approach is to do ZF nulling with the *pseudo-inverse* of $\mathbf{H}(k)$ (denote as $\mathbf{H}(k)^+$) [Fosc96]. Thus the estimated signal can be shown as

$$\begin{aligned} \widehat{\mathbf{s}}(k) &= \mathbf{H}(k)^+\mathbf{y}(k) = (\mathbf{H}(k)^H\mathbf{H}(k))^{-1}\mathbf{H}(k)^H\mathbf{y}(k) \\ &= \mathbf{s}(k) + (\mathbf{H}(k)^H\mathbf{H}(k))^{-1}\mathbf{H}(k)^H\mathbf{n}(k) \ . \end{aligned} \tag{2.34}$$

Observing the Equation 2.34, the ZF receiver suffers from noise enhancement. To encounter that, the Minimum Mean Square Error (MMSE) receiver is a more popular solution for spatial multiplexing MIMO detection [Zels04]. The receiver signal can be recovered by multiplex with

$$\mathbf{W}(k) = (\alpha\mathbf{I}_{N_t} + \mathbf{H}(k)^H\mathbf{H}(k))^{-1}\mathbf{H}(k)^H \ , \tag{2.35}$$

where $\alpha = N_t\sigma_n^2/P_t$. As shown, the MMSE receiver can trade off interference stream nulling for noise enhancement reduction. Thus it is considered for all spatial multiplexing schemes in this thesis.

The advantage of the JC is the simplicity in processing and the low CQI requirement since the same MCS is employed on both streams. In some 3GPP contributions, JC is also called single-codeword SDM [Qual06a]. JC is not suitable to support advanced nonlinear Successive Interference Cancellation (SIC) receiver in MMSE detection stage. With SIC, different streams which are coded together will demonstrate different channel quality. But the fact that turbo coder dislikes variations within a code block, will deteriorate the turbo decoder performance [Zels04].

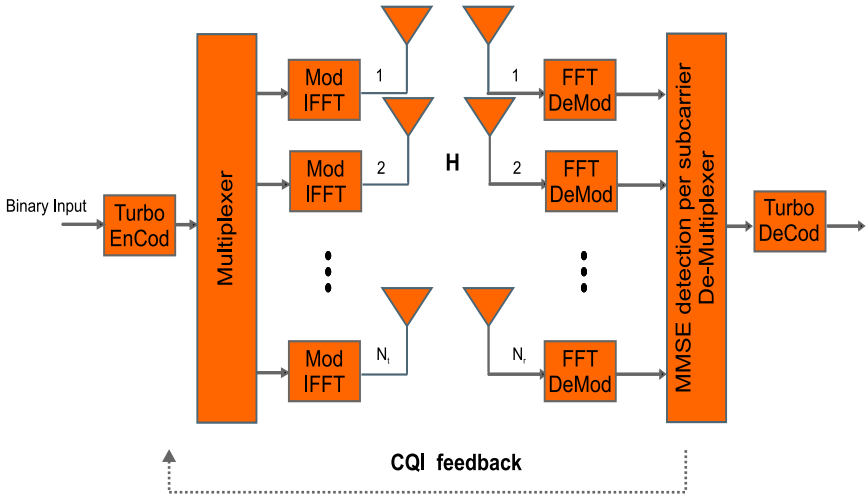

Figure 2.10: Illustration of Joint Coding with MMSE receiver.

2.4.3 PARC

Per Antenna Coding and Rate Control (PARC) refers to the case that the MCS can be adapted separately on each spatial stream [Chun01]. For the uncorrelated cases, the channel quality is usually different on different streams. From an information theory point of view, PARC is more efficient than JC since it can allocate the data rate separately for each spatial stream. As shown in Figure 2.11, compared to the JC, the PAC multiplexes the information bits into several streams (may have different data length) and code them separately.

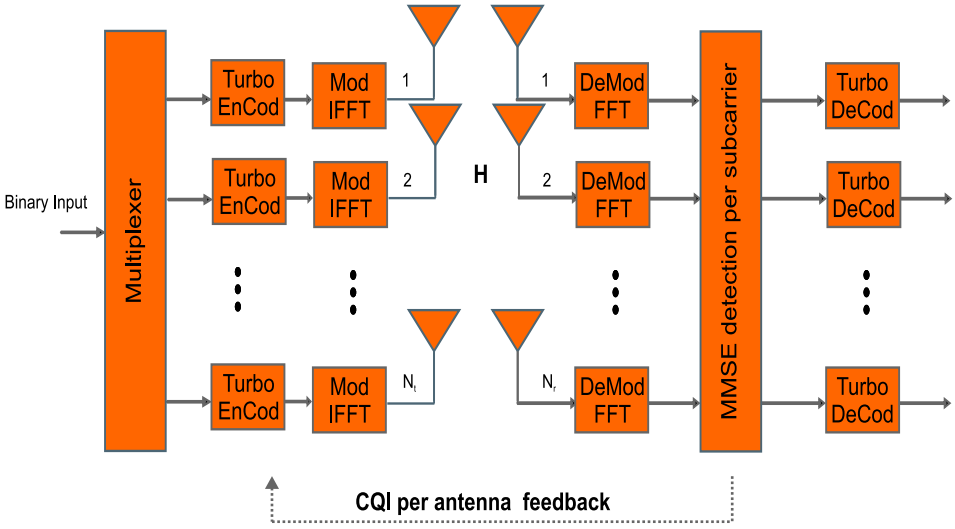

Figure 2.11: Illustration of PARC with MMSE receiver.

With separate coding for each stream, PARC can also potentially be equipped with coding aided SIC (PARC-SIC) which offers better performance since the interference from the other stream could be cancelled [Qual05]. The gain is at the cost of the complexity and delay. Moreover, the SIC will suffer from error propagation. The PARC is also referred as multiple codeword SDM [Qual06a].

2.4.4 D-TxAA

It is known that for the TxAA case, the antenna weights are selected to maximize the SNR at the UE. The weights are usually chosen to be the first eigenvector (corresponding to maximum eigenvalue), and thus maximize the link quality. A natural extension of TxAA is referred to as (D-TxAA) [Moto06]. For this case, two separate data streams are transmitted on both eigenmodes of the MIMO channel, *i.e.* , to maximize the total throughput of the channel. The D-TxAA can also be called precoded PARC or equal power eigenmode transmission.

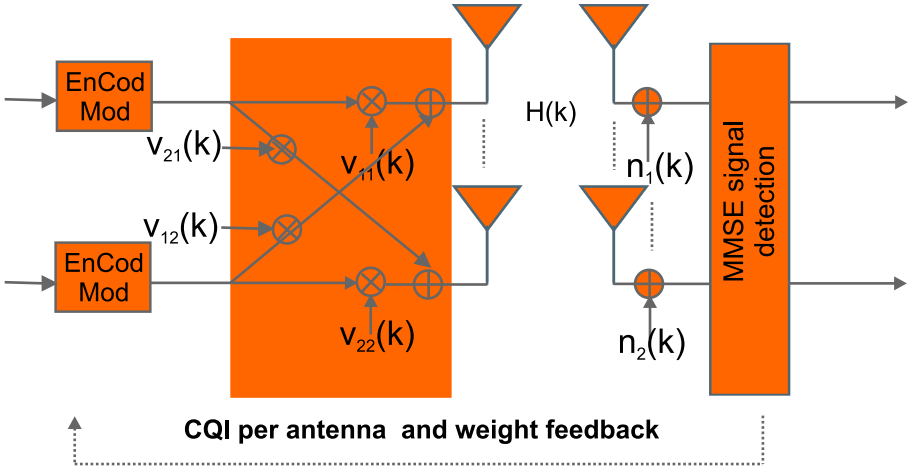

Figure 2.12: Illustration of D-TxAA with MMSE receiver on the k^{th} subcarrier.

Following the eigenvalue analysis in Subsection 2.2.1, the transmit and receive eigen filter $\mathbf{V}$ and $\mathbf{U}$ can be found from the SVD computation of channel matrix. Ideally the signal will be decomposed into several data pipes without any interference. However, similar to the TxAA, D-TxAA will also suffer from imperfections from non-ideal CSI. The eNode-B may choose a non-ideal weight matrix $\widehat{\mathbf{V}}$ due to quantization, grouping, delay, error etc. Thus the effective channel matrix with non-ideal weighting will be given as

$$\widehat{\mathbf{H}} = \mathbf{H}\widehat{\mathbf{V}} \ . \tag{2.36}$$

Under the unit norm constraint on receiver filter, the MMSE solution for the

receive weight matrix $\widehat{\mathbf{U}}$ will be given as

$$\widehat{\mathbf{U}} = (\alpha\mathbf{I} + \widehat{\mathbf{H}}^H\widehat{\mathbf{H}})^{-1}\widehat{\mathbf{H}}^H \quad . \tag{2.37}$$

The weight matrix feedback for D-TxAA will not involve higher feedback compared to TxAA due to its unitary property. That is, knowledge of one of the eigenvectors will completely specify the direction of the second eigenvector [Paut01]. The following equations represent this property mathematically. Because the V matrix is unitary, it has a structure that allows it to be written as

$$\mathbf{V} = \begin{bmatrix} v_{11} & v_{12} \\ v_{21} & v_{22} \end{bmatrix} \Rightarrow \begin{bmatrix} A & \sqrt{1-A^2} \\ \sqrt{1-A^2}\cdot e^{j\Delta\theta} & -A\cdot e^{j\Delta\theta} \end{bmatrix} \quad , \tag{2.38}$$

where

$$A = |v_{11}| \quad , \tag{2.39}$$

$$\Delta\theta = phase(v_{21}) - phase(v_{11}) \quad . \tag{2.40}$$

Note that the solution is not unique, phase shift on both eigenvectors will still keep two eigenvectors orthogonal.

2.5 Summary

In this chapter the necessary background information for reading this thesis is presented. More specifically, a basic understanding of the MIMO-OFDM technology which is essential for the LTE systems is presented. We firstly introduced the main principles of MIMO, in which its large capacity potential are addressed. The concept of parallel sub-channeling was introduced by mean of eigen-analysis. Together with that the MIMO gain mechanisms and the MIMO categorizations are discussed with examples.

Moreover, to gain insight into the MIMO-OFDM systems, we formulated a unified framework of MIMO-OFDM based on antenna elements and sub-carrier equivalence concept from Molisch etc. The formulation is performed by extending the linear dispersion code (LDC) from Hassibi to frequency domain as well. As this framework covers most of the MIMO-OFDM schemes, it is found to be too complex for practical usage. As a result, we consider a simplified version of MIMO-OFDM framework with a detached frequency and space-time processing which is able to achieve most of the potentials with a much reduced complexity. This also serves as the guideline for the selection of the MIMO-OFDM schemes for further evaluation.

At last, the MIMO schemes to be used throughout this thesis are introduced in details, and the different complexity and feedback requirements for different

schemes are discussed. Now we are ready to continue with the link-level and the system-level study of MIMO for LTE systems in later chapters.

Chapter 3

Baseline Link-Level LTE Evaluation

3.1 Introduction

To define common grounds for benchmarking performance and complexity of different advanced physical layer enhancements, a baseline downlink parameter set for the UTRA LTE system was decided and described in [3GPP06a]. Using these physical layer parameters as a starting point, a detailed link-level evaluation of LTE downlink air interface has been carried out in this study. Important LTE features such as *link adaptation* (LA) based on *adaptive modulation and coding* (AMC) and *Hybrid ARQ* (HARQ) have been included. Since multiple antennas at both transmitter and receiver ends are envisioned for LTE, we have investigated the potential benefit of some of the most popular antenna schemes, namely SISO, SIMO, SFC and JC as introduced in the previous chapter.

The LTE system parameters are first introduced in Section 3.2. After that, the details of the link-level simulator developed are discussed in Section 3.3. The SINR distribution for various MIMO schemes are discussed in Section 3.4 both for the purpose of verification and performance analysis. Further, the link-level results are summarized in Section 3.5. More specifically, for various MIMO schemes, the spectral efficiency performance with long-term and short-term LA adaptation are presented and compared. To support LA, the CQI related issues are discussed as well. Moreover, the link-level throughput is mapped to corresponding single-user cell spectral efficiency using available *Geometry factor* (G-factor) [1] distributions for the macro and microcell scenarios with LTE assumptions.

[1]The G-factor is the ratio of the total received wideband BS power and othercell/noise interference at the UE. It is averaged over short-term fading, but not shadowing.

3.2 LTE System Parameters

The main system parameters of LTE downlink evaluation are listed in Table 3.1 [3GPP06a].

Table 3.1: Parameters for downlink transmission scheme

Transmission BW	1.25 MHz	2.5 MHz	5 MHz	10 MHz	15 MHz	20 MHz
Sub-frame duration	0.5 ms					
Sub-carrier spacing	15 kHz					
Sampling frequency	1.92	3.84	7.68	15.36	23.04	30.72
FFT size	128	256	512	1024	1536	2048
Number of sub-carriers [a]	76	151	301	601	901	1201
No. of OFDM symbols per sub-frame (short/long CP)	6/7					
Short CP [b] (μs/samples)	(4.69/9), (5.21/10)	(4.69/18) (5.21/20)	(4.69/36), (5.21/40)	(4.69/72), (5.21/80)	(4.69/108), (5.21/120)	(4.69/144), (5.21/160)
Long CP (μs/samples)	(16.67/32)	(16.67/64)	(16.67/128)	(16.67/256)	(16.67/384)	(16.67/512)
Channel code	3GPP Rel. 6 compliant Turbo code with basic rate 1/3					
Rate Matching	3GPP Rel. 6 compliant					

[a] Includes DC sub-carrier which contains no data.
[b] The first row is for the first 6 symbols, and the second row is for the last symbol.

For the link adaptation purpose, we consider the MCS as summarized in Table 3.2. From that we can predict that with variable-rate turbo coding up to 4/5 code rate, and up to 64QAM modulation, the LTE system with the maximum 20 MHz bandwidth supports peak data rates from 5.6 Mbps up to 80.6 Mbps for single

stream scenario. For the dual stream MIMO like JC, the peak data rate can vary from 11.2 Mbps up to 161.2 Mbps. Obviously dual stream schemes are necessary to reach the ambitious LTE target of 100 Mbps peak data rate. With a realistic 20-30% estimate of overhead due to signalling and pilot channels, at least dual stream with 16QAM and no coding will be required.

Table 3.2: LTE bandwidth efficiencies in a 20 MHz bandwidth for example

MCS	Single Stream Data Rate	Dual Stream Data Rate
QPSK 1/6	5.6Mbps	11.2Mbps
QPSK 1/3	11.2Mbps	22.4Mbps
QPSK 1/2	16.8Mbps	33.6Mbps
QPSK 2/3	22.4Mbps	44.8Mbps
16QAM 1/2	33.6Mbps	67.2Mbps
16QAM 2/3	44.8Mbps	89.6Mbps
16QAM 3/4	50.4Mbps	100.8Mbps
64QAM 1/2	50.4Mbps	100.8Mbps
64QAM 2/3	67.2Mbps	134.4Mbps
64QAM 4/5	80.6Mbps	161.2Mbps

*:The overhead due to signalling and pilot channels is not considered here.

3.3 Overview of Link-Level Simulator

Based on the LTE system parameters, a link-level simulator was constructed. It will be described in two parts, the link adaption/HARQ process part and the physical layer part. Among the practical implementation issues, we found the calculation of the soft information for turbo decoder need special clarification, and that is discussed in Appendix B. The validation of the simulator implementation is provided in Appendix C.

3.3.1 Link Adaptation and HARQ Process

The working process of LA and HARQ is shown in Figure 3.1. To allow for processing and propagation delays, the HARQ retransmission scheme is based on the stop and wait (SAW) principle with several independent HARQ processes

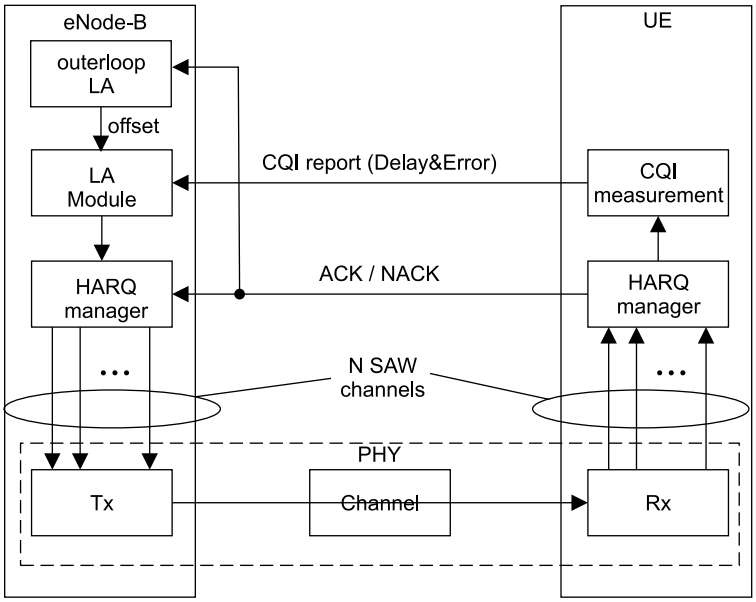

Figure 3.1: Diagram of the LA and HARQ process.

per user [Kold02]. Note that in this study we have only considered synchronous HARQ, and the transmission format (MCS and MIMO) remains the same between transmissions. The UE first feed back the measured CQI and ACK/NACK information to the eNode-B. Then LA module in eNode-B performs two tasks. Firstly, it will consult the HARQ manager module on whether the next transmission should be a new packet or a retransmission of a failed packet. Secondly, it will estimate the supportable throughput by using link to system mapping table based on the CQIs from the user.

The link to system mapping table adopted here is based on the Exponential Effective SIR Mapping (EESM) [Eric03] [Eric04a]. The motivation behind such a model is to avoid the generation of all BLER curvers for any geometry and channel conditions in the OFDM systems. Derivation of EESM is based on the Union-Chernoff bound for error probabilities. The basic idea is to map the current geometry and channel conditions (which will involve frequency selective fading for a multi-path channel, for example) to an effective SIR value that may then be used directly with the AWGN BLER curves to determine the appropriate block error rate. The effective SINR is defined as

$$\text{SINR}_{eff} = -\beta \cdot \ln(\frac{1}{N_u}\sum_{k=1}^{N_u} e^{-\frac{\gamma_k}{\beta}}) \ , \tag{3.1}$$

where N_u is the number of useful sub-carriers being considered, and γ_k is the SINR for the k^{th} OFDM sub-carrier. The β is a parameter that must be estimated from extensive link-level simulations for every MCS being considered, and it could be

taken as a parameter to describe the sensitivity of turbo decoder performance towards frequency selectivity. The general trend is that the higher the modulation order and code rate, the worse the decoder performance towards frequency selectivity. The EESM model will be further explained and validated in Appendix E.

Given one specific MCS i, the effective SINR can be calculated, and the BLER can be looked up from a AWGN channel BLER curve of this specific MCS. Then the throughput for i^{th} MCS can be predicted as

$$\mathrm{TP}_i = (1 - \mathrm{BLER}_i) \times \mathrm{TBS}_i \ , \tag{3.2}$$

where the TBS_i is the transport block size of a certain MCS i and the BLER_i is the BLER for a certain MCS i. The procedure is repeated for all MCS available, and the MCS gives best throughput, while maintaining the BLER target is chosen for transmission, as explained in Equation 3.3.

$$\mathrm{MCS\_SEL} = \arg \max_{i|\mathrm{BLER}_i < \mathrm{BLER}_{\mathrm{target}}} \{\mathrm{TP}_i\} \ . \tag{3.3}$$

After that, as shown in Figure 3.2, the MCS selection information (or potentially MIMO selection) from LA module is then fed into the rate matcher, modulation, and MIMO processing modules in physical layer process.

The system explained above can work with ideal CQI feedback. However, if the CQI is perturbed by measurement or quantization error, the LA module will make incorrect decisions. As a remedy mechanism, an *outer-loop link adaptation* (OLLA) is utilized as well, as shown in Figure 3.1. The main principle of OLLA is to stabilize the 1st transmission *Block Error Probability* (BLER) taking into account link adaptation errors due to incorrect CQI reports [Naka02] [Pokh06]. The adaptation algorithm uses a certain 1st transmission BLER target (20% is assumed here) and is implemented by adding an adaptive offset to the available CQI reports for the UE. The offset is updated by using ACK/NACKs from the first transmission based on actual transmissions and uses different up and down step-size in the SINR domain. In case of multi-stream MIMO, since there are separate ACK/NACKs for each spatial streams, the offset will be updated sequentially with each ACK/NACKs. In general, the OLLA algorithm is similar to the well-known outer loop power control algorithm for adjustment of SINR targets for dedicated WCDMA channels [Samp97].

3.3.2 Physical Layer Link Chain

The block diagram of the physical layer link chain used in the analysis of LTE downlink is shown in Figure 3.2. As shown, the left side is the eNode-B (transmitter), and the right side is the UE (receiver). The link adaptation module, as

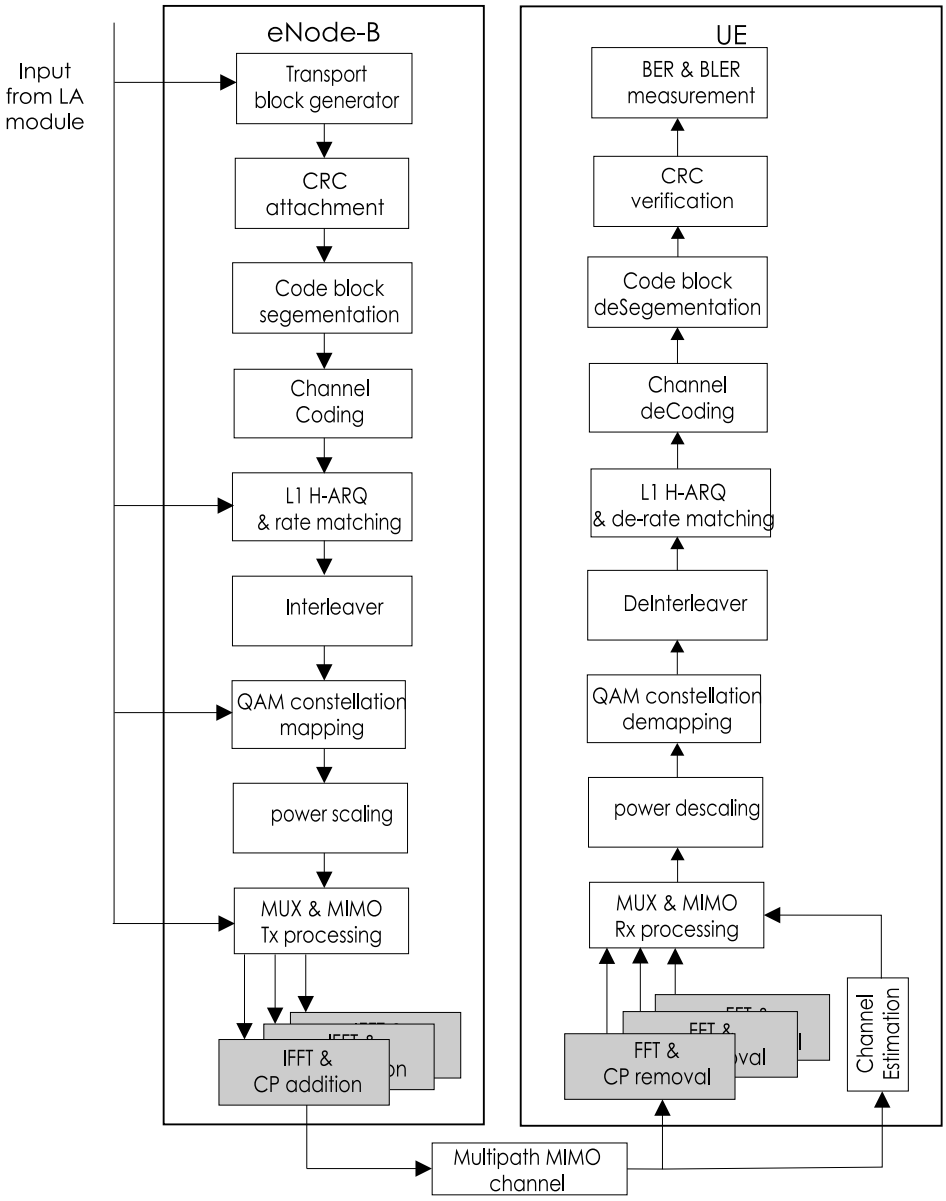

Figure 3.2: Diagram of the physical-layer link chain.

shown in Figure 3.1, selects a *transport format and resource combination* (TFRC) for transmission on the basis of CQI measurement from the UE. The TFRC decision is passed to the Transport Block Generator which generates a packet of the requested size. Obviously we assume that there is always data to transmit. It is followed by *cyclic redundancy check* (CRC) encoding. Then according to the packet size and the maximum code block size, the packet is divided into several blocks before being fed to the channel encoder. The UTRA Release 6 Turbo cod-

ing is used in this study. According to the code rate requirement, the output coded bits are punctured/repeated by the rate matcher (approximately from 1/6 to 1/1). The coded and interleaved bits are modulated, and for QAM modulation, a QAM remapping is performed [3GPP01]. The purpose is to put the systematic bits at more reliable constellation points as this can improve the decoder performance. The modulated symbols are space-time processed according to the selected MIMO scheme. For each spatial channel, an IFFT is applied, and the cyclic prefix is added. At receiver side, the UE basically performs the reverse operation. If the CRC decoder determines that the data packet is error free, an acknowledgement (ACK) is signalled back to the BS, otherwise, the soft bits remain in the UE buffer, and a negative acknowledgement (NACK) is signalled back. Upon reception of a NACK, the eNode-B performs fast L1 retransmission of the data packet. The MIMO multipath channel used is based on the implementation in [Schu01] from the I-METRA project [2]. The path loss, shadowing and other cell interference (modeled as AWGN) loss are modeled as the G-factor [Holm01]. Based on this AWGN assumption, the G-factor is equivalent to average SNR throughout this thesis.

3.4 SINR Distribution for MIMO Schemes

The SINR distribution for various MIMO schemes is revisited in this section. It is not only useful for verification of the MIMO implementation, but also for simple performance analysis. The discussion below covers both uncorrelated and correlated cases.

3.4.1 Uncorrelated Channel

The *cumulative density function* (cdf) for many single stream diversity MIMO schemes in uncorrelated Rayleigh channel is presented in [Jake94] as:

$$F(\gamma \leq \Gamma) = 1 - e^{-\frac{\Gamma}{\gamma_0}} \sum_{n=1}^{N} \frac{(\frac{\Gamma}{\gamma_0})^{n-1}}{(n-1)!} \ , \tag{3.4}$$

where γ is the instantaneous SINR, and N is the diversity order. As shown in [Wint94], for spatial multiplexing schemes with Zero Forcing (ZF) receiver, the end-to-end system is decoupled into a set of parallel SISO channels. The SINR on each stream is Chi-squared distributed with $2(N_r - N_t + 1)$ degree of freedom. The *probability density function* (pdf) of SINR on k^{th} stream is then given by:

$$p(\gamma_k) = \frac{N_t e^{-\frac{N_t \gamma_k}{\gamma_0}}}{\gamma_0 (N_r - N_t)!} (\frac{N_t \gamma_k}{\gamma_0})^{N_r - N_t} \ . \tag{3.5}$$

[2] http://www.ist-imetra.org/

3.4.2 Correlated Channel

It is well known that the antenna correlation has adverse effect on the performance of MIMO. The loss of performance for orthogonal space-time block codes (OSTBC) is discussed in [Jors04]. It is shown that the OSTBC schemes are robust against spatial correlation and experience a diversity advantage degradation only with singular correlation matrices. For spatial multiplexing schemes with ZF receiver in presence of transmit correlation, the pdf of SINR on k^{th} stream is given by [Gore02]:

$$p_{corr}(\gamma_k) = \frac{N_t \sigma_k^2 e^{-\frac{N_t \sigma_k^2 \gamma_k}{\gamma_0}}}{\gamma_0 (N_r - N_t)!} \left(\frac{N_t \sigma_k^2 \gamma_k}{\gamma_0}\right)^{N_r - N_t} \quad , \tag{3.6}$$

where R_{tx} is the transmit spatial correlation matrices as defined in Equation 2.14 in Chapter 2, and σ_k^2 equals to $[R_{tx}^{-1}]_{kk}$, which is defined as the k^{th} diagonal entry of R_{tx}^{-1}. Besides, the receiver antenna elements are assumed to be uncorrelated, *i.e.* , the R_{rx} is a diagonal matrix with all 1 on its diagonal. Equation 3.6 shows that the transmit correlation causes a degradation in effective SINR, best described as a mean SNR loss with the degradation on k^{th} stream accurately quantified by $[R_{tx}^{-1}]_{kk}$. As shown, spatial multiplexing schemes are much more vulnerable to correlation than OSTBC.

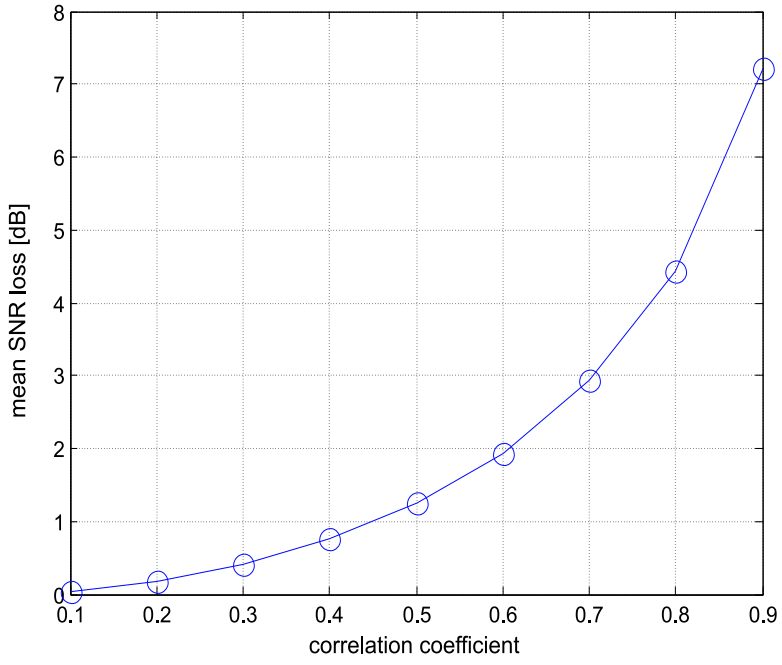

Figure 3.3: Mean gain loss of JC with ZF receiver against the level of correlation coefficients.

For illustration purposes, we use Zelst's double-coefficient spatial correlation

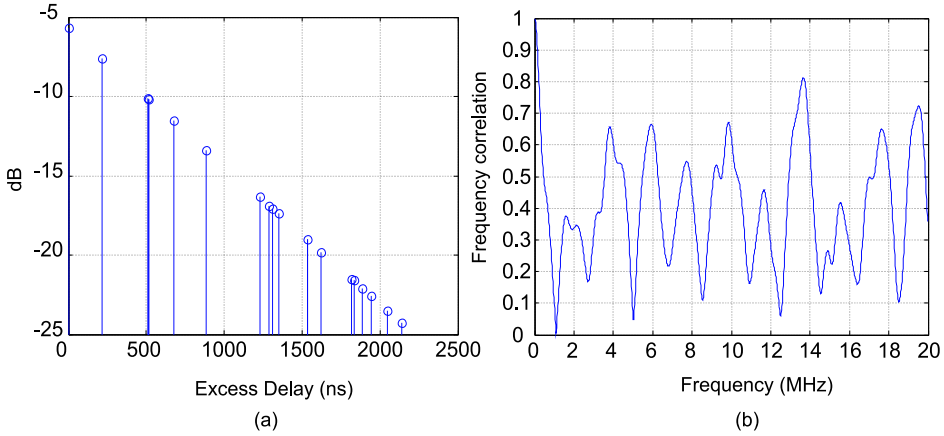

Figure 3.4: 20-ray Typical Urban channel (a) Power delay profile (b) frequency correlation over 10MHz

model [Zels04] to show the impact of correlation on the performance. The nice property of such a transmit correlation matrix as Equation 2.12 in Chapter 2 is that the inverse of it is rather simple [Kavc00],

$$R_t^{-1} = \frac{1}{1-r^2}\begin{bmatrix} 1 & -r & 0 & \dots & 0 \\ -r & 1+r^2 & -r & \ddots & \vdots \\ r^2 & -r & 1+r^2 & \ddots & 0 \\ \vdots & \ddots & \ddots & \ddots & -r \\ 0 & \dots & 0 & -r & 1+r^2 \end{bmatrix}. \tag{3.7}$$

With the assumptions above, the mean gain loss of 2x2 spatial multiplexing schemes with ZF receiver $[R_t^{-1}]_{kk}$, is plotted with a different level of correlation in Figure 3.3. It is observed that with a correlation of 0.3, the mean SNR loss is less than 0.5dB, and the loss is around 1.2dB for correlation of 0.5 and is increased to 3dB with correlation of 0.7dB. The loss will be further illustrated with spectral efficiency loss for JC in Subsection 3.5.3.

3.5 Performance evaluation

To analyze the baseline LTE performance, we choose the following simulation assumptions in Subsection 3.5.1 with reference on the Table 3.1 from [3GPP06a]. After that the spectral efficiency performance for long-term and short-term LA is presented and explained. Next, the CQI to support various LA strategies is analyzed, and the cell level spectral efficiency is estimated for different cell scenarios.

3.5.1 Simulation Assumptions

Table 3.3: Main Simulation Parameters

Parameter	Value
Carrier frequency	2 GHz
Transmission BW	10 MHz
OFDM PHY parameters	short CP 7 data sym/sub-frame
FFT size	1024
Number of useful subcarriers	600
Channel Profile	20-ray Typical Urban channel model ([3GPP05], Section 5.1)
Transmit antenna correlation	double-coefficient spatial correlation model [Zels04]
Receive antenna correlation	uncorrelated
MCS settings	QPSK: 1/6, 1/3, 1/2, 2/3 16QAM: 1/2 , 2/3, 3/4 64QAM: 2/3, 4/5
Channel estimation	Ideal
Antenna schemes	SISO, SIMO, SFC, JC
Speed	3 km/h
HARQ SAW channels	6
HARQ Max No. of transmission	4

For the performance evaluation in this thesis, we use 10MHz system bandwidth as recommended by [3GPP06a]. The channel profile we choose is the 20-ray Typical Urban channel [3GPP05]. The PDP and its corresponding frequency correlation property is presented in Figure 3.4. As shown the chosen channel profile demonstrates a reasonably low frequency correlation up to 20MHz. The main parameters are summarized in Table 3.3. The signalling or pilot overhead is not considered. No errors are assumed in the transmission of CQI and ACK/NACK messages. Further, the channel estimation is assumed to be ideal throughout this thesis. Since the detailed MIMO channel with antenna correlation is not available

in 3GPP when this study is carried out, we choose the simple double-coefficient spatial correlation model from [Zels04], as introduced in Subsection 2.2.1, as the model for correlated cases.

3.5.2 Discussion of the Long-Term and Short-Term LA

Considering the LA approach with long-term channel statistics, the MCS adaptation is based on average received SNR (i.e., G-factor). This kind of LA strategy is also called long-term LA. Practically, this type of long-term LA is more suitable for high speed users when the instantaneous channel information is not obtainable. On the contrary, if the instantaneous channel quality is available in eNode-B, LA can perform fast link adaptation per TTI. This kind of LA strategy is also called short-term LA. Practically, this type of LA is intended for low mobility users when the instantaneous channel information is feasible. Both potential LA strategies are discussed in this subsection and the corresponding performance results will be presented in the next two subsections.

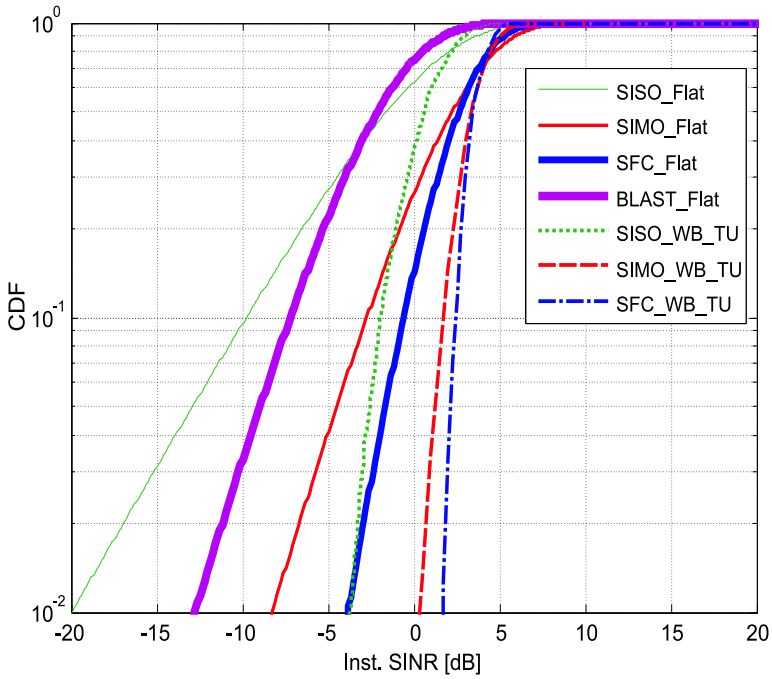

Figure 3.5: CDF of measured SINR at a G-factor of 0dB. The four solid line (Flat) curves represent the statistics of SINR measured on a Flat-Rayleigh channel profile. The three dashed line (WB_TU) curves represent average SINR measured over 10MHz bandwidth in Typical Urban channel profile.

To see how different the LA strategy behaves, the SINR dynamics should be

analyzed. As shown in Figure 3.5, for the cases of flat rayleigh channel, the dynamics range of SINR for a certain G-factor is up to 25dB for SISO. However, the dynamic range of the measured average whole bandwidth SINR for selected cases is very limited for a single user with full bandwidth available. This is due to the large bandwidth (10MHz) and the very frequency selective TU channel profile. For example, the SINR dynamic range is only 3dB for SFC wholeband case. Intuitively speaking, when the SINR dynamics is high, the MCS adaptation should be made fast enough to track that, otherwise the performance will degrade. However, although the short-term LA is always more efficient than the long-term LA, the gain is much smaller when the SINR dynamics is low, *i.e.* , the selection of modulation and coding is almost constant for given G-factor. In those cases, the long-term LA is more efficient since the required CQI feedback is much lower than the short-term LA.

3.5.3 LA with Long-Term Channel Information

This subsection presents the long-term LA results. The spectral efficiency, defined as useful throughput achieved over bandwidth, of different modulation and coding sets with or without HARQ is plotted versus the G-factor in Figure 3.6 for the SIMO case. The individual curves have the characteristic steep slope without HARQ. The combining gain of HARQ can be seen in the smoothening out of the spectral efficiency curve. This results from the gradual degradation of the BLER when HARQ is present. This HARQ property enables easier implementation of AMC by reducing the number of required MCS levels and the sensitivity to measurement error and traffic fluctuations.

Figure 3.7 shows the LA curve for SFC scheme with HARQ, including the detailed curves of different modulation and coding sets. The IR combining scheme is preferred over CC scheme at code rates above 0.5. The usage of a very low code rate 1/6 (achieved from rate matching) and HARQ greatly enhances the cell edge coverage. Since the effective code rate is reduced after each IR retransmission, the IR curves have a distinct stair-case like pattern. The property of the HARQ will be further explained in Figure C.3 of Appendix C.

The effect of transmit antenna correlation on the spectral efficiency performance of JC and SFC is shown in Figure 3.8 and Figure 3.9, respectively. As expected, the loss due to correlation for JC is significant, while SFC is quite insensitive to correlation. The observation is consistent with the conclusions from [Gore02] for spatial multiplexing schemes and [Jors04] for SFC. Further, due to the interaction of MCS and correlation loss, one interesting observation about JC is that the spectral efficiency loss due to correlation varies significantly for different MCS. The general trend is that the higher modulation order and/or code rate, the more severe the spectral efficiency loss. For example with a correlation coeffi-

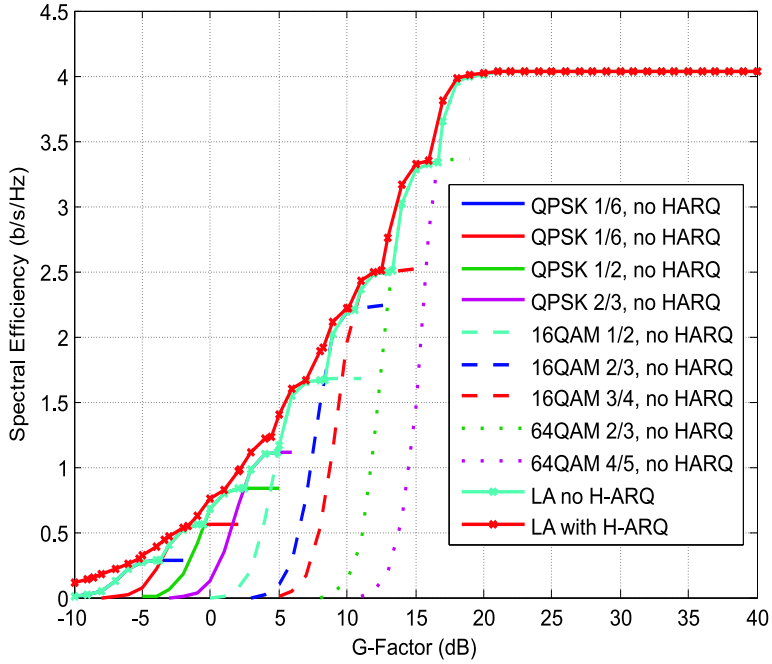

Figure 3.6: Spectral Efficiency of 1x2 SIMO with and without HARQ.

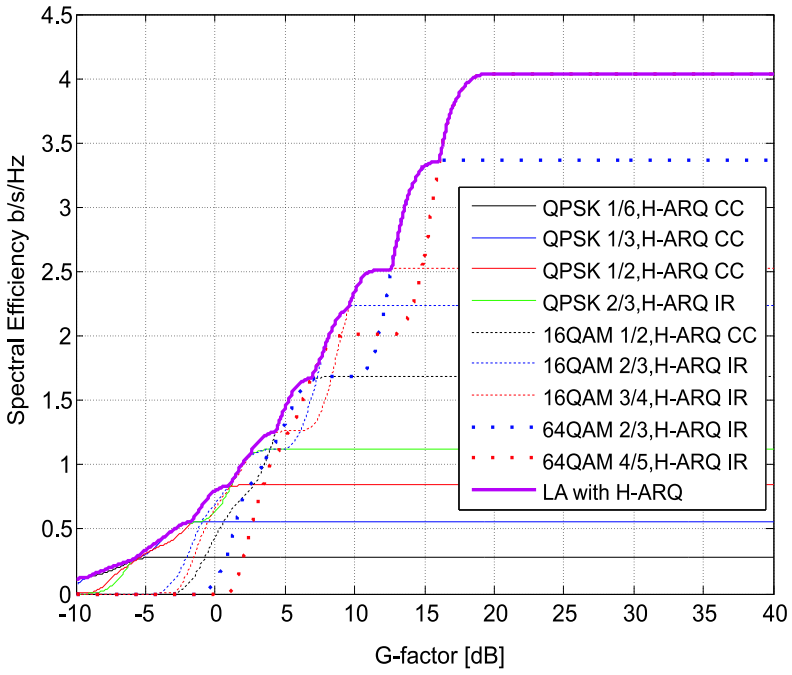

Figure 3.7: Spectral Efficiency of 2x2 SFC with different MCS.

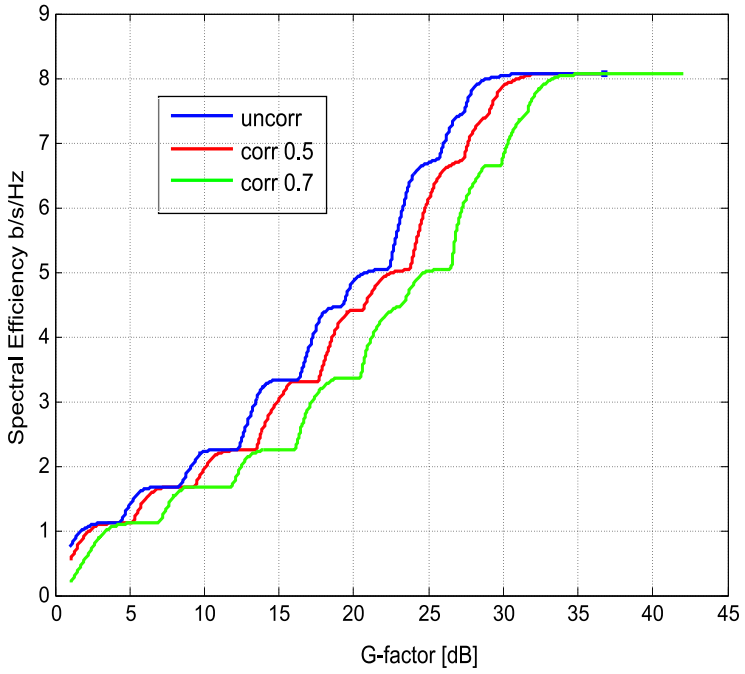

Figure 3.8: Spectral Efficiency of 2x2 JC scheme with or without antenna correlation.

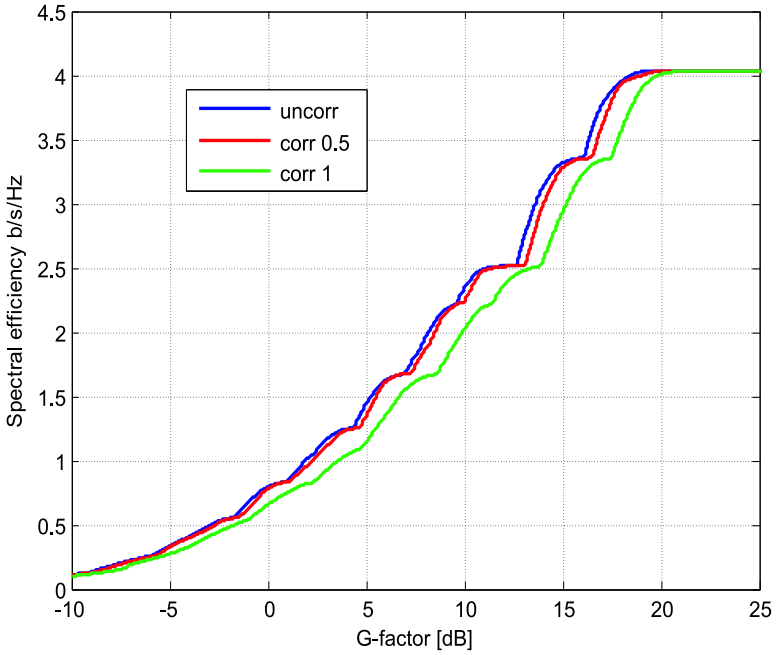

Figure 3.9: Spectral Efficiency of 2x2 SFC scheme with or without antenna correlation.

cient of 0.5, the average SNR loss is around 1.2dB from the simplified analysis in Figure 3.3. Considering spectral efficiency, around 2-3dB loss is seen for 64QAM cases, while only 0.5dB loss is seen for the QPSK 1/2 case, and around 1dB loss for QPSK 1/3 is seen. As for SFC, the transmit antenna correlation introduces transmit diversity loss only. With the presence of receiver diversity for SFC, the loss due to transmit diversity loss is smaller. Up to a correlation of 0.5, there is only a marginal loss for SFC. With a fully correlated scenario, the spectral efficiency of SFC is reduced to the SIMO performance.

3.5.4 LA with Short-Term Channel Information

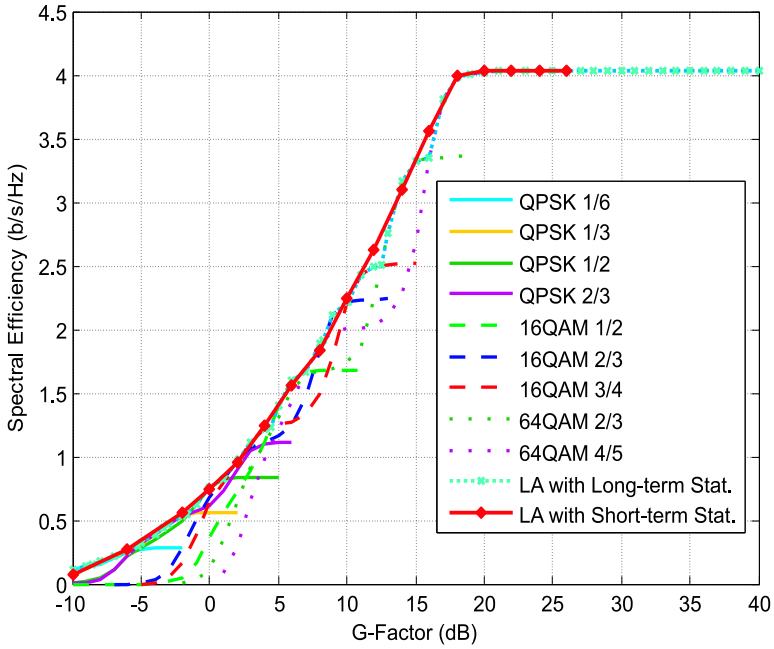

Figure 3.10: Comparison of short-term LA and long-term LA for 1x2 SIMO.

For the whole bandwidth transmission performed here, as discussed in Subsection 3.5.2, the spectral efficiency results will not differ much from the LA results with long-term channel information. The performance comparison of the two LAs is shown in Figure 3.10 for SIMO. The performance curve of short-term LA smooth the spectral efficiency curve of long-term LA further and offers some gain especially in the transition range of different MCS. But in the cases where the bandwidth is small or the channel is frequency flat, the LA with short-term channel information will be significantly higher than the LA with long-term channel information.

In Figure 3.11, the spectral efficiency curves with short-term LA for different

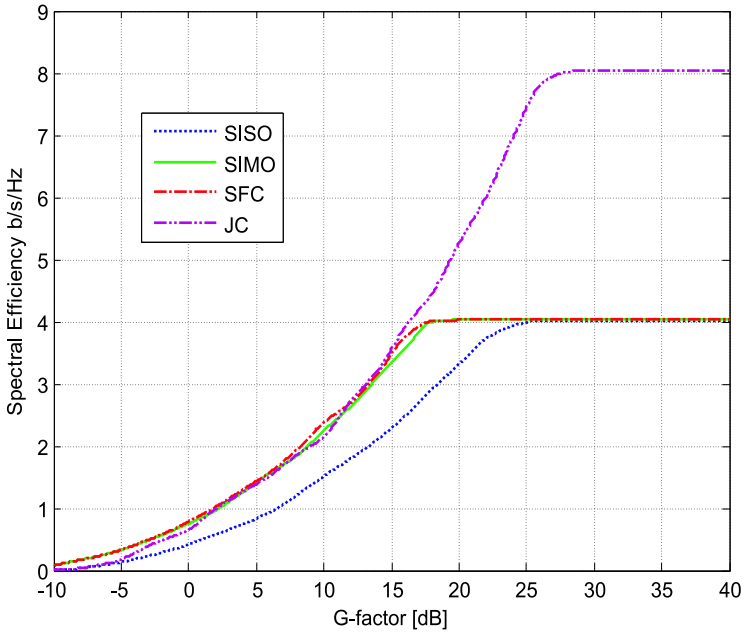

Figure 3.11: Spectral Efficiency for different MIMO schemes with short-term LA.

antenna configurations considered are shown for comparison. With two receive antennas, the SIMO scheme shows a very rapid rise over SISO of throughput with G-factor due to the 3dB array gain and diversity gain. The additional gain from increasing the diversity order from 2 to 4 when SFC is introduced is, as we can expect, of less significance. As for dual stream MIMO scheme JC, the system shows a clear gain when the G-factor is above 12 dB. This is consistent with the intuitive observation that only high G-factors allow us to have sufficiently high SINRs on both streams to effectively boost the throughput. In comparison, the single stream cases are limited by 64QAM modulation. The spectral efficiency of JC and SFC is quite similar in low G-factor range due to the ideal channel estimation assumption. The spectral efficiency of JC will deteriorate more than SFC when real channel estimation is used since it is more sensitive to channel estimation errors. Thus the adaptive MIMO case is also considered for the 2x2 configuration, denoted as *adapMIMO*, where the SFC is taken as a backup for JC in low G-factor range. The spectral efficiency curve for this case is obtained by combining the SFC curve in low G-factor range ($<$10dB) and JC curve in high G-factor range ($>$10dB). As it will be explained later in Chapter 5, this type of MIMO adaptation is also called slow adaptive MIMO.

3.5.5 CQI Analysis

The quality of CQI reports determines the obtainable LA performance, and therefore, we further consider the CQI issues in this subsection. To support the link adaptation, the CQI needs to be sent back from the UE to the eNode-B within a certain time interval. For LA with long-term channel information, the CQI is measured for a long period, whereas for the LA with short-term channel information, the CQI is measured every TTI. In our study, the CQI is simply modeled as the linear averaged SINR over a certain number of sub-carriers as

$$\text{CQI} = \sum_{i=1}^{M} \gamma_i / M \ , \tag{3.8}$$

where the γ_i is the SINR on sub-carrier i, and M is the number of the sub-carriers considered. The CQI is usually perturbed by measurement and quantization errors.

For frequency selective channel, if we support Frequency Domain Link Adaptation (FDLA) [Kold05], the CQI should be reported per frequency chunks, *i.e.* , a number of neighboring sub-carriers. However, even if we perform a whole-band transmission, CQI should contain sufficient information such that the LA in the transmitter can make a reasonable throughput prediction for each MCS and make an MCS selection for next transmission. To illustrate that we plot the spectral efficiency performance with different number of CQIs over frequency in Figure 3.12. As shown, for whole-band transmission in Typical Urban channel, there is no noticeable difference between using 600 CQIs or 24 CQIs (each over 25 sub-carriers) per TTI. Considering the coherence bandwidth of the channel, 24 CQIs are enough to reflect the frequency selectivity. And it is also observed that if only one linear averaged CQI is used, there is a significant loss when 16QAM start to be used where the one value CQI is not sufficient any more to reflect the frequency variation. The normal OLLA is running for this case as a remedy method, where same offset is used on CQI report for all MCS's effective SIR calculation. This is based on the assumption that the effect on performance from measurement error in average is the same for different MCS.

To keep the CQI feedback minimal, one way to solve the problem is to use one geometry averaged CQI, and make OLLA adjustment per MCS. The geometry averaged CQI is defined as

$$CQI = (\prod_{i=1}^{M} \gamma_i)^{1/M} = \exp(\frac{1}{M} \sum_{i=1}^{M} \ln \gamma_i) \ , \tag{3.9}$$

where the effect of frequency variation is better described. Besides, by making OLLA offset adjustment separately for each MCS, higher offsets will be given for higher MCS due to a higher sensitivity towards frequency selectivity. As shown

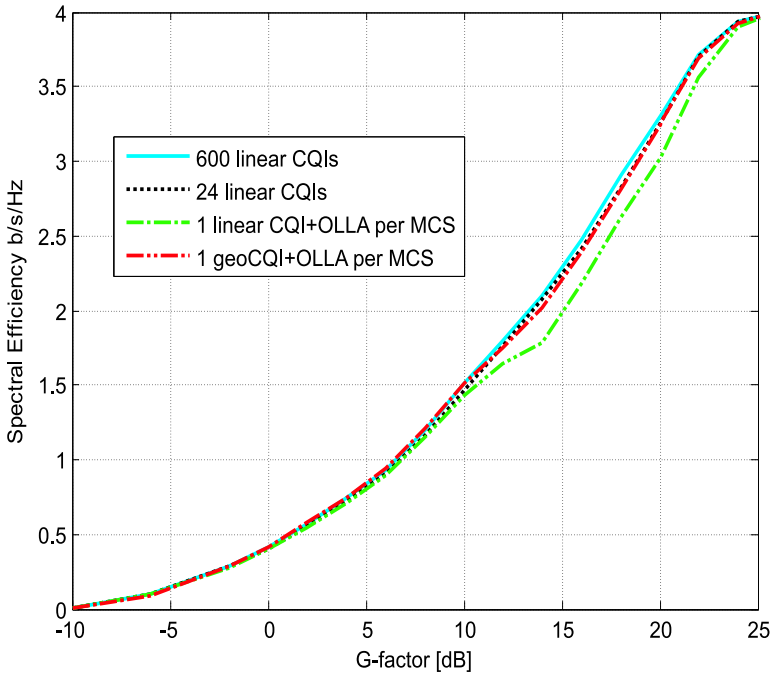

Figure 3.12: The effect of CQI on the spectral efficiency performance with short-term LA for SISO.

in Figure 3.12, the performance of the case with combination of 1 geometry CQI and OLLA per MCS is on top of the optimal performance. In this specific case, the generalized OLLA could be considered as a remedy for CQI inefficiency.

3.5.6 Single-User Cell Capacity

The G-factor distributions used for the macrocell outdoor and the microcell indoor/outdoor scenarios are shown in Figure 3.13 [Kova06]. The statistics is collected from the extensive system level simulation following the cell assumptions in [3GPP06a]. The single user spectral efficiency at cell level is evaluated by conditioning the G-factor dependent throughput with the probability of obtaining a given G-factor and integrating this over the whole G-factor range available in a certain cell scenario. Figure 3.14 shows a bar plot of the single user cell level spectral efficiency obtained for the various test cases considered. Considering uncorrelated antennas and the macrocell scenario, it is shown that the SIMO and SFC schemes can provide a gain in the order of 61% and 76% respectively over the SISO case. The *adapMIMO* does not provide much improvement over SFC in this case. This results from the limited dynamic range in the macrocell scenario, in which only 3% users have G-factor greater than 15 dB. Meanwhile, in microcell scenario the gain of *adapMIMO* over SISO is in the order of 80%, which is around 50% more than

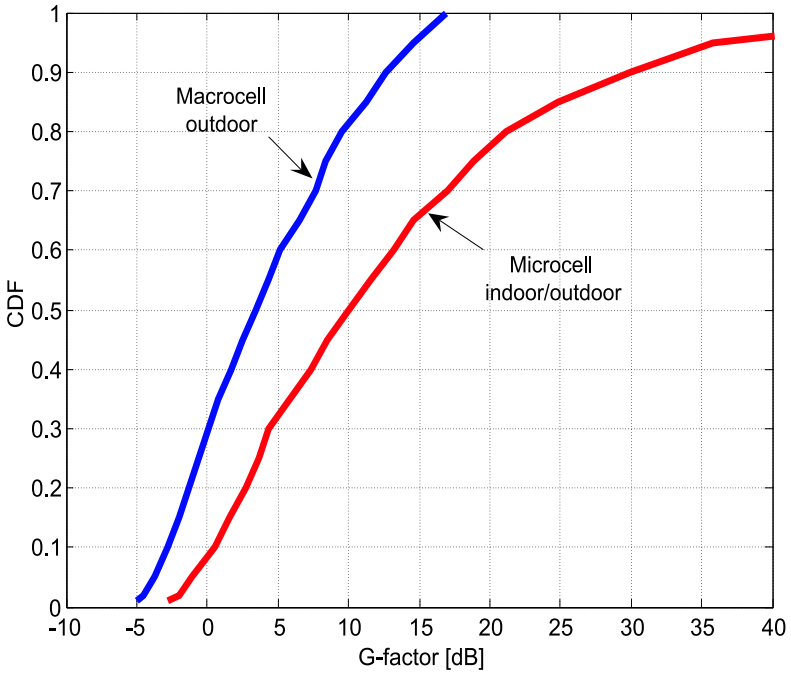

Figure 3.13: CDF of G-factor in macro and micro cell scenarios.

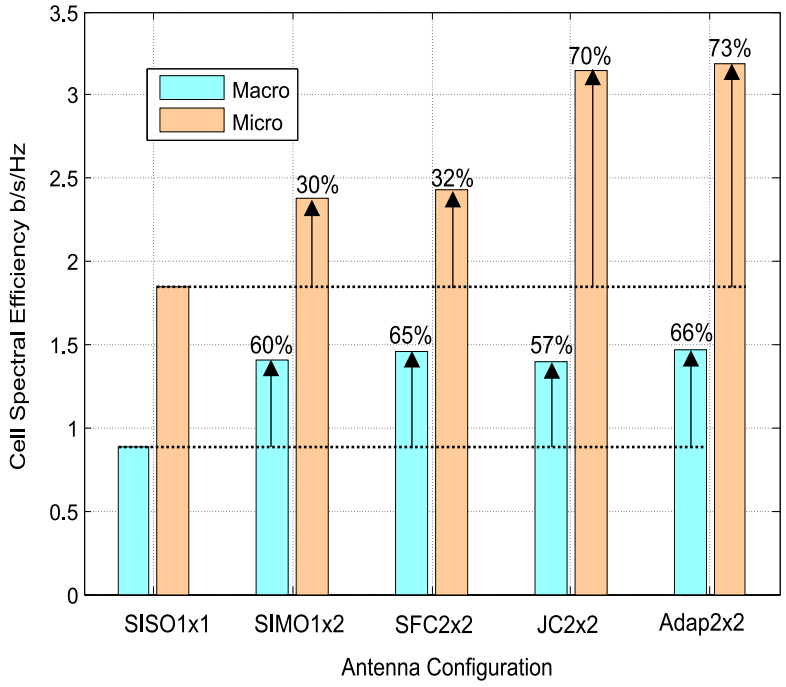

Figure 3.14: Single-user Cell Spectral Efficiency of different antenna configurations.

what SFC can achieve. The *adapMIMO* with dual stream JC in good conditions benefits from the extended dynamic range available in this scenario. Further, the SIMO scheme can provide a gain of around 28% over SISO.

3.6 Summary

In this chapter we have investigated the performance of the OFDMA based radio access technique proposed by the 3GPP Study Item on Long Term Evolution of UTRA. A detailed link level simulator implementation of the LTE downlink has been developed for this purpose. It includes the majority of LTE features, including turbo coding, rate matching, adaptive modulation and coding, as well as fast L1 HARQ. This chapter also presented the baseline simulation settings for future study. The long-term LA and short-term LA algorithms are used and compared. These results are to be considered as upper-bound estimates as the simulations do not consider overhead due to pilot and other control channels as well as real channel estimation. Since multiple antenna schemes are expected to be an integral part of the LTE system, we have selected four reference schemes for the link level analysis. Detailed link level simulations were carried out for the Typical Urban channel model, keeping the system bandwidth fixed at 10 MHz. The throughput obtained at the link-level was mapped to single user cell level spectral efficiency using available G-factor distributions for the macrocell and microcell scenarios. The single user cell spectral efficiency performance of both SFC and adapMIMO scheme in the macrocell case is quite similar, around 1.5 b/s/Hz. However, in the microcell case, adapMIMO with dual stream JC in good conditions performs significantly better than SFC, and their respective spectral efficiency figures are 3.4 b/s/hz and around 2.5 b/s/Hz. Taking into account other imperfections normally associated with a practical system it becomes important to investigate more advanced features in order to improve system performance further. Some of the techniques like closed-loop MIMO, fast adaptive MIMO, and frequency domain packet scheduling, will be investigated in the following chapters.

Chapter 4

Design and Analysis of CLTD with Limited Feedback

4.1 Introduction

Transmit diversity schemes can be divided into *open-loop* and *closed-loop* schemes. Under ideal assumptions they provide the same diversity gain, but the closed-loop scheme will also obtain array gain at the extra cost of feedback signalling [Lo99]. The closed-loop schemes such as CLTD are shown to be able to provide a significant gain over SISO for previous cellular systems like WCDMA, HSDPA [More03]. Therefore, in this chapter we consider the potential benefit from CLTD as an advanced technique to further increase the performance of the UTRA long term evolution. To support CLTD in FDD system, transmit weight information has to be fed back through uplink signalling [Moto05]. The narrowband CLTD techniques can be extended to wideband frequency selective channels by combining them with OFDMA. The CLTD in OFDMA system potentially requires feedback with weight vector information for each subcarrier at every update. The limited uplink bandwidth and the extensive feedback requirements have motivated researchers to develop efficient methods to bring down the amount of required feedback information. The approach we took is to optimize the choice of weight for a group of neighboring sub-carriers so that the majority of the sub-carriers maintain the CLTD gain. This simple approach makes it possible to trade off the performance gain and feedback requirement depending on the available uplink resources. Besides, a theoretical analysis on loss of different quantization resolution and size of groups is performed in Section 4.2. There are also other gain mechanisms like *Adaptive Modulation and Coding* (AMC) based *link adaptation* (LA) and the *Hybrid-ARQ* (HARQ) in UTRA LTE. An important issue that should be carefully considered is the compatibility of CLTD with those essential features.

To see whether the theoretical CLTD gain can be effectively mapped to spectral efficiency in the system, we use detailed link level simulation experiments to evaluate the attainable spectral efficiency. Those results are shown and explained in Section 4.3 together with estimates on single-user cell level spectral efficiency. Several practical issues affecting the CLTD gain such as high velocity, feedback delay are addressed as well. Concluding remarks are given in Section 4.4.

4.2 Design of Limited Feedback Strategy

The optimum CLTD requires the weights for each subcarrier with infinite resolution. To keep a minimal feedback requirement while maintaining most of the gain, two strategies are considered as follows:

4.2.1 Quantization

The amplitude and phase of the optimum weights must be quantized to minimize signaling overhead. For notational convenience, the subcarrier index is implicit from now on. From the channel matrix **H**, the UE selects the optimum quantized weights from a set of predetermined weights. As reference, two CLTD modes defined in 3GPP for WCDMA are considered in this study [3GPP00a]. The 'Mode1' (CLM1) splits the power equally between antennas and quantizes the phase of weight w_2 into four equally spaced phases since the weight w_1 is assumed to be real. The 'Mode2' (CLM2) defines eight phases and two distinct amplitudes ($\sqrt{0.8}$ and $\sqrt{0.2}$). The feedback bits for each weight are 2 and 4 bits for CLM1 and CLM2, respectively. As an upper bound, we also define CLM0 to be the case when ideal transmit array gain can be achieved, *i.e.* , with ideal antenna weight and with no feedback delay. The theoretical loss of mean SNR due to quantization without feedback delay is 0.7dB and 0.3dB for 2x1 CLM1, and 2x1 CLM2 respectively [Gerl02].

4.2.2 Grouping

Another common approach to reduce the feedback is to exploit the frequency correlation. A spherical interpolation based approach is proposed in [Choi05], in which a sub-sampled weight vector and some extra phase adjustment information is fed back to the transmitter. The feedback requirement with this method is still a bit high since the weight vector has to be sampled frequently to keep the interpolation work reasonably. Instead we consider a group of K sub-carriers together (referred to as "grouping") by optimizing the weight for the whole group of sub-carriers.

The feedback with grouping is reduced by $1/K$ at every update. The weight for each group $\mathbf{W}_g$ is selected as the weight which maximizes the group mean SNR

$$\mathbf{W}_g = \arg\max_{q \in \mathcal{W}} \frac{\sum_{j=1}^{K} ||\mathbf{H}(j)q||}{K} \ , \tag{4.1}$$

where $\mathcal{W} = [q_1, ...q_i, ...q_{2^Q}]$ is the set of weight choices with quantization resolution of Q bits.

4.2.3 Loss Analysis

Different quantization resolution and grouping size will generate a certain amount of uplink signalling as summarized in Table 4.1 assuming 10MHz bandwidth. The tradeoff between performance and signalling is to be discussed in this section in terms of loss analysis.

Table 4.1: Feedback requirements of different quantization resolution and group size

Quantization/group size	**(bits/update)**
SFC	0
CLM0	infinite
CLM1 K=1	1200
CLM1 K=10	120
CLM1 K=25	48
CLM1 K=40	30
CLM1 K=50	24
CLM2 K=1	2400
CLM2 K=20	120
CLM2 K=50	48

We consider a general $2 \times N_r$ antenna configuration in flat Rayleigh channel. For the simplicity of analysis, we only consider the weight phase quantization with equal amplitude, or the so called "co-phase" algorithm [Hama01]. Further we assume that w_1 is $1/\sqrt{2}$ with phase of 0, the weight selection for w_2 can be found as

$$\arg\max_{w_2 \in \mathcal{W}} ||\mathbf{h}_1 + w_2\mathbf{h}_2|| \ , \tag{4.2}$$

where $\mathcal{W} = \{e^{-j\pi(n-1)/2^{(Q-1)}}/\sqrt{N_t} : n = 1, ..., Q\}$. By following the assumption and analysis approach in ([Hott03a], section 11.4), the mean SNR gain with CLTD over open loop can be obtained as follows: Assuming no delay in feedback weight, the instantaneous received SNR is obtained as

$$||\mathbf{Hw}||^2 = \frac{1}{2}\left(||\mathbf{h}_1||^2 + ||\mathbf{h}_2||^2\right) + |\mathbf{h}_1^H\mathbf{h}_2|\cos(\theta_m) \ . \tag{4.3}$$

Further phase mismatch θ_m is found to be equal to $\angle(\mathbf{h}_1^H\mathbf{h}_2) - \angle(w_2)$ and $\angle(\cdot)$ denotes the angle information of the argument. The SNR gain γ_g is thus given as

$$\gamma_g = 1 + \frac{E\{|\mathbf{h}_1^H\mathbf{h}_2|\} \cdot E\{\cos(\theta_m)\}}{2\left(||\mathbf{h}_1||^2 + ||\mathbf{h}_2||^2\right)} \ , \tag{4.4}$$

where $E\{\cdot\}$ denotes the expectation operator.

By using the Lemma 2 in [Hama01], we have

$$E\{|\mathbf{h}_1^H\mathbf{h}_2|\} = \frac{\Gamma(\frac{1}{2})\Gamma(L+\frac{1}{2})}{\Gamma(L)} \ , \tag{4.5}$$

and

$$E\{\cos(\theta_m)\} = \int_{-\pi}^{\pi} p(\theta_m)\cos(\theta_m)d\theta_m \ , \tag{4.6}$$

where the L is equal to the number of receive antennas N_r, $\Gamma(\cdot)$ is the Gamma function [1] and $p(\theta_m)$ is the pdf of θ_m.

For the CLM1 2x2 without grouping, the SNR gain can be shown to be

$$\begin{aligned} \gamma_g &= 2 \cdot \left(1 + \frac{\Gamma(\frac{1}{2})\Gamma(L+\frac{1}{2}) \cdot \frac{4}{\pi} \cdot \sin\frac{\pi}{4}}{\Gamma(L)\cdot 2}\right) \\ &= 3.06 \ , \end{aligned} \tag{4.7}$$

where the factor of 2 is used to take into account the receiver antenna maximal ratio combining gain. Thus the array gain can be found to be around 4.86dB compared to up to 6dB in fully correlated environment. Note that due to equivalence, the analysis also applied to multi-path Rayleigh channel with a proper scaling [Hott03a].

As for the case with grouping, the loss due to grouping depends on the frequency selectivity as well as the group size. The channel profile we considered is COST 259 Typical Urban with 20 taps [3GPP05], and an rms delay of 0.5μs. The corresponding *coherence bandwidth* (CB) defined on envelope correlation of 0.5 is around 320kHz. Due to the difficulty in deriving a closed-form solution, we apply Monte Carlo simulation in analyzing the phase mismatch. First, we record both the applied weight $\hat{\mathbf{w}}_2$ (due to grouping and quantization) and perfect weight $\widetilde{\mathbf{w}}_2$ for each subcarrier over a time period long enough to have sufficient statistics. Then we define a weight phase mismatch as $\theta_m = \angle(\hat{\mathbf{w}}_2) - \angle(\widetilde{\mathbf{w}}_2)|$, $0 \le \theta_m < \pi$. Due to the cyclic property of phase, the relative phase difference is used because it is a more direct reflection of performance. The sample distribution of θ_m with different group size and quantization resolution is shown in Figure 4.1. As shown, the mismatch in phase for CLM1 and CLM2 without grouping is uniformly distributed within 45^o and 22.5^o, respectively. When a larger group size is used, the

[1] see definition details in http://en.wikipedia.org/wiki/Gamma_function

phase mismatch is increased up to 180^o, and the higher phase mismatch will result in lower array and diversity gain. The SNR gain for various grouping cases can be obtained from the calculation of the numerical integration of Equation 4.6 of the corresponding sample distribution in the interval $[0, \pi]$.

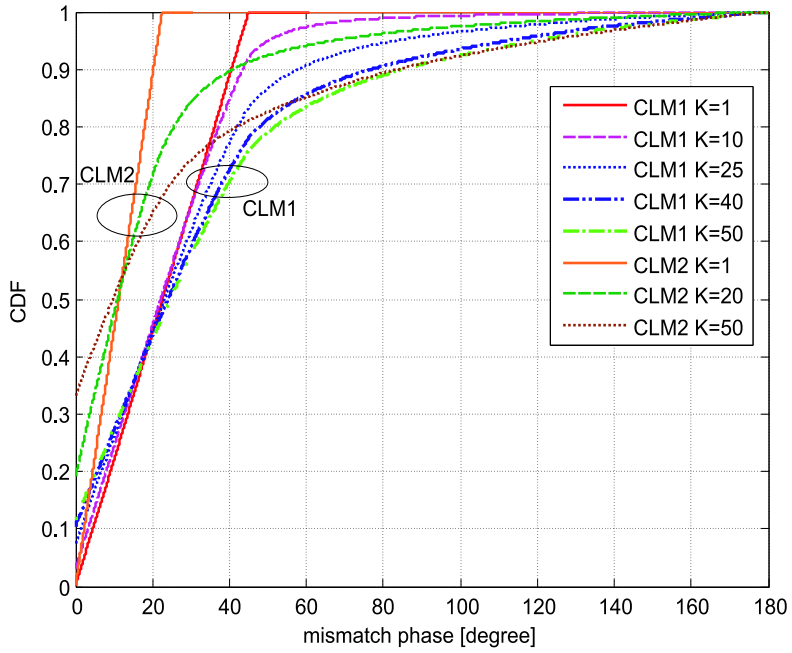

Figure 4.1: Sample distribution of phase mismatch for different group size and phase quantization resolution.

The mean SNR loss alone cannot describe loss due to grouping since severe diversity loss also occurs, and therefore an analysis of bit error rate is also necessary. The uncoded *bit error rate* (BER) for different quantization resolution and group size are shown against G-factor in Figure 4.2. SFC is the reference *open loop* scheme with Alamouti space time coding applied on adjacent sub-carriers as introduced in Chapter 2.4. The G-factor range covers most of the range where QPSK will be selected when AMC is used. It is interesting to note that when the group size is relatively small, higher quantization resolution is more advantageous: As shown, although the CLM1 K=10 and CLM2 K=20 have the same feedback requirement, CLM2 shows better performance. For a large group size, however, comparing the performance of CLM1 K=25 and CLM2 K=50 it is more efficient to use fewer bits on quantization and more bits on grouping.

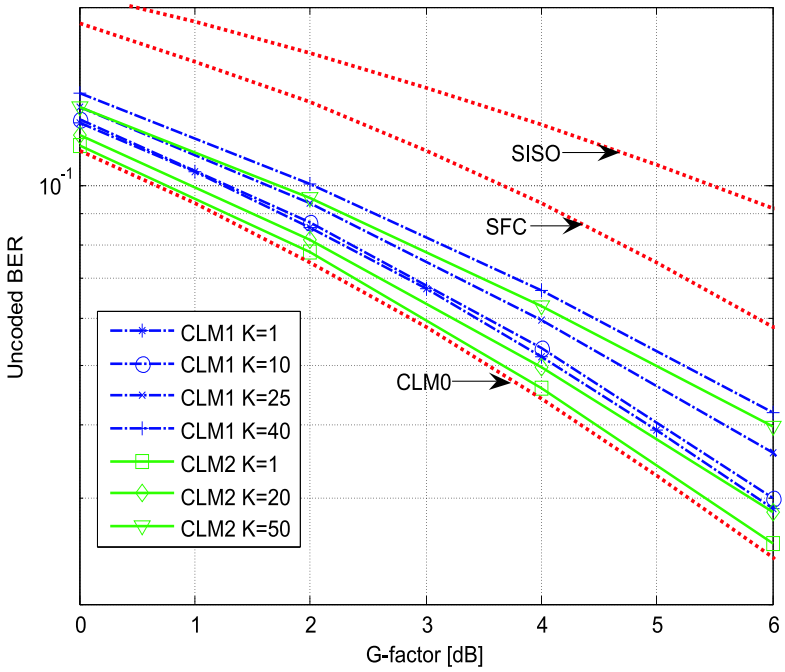

Figure 4.2: Simulated Uncoded BER comparison for different group size and quantization resolution with QPSK modulation and antenna configuration 2x1.

4.3 Performance Evaluation

In this section, the performance is evaluated in terms of spectral efficiency, defined as useful throughput achieved over bandwidth. The detailed link simulator introduced in the previous chapter is further extended to support CLTD. The main upgrades of the simulator include some new functionalities such as weight calculation, weight feedback delay and error, weight multiplication at both transmitter and receiver. The basic simulation parameters are set according to [3GPP06a] for UTRA LTE as in Table 3.3 in Chapter 3. Moreover, the delay of weight feedback is assumed to be 3ms for all simulations.

4.3.1 Limited Feedback

To reduce the feedback, the two strategies of quantization and grouping are considered. To keep the weight signalling overhead reasonably low, larger group size is highly preferred. Since with larger group size, the higher quantization is not useful anymore based on the previous analysis, only CLM1 is considered for further study. For antenna configuration 2x1, the performance is first compared for different code rates with different feedback options in Figure 4.3. The perfect weighting option (CLM0) shows 3dB array gain over the open loop SFC in uncoded BER.

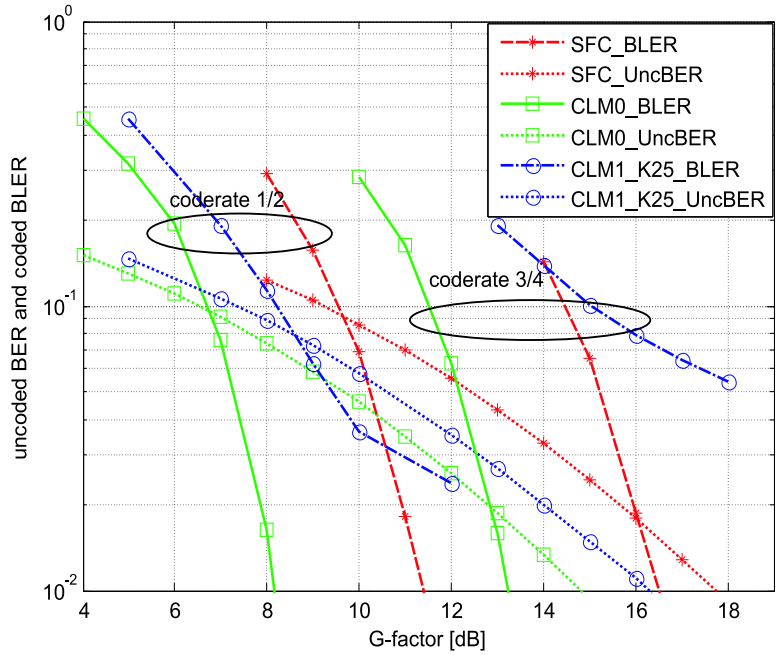

Figure 4.3: Comparison of uncoded BER and coded BLER for different code rate with 16QAM in 2x1.

The uncoded BER of CLM1 with K=25 shows a mean SNR loss as well as reduced diversity order as compared to CLM0, while the loss is reflected significantly different with coded *block error rate* (BLER) curves for different code rates. Higher code rate shows higher BLER loss due to higher sensitivity to reduced diversity order. This also reveals that including the effect of AMC and HARQ is important to make conclusions on CLTD performance in terms of spectral efficiency.

The spectral efficiency is first evaluated for antenna configuration 2x1 in Figure 4.4 with LA based on long-term statistics. As shown, the top-most curve CLM0 serves as the upper bound, and the open loop scheme SFC serves as the lower bound. When quantization is introduced by using CLM1, the spectral efficiency loss is rather small. With a group size of 10 there is almost no noticeable loss compared to the case without grouping. When the grouping size is further increased, the performance degrades significantly in high G-factor range. The CLTD loses its advantage over open loop SFC at a G-factor of around 5dB and 20dB for group size of 40 and 25 respectively.

In comparison, the LA with instantaneous CQI feedback is performed as well, as shown in Figure 4.5. Similar to the results in Chapter 3, the LA based on short-term statistics can further smooth the throughput curve compared to long-term LA. Besides, it is also interesting to observe that the loss due to grouping with the short-term LA is reduced compared to the long-term LA, especially in the high G-factor

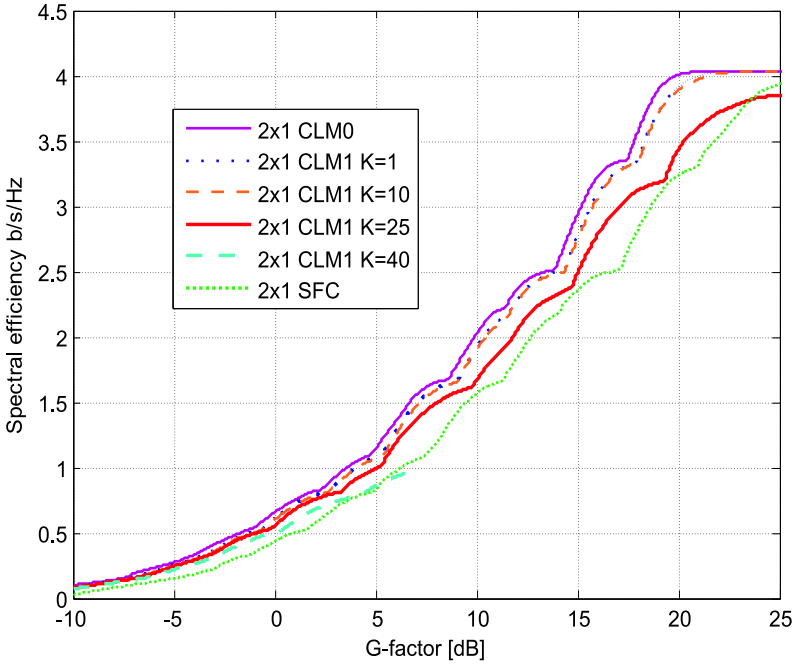

Figure 4.4: Spectral Efficiency comparison of open loop SFC and CLTD with different feedback requirements in 2x1 with long-term LA.

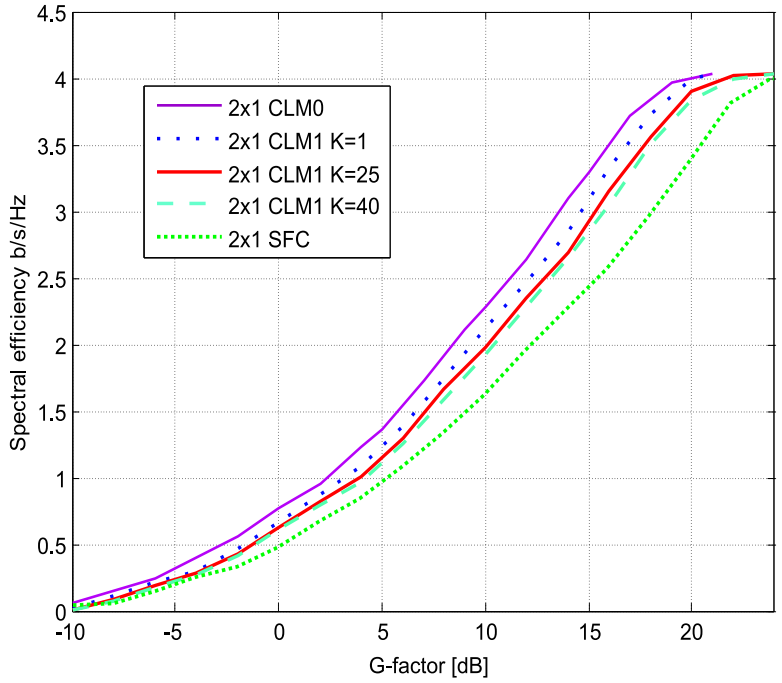

Figure 4.5: Spectral Efficiency comparison of open loop SFC and CLTD with different feedback requirements in 2x1 with short-term LA.

range. For a grouping size of 25 and 40, the spectral efficiency performance with short-term LA is always better than open loop SFC. This could be explained as follows: The diversity loss due to grouping increases the SINR dynamics. With the short-term LA, the LA module can make a good use of this larger variation since it can adaptively change the MCS on an almost instantaneous basis. This exemplifies how different diversity gain mechanisms may complement each other.

Further, the spectral efficiency is also evaluated for 2x2 in Figure 4.6 with short-term LA. With one additional receive antenna, the transmit weight cannot optimally produce a beam towards both receive antennas in uncorrelated scenario, and therefore, the maximum mean array gain is only 2.44dB for CLM0, and only 1.86dB for CLM1 quantization as compared to open loop SFC [Berg05]. Because of the existence of receive diversity, the reduced diversity order with grouping is less significant: the spectral efficiency is mostly determined by the mean gain. With grouping, most of the gain can be maintained as compared to CLM1 K=1. Higher quantization resolution has to be explored to get even closer to the CLM0.

For cell edge users, we plot the relative throughput gain from CLTD over open loop schemes in Figure 4.7. For 2x1, up to 70% gain is achieved with CLM1, K=1, over open loop at the G-factor of -5dB, and the gain is reduced to 60% with grouping K=25. Similarly, for 2x2, up to 40% gain is achieved with CLM1 over open loop, and the gain reduced to 30% or 25% with grouping K=25 or K=40, respectively. This confirms that the CLTD is a good strategy for coverage improvement. Quite significant gain can be achieved with much reduced weight feedback requirements. The reduction in feedback is critical to consider here since the users who desperately need the coverage gain, is usually also the users who lacks uplink capability.

Based on the G-factor distribution for Micro- and Macro- cell in Figure 3.13 in Chapter 3, the cell level spectral efficiency is estimated for different feedback options as summarized in Figure 4.8 and Figure 4.9 for antenna configuration of 2x1 and 2x2 respectively. The relative gain of CLTD over open loop is shown as well. For 2x1, the relative gain of CLM0 over reference open loop has around 25% and 51% gain in micro- and macro- cell, respectively. When quantization is introduced with CLM1, the gain is reduced to around 19% and 36%. With CLM1 and a group size of K=25, 92% and 85% of the cell spectral efficiency of CLM0 is maintained in the two cell scenarios. As for 2x2, maximum gain achieved with CLM0 over open loop is 13% in microcell, and 24% in macrocell. With the quantization of CLM1, 94% and 88% of the cell spectral efficiency of CLM0 is still maintained for the respective cell scenarios, even at a group size of 40.

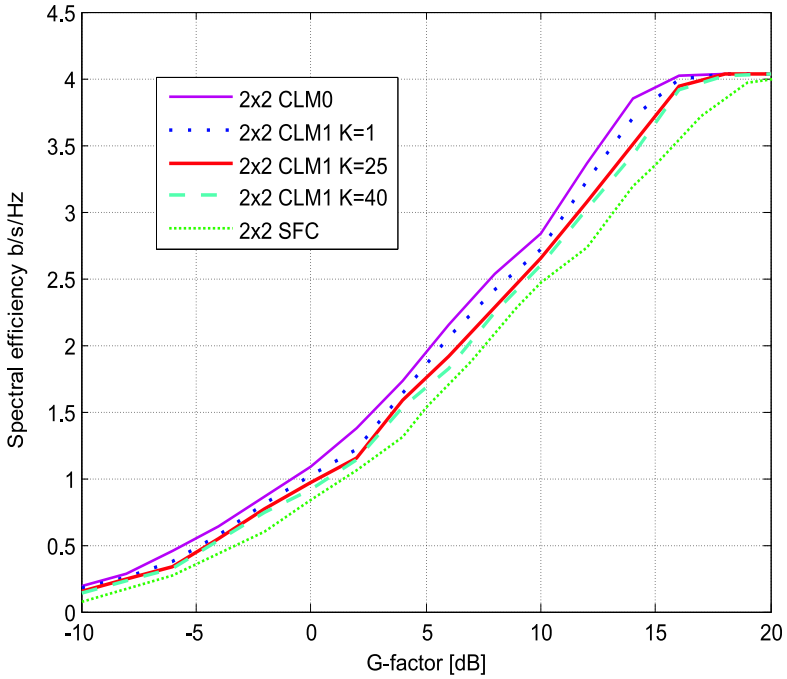

Figure 4.6: Spectral Efficiency comparison of open loop SFC and CLTD with different feedback requirements in 2x2 with short-term LA.

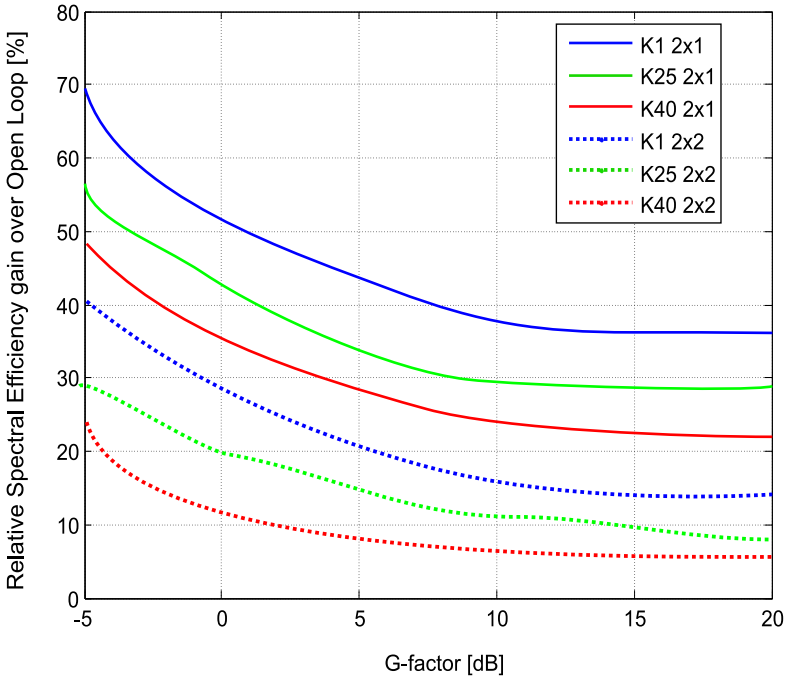

Figure 4.7: The relative gain of CLTD with different group size over the open loop.

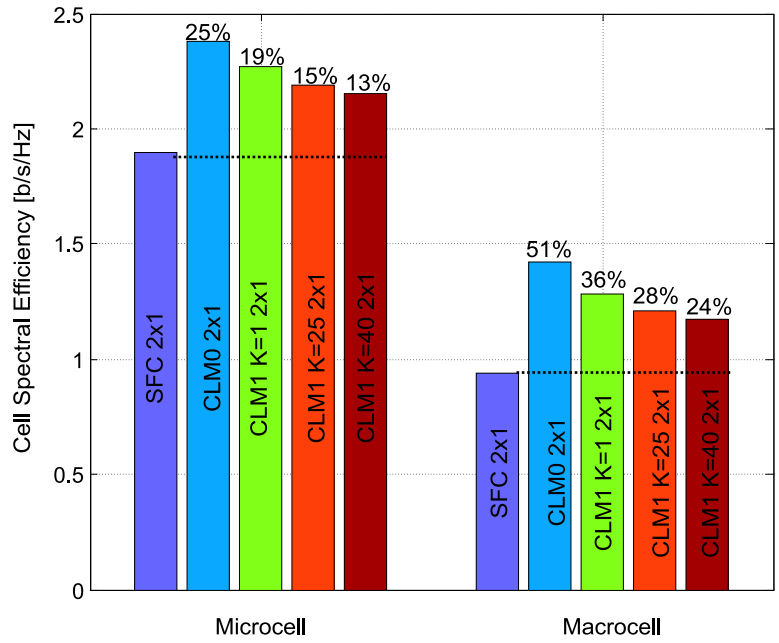

Figure 4.8: Single-user cell spectral efficiency for CLTD 2x1 with different feedback requirements.

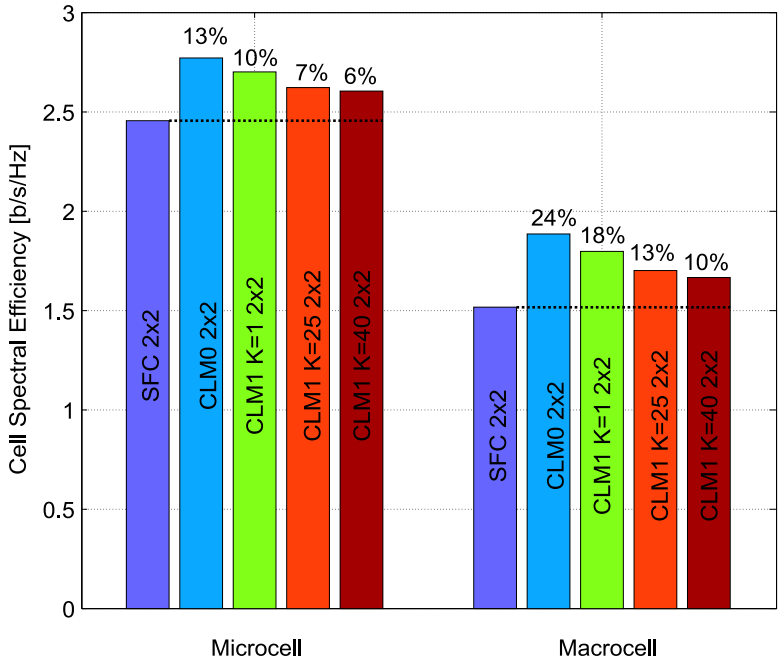

Figure 4.9: Single-user cell spectral efficiency for CLTD 2x2 with different feedback requirements.

4.3.2 Sensitivity Towards Mobility

The CLTD is quite sensitive to high mobility and feedback error. For illustration we use 16QAM and code rate 1/2 in 2x1 configuration and show the impact in terms of BLER in Figure 4.10. By assuming 3ms delay due to signalling and processing, no noticeable loss due to delay is observed for low speed users at 3kmph. But when the speed increases to 10kmph, quite significant loss is observed. If we look at the 10% BLER point, the loss with 10kmph compared to 3kmph is 0.6dB without grouping, but the loss is increased to 3.7dB with grouping because of reduced diversity order.

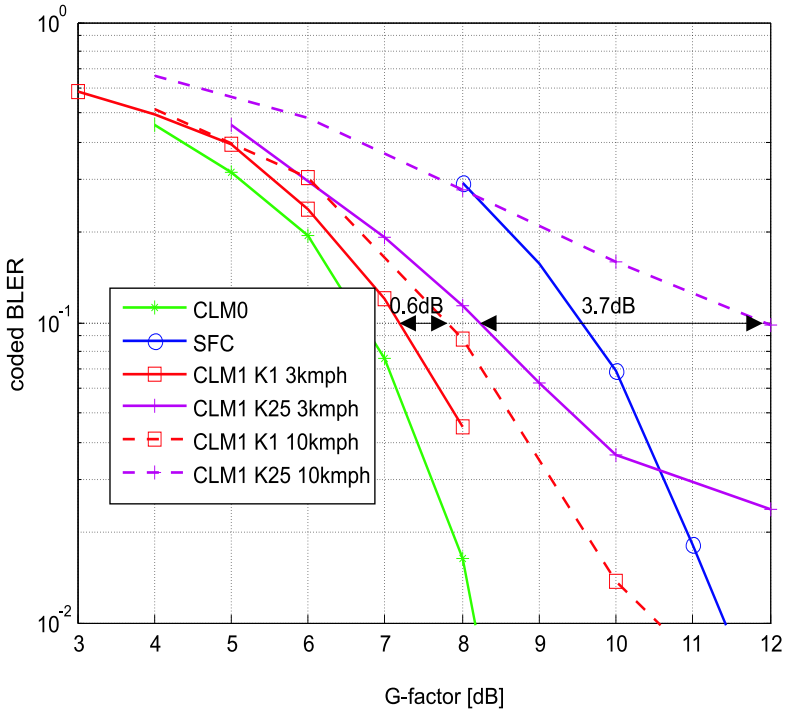

Figure 4.10: Loss due to high mobility with or without grouping for 16QAM.

4.4 Summary

In this chapter we have evaluated the spectral efficiency of Closed-Loop Transmit Diversity for UTRA long term evolution system in macro- and micro-cell scenarios. The emphasis was on reducing the amount of required feedback for the CLTD, specifically we explored the potential of using quantization and grouping over frequency. The estimated cell level spectral efficiency gain of CLTD is limited. In 2x1, even with full CSI, only moderate gain is observed over open loop SFC (25% and 51%) in micro- and macrocell. With CLM1 and grouping of 25 sub-carriers,

the gain is reduced to 15% and 28% respectively. The gain with one extra receive antenna is even smaller. However, the spectral efficiency gain at cell edge brought by CLTD is significant and this indicates that CLTD is potentially a good method to increase cell coverage for low mobility users. Up to 60% and 40% gain is achieved with CLM1 over open loop SFC with grouping of up to 25 and 40 sub-carriers for 2x1 and 2x2, respectively. The attainable gain is shown to be less in the presence of increased terminal mobility and feedback delays, etc.

Chapter 5

Design and Analysis of LA with Fast MIMO Adaptation

5.1 Introduction

The spatial freedom introduced by a MIMO system can be used in different ways, i.e., either to improve link quality or to enhance throughput. The authors in [Fern04] proposed the adaptive selection of MIMO schemes on average channel quality metrics. This type of MIMO adaptation is often referred to as long-term, or *slow*, adaptive MIMO. On the other hand, it is proposed in [Catr02] that the system can adaptively choose among MIMO schemes based on instantaneous channel conditions to maximize the spectral efficiency. We call this type of MIMO adaptation short-term, or *fast*, adaptive MIMO. *Link Adaptation* (LA) based on *adaptive modulation and coding* (AMC) according to the channel quality variations experienced is one of the key mechanisms to enhance spectral efficiency of packet switched data transmissions. Due to subtle interactions, the efficient utilization of adaptive MIMO has to be considered together with the LA module.

In this chapter the combination of adaptive MIMO and short-term LA are addressed to further increase the spectral efficiency performance of LTE. For simplicity, LA is only referred to as short-term LA within this chapter. The capacity gain of introducing fast MIMO adaptation to LA layer is first formulated from the instantaneous SINR distribution perspective in Section 5.2. The instantaneous SINR is defined as the measured/predicted SINR within each *Transmission Time Interval* (TTI) [1]. To make a fair comparison between MIMO schemes with a different number of effective spatial streams and different receiver features, a unified

[1] TTI is the minimum time resolution for adjustment of transmission format, it is defined as 2ms in HSDPA [3GPP01], 1ms in LTE [3GPP06a].

SINR is defined to translate all multistream MIMO SINRs to an equivalent effective SINR. The capacity of LA including fast MIMO adaptation is then derived on the basis of this. As a case study, the theoretical analysis framework is afterwards used to compare the capacity potential of LA including fast MIMO adaptation of SFC with three commonly used multi-stream MIMO schemes with different level of complexity and feedback requirement. After that, the practical selection metric design for LA with fast MIMO adaptation is discussed in Section 5.3. More specifically for JC, to capture the instantaneous channel condition, we propose the usage of a two dimension lookup table based on two instantaneous metrics, average SINR and SINR ratio, and the Modulation and Coding sets (MMCS) are selected regardless of the correlation degree of channel, since the effect of correlation is already reflected in the measured/predicted SINR. Detailed link level simulation is then performed to evaluate the attainable spectral efficiency gain in Section 5.4.

5.2 Theoretical Analysis of Fast Adaptive MIMO

5.2.1 Channel Model

Recall that the signal model of a MIMO channel can be expressed as in Chapter 2

$$\mathbf{y} = \mathbf{H}\mathbf{s} + \mathbf{n} \ . \tag{5.1}$$

The average SNR per receive antenna is $\gamma_0 = E_s/N_o$, where the E_s is the signal power, and N_o is the noise variance. We consider multi-stream MIMO scheme with K spatial streams, where K is less than or equal to $\min(N_t, N_r)$. If we define γ_k as the instantaneous SINR on the k^{th} spatial stream, the instantaneous capacity for this MIMO scheme is defined as in Chapter 2

$$C_{inst} = \sum_{k=1}^{K} \log_2(1+\gamma_k) \ . \tag{5.2}$$

If there are M MIMO scheme with different diversity and spatial multiplexing gain available for adaptation, for each time instance, the MIMO scheme that gives the highest capacity is chosen such that

$$C_{LA\_inst} = \max[C_{inst\_1} \quad C_{inst\_2} \quad ... \quad C_{inst\_M}] \ . \tag{5.3}$$

In Eqn. (5.3), $[C_{inst\_1} \quad C_{inst\_2} \quad ... \quad C_{inst\_M}]$ is the instantaneous capacity of MIMO scheme 1 to M offered in a particular channel condition. For the comparison between the different adaptive, or non-adaptive $(M = 1)$, schemes we evaluate the time-ergodic capacity by taking the expectation over the possible channel conditions. The ergodic capacity for LA including MIMO adaptation could thus be formulated as

$$C_{LA\_erg} = E\{C_{LA\_inst}\} \ , \tag{5.4}$$

where the $E\{\cdot\}$ denotes the expectation operator. Equations (5.3) and (5.4) reveal that the LA including fast MIMO adaptation always chooses the scheme with maximum instantaneous capacity. Similar to the short-term AMC, the MIMO adaptation is also performed at a very fast pace now. As will be shown next, we will represent the capacity gain of LA including fast MIMO adaptation in terms of a unified SINR which translates all multi-stream MIMO SINRs into an equivalent single SINR. This will allow a closed-form solution to Eqn. (5.4) under the assumption of a zero-forcing (ZF) receiver.

5.2.2 Definition of Unified SINR

To analyze the MIMO scheme with K streams, the unified SINR for MIMO is defined as the equivalent single SINR that offers the same instantaneous capacity. Since we assume ZF receiver, all streams are uncorrelated. The unified SINR γ_u can be formulated as:

$$\begin{aligned} \log_2(1+\gamma_u) &= \sum_{k=1}^{K} \log_2(1+\gamma_k) \\ \Leftrightarrow \gamma_u &= -1 + \prod_{k=1}^{K}(1+\gamma_k) \ . \end{aligned} \tag{5.5}$$

As shown in [Wint94], for spatial multiplexing schemes with ZF receiver, the end-to-end system is decoupled into a set of parallel uncorrelated SISO channels (streams). For Gaussian distributed interference this leads to independence between the streams which allows us to write the *cumulative density function* (cdf) of the unified SINR as:

$$\begin{aligned} & F(\gamma_u \le U) \\ &= \int_1^{U+1} p_{x_1}(x_1) \int_1^{\frac{U+1}{x_1}} p_{x_2}(x_2) \ldots dx_1 \ldots dx_K \\ &= \int_1^{U+1} p_{\gamma_1}(x_1-1) \int_1^{\frac{U+1}{x_1}} p_{\gamma_2}(x_2-1) \ldots dx_1 \ldots dx_K \ , \end{aligned} \tag{5.6}$$

where the $p_{\gamma_k}(\gamma_k)$ is the *probability density function* (pdf) of γ_k, the $p_{x_k}(x_k)$ is the pdf of $x_k = \gamma_k + 1$. The second line follows because of the pdf relation of a linear function. In the general case, Eqn. (5.6) is a K dimensional integral. For the case of only a few streams Eqn. (5.6) can be used for closed-form evaluations, whereas Monte Carlo integration is more practical for a higher number of streams.

5.2.3 Capacity of LA Including Fast MIMO Adaptation

Based on the SINR analysis in Section 3.4 of Chapter 3 and unified SINR definition in previous section, the LA including fast MIMO adaptation is analyzed in terms of the capacity and selection probability. For simplicity, the following evaluation considers adaptation between only two MIMO schemes, but could be extended to more schemes if needed. If we define the γ_x and γ_y as the instantaneous unified SINR of scheme X and Y, p_X and p_Y are the corresponding unified SINR pdf, the ergodic capacity from LA including fast MIMO adaptation of scheme X and Y at a certain average SNR, *i.e.* , G-factor, can be calculated by:

$$C_{LA\_erg} = \int_0^\infty p_Y(\gamma_y) \int_{\gamma_y}^\infty p_X(\gamma_x) \log_2(1+\gamma_x) d\gamma_x d\gamma_y + \int_0^\infty p_Y(\gamma_y) \int_0^{\gamma_y} p_X(\gamma_x) \log_2(1+\gamma_y) d\gamma_x d\gamma_y \quad . \tag{5.7}$$

The first line in Equation (5.7) means that when γ_x is larger than γ_y, the capacity of scheme X is chosen, while the second line means that when γ_x is smaller than γ_y, the capacity of scheme Y is chosen.

Moreover, we can get the probability of scheme X being selected by:

$$\begin{aligned} P(X) &= \int_0^\infty p_X(\gamma_x) P(\gamma_y < \gamma_x) d\gamma_x \\ &= \int_0^\infty p_X(\gamma_x) \int_0^{\gamma_x} p_Y(\gamma_y) d\gamma_x d\gamma_y \quad , \end{aligned} \tag{5.8}$$

where $P(\gamma_y < \gamma_x)$ is the probability that γ_y is less than γ_x. The actual numbers are obtained by specifying the different MIMO schemes along with the appropriate unified SINR distributions. We will now look at four different MIMO schemes.

5.2.4 Examples

We consider SFC with three commonly used spatial multiplexing MIMO schemes: JC, PARC with MMSE receiver and PARC with SIC receiver separately. As introduced in Section 2.4 of Chapter 2, these multi-stream schemes have different levels of complexity and feedback requirements, as summarized in Table 5.1. By complexity order we mean estimated hardware processing complexity as given in [Texa05]. Moreover, for the simplicity of the analysis, we assume equal power allocation across antennas and ZF receiver for all multi-stream schemes.

Table 5.1: An overview of the considered MIMO schemes

Notation	SFC	JC	PARC-MMSE	PARC-SIC
Gain mechanisms	diversity and array gain	multiplexing gain	multiplexing gain	multiplexing gain
Complexity order	1	2	2	6
Feedback requirement every TTI	one CQI feedback	one CQI feedback	CQI feedback for each stream	CQI feedback for each stream

We now concentrate on dual-stream $(K = 2)$ spatial multiplexing schemes. It is noted that for JC a single coded packet will be transmitted over two streams. With conservative LA, MCS selection will therefore be based on the channel condition on the weaker stream, hence the capacity is twice that of the weaker stream:

$$\begin{aligned} \log_2(1+\gamma_u) &= 2\log_2(1+\gamma_{weak}) \\ \Longleftrightarrow \gamma_{weak} &= \sqrt{1+\gamma_u} - 1 \ , \end{aligned} \tag{5.9}$$

where γ_{weak} is the instantaneous SINR of the weaker stream, the distribution of γ_{weak} has same diversity order as γ_k, with the mean value m' of $\frac{\gamma_0}{K\sigma_k^2} - \Delta$. The σ_k^2 is the mean loss due to correlation as defined in Equation 3.6 of Chapter 3 and the Δ is the average SNR loss of the weak stream compared to the average SINR of the two streams. Thus the CDF of unified SINR for JC can be derived with Equation 5.9 as

$$F_1(\gamma_u \leq U) = 1 - e^{-\frac{\sqrt{U+1}-1}{m'}} \ . \tag{5.10}$$

By using the pdf from equation (3.6 in Chapter 3) and equation (5.6), the uni-

fied SINR of PARC-MMSE is calculated as follows:

$$\begin{aligned} & F_2(\gamma_u \le U) \\ = & \int_1^{U+1} \frac{1}{m} e^{-\frac{x_1-1}{m}} (1 - e^{-\frac{\frac{U+1}{x_1}-1}{m}}) dx_1 \\ = & \int_1^{U+1} \frac{1}{m} e^{-\frac{x_1-1}{m}} dX_1 - \int_1^{U+1} \frac{1}{m} e^{-\frac{x_1+\frac{U+1}{x_1}-2}{m}} dx_1 \\ = & 1 - e^{-\frac{U}{m}} - \int_1^{\sqrt{U+1}} \frac{1}{m} e^{-\frac{x_1+\frac{U+1}{x_1}-2}{m}} dx_1 - \int_{\sqrt{U+1}}^{U+1} \frac{1}{m} e^{-\frac{x_1+\frac{U+1}{x_1}-2}{m}} dx_1 \ , \end{aligned} \tag{5.11}$$

where m is $\frac{\gamma_0}{K\sigma_k^2}$. When the average SNR is very high, *i.e.* , $\gamma_0 \gg 1$, the third item of Equation 5.11 is quite small and can be ignored. Moreover, the fourth item of Equation 5.11 can be approximated as

$$\int_{\sqrt{U+1}}^{U+1} \frac{1}{m} e^{-\frac{x_1+\frac{U+1}{x_1}-2}{m}} dx_1 \approx \int_{\sqrt{U+1}}^{U+1} \frac{1}{m} e^{-\frac{x_1-2}{m}} dx_1 \ , \tag{5.12}$$

since $x_1 \gg \frac{U+1}{x_1}$ in the integration range $[\sqrt{U+1}, U+1]$. Thus when the average SNR is high, the unified SINR of PARC-MMSE can be approximated as

$$\begin{aligned} & F_2(\gamma_u \le U) \\ \approx & 1 - e^{-\frac{U}{m}} \int_{\sqrt{U+1}}^{U+1} \frac{1}{m} e^{-\frac{x_1-2}{m}} dx_1 \\ = & 1 - e^{-\frac{U}{m}} - \left(-e^{-\frac{x_1-2}{m}}\right) |_{\sqrt{U+1}}^{U+1} \\ = & 1 - e^{-\frac{U}{m}} - e^{\frac{2-\sqrt{U+1}}{m}} + e^{\frac{1-U}{m}} \ . \end{aligned} \tag{5.13}$$

Finally, assuming that the effect of the first stream is completely canceled when detecting the second stream for PARC-SIC, and replacing the p_{γ_2} in (5.6) with the SIMO 1x2 SINR distribution, we can obtain the unified SINR for PARC-SIC as

$$\begin{aligned} & F_3(\gamma_u \le U) \\ = & \int_1^{U+1} \frac{1}{m} e^{-\frac{x_1}{m}} \left(1 - e^{-\frac{x}{m''}} - \frac{x}{m''} e^{-\frac{x}{m''}}\right) |_1^{\frac{U+1}{x}} \\ = & \int_1^{U+1} \frac{1}{m} e^{-\frac{x_1}{m}} \cdot (e^{-\frac{1}{m''}}(1 + \frac{1}{m''}) - e^{-\frac{U+1}{m'' x_1}}(1 + \frac{U+1}{m'' x_1})) dx_1 \ , \end{aligned} \tag{5.14}$$

where m'' is $\frac{\gamma_0}{K}$ since the correlation will have adverse effect on the first detected stream, but no effect on the second stream.

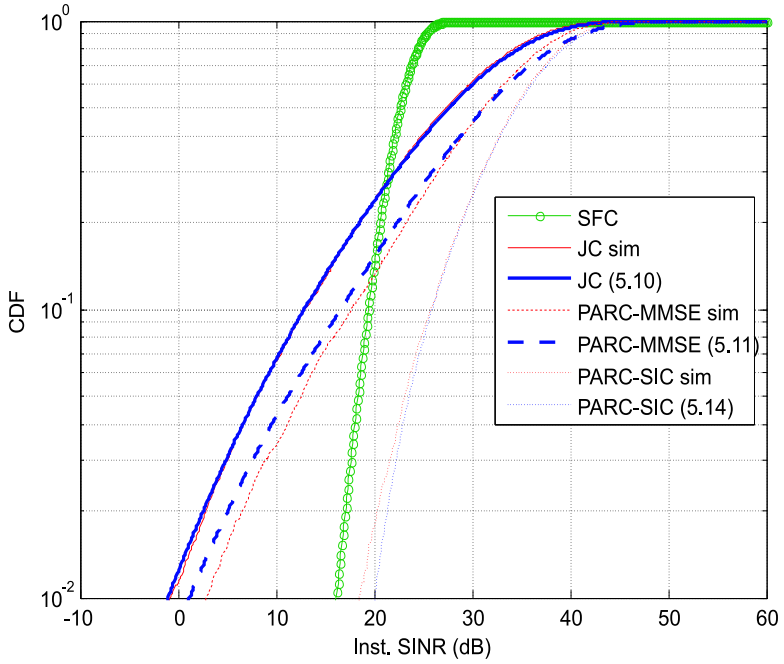

Figure 5.1: CDFs of unified SINR for different MIMO schemes with average SNR of 20dB. Equations (13)-(15) are verified against simulation results.

The unified SINRs of different spatial multiplexing schemes based on (Equation 5.10)-(Equation 5.14) at an average SINR of 20dB are compared in Figure 5.1 with corresponding distributions obtained from simulation. At each TTI, although the channel matrix is identical for diversity and SM schemes with same antenna configuration, the instantaneous unified SINR is different. By adaptively choosing the MIMO scheme with the highest instantaneous unified SINR (equivalent to instantaneous total capacity) leads to a capacity gain.

The capacity of LA including fast MIMO adaptation for the three different possible combinations of one diversity and one spatial multiplexing scheme $(M = 2)$ is shown in Figure 5.2 together with the capacity of the corresponding individual (non-adaptive) schemes. Looking first at the capacity of the individual schemes it can be seen that SFC shows advantage over spatial multiplexing in the low average SNR ranges, whereas the opposite is true for high SNR ranges. Now, looking at the adaptive schemes, they can be seen to always perform better than LA with fixed MIMO (non-adaptive), and in the transition range, better than both the diversity and the spatial multiplexing scheme individually. This latter observation is most significant for the case of JC, whereas the adaptation between SFC and PARC-SIC has almost no capacity advantage. This could be explained by the cdfs of unified SINR of SFC and PARC-SIC in Figure 5.1, in which the PARC-SIC always has

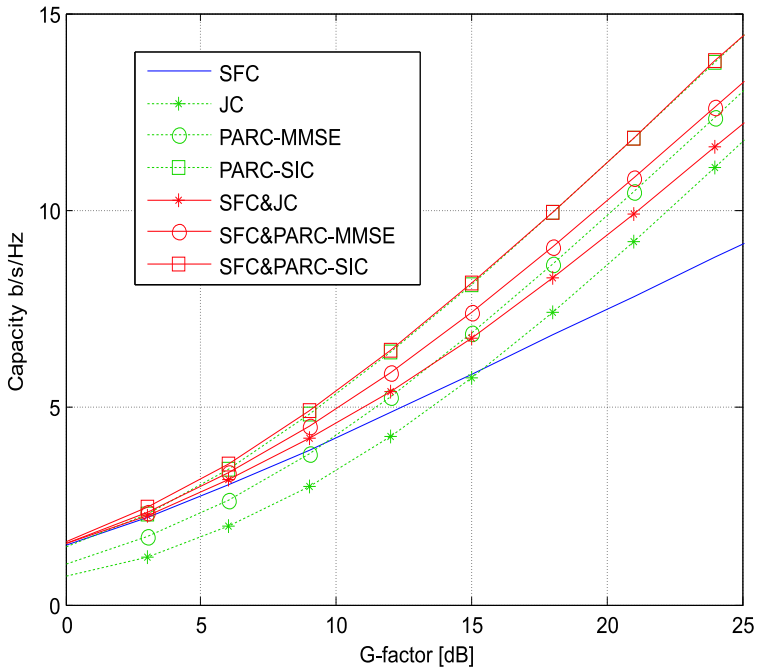

Figure 5.2: Capacity for LA including fast MIMO adaptation in uncorrelated Flat Rayleigh channel. SFC is paired with three spatial multiplexing schemes separately.

better instantaneous SINR than SFC. For the other two combinations, it is observed that the unified SINR curves cross over each other, *i.e.* , different MIMO schemes gain over the others at different time instance. With fast adaptive MIMO, up to 16% gain is observed in the transition range.

An intuitive explanation of Figure 5.2 can also be found considering different levels of tolerance towards unevenness between streams. For JC, since the decoder will take both streams and decode them together, the decoder will perform well only if we have similar SINR on all streams. While for PARC-MMSE, where each stream is coded and decoded separately, the tolerance to unevenness is higher compared to JC. And for PARC-SIC, since before decoding the next stream, the effect of the other stream will be canceled, the tolerance towards unevenness is even higher. As a consequence, different schemes and receiver types having different level of tolerance towards unevenness of streams will lead to different attainable fast adaptive MIMO gain.

Figure 5.3 shows the selection probability for the diversity and spatial multiplexing schemes in each of the three different combinations. Only an average SINR of 1dB is required to select the PARC-SIC more often than SFC. The corresponding numbers for PARC-MMSE and JC are around 8 and 14dB respectively, which again shows the bigger potential for MIMO adaptation with these combinations.

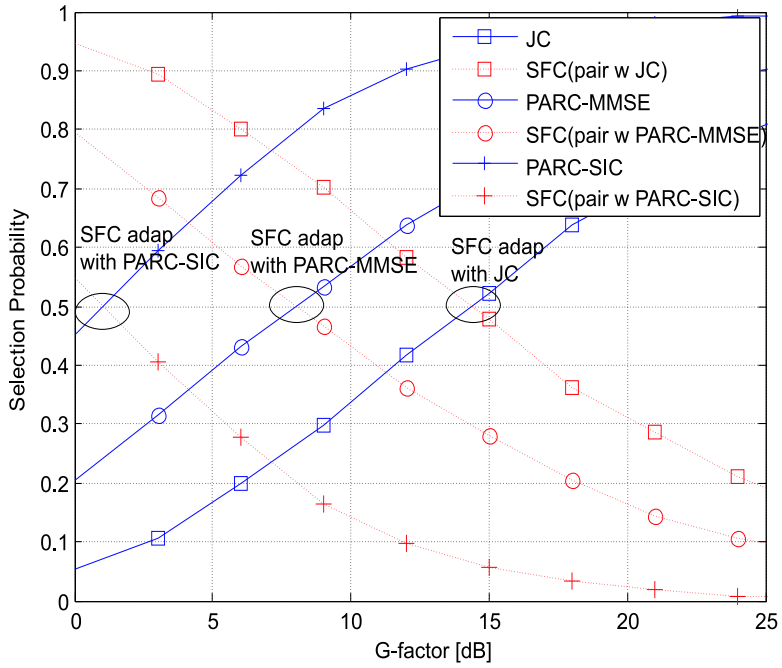

Figure 5.3: Selection Probability for fast MIMO adaptation in uncorrelated Flat Rayleigh channel. SFC is paired with three spatial multiplexing schemes separately.

The correlation effect for adaptation between SFC and PARC is shown in Figure 5.4. As shown, there is increased capacity gain over a larger average SNR range in more correlated scenarios. This is due to the fact that spatial multiplexing schemes are more sensitive to correlation compared to SFC. Since diversity MIMO can be used as a backup for spatial multiplexing scheme in very ill-conditioned channel realizations, the capacity loss due to correlation is smaller when adaptation is used.

5.3 Channel Quality Metric Design of LA with Fast MIMO Adaptation

To reach the capacity potential, special attention should be given to the practical application of LA with fast MIMO adaptation. This is addressed in this section. Following the terminology in [Fore05], the combination of MCS and MIMO is considered as transmission mode, denoted as MMCS. In [Fore05], a spatial selectivity indicator is defined to characterize the long term spatial correlation of the channel. Thus for different typical channel scenarios, different lookup tables based on average SNR are used for mode selection. However, for the fast adaptive MIMO considered in this study, the spatial selectivity indicator together with average SNR

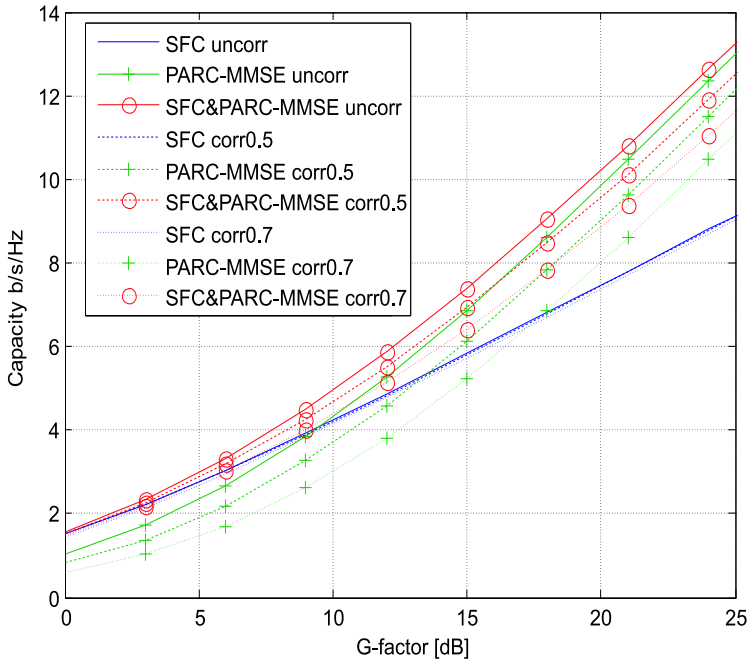

Figure 5.4: Capacity for fast MIMO adaptation with SFC and PARC in Flat Rayleigh channel with different correlation.

is not suitable since it cannot reflect the instantaneous channel variation and different receiver capability. Instead the following instantaneous SINR metrics are considered as channel quality metrics.

For PARC-MMSE and PARC-SIC, since the channel coding and modulation are done separately for each stream, the solution could be quite straightforward. At each TTI, SINR for SFC γ_{SFC} and SINRs for each stream with PARC-MMSE or PARC-SIC γ_1 and γ_2 are fed back. Then the eNode-B predicts the throughput of the two cases and chooses the MIMO mode which gives the best total throughput, as described in [Fern04]. After that, the MCS is selected accordingly.

As for JC, since all streams are coded together, the throughput prediction is not that straightforward. Thus we propose a two dimensional look up table based on two metrics `AvgSINR` and `DiffRatio`. The `AvgSINR` is the averaged SINR over all streams to represent an averaged quality of all streams, while the `DiffRatio` is used to take into account the difference of streams. If we assume that a system can support up to K spatial streams, and the instantaneous SINR per stream is sorted in ascending order as $[\gamma_1, \gamma_2, ..., \gamma_K]$, the two metrics for the LUT are defined as:

$$\texttt{AvgSINR} = \frac{\sum_{i=1}^{K}(\gamma_i)}{K} \quad , \tag{5.15}$$

$$\texttt{DiffRatio} = \frac{\gamma_K}{\gamma_1} \quad . \tag{5.16}$$

The idea behind this proposal is that the more unevenness of stream quality, the worse the performance from JC, and the higher the chance that single stream schemes should be used instead. Extensive simulations are performed to obtain such a lookup table with the BLER target and power constraints. At each TTI, certain `AvgSINR` and `SINRratio` are observed, and its corresponding *Block Error Indicator* (BLEI) ("0" is for ACK and "1" is for NACK) is stored. For each 2D bin, enough samples are saved to have enough statistics. The general trend is that when the unevenness exceeds some thresholds, it is more efficient to use schemes with less stream. Also the higher the `AvgSINR`, the higher the `SINRratio` threshold, i.e., the more tolerance of unevenness.

5.4 Performance Evaluation

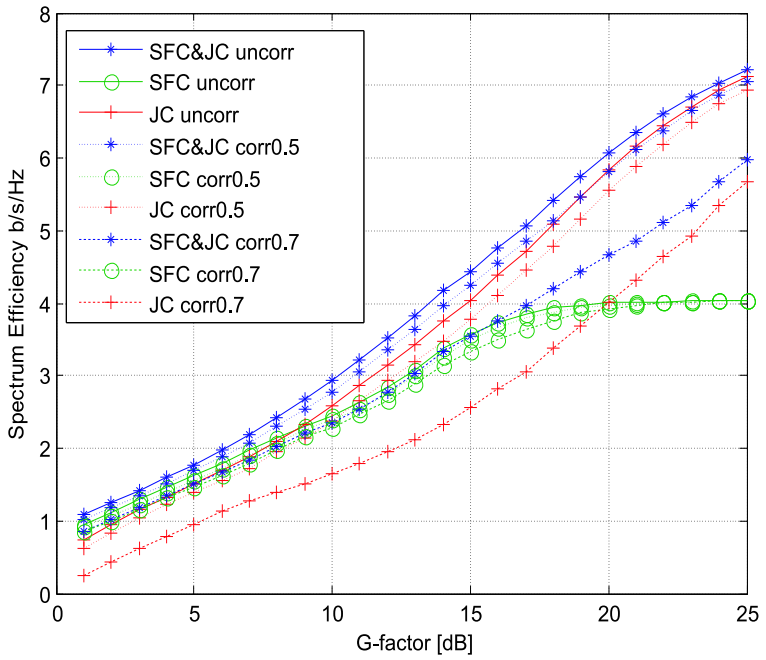

Figure 5.5: Spectral Efficiency in Flat Rayleigh channel with different correlation.

To evaluate the LA with fast MIMO adaptation in terms of attainable spectral efficiency, a detailed link level simulation is done. The theoretical analysis has shown that the potential gain for advanced receivers is quite limited, so the simplest JC (2str) with MMSE receiver together with SFC (1str) is considered here for further study. This simpler receiver is of special interest also because it requires much less processing power compared to the other two multi-stream schemes.

The system parameters and configurations assumed are set according to [3GPP06a] for 3GPP E-UTRA. 9MCS considered are QPSK (1/6, 1/3, 1/2, 2/3), 16QAM(1/2

, 2/3, 3/4), 64QAM(2/3, 4/5). With 9 MCS and 2 MIMO schemes, a total of 18 MMCS modes are considered. Further, the flat Rayleigh channel is considered. As for frequency selective channel, we would consider the case that the MMCS is selected per frequency chunk. If the frequency chunk size is smaller than the coherence bandwidth, the system is still equivalent to flat Rayleigh channel. Other simulation parameters is set according to the Table 3.3 in Chapter 3.

The spectral efficiency of LA with and without MIMO adaptation in uncorrelated and correlated channel is compared in Figure 5.5. The attainable spectral efficiency is much lower than the capacity in Section 5.2, but the same trend is observed. As shown, LA with fast MIMO adaptation shows significant gain over LA with fixed MIMO. Up to 0.5 b/s/Hz and 0.8 b/s/Hz is observed for LA with fast MIMO adaptation over slow MIMO adaptation for transmit antenna correlation of 0.5 and 0.7, respectively. The gain of including fast MIMO adaptation diminishes faster than the theoretical analysis because the maximum spectral efficiency for SFC saturates at 4 b/s/Hz, which is limited by the highest modulation used, 64QAM. Since JC and other spatial multiplexing schemes are more sensitive to channel estimation errors in practice, the potential of LA with fast MIMO adaptation is expected to be even higher when real channel estimation is applied.

5.5 Summary

The capacity of including fast MIMO adaptation into LA layer is derived in this chapter. The analysis shows that the potential of including instantaneous MIMO adaptation into LA is quite limited for advanced receiver, while significant capacity can be achieved in combination with simpler receivers and/or more correlated scenarios. The channel quality metric issues for practical utilization are discussed based on instantaneous SINRs. Furthermore, extensive link level simulation is done to evaluate this with more realistic factors. Results show that significant spectral efficiency gain from LA including fast MIMO adaptation is observed, and is even more effective for correlated scenarios. The LA including fast MIMO adaptation is shown to be a good LA strategy for fast changing mixed correlation scenario and simple receivers.

Chapter 6

System Model for Network Evaluation

This chapter introduces the simulation methodology and assumptions for system-level evaluation in Chapter 7 and Chapter 8. More specifically, the overall detached link and system simulation methodology is introduced in Section 6.1. After that, the modeling of each module in the network overlay is discussed in Section 6.2. Special attention is given to the analysis of two different traffic models. The key performance indicators and default simulation assumptions are further presented in Section 6.3 and Section 6.4 respectively.

6.1 Detached Link and System Methodology

As shown in Figure 6.1, we consider a detached link and system methodology for the system-level evaluation. This technique is a practical trade-off between simulation inaccuracy due to the modeling simplifications and the processing load caused by the complexity of the joint modeling of link and system levels in real-time [Berg05]. The operation of such an approach is that the link-level processing is abstracted in the form of pre-generated SINR traces from link-level simulation, while the system-level related processing is implemented in a network overlay including system level parameters. The link level simulator used is as introduced in Chapter 3.

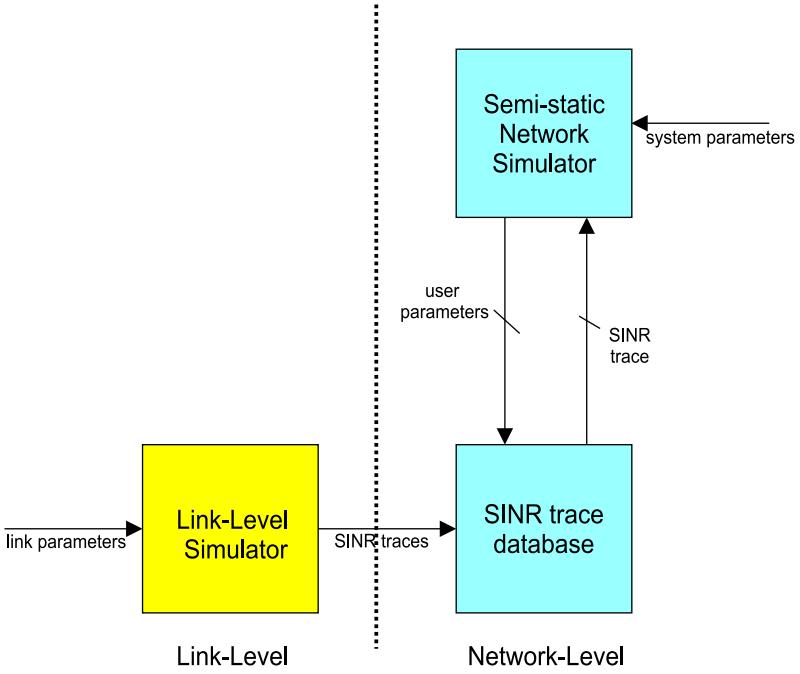

Figure 6.1: Decoupled link and network simulation methodology for run-time efficient network performance evaluation, inspired by Figure 1.9 [Berg05]

6.2 Network Simulator Modeling

This network simulator provides traffic modeling, multiuser scheduling, and link adaptation including Chase Combining HARQ under the UTRAN LTE downlink parameters and assumptions described in [3GPP06a]. The system is based on a simple *admission control* (AC) strategy which keeps the number of UEs per cell constant. UEs within the reference cell are simulated in detail, while other-cell interference, path loss, and shadowing is modeled as AWGN adjusted to an equivalent G-factor distribution [Kova06]. The average G-factor remains constant for a UE during a session, thus assuming that the packet call is short compared to the coherence time of the shadow fading and distance dependent path loss. Besides, with practical signalling constraints, we assume equal power allocation over the PRBs, and same MCS is used for all PRBs on each spatial stream for one UE per TTI. The modeling details of modules such as Link Adaptation, CQI, HARQ, Link to system mapping and traffic models are further introduced as follows:

6.2.1 Link Adaptation

As introduced in Section 3.3.1 in Chapter 3, link adaptation consists of both inner loop link adaptation (Adaptive modulation and coding) and outer loop link adapta-

tion. The inner LA selects the MCS which gives the best throughput while maintaining the BLER target, as explained in Equation 3.3. Further, an outer loop LA (OLLA) module is used to maintain the 1st transmission target BLER by adding an adaptive offset to the available CQI reports for the UE based on the ACK/NACKs [Naka02] [Pokh06]. The OLLA is shown to be very effective in combating the CQI error.

6.2.2 CQI Error and Delay Modelling

To support the link adaptation, the transmitter should have knowledge of the channel variation for each UE. In the FDD system, this information is obtained by CQI feedback from each UE to eNode via uplink. The quality of CQI is an important factor for the efficient application of LA.

To take into account the practical imperfections, the CQI reports are modeled with errors associated to (i) measurement inaccuracy modeled as a lognormal error in the SINR domain and quantization loss with 1dB resolution (ii) reporting delay corresponding to 2 ms.

6.2.3 Layer One HARQ Retransmission Model

In this network simulator, explicit scheduling of multiple HARQ processes per user has not been performed due to complexity. Instead we include the effect of HARQ in terms of Chase Combining using a simple HARQ process model from [Fred02].

The soft combined SINR after each transmission is given by:

$$\{\text{SINR}\}_n = \eta^{n-1} \cdot \sum_{k=1}^{n} (\text{SINR})_k \ , \tag{6.1}$$

where $\{\text{SINR}\}_n$ represents the combined SINR after n transmissions, η denotes the chase combining efficiency and $(\text{SINR})_k$ denotes the SINR of the k^{th} transmission. $\eta = 0.95$ is assumed in this study, which is the recommended value in [Fred02]. Note that Equation 6.1 is only valid when n is relatively small, e.g., around 3-4, which is also practical. In this study the HARQ process allows a maximum of three retransmissions per block before it is discarded, i.e., $n = 4$. Moreover, we use the simple statistical recursive HARQ model given below to calculate the effective block throughput after retransmissions:

$$\text{TP}_{\text{eff}} = \sum_{k=1}^{n} \frac{\text{TBS}}{k} (1 - \text{BLER}_k) \ , \tag{6.2}$$

where TP_{eff} denotes the effective throughput after HARQ combining gain, TBS denotes the transport block size given by the MCS employed, $BLER_k$ denotes the BLER for the k^{th} transmission. Note that Equation 6.2 is applicable only if the block is finally correctly received after the fourth transmission, i.e., $BLER_4 = 0$, otherwise the block is considered to be lost. Note that the HARQ model presented here assumes non-adaptive HARQ operation. This is also clear from Equation 6.2 since we assume that the transmit parameters are not changed between transmissions of the same code block. Further, no signaling delays or errors in the transmission of HARQ ACK/NACKs are assumed.

6.2.4 Link to System Mapping

For complexity reasons, a link level simulation of all links between eNode-B and UEs is not feasible. In practice, we utilize this detached link and system approach and use single link level simulation results in terms of the BLER as a function of SINR to predict each UE's throughput. One commonly used link to system interface is the *exponential effective-SINR mapping* (EESM) [Brue05], as introduced in Section 3.3.1 in Chapter 3. The only difference is that the EESM is not only used to predict the throughput from the CQIs in LA module in transmitter (as in Chapter 3), but also used to calculate the actual throughput from the experienced SINRs per sub-carrier at the receiver. This means that for each transmission, the associated packet error is obtained. The validation of EESM link to system interface model is discussed in Appendix E.

6.2.5 Traffic Model

We have considered the infinite buffer and the finite buffer traffic models in this study to abstract the behavior of best effort traffic. Infinite buffer is the simplest traffic model for system level evaluation, in which the users always have data packets to transmit. In the infinite buffer model all users experience equal session time irrespective of their location within the cell. This implies that the users close to the eNode-B download a much larger amount of data in comparison to those located near the cell edge (due to superior SINR conditions near the cell center). For this model, the cell and user throughput statistics are collected over a large number of simulation runs with the same duration. In each run a given number of user locations within the cell are sampled.

The finite buffer model allows downloading of an equal amount of data by each active user, and when the session is terminated, a new UE is immediately admitted. As a consequence, the session time for a UE with finite buffer is inverse-proportional to the experienced data rates, and the users close to the cell edge are expected to stay longer in the system in comparison to the users located near the

cell center. The data rates delivered to the cell edge users will dominate the resultant cell throughput. Only a single simulation run is performed in this case, which is of a long duration in order to have sufficient number of completed sessions. This is required to sample all the locations in the cell. In both cases user locations within the reference cell are generated on the basis of the G-factor distribution for the simulated deployment scenario [Kova06]. In this study, macro-cell case 1 and micro-cell outdoor to indoor environment are considered. Further, data is always available in the eNode-B, waiting to be served by the scheduler. Note that burstiness of packet arrival within an ongoing session has not been modeled in either case.

The important property of two models is the session time distribution among the users. Equal session time distribution is observed for infinite buffer model, while unequal session time is observed for finite buffer depending on the user throughput distribution. To gain insight in this, we perform the following analysis of the *effective* G-factor distribution. For infinite buffer model, the previous study shows that if we condition the user throughput on the user G-factor distribution, the cell level throughput can be estimated, and it is quite accurate compared to the real system simulation results [Moge07b]. However, for finite buffer the experienced G-factor distribution will change since the session time for each user is different. To take that into account, we define effective G-factor as the actually experienced G-factor over the simulation length. To measure that we stored the G-factor trace at each TTI from all the active users and computed the distribution from that trace as the effective G-factor distribution. Since the session time is uniformly distributed for all users for infinite buffer model, the effective G-factor distribution remains the same. However, the effective G-factor distribution for finite buffer will vary depending on the session time. To quantify the effect of the unequal session time, we approach the problem of calculation of effective G-factor distribution for finite buffer with a statistic method called *weighted distribution*.

Weighted distribution is a common method first appeared in statistics, where the certain factors are modeled with a distribution, while uncertain factors are modeled as another distribution. Under specific situation, the certain factor distribution is weighted with uncertain factors to get the effective distribution [Rao85]. The same approach is considered here to take into account the unequal session time distribution for users with different physical locations. The effective G-factor distribution for finite buffer can be described by weighting the user G-factor distribution $p_u(x)$ with the actual session time distribution $T_s(x)$ as

$$p_{\text{effG}}(x) = \frac{T_s(x) \cdot p_u(x)}{\omega} \quad , \tag{6.3}$$

where ω is a normalizing factor obtained to make the total probability equal to unity by choosing $E\{T_s(x)\}$, and both distributions are a function of G-factor x. If we assume a total packet size of M bits in the buffer for all the users, and an

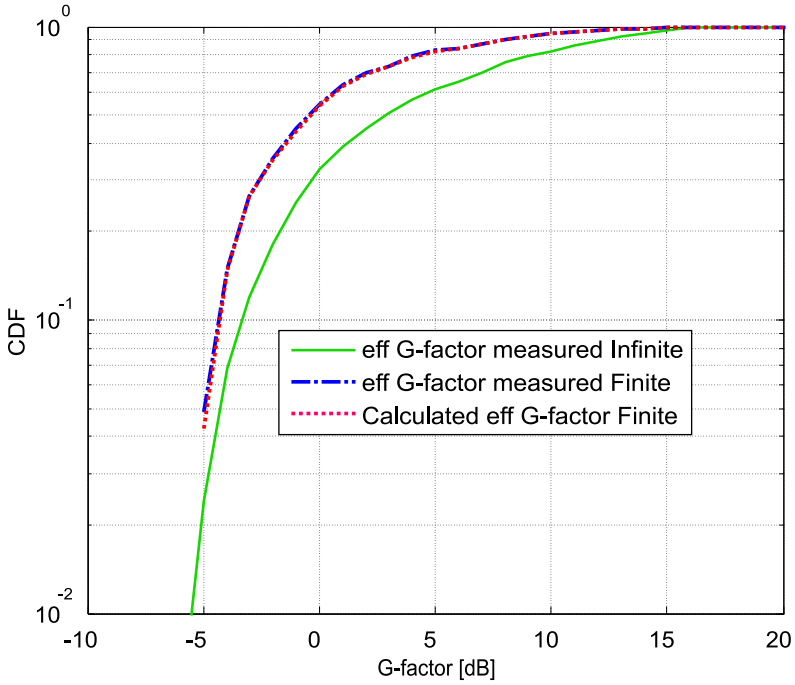

Figure 6.2: The comparison of effective G-factor distribution and user G-factor distribution for finite and infinite cases in macro cell scenario.

average user throughput of $\text{TP}_{user}(x)$ which is also a function of G-factor, $T_s(x)$ is given by

$$T_s(x) = \frac{M}{\text{TP}_{user}(x)} \quad . \tag{6.4}$$

We measured the effective G-factor distribution for both infinite and finite buffer models from simulation for 1x2 FDPS macro cell, as shown in Figure 6.2. If we weighted the user G-factor distribution with the user session time for finite buffer model, the calculated weighted distribution is shown on top of the measured effective G-factor distribution for finite buffer and validates the above analysis. The cell throughput estimate for finite buffer can also be done similarly as in [Moge07b] by condition the user throughput on the effective finite buffer G-factor distribution. It is noted that the effective G-factor distribution analysis will only be used to gain insight of the impact from traffic model, while the detailed system evaluation simulation results in Chapter 7 and Chapter 8 are not based on this analysis.

6.3 Key Performance Indicators

For the system-level study, we will use the Key Performance Indicators (KPIs), namely average cell throughput, spectral efficiency, average user throughput, and

coverage. The average cell throughput $\overline{TP_{cell}}$ is defined as the ratio between the total correctly decoded bits and the total simulation time,

$$\overline{TP_{cell}} = \frac{\text{total bits correctly delivered}}{\text{simulation time}} \quad . \tag{6.5}$$

The corresponding spectral efficiency is given by the ratio of total cell throughput divided by the bandwidth occupied:

$$\text{spectral efficiency} = \frac{\overline{TP_{cell}}}{\text{Bandwidth}} \quad . \tag{6.6}$$

The average user throughput for the ith active user is defined as:

$$TP_i = \frac{\text{bits correctly delivered to user } i}{\text{session time for user } i} \quad . \tag{6.7}$$

Coverage, denoted by $TP_{coverage}$, is determined from the CDF curve of the average user throughput taken over all the completed sessions. Coverage is defined as the data rate corresponding to the 5% quantile in the CDF curve, i.e., 95% of the users experience a higher average data rate than the rate specified by the coverage parameter. This KPI indicates data rate experienced by users around the cell edge. Further, it can be used to differentiate packet schedulers in terms of fairness in the distribution of throughput among users.

6.4 Default Simulation Parameters

The main default simulation assumptions are summarized in Table 6.1. The validation of the network simulator used is provided in Appendix E.

Table 6.1: Default simulation parameters and assumptions.

Parameter	**Setting**
Physical parameters	See [1]
System bandwidth	10 MHz
Cell-level user distribution	Uniform
PRB width	375 kHz
User diversity order (UDO)	10 (default)
Traffic model	Single 2 Mbit packet
Power delay profile	Typical Urban
LA delay	2 ms
CQI error std	1 dB
CQI reporting resolution	1 dB
Modulation/code rate settings	QPSK: 1/3, 1/2, 2/3 16QAM: 1/2, 2/3, 4/5 64QAM: 1/2, 2/3, 4/5
H-ARQ model	Ideal chase comb.
LA target	20% BLEP (1st TX.)
UE speed	3 km/h
Channel estimation	Ideal
Carrier frequency	2 GHz
autoregressive moving window	150 TTIs
Initial T_k value	log2(1+G/2.5)/UDO
Weight info feedback delay	2 ms

Chapter 7

Design and Analysis of MIMO with FDPS

7.1 Introduction

OFDMA facilitates FDPS which promises up to 40%-60% gain over time-domain only scheduling, based on 1x2 with MRC receiver [Pokh06] under LTE downlink assumptions. The Multiple-Input Multiple-Output (MIMO) technology can potentially increase the diversity and array gain (diversity mode) and/or can provide a large spectral efficiency gain without increasing the bandwidth (SDM mode). It is therefore quite natural to consider the combination of MIMO and FDPS (MIMO-FDPS). However, due to the interaction of MIMO and FDPS, it is not a trivial task to combine them effectively.

The MIMO-FDPS performance for UTRA LTE downlink is analyzed in this chapter. Since the interaction of diversity MIMO and FDPS is extensively studied in literature, (see for example [Weng05], [Pokh07]), the emphasis of this thesis is put on SDM type of MIMO with FDPS (SDM-FDPS). Depending on whether the spatial freedom of SDM is given to the packet scheduler or not, two concepts are currently discussed in 3GPP, namely SU- and MU- MIMO, following the terminology in [3GPP06a]. The SU-MIMO has the restriction that only one UE can be scheduled over the same time-frequency resource, whereas MU-MIMO offers greater flexibility to the scheduler so that different UEs can be scheduled on different spatial streams over the same time-frequency resource. The MU-MIMO offers greater flexibility in the spatial domain, but it also imposes higher requirements on the resource allocation signalling. The two concepts have been analyzed in the literature, see e.g. [Heat01b] and references therein. Most studies are conceptual in nature and disregard fairness between UEs and practicalities, such as practical

SINR dynamic range, amount of signaling overhead, adaptation uncertainties, etc. Such factors are highly relevant in wireless system design. To include those factors, we analyze by simulation the combination of SDM and Proportional Fair (PF) FDPS under the influence of these factors with finite or infinite buffer best effort traffic model. The signalling overhead to support SDM-FDPS will be addressed in Chapter 8.

The organization of this chapter is as follows: In Section 7.2, the basic FDPS terminology when combined with MIMO schemes is introduced. The practical SDM MIMO aware FDPS algorithms are proposed in Section 7.3. To gain insight, Section 7.4 provides an analysis of post scheduling SINR distribution for all MIMO-FDPS schemes based on the unified SINR concept from Chapter 5. Based on that, the cell performance bounds are derived. Detailed system-level simulation results are shown and explained in Section 7.5. The simulation results are further compared with the theoretical bounds in Section 7.6. After that, the main conclusions are summarized in Section 7.7.

7.2 System Model

Recall a UTRA LTE downlink consisting of a scheduling node (eNode-B) with FDPS functionality and several UEs with SDM capability as mentioned in Section 1.1.6 of Chapter 1. As seen in Figure 1.6, three types of schemes are considered for MIMO-FDPS, namely beamforming and diversity MIMO FDPS, SU-MIMO FDPS or MU-MIMO FDPS. The UEs assist the scheduler by reporting the CQI per scheduling unit to the eNode-B in order to support fast channel aware scheduling. The basic scheduling unit is denoted as a physical resource block (PRB). As stated in [3GPP06a], there are two ways of creating the PRB as shown in Figure 7.1:

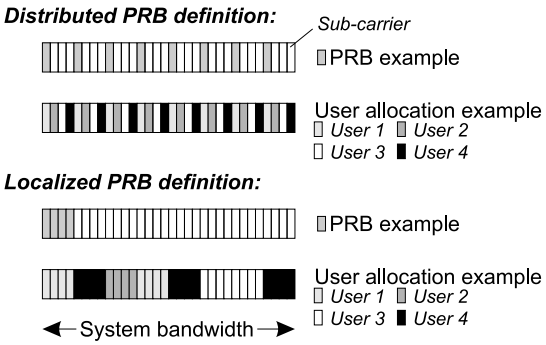

Figure 7.1: Distributed vs Localized PRB concept.

- *Distributed*: The PRB is defined by non-consecutive sub-carriers distributed

over the operating bandwidth to maximize the frequency diversity. None, or limited user/selection diversity can be exploited since all RPBs will experience similar average channel condition.

- *Localized*: The PRB is defined by consecutive sub-carriers (within coherence bandwidth): *e.g.* isolated to a certain sub-band within the system bandwidth.

In general, the distributed PRB can still be combined with time domain PS to exploit the multiuser diversity in time domain. The localized PRB definition facilitates the user/selection diversity in the frequency domain and thus FDPS, while the distributed PRB definition is used when frequency diversity is to be utilized instead. In this study, we concentrate on localized PRB definition since FDPS gain is our main concern.

For diversity MIMO and SU-MIMO, the minimal scheduling flexibility, one PRB, covers a group of 25 neighboring sub-carriers with around 375kHz bandwidth over 7 OFDM symbols. However, the PRB size of MU-MIMO only covers one spatial stream on a 25 subcarrier and 7 OFDM symbols grid. The Figure 7.2 illustrates the definition of PRB for the two SDM-FDPS concepts under investigation. Note that the SU-MIMO is a special case of the MU-MIMO, i.e., when the same UE gets allocated two streams on the same time-frequency resource.

The actual PRBs allocated to a UE are determined by the eNode-B scheduler together with the Modulation and Coding Scheme (MCS) for these resources. It encompasses entities such as LA and HARQ manager to perform overall scheduling decision. In our work, the CQI is simply the linearly averaged SINR over the PRB, but with a measurement and quantization error added. The overhead due to reference symbols or control information assumed is two OFDM symbols per TTI (28% overhead).

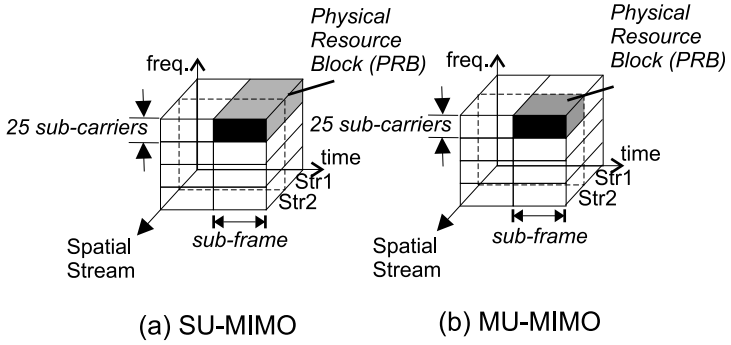

Figure 7.2: Illustration of SU-MIMO and MU-MIMO concepts.

7.3 MIMO Aware FDPS Algorithm

As a basis for this study we consider the well-known PF algorithm which provides an attractive trade-off between throughput and coverage gain [Weng05]. Here we extend it to the spatial domain for MU-MIMO. We estimate the equivalent and instantaneously supported throughput $R_{k,b,s}(t)$ for each UE k, on each frequency chunk b and for each stream s in the scheduling interval t. The PF scheduler selects the k^*th UE on each PRB which maximizes the PF metric $\frac{R_{k,b,s}(t)}{T_k(t)}$,

$$k^* = \arg\max_k \left\{ \frac{R_{k,b,s}(t)}{T_k(t)} \right\}, \quad k = 1...K, \quad \forall b, s \tag{7.1}$$

where $T_k(t)$ is the average delivered throughput to UE k in the past, which is calculated by an autoregressive filter [Holm01]. Note that for SU-MIMO and diversity MIMO, since the size of a PRB covers both streams on the same frequency chunk, we still use Equation 7.1, but without the spatial domain flexibility.

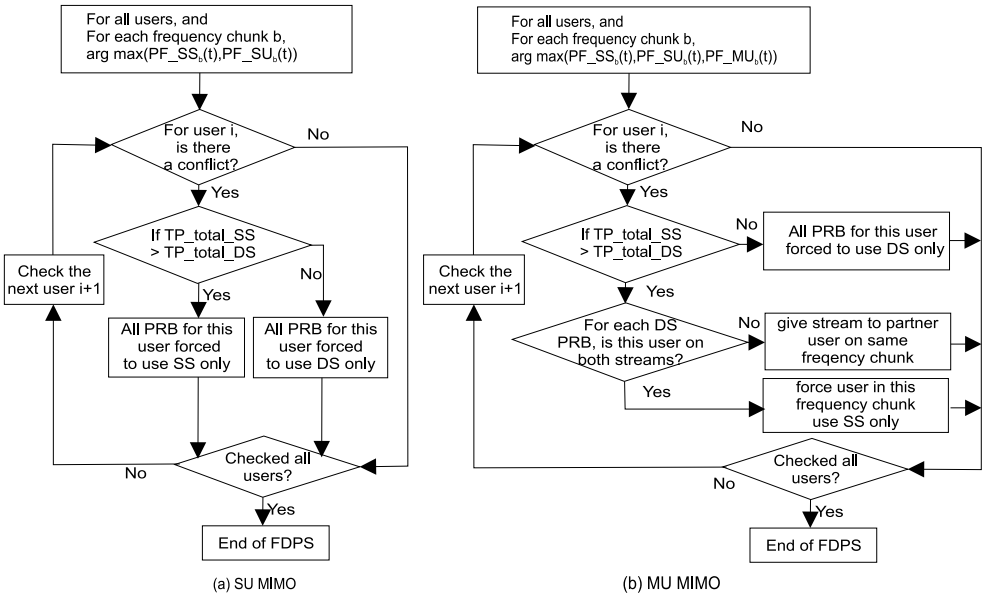

Figure 7.3: Flow chart of FDPS algorithm for SU- and MU- MIMO.

To extend the FDPS to work with SDM, an FDPS algorithm that takes the extra spatial dimension into account, particularly MIMO mode selection, is needed. Most of the previous work considers exhaustive and iterative search methods for optimal power, bit loading and MIMO selection, which is too complex for practical application, see for example [Digh03], [Jung04]. Moreover, although it is still an open issue in 3GPP, the flexible MCS adaptation per PRB is hard to achieve due to signaling constraints, thus only one MIMO mode for one UE within a TTI is supported in this study, which makes the performance suboptimum. However, the

algorithm design is efficient and suitable for practical implementation. Moreover, since SDM only makes sense for time-frequency resources in favorable channel conditions, we select transmit diversity schemes as the fallback MIMO mode. Thus to support FDPS with full flexibility, we further assume that CQIs for both *single-stream* (SS) and *dual-stream* (DS) MIMO are reported from the UE to eNode-B. The CQI is reported per stream for DS MIMO. Based on these considerations we propose the following simple, yet efficient algorithm which offers a good trade-off between performance and complexity.

In both cases, the first step is to estimate the user throughput using a SNR to supportable throughput mapping table (Figure 1.4 in Chapter 1) based on the CQIs reported for the individual PRBs for each user. Afterwards the PF metric is calculated for all MIMO cases. For single-stream MIMO and SU-MIMO, we denote PF_SS$_{k,b}(t)$, PF_SU$_{k,b}(t)$ as the PF metric value for each user k within each frequency chunk b at time interval t. And for MU-MIMO, PF_MU$_{k,b,s}(t)$ is assumed as the corresponding PF metric value used with smaller PRB definition. After that, for each frequency chunk b, the best user (or best users for MU-MIMO) is chosen to maximize the PF metric over all available MIMO schemes denoted as PF_SS$_b(t)$, PF_SU$_b(t)$ and PF_MU$_b(t)$ respectively. Note that special care should be taken when precoding is performed with MU-MIMO. The restriction is that the scheduler can only multiplex users with the same preferred precoding matrix, but with orthogonal precoding vectors (i.e., occupy different stream on the same time-frequency resource). The effect of this will be further explained in Section 7.5. On the basis of this, a first round MIMO mode selection is made for each frequency chunk, and user selection is done implicitly as well, as in the first block of the diagram of the proposed FDPS algorithms for SU- and MU- MIMO in Figure 7.3 (a) and (b) respectively.

A potential problem is that multiple MIMO modes can be selected for a single user, i.e., both dual-stream and single-stream mode are selected for the same user on different PRBs, within one TTI, which is contradicting the constraint we made. To avoid an iterative optimization process, the following simple and efficient approach is proposed for the two cases. As shown in Figure 7.3 (a) for SU-MIMO, whenever there is a conflict, we compare the total throughput from all the single-stream PRBs for this user (TP_total_SS) with that from all the dual-stream PRBs (TP_total_DS). Then the user is forced to use the MIMO mode which gives better total throughput. For the MU-MIMO case as shown in Figure 7.3 (b), when the single-stream mode is favored for a user, we make a decision for each dual-stream PRB depending on whether the other stream on the same frequency chunk is selected for this user or not. If the user is selected on both streams, this user is forced to single-stream for this frequency chunk, whereas this stream is assigned to partner user on the same frequency chunk if the opposite is true. Once the assignment of PRBs to users has been performed, the scheduler asks the LA to calculate the supported data rate for each user, also taking the selected MIMO mode into

account.

7.4 Theoretical Analysis

7.4.1 Post-Scheduling SINR Analysis

To gain insight into MIMO-FDPS principles, especially for SDM-FDPS, we consider the post scheduling SINR distribution using a simple analytical model for the PF scheduler which was originally used for SISO with time domain scheduling in [Holt00]. Assuming that the frequency chunk bandwidth is smaller than the coherence bandwidth of the channel, the per frequency chunk fading characteristics are equivalent to the flat-fading Rayleigh channel, and FDPS in frequency selective channel is equivalent to time domain Packet Scheduler (PS) in flat Rayleigh channel. Besides, as in [Holt00] some simplifying assumptions are adopted to enable this simple analytical model:

1. The fading statistics of all users are independent and identically distributed (i.i.d.). Users move with the same speed and have equal access probability.

2. A user's achievable data rate is (approximately) linearly related to its instantaneous received SINR.

3. A sufficiently long averaging window is used, so that the average received data rate of a user is stationary.

While these assumptions are unlikely to be perfectly fulfilled in reality, they suffice to provide insight into the PF scheduler. Based on these arguments and assumptions, we can directly adopt the model from [Holt00] where the PF metric in Equation 7.1 can be approximated by

$$k^* = \arg\max_k \left(\frac{\gamma_k(t)}{\overline{\gamma_k}}\right), \;\; k = 1...K \;\; , \tag{7.2}$$

where $\gamma_k(t)$ is the instantaneous SINR for the kth user at scheduling interval t, and $\overline{\gamma_k}$ is the average received SINR for the kth user. Let the *cumulative distribution function* (cdf) of the SINR for the kth user be $F_{\gamma_k}(\gamma)$. With K active users available for scheduling, denoted as User Diversity Order (UDO), the cdf of the normalized post-scheduling SINR γ^* is given by [Berg03]

$$F_{\gamma^*}(\gamma) = \left(F_{\gamma_k}\left(\frac{\gamma_k}{\overline{\gamma_k}}\right)\right)^K \;\; . \tag{7.3}$$

The normalized post-scheduling SINR distribution for various diversity MIMO schemes are shown in Figure 7.4. It can be seen that PF scheduling increases not only the diversity order, but also the mean SINR. As for the case of SFC with multi-user diversity, the so-called "channel hardening" effect makes it even worse compared to 1x2 SIMO in terms of the probability of having high SINRs [Hoch04]. The reason is that the SFC with more space diversity not only reduces the severity of destructive fades, but also the probability of encountering very high constructive fading peaks.

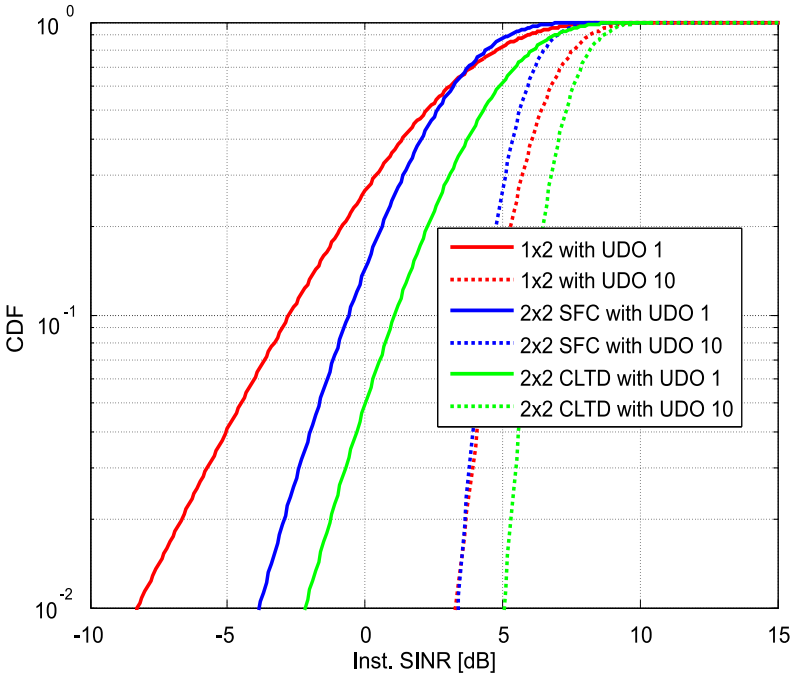

Figure 7.4: normalized post-scheduling SINR distributions of various diversity MIMO schemes, with and without user diversity order of 10.

In case of SDM scheme for one user with equal power allocation, the *cumulative distribution function* (CDF) of the per frequency chunk and per stream SINR is shown in Figure 7.5, curve (1). It is based on a *zero-forcing* (ZF) receiver and assumes that the G-factor is equal to 20 dB. For simplicity we consider all users to have the same G-factor for analysis in SDM-FDPS. The reason is that for SDM-FDPS, the users in lower G-factor will use single-stream MIMO schemes instead, which makes the analysis quite complicated. A high value of the G-factor was selected for illustration here since dual stream operation presupposes good channel conditions. To include the effect of two streams for SU-MIMO, The unified SINR approach proposed in Chapter 5 is utilized here to translate the streams SINRs γ_k into one effective SINR γ_u, which gives the same total capacity. Recall that the

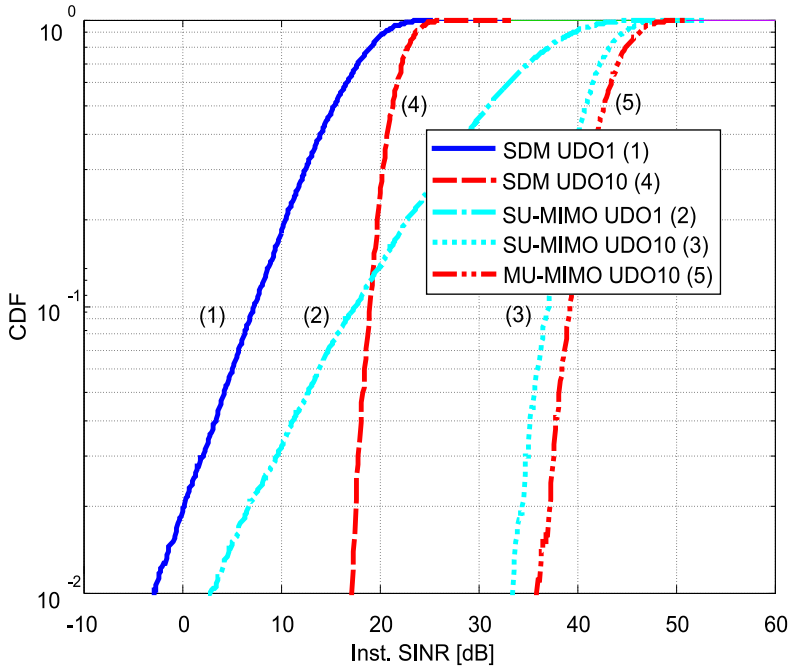

Figure 7.5: SINR distributions of the SU-MIMO and MU-MIMO schemes, with and without multi-user diversity of 10, at the G-factor of 20 dB.

unified SINR can be formulated as:

$$\log_2(1+\gamma_u) = \sum_{k=1}^{2} \log_2(1+\gamma_k) \tag{7.4}$$
$$\Leftrightarrow \gamma_u = -1 + \prod_{k=1}^{2}(1+\gamma_k) \ ,$$

and the CDF of the unified SINR as:

$$F(\gamma_u \leq U) \tag{7.5}$$
$$= \int_{1}^{U+1} p_{x_1}(x_1) \int_{1}^{\frac{U+1}{x_1}} p_{x_2}(x_2) \ldots dx_1$$
$$= \int_{1}^{U+1} p_{\gamma_1}(x_1-1) \int_{1}^{\frac{U+1}{x_1}} p_{\gamma_2}(x_2-1) \ldots dx_1 \ ,$$

where the $p_{\gamma_k}(\gamma_k)$ is the *probability density function* (PDF) of γ_k, the $p_{x_k}(x_k)$ is the PDF of x_k, and $x_k = \gamma_k + 1$. In this case, Equation 7.5 is a two-dimensional integral. By inserting the SDM stream SINR distribution (curve (1)) in Equation

7.5 for both $p_{\gamma_1}(\gamma_1)$ and $p_{\gamma_2}(\gamma_2)$, the distribution of unified effective SINR for SU-MIMO can be derived as

$$F_{SU-MIMO}(\gamma_u \leq U) = \int_1^{U+1} \frac{1}{m} e^{-\frac{x_1-1}{m}} (1 - e^{-\frac{\frac{U+1}{x_1}-1}{m}}) dx_1 \quad , \tag{7.6}$$

where $m = \frac{\gamma_0}{2}$ and γ_0 is the average SINR per receive antenna. The CDF of Equation 7.6 is shown in Figure 7.5, curve (2). Applying the PF criterion, *i.e.* , add the multiuser diversity on top of that, the CDF of the post scheduling per PRB unified SINR for SU-MIMO can be given as

$$F_{SU-MIMO\_K} = (F_{SU-MIMO})^K \quad , \tag{7.7}$$

The CDF curve given by Equation 7.7 for UDO equal to 10 is shown in Figure 7.5, curve (3).

In case of MU-MIMO, since the multi-user diversity can be exploited even in the spatial dimension, the multiuser diversity should be utilized before translated into the unified SINR. Therefore, the CDF of the post-scheduling SINR on each stream with multiuser diversity of 10 is given by

$$F_{SDM\_K} = (F_{SDM})^K \quad , \tag{7.8}$$

This is shown in Figure 7.5, curve (4). Then the two stream SINRs with the same distribution as in Equation 7.8 are combined into a single effective unified SINR, as given by

$$F_{MU\_MIMO\_K}(\gamma_u \leq U) = \int_1^{U+1} K(1 - e^{-\frac{x_1-1}{m}})^{K-1} \frac{1}{m} e^{-\frac{x_1-1}{m}} (1 - e^{-\frac{\frac{U+1}{x_1}-1}{m}})^K dx_1 \ . \tag{7.9}$$

The post-scheduling per frequency chunk unified SINR distribution for MU-MIMO of Equation 7.9 is shown in Figure 7.5, curve (5). Comparing the curve (4) and curve (5) in Figure 7.5, the unified SINR of the MU-MIMO scheme has a mean SINR gain over that of the SU-MIMO scheme with the same UDO due to the extra flexibility of the spatial domain, although the diversity order is approximately the same. The above analysis could also be extended to other antenna configurations.

7.4.2 Throughput Analysis

Based on the post-scheduling SINR analysis, we are ready to get the performance bounds for each SDM-FDPS cases. One important prerequisite is the choice of

the SINR to throughput mapping metric. The most common metric is the Shannon Formula [Shan48] given as:

$$C = \log_2(1 + SNR) \ . \tag{7.10}$$

As shown in [Moge07b], a better approximation to realistic link adaptation model with realistic MCS is the "***Scaled Shannon***" formula, as proposed in [Moge07b]. It is given by

$$C = BW_{eff} \times \log_2(1 + SNR/SNR_{eff}) \ . \tag{7.11}$$

Here the BW_{eff} is adjusted according to the system bandwidth (BW) efficiency of the system and SNR_{eff} is adjusted according to the SNR implementation efficiency. The BW_{eff} is 0.83 considering LTE system parameters and SNR_{eff} is 1.6dB in AWGN channel with realistic modulation and coding [Moge07b]. Furthermore we upper limit C according to the hard spectral efficiency given by the MCS supported in simulation study, e.g. 64QAM, Rate 4/5.

The throughput at a certain G-factor TP_G is given as

$$TP_G = \int_0^\infty F_{Map}(x) \cdot p_\gamma(x) \cdot dx \ , \tag{7.12}$$

where the F_{Map} is the SINR to throughput mapping function which can use either Shannon formula (Eqn. (7.10)) or Scaled Shannon (Eqn. (7.11)). The $p_\gamma(x)$ is the PDF of post-scheduling SINR distribution, which can be obtained by taking the derivative of Eqn. (7.7) for SU-MIMO or Eqn. (7.9) for MU-MIMO.

With the knowledge of TP_G for each G-factor and the PDF of the G-factor distribution p_G for a certain cellular deployment scenario [Kova06], the cell level throughput can be written as:

$$TP_{cell} = \int_0^\infty TP_G(G) \cdot p_G(G) \cdot dG \ , \tag{7.13}$$

where the TP_G is a function of G. Note that the simplified analysis above will only be used to obtain the theoretical bounds, while the detailed system simulation based evaluation in section 7.5 is not limited by these simplifications.

7.5 Performance Evaluation

7.5.1 Evaluated MIMO Schemes

Although the main contribution from this PhD study is on SDM-FDPS, we show results for diversity MIMO FDPS as well as SDM-FDPS for completeness. Thus

for diversity MIMO, we consider the 2x2 SFC and 2x2 CLTD. As for SDM, the schemes need to be divided into precoding cases and without precoding cases. Since the SDM can only be efficiently utilized for users with good channel quality and high rank MIMO channel, single-stream MIMO schemes should be used as fallback mode for the users in the cell edge or low rank MIMO channel conditions. For no precoding case, we use *per-antenna rate control* (PARC) with *space frequency coding* (SFC) as fallback mode. In the unitary precoding case, we utilize the CLTD (CL Mode 1) for single stream transmission [Wei06d], and dual stream TxAA (D-TxAA) [Moto06] for dual stream transmission. In both cases, the weight is optimized for a group of sub-carriers within a PRB, and the feedback requirements are 2 bits per PRB. Since the optimal design of codebooks specifically for D-TxAA is still an open issue, the TxAA codebooks are adopted for D-TxAA as well in this study. For comparison purposes, we consider as reference scheme the 1x2 SIMO with PF FDPS [3GPP06a]. The MIMO schemes and the receiver types considered are summarized in Table 7.1. Other system assumptions are as explained in Chapter 6.

Table 7.1: MIMO schemes and receiver types considered.

MIMO mode	No precoding	With precoding	Receiver Type
(SU-) MU- MIMO (Dual-stream)	PARC	D-TxAA	Linear MMSE
Fallback mode (Single-stream)	SFC	CLTD	Maximal Ratio Combining (MRC)

7.5.2 Finite Buffer Performance

This subsection considers the finite buffer best effort traffic model, while the comparison against infinite buffer model is shown in next subsection.

The average cell throughput is first plotted against number of active users for different single-stream MIMO schemes in macro-cell scenarios in Figure 7.6. The localized RPB results are with FDPS, and the distributed PRB results are with time domain Packet Scheduler (TDPS) only. As shown, for results with TDPS only, the CLTD 2x2 achieves the best performance, and the 1x2 SIMO is the worst. Moreover, we can see that the gain from TDPS is quite limited with increase in UDO for such a frequency selective channel profile considered. When the FDPS is utilized, the cell throughput increases much faster than the TDPS with the increase in UDO. The CLTD 2x2 with FDPS still achieves the best performance among them. However, the performance of 1x2 SIMO FDPS is better than 2x2 SFC FDPS with UDO larger than 2. This is called the “channel hardening” effect of SFC, which is extensively studied by [Hoch04]. The trend of results can also be well

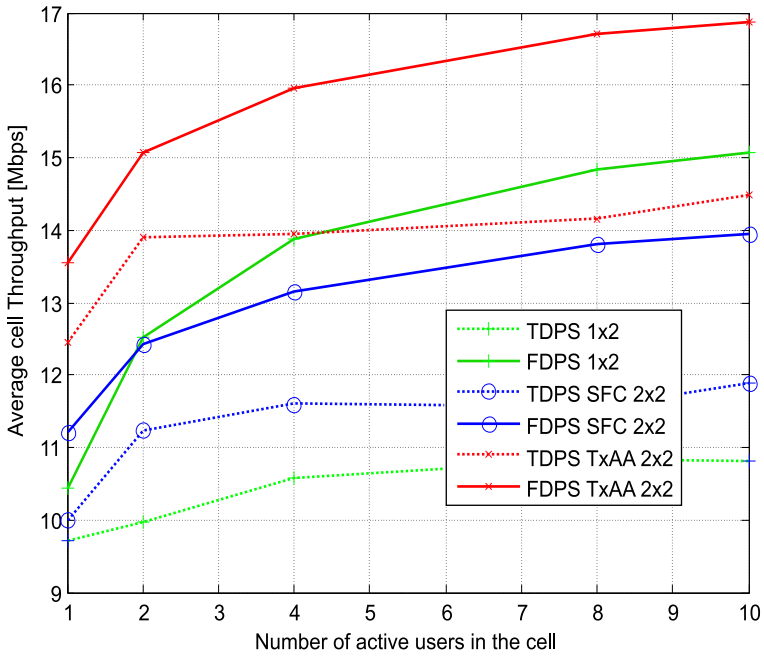

Figure 7.6: Average cell throughput comparison of diversity MIMO schemes with distributed PRB or localized PRB definition in macro cell with finite buffer best effort traffic model.

predicted from the SINR analysis in Figure 7.4. Of course the required signalling for TDPS is lower than FDPS. That is, only one CQI for the whole bandwidth for TDPS while CQI per PRB is necessary to obtain the full flexibility in FDPS. The tradeoff between the amount of CQI signalling and scheduling flexibility and will be further explained in Subsection 8.2.3.

The average cell throughput is plotted against number of active users for different SDM-FDPS schemes in macro-cell and micro-cell scenarios. For the macro-cell case shown in Figure 7.7 it is observed that both SDM schemes without precoding offer only marginal gain over 1x2 SIMO case, over the considered range. This is due to limited SINR dynamic range available in macro-cells, e.g., the highest G-factor is limited to 17 dB. However, the gain of SDM schemes increases with precoding cases, e.g., at UDO of 10 the gain is around 20% over reference scheme. The gain comes mostly from cell edge users benefiting from the CLTD feature, as illustrated in Figure 4.7. The drawback of precoding cases is the extra weight feedback requirement. Among the precoding cases MU-MIMO outperforms SU-MIMO especially when the UDO is low, due to the increase in degree of spatial freedom available to the scheduler.

As for the micro-cell scenario, the results in Figure 7.8 convey a slightly different picture. If we take UDO of 10 as an example, the SU-MIMO scheme without precoding gives a gain of around 10% over the reference case. When precoding

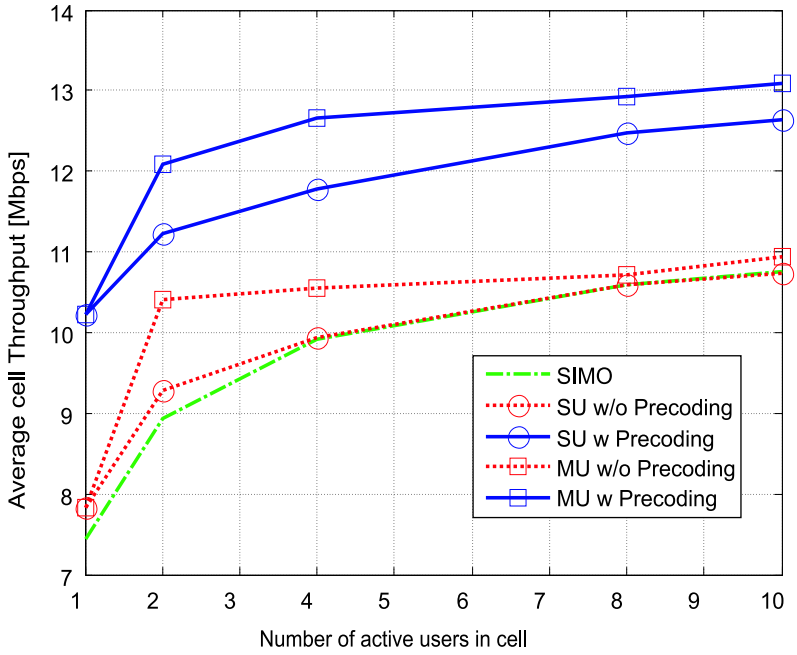

Figure 7.7: Average cell throughput comparison of SDM MIMO schemes in macro cell with finite buffer best effort traffic model.

is introduced, the gain from SU-MIMO increases to around 15%. With increasing UDO the cell throughput increases very slowly. The behavior of MU-MIMO without precoding is quite different as the cell throughput has a steeper increase than the SU-MIMO curves. Although it is worse than SU-MIMO with precoding when the UDO is low, it outperforms SU-MIMO with precoding when UDO exceeds 21. Compared to that of MU-MIMO without precoding, the results of MU-MIMO with precoding grow much slower with the increase in the UDO. One of limitations comes from the reduced effective UDO due to precoding restriction. As mentioned earlier, for MU-MIMO with precoding, we can only multiplex users with the same preferred precoding matrix, but with orthogonal precoding vectors. For the precoding schemes we considered, namely D-TxAA with 4 precoding quantization matrix options, the active users are divided into 4 groups. Then the effective UDO is the number of users with same preferred precoding matrix selection. To further explain this, the probability of distribution of the effective UDO traces collected from simulation of MU-MIMO with precoding is shown for UDO of 4, 10, 30 in Figure 7.9. As shown, when UDO is 4, the effective UDO is around 1.8 in average. The average effective UDO is only around 3.4 and 8.9 for a UDO of 10 and 30. This also suggests a dilemma we might face when MU-MIMO with unitary precoding is used. If we increase the quantization resolution in the precoding matrix, we can improve the link performance since the spatial streams will be made more orthogonal to each other. On the other hand, the effective UDO will be reduced, and the gain from FDPS will be lower with less multi-user diversity. Another

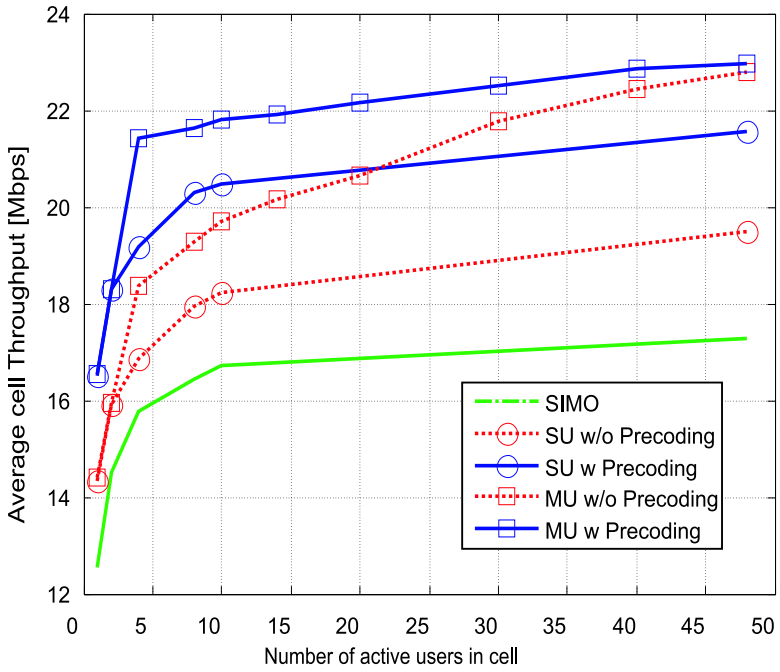

Figure 7.8: Average cell throughput comparison of SDM MIMO schemes in micro cell with finite buffer best effort traffic model.

limiting factor for the results of MU-MIMO comes from the limited modulation order. As shown in Figure 7.10, we plot the CDF of the post-scheduling effective SINR from simulation for selected cases of MU-MIMO with or without precoding. The highest MCS we have used is the 64QAM and 4/5, and for this MCS an effective SINR of 17dB will always have a BLER of 0, *i.e.* , the throughput with effective SINR higher than 17dB will saturate. At the UDO of 30, the MU-MIMO without precoding has 15% of the time entering the saturation range, while the MU-MIMO with precoding has 24% of the time being in the saturation range. In summary, when the UDO is 10, the gain of MU-MIMO scheme over reference is in the order of 16-30% depending on whether precoding is used. When the UDO is around 48, the gain is in the order of 35%. Results confirm that the SDM concepts are mainly features for the micro-cell scenario. The complete results for different MIMO schemes in micro and macro scnearios are summarized in Table 7.2.

To show the average user data rate performance, the CDF of user throughput distribution is plotted for various cases in micro cell, as shown in Figure 7.11, assuming 10 active users in the cell. For the 5% outage point for various cases, the coverage user throughput is around 900k bits/s in the cases without precoding, while the coverage user throughput can be increased to 1100k bits/s in the precoding cases. Regarding the peak user throughput, the MU-MIMO without precoding achieves the highest peak data rate, but with a sacrifice in the coverage user performance.

Table 7.2: Comparison of the average cell throughput [Mbps] with different MIMO schemes for UDO of 10 with finite buffer traffic model

MIMO schemes	1x2	2x2 SFC	2x2 CLTD	2x2SU w/o pre-coding	2x2SU w pre-coding	2x2MU w/o pre-coding	2x2MU w pre-coding
Macro cell	10.76	9.96	12.05	10.74	12.63	10.93	13.07
(Gain over 1x2 %)	(0%)	(-7%)	(12%)	(-0.2%)	(17%)	(1.6%)	(21%)
Micro cell	16.64	15.71	17.97	18.21	20.48	19.71	21.79
(Gain over 1x2 %)	(0%)	(-5%)	(8%)	(9.4%)	(23%)	(18%)	(31%)

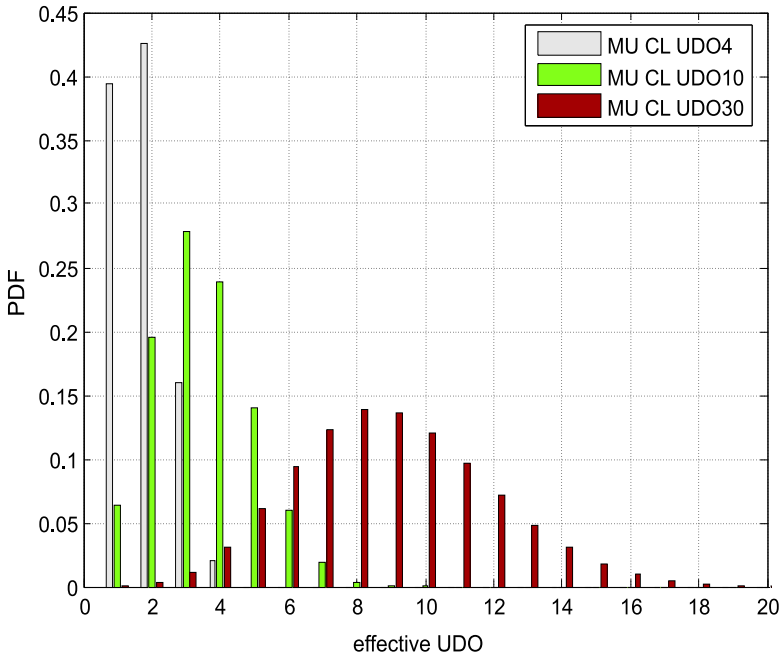

Figure 7.9: The sample PDF distribution of the effective UDO measured from simulation.

7.5.3 Performance of Finite Buffer versus Infinite Buffer

The traffic model has a significant impact on SDM performance. The average cell gain over 1x2 MRC case with FDPS is plotted for different traffic models

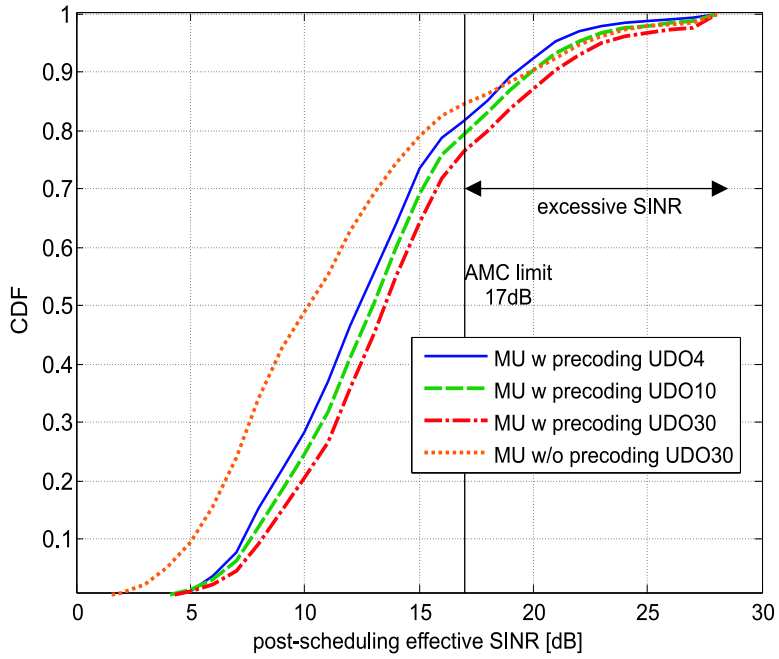

Figure 7.10: The sample CDF distribution of post-scheduling effective SINR from simulation.

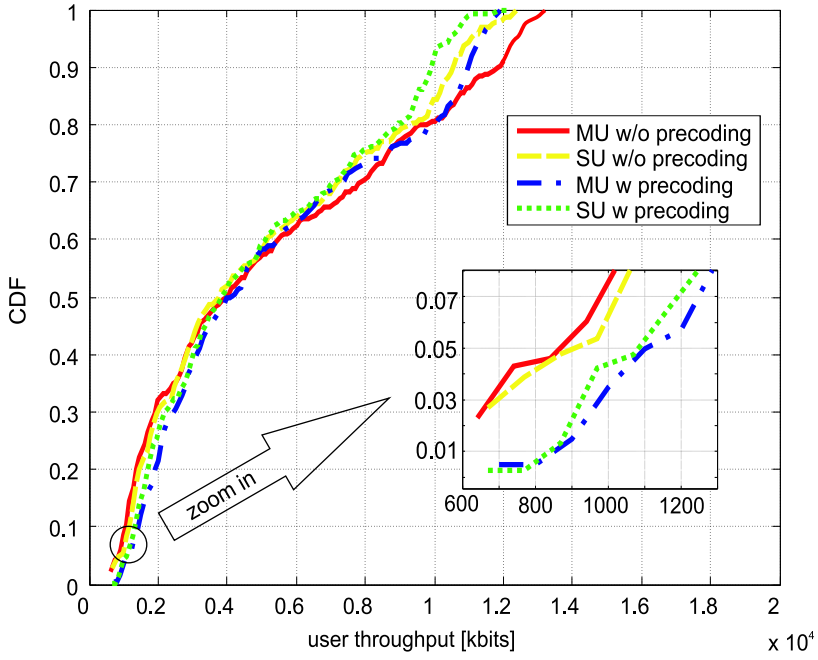

Figure 7.11: The user throughput distribution for various SDM-FDPS case in micro cell.

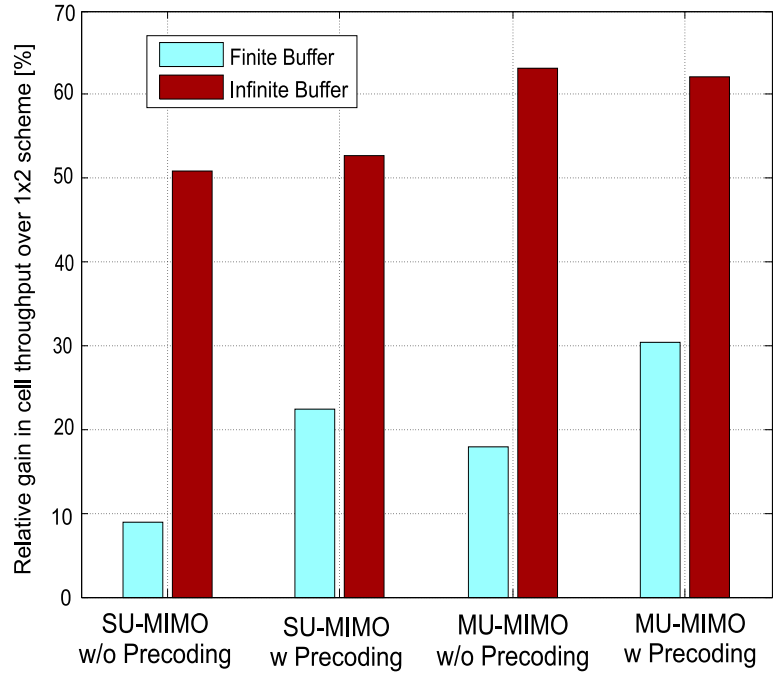

Figure 7.12: Relative cell throughput gain of SDM FDPS over 1x2 FDPS in micro cell for different traffic model at UDO of 10.

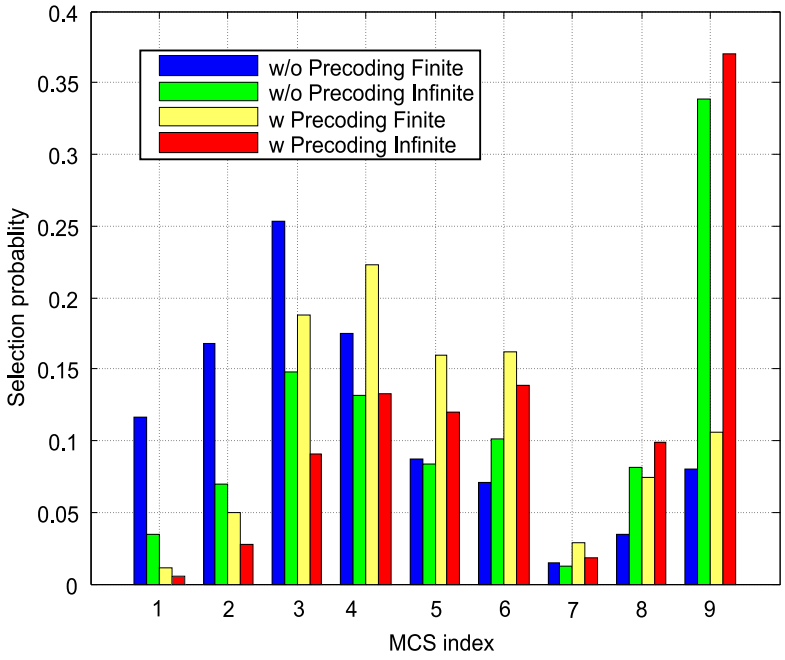

Figure 7.13: MCS selection probability for MU-MIMO for different traffic model in micro cell at UDO of 10.

in Figure 7.12. As shown with finite buffer, the gain is from 10-30%, and for infinite buffer, the gain is in the order of 50-60%. The reason for higher gain with infinite buffer model can be explained by the analysis in Subsection 6.2.5. Since equal amount of data is sent to all users in the cell, the finite buffer model results in a longer session time for the low data rate cell edge users than the users in good condition. On the other hand, for the infinite buffer model all users will be given equal access time, and the users supporting high data rate can download much more data than users in the cell edge, thus the average cell throughput is increased. In Figure 7.13, the MCS selection probability is shown for MU-MIMO with both traffic models. The MCS from QPSK 1/3 to 64QAM 4/5 is numbered incrementally as 1 to 9. The results clearly indicate that the probability of selecting the highest MCS is increased significantly when using infinite buffer best effort model compared to the finite buffer model. Considering the finite buffer traffic model cases only, the probability of selection of MCS 4-9 for the scheme with precoding is shown to be higher than the scheme without precoding. This implies that the precoding increases the user experienced SINR and thus increases the cell throughput.

7.6 Comparison of Theoretical Bounds with Simulation Results

The derived theoretical bounds in section 7.4 and the system-level simulation results in section 7.5 are compared here to illustrate the effect from practical factors which is not feasible to be included in theoretical analysis.

The user throughput with SDM-FDPS against G-factor curves are first plotted for the theoretical bounds (using Eqn. (7.12)) and simulation results in Fig. 7.14. As observed, a quite good approximations can be found with the scaled Shannon bounds by including realistic LA effect. The remaining difference between the theoretical bounds with the simulation results can be due to some imperfection factors such as the frequency selectivity within a frequency chunk, non-ideal CQI as well as signalling constraints. Further, we compare the cell level throughput for theoretical approaches (using Eqn. (7.13)) and simulation results for different cell scenarios, as shown in Fig. 7.15. The approach using scaled Shannon can make the bound quite close to the Monte Carlo simulations results, i.e., within a 10%-30% range.

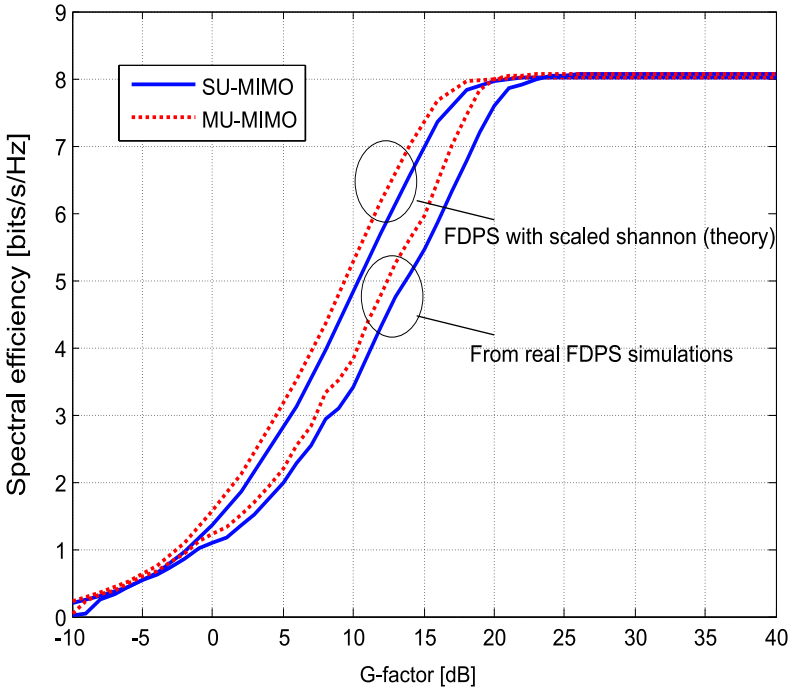

Figure 7.14: Comparison of G-factor versus throughput between theoretical bounds and simulation results.

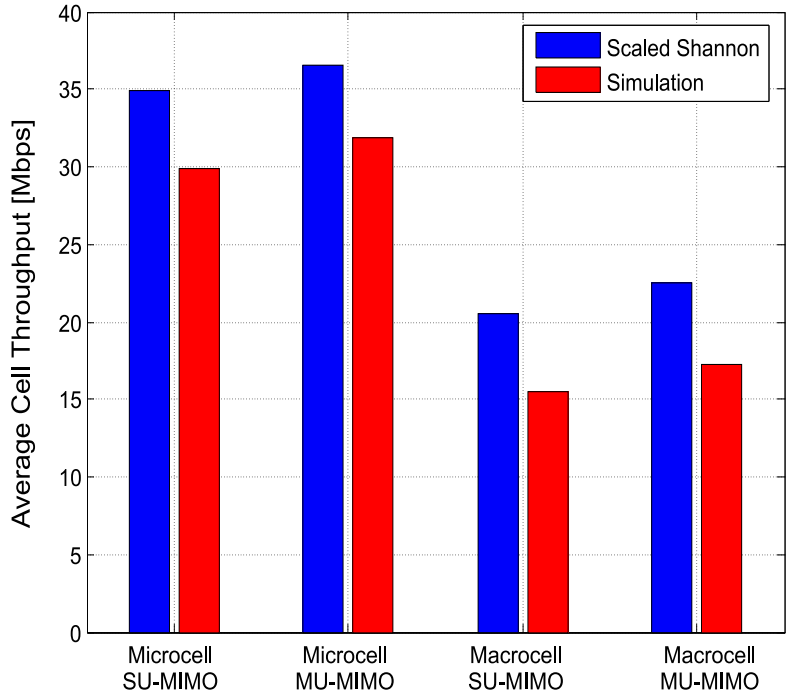

Figure 7.15: Comparison of cell throughput between theoretical bounds and simulation results under infinite buffer best effort traffic model.

7.7 Summary

In this chapter we evaluated the obtainable average cell throughput for MIMO combined with FDPS based on UTRAN LTE downlink. The special emphasis is put on spatial multiplexing mode MIMO. A proportional fair scheduler extended to frequency and spatial domains is used in the study. The theoretical analysis of post-scheduled SINR distribution is first carried out for various MIMO-FDPS schemes. The impact of traffic model is shown to be a critical factor in performance evaluation. With the more realistic finite buffer best-effort traffic model, results show no observable gain from SDM-FDPS without precoding in the macro-cell case over the 1x2 MRC (reference case), while the gain with precoding is around 20%. Results also reveal that in the micro-cell scenario a gain in cell throughput of around 10% and 18% is obtainable with SU- and MU- MIMO schemes respectively without precoding. With precoding, the gain can be increased to 22% and 30% respectively. These results assume 10 active users in the cell. Finally, the theoretical bounds are shown to be able to predict the realistic system simulation results within a 10%-30% range. Although good potential of MIMO with FDPS is shown in this chapter, the signalling overhead to support MIMO-FDPS is a crucial issue for its practical usage. This will be addressed in the next chapter.

Chapter 8

Design and Analysis of Signalling Reduction for FDPS MIMO

8.1 Introduction

The studies in the previous chapter show that the MIMO in SDM mode combined with FDPS (SDM-FDPS) can further enhance the LTE performance [Wei07b]. To enable SDM-FDPS, the uplink CQI report from each UE is required per stream and per frequency chunk. Moreover, since SDM can only be used when the channel conditions are quite good, a fallback MIMO mode is also required. Thus, in order to provide full flexibility at the packet scheduler, the UE needs to report CQIs for all the available MIMO modes, thus making the overhead impractically large. In terms of downlink control signaling, the eNode-B needs to inform the UE about the current resource allocation. This overhead is also a function of the number of available frequency chunks and MIMO streams.

In this chapter the methods to mitigate the signaling requirement for SDM-FDPS are investigated. For example, in order to reduce the signaling of CQI reports for all the available MIMO modes, we consider a semi-adaptive approach where each UE supports only one MIMO mode at a certain time interval. The MIMO mode can only be updated on a slow basis, e.g., every 100 ms. In terms of CQI bandwidth reduction, previous work in [Gesb04] proposed an efficient technique to reduce the CQI overhead for time-domain only packet scheduling by letting the UE report the CQI only when the channel is "good", i.e., when channel quality exceeds a certain threshold. Another efficient threshold-based CQI scheme proposed in [Kold06] reduces the CQI signaling overhead for FDPS significantly by including both threshold-based signaling and time-staggered reporting methods. In this study we extend these techniques to support SDM-FDPS as well. The trade-off be-

tween the reduction in uplink signaling and achievable SDM-FDPS performance is evaluated using system-level simulations. The rest of the chapter is organized as follows: To reduce the increased signalling requirement for SDM-FDPS, Section 8.2 proposed several efficient methods, and the signalling is estimated as well. Detailed simulation results are shown and explained in Section 8.3, while the main conclusions are summarized in Section 8.4.

8.2 Signalling Reduction Methods

The reference case in terms of signaling is based on fast-adaptive MIMO selection, such that the MIMO mode (single or dual-stream) is selected every TTI. The SDM scheme utilizes separate data rate adjustment on each stream, i.e., the multi-codeword (MCW) is used. The UEs need to report CQIs for all the available MIMO modes based on the absolute CQI (AB-CQI) scheme. In order to reduce the signaling overhead the following reduction methods are considered.

8.2.1 Semi-adaptive MIMO Mode Selection

If we recall from the analysis in Chapter 5, the fast-adaptive MIMO selection is always better than semi-adaptive MIMO selection in flat Rayleigh channel in a single-user link. Most of the fast adaptive MIMO gain comes from the flexibility to use less streams when there is channel condition deficiency for higher multi-stream transmission on some time instances. However, when combined with FDPS, the scheduler behavior needs to be considered as well. As an example we perform fast adaptive MIMO together with FDPS for SU-MIMO without precoding as shown in Figure 8.1. The slow adaptive MIMO will use SFC when G-factor is below 0 dB, and use PARC when G-factor is higher than 0 dB. As shown, there is almost no gain from fast adaptive MIMO over slow adaptive MIMO when FDPS is utilized. The reason is that the scheduler will only utilize the very best channel conditions from many active users in the cell, and the probability of encountering bad channel condition is quite low.

Motivated by the above analysis, we consider a semi-adaptive approach for MIMO mode selection with SDM-FDPS, in which the MIMO mode is chosen on a slow update basis ($\sim$100ms), and the UE only needs to feed back CQI for the selected MIMO mode. Semi-adaptive MIMO selection will put more restriction on the scheduling freedom, but with a reduced signaling requirement specially on CQI feedback.

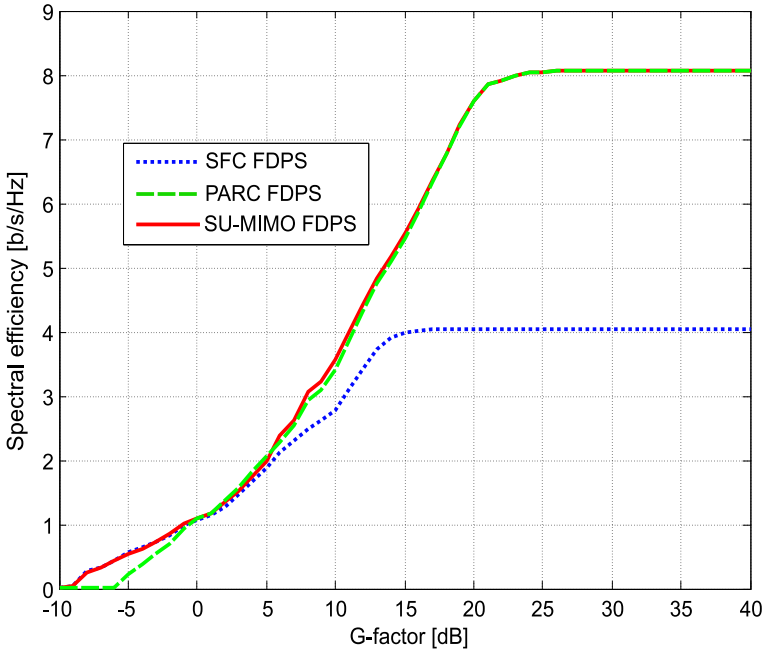

Figure 8.1: Spectral Efficiency of fast adaptive MIMO with FDPS at UDO of 10.

8.2.2 Single Codeword (SCW) for SDM

Previous link level studies show that the MCW can achieve better performance compared to SCW if simple linear receivers are used [Noki06a] since the MCW can adapt to the unevenness between the streams better than SCW. However, when combined with FDPS, we also need to consider the effect from the scheduler behavior. The loss of using SCW instead of MCW is expected to be quite low in this case. For MU-MIMO, the scheduler tends to schedule only the better stream if the unevenness between streams gets high. On the other hand, the scheduler for SU-MIMO will select only the user whose streams are quite similar in quality since the scheduler decision is based on total throughput from both streams. Besides, considering the practical restriction that only one MCS is used per user per stream, the variation between channel quality in different scheduled RPBs for same UE also becomes an important factor. As shown in Figure 8.2, we plot the average number of users scheduled versus available users in the cell for SU-MIMO with or without precoding as examples. When the UDO is low, the number of users scheduled is also low, and the number of RPBs allocated to one scheduled user is high. Considering the frequency selectivity, the average quality of two streams for one UE over so many PRBs gets quite similar. Of course we can foresee that when the UDO is high, and one UE gets only around one frequency chunk, the unevenness between two streams will certainly make the MCW more efficient than SCW. But at that time the gain of FDPS usually starts to saturate. Based on these arguments,

we consider to evaluate the performance of using only SCW for SDM-FDPS, by which the downlink control signalling concerning transport format can be reduced.

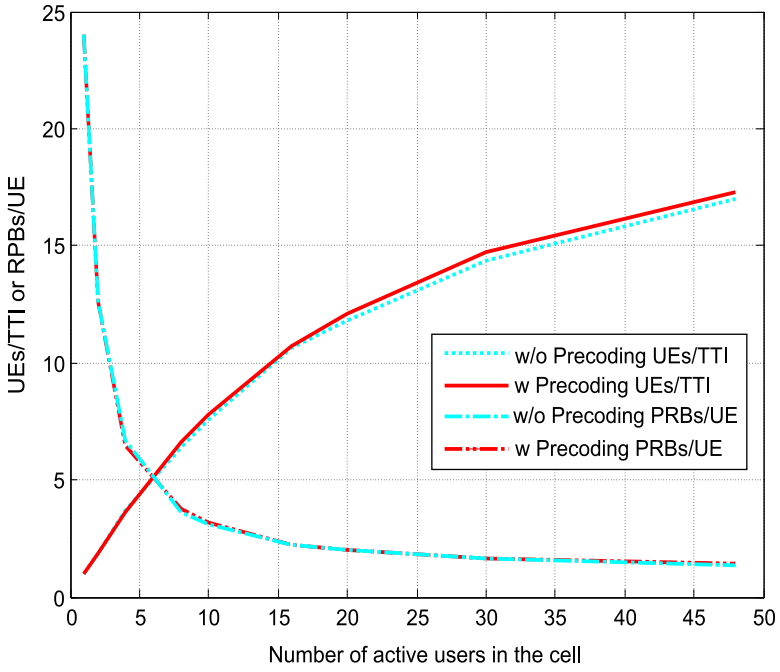

Figure 8.2: Average number of UEs scheduled per TTI and average number of RPBs allocated to one scheduled UE versus the UDO.

8.2.3 Threshold Based CQI Reduction

As mentioned earlier, the CQI signalling requirement will increase linearly with the number of scheduling units and the number of UEs. With limited uplink resources, the CQI bandwidth reduction is crucial for the system design. The technique proposed in [Gesb04] for time domain PS can reduce the CQI signalling by letting the UE report the CQI only when the channel is "good", i.e., when the channel quality exceeds a certain threshold. The variant of this for FDPS is called "best-M" scheme [Noki07a] in which only the full CQIs for the M selected PRBs are reported. To further compress the required signalling, another efficient threshold-based CQI scheme proposed in [Kold06] reduces the CQI signaling overhead for FDPS significantly by including both Threshold CQI (TH-CQI) signaling and time-staggered reporting methods. One variant of the TH-CQI scheme is illustrated in Figure 8.3. As shown, the threshold is given in terms of a SINR value with an offset $\triangle TH$ added to the average wide-band SINR, *i.e.* , the G-factor. The "best PRBs" are those that have a better channel quality than the sum of average SINR and the offset. The TH-CQI consists of the linear average of the SINR over the best PRBs and a bitmap indicating the identity of those PRBs. The main drawback

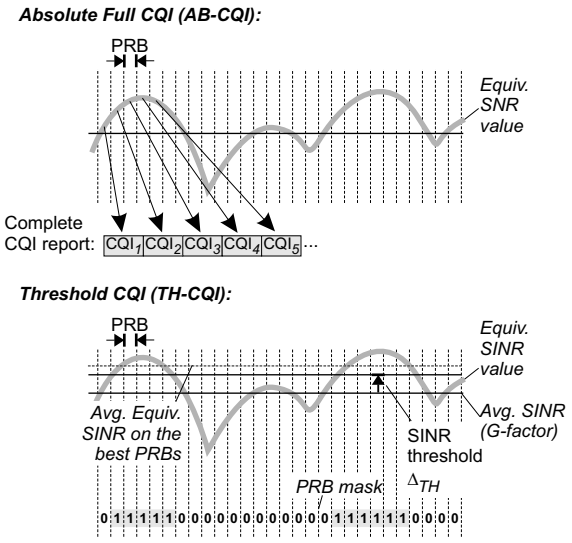

Figure 8.3: Graphical illustration of the full CQI and reduced CQI schemes.

of this scheme is that it limits the flexibility of the downlink scheduler. Apparently since TH-CQI only has one averaged quality value of all selected M PRBs, the variation within the multiple PRBs should be low enough to maintain a good scheduling decision. On the other hand, the number of selected RPBs should also be large enough such that the scheduling outage can be kept low. The scheduling outage is defined as the probability that there is no user reporting on a certain PRB. Another problem is that the optimized threshold value is potentially dependent on other factors such as the channel profile, G-factor, UDO, scheduling algorithm, etc. All the problems listed make the optimization of the threshold a quite complicated task which may require quite extensive simulations.

For reasonable complexity we choose to use the theoretical analysis on CDF curves of post-scheduled SINR in Figure 7.5 to determine the threshold values instead. When the scheduling outage happens, we will randomly pick one UE to schedule on this PRB. Therefore, in case of MU-MIMO, since the PRB is only one stream of a frequency chunk, the CDF curve of SDM with UDO 10 is used as reference, *i.e.* , the Figure 7.5, curve (4). The threshold is selected to be 17 dB for a G-factor of 20dB, which corresponds to the 1% outage point. Since the relative offset is constant for MU-MIMO, the threshold will always be 3dB below the G-factor for each UE with different G-factor. As for SU-MIMO, we use the 1% outage point in curve (3) in Figure 7.5 as the threshold value for RPB unified SINR threshold. Only when the PRB unified SINR exceeds the threshold, the RPB is selected. Note that contrary to MU-MIMO, the offset value for SU-MIMO varies with the G-factor.

8.2.4 Signalling Analysis

We now consider an estimation of the various signalling reduction schemes discussed above. As the detailed signaling format is still an open issue in LTE, only a rough estimate of the overhead is made.

Table 8.1: Signalling estimation for various MIMO schemes with FDPS.

MIMO schemes with various signalling reduction	Uplink Signalling bits/update/user		Downlink Signalling bits/update
	w/o precoding	w precoding	
Diversity MIMO AB-CQI (reference)	120	168	184
Diversity MIMO TH-CQI	29	29+2M	184
2x2 SU-MIMO AB-CQI fast-adaptive MCW (reference)	360	456	254
2x2 SU-MIMO AB-CQI semi-adaptive MCW	180	228	234
2x2 SU-MIMO AB-CQI semi-adaptive SCW	180	228	184
2x2 SU-MIMO TH-CQI semi-adaptive SCW	32	32+2M	184
2x2 MU-MIMO AB-CQI fast-adaptive MCW	360	456	337
2x2 MU-MIMO AB-CQI semi-adaptive MCW	180	228	317
2x2 MU-MIMO AB-CQI semi-adaptive SCW	180	228	267
2x2 MU-MIMO TH-CQI semi-adaptive SCW	44	44+2M	267

In terms of uplink signaling the resolution for CQI is assumed to be 5 bits per frequency chunk per stream (assuming similar SINR dynamics as Rel. 6 HSDPA [Holm01]), and the 10 MHz divided into 24 frequency chunks. The CQI signaling overhead for the diversity MIMO scheme with FDPS will be equal to $N_{\text{FC}} \times N_{\text{CQI}} = 24 \times 5 = 120$ bits/update/user with the AB-CQI scheme, where N_{FC} is the number of frequency chunks and N_{CQI} is the CQI resolution. The overhead can be reduced to $N_{\text{FC}} + N_{\text{CQI}} = 24 + 5 = 29$ bits/update/UE if the

TH-CQI is used instead, in which 5 bits are used for the CQI value and 24 bits are the mask bits. SDM-FDPS with fast-adaptive MIMO mode selection requires $N_{\text{CQI}} \times N_{\text{FC}} \times 2 + N_{\text{CQI}} \times N_{\text{FC}} = 24 \times 5 \times 3 = 360$ bits/update/user, based on AB-CQI and three CQI reports (two CQIs for dual-stream and one CQI for single-stream) per user. Semi-adaptive MIMO mode selection can reduce the CQI signaling by 50% compared to the fast-adaptive case, *i.e.* , $0.5 \times N_{\text{CQI}} \times N_{\text{FC}} \times 2 + 0.5 \times N_{\text{CQI}} \times N_{\text{FC}} = 0.5 \times 240 + 0.5 \times 120 = 180$. This assumes that there is an equal number of single-stream and dual-stream users in the cell, thus half of the users need 240 bits/update, and half of the users need 120 bits/update. The actual ratio between dual-stream and single-stream user will vary depending on scenarios. When the TH-CQI scheme is utilized together with the SU-MIMO semi-adaptive approach, the CQI overhead can be reduced to $0.5 \times (N_{\text{FC}} + N_{\text{CQI}}) + 0.5 \times (N_{\text{FC}} + (N_{\text{CQI}} \times 2)) = 0.5 \times 29 + 0.5 \times 34 \approx 32$ bits/update/user, i.e., 91% reduction of the overhead can be achieved compared to the fast-adaptive scheme with AB-CQI. As in the case where TH-CQI is combined with MU-MIMO semi-adaptive selection, the CQI signalling is $0.5 \times (N_{\text{FC}} + N_{\text{CQI}}) + 0.5 \times (2 \times N_{\text{FC}} + (N_{\text{CQI}} \times 2)) = 0.5 \times 29 + 0.5 \times (48 + (5 \times 2)) \approx 44$ bits/update/user.

Concerning the precoding schemes, the extra weight feedback of Q bits has to be considered in uplink signalling as well. In this study we assume 2 bits per frequency chunk. For diversity MIMO with FDPS, the reference uplink signalling is increased to $N_{\text{FC}} \times N_{\text{CQI}} + N_{\text{FC}} \times Q = 120 + 24 \times 2 = 168$ bits/update/user. With TH-CQI, obviously we only need feedback weight for the M selected RPBs, thus the total signalling will be $29 + Q \times M$ bits/update/user. Similarly, for SDM-FDPS, the extra weight feedback with fast MIMO adaptation is $2 \times N_{\text{FC}} \times Q = 96$ bits/update/user since both weights for single-stream and dual-stream schemes should be fed back. And this can be reduced to $N_{\text{FC}} \times Q = 2 \times 24 = 48$ bits/update/user if semi-adaptive MIMO selection is utilized. If we further combine it with TH-CQI, the extra weight feedback is $M \times Q$ bits/update/user, thus the total feedback is the sum of CQI feedback and weight feedback as $44 + M \times Q$ bits.

The downlink control signaling overhead can be estimated for the 10 scheduled users as an example. The estimation assumes that all users are scheduled per TTI and that there is an equal proportion of single and dual-stream users. Following the assumptions in [3GPP06a], Table 7.1.1.2.3.1-1, the downlink transport format signaling N_{TF} takes around 8 bits per user and per spatial stream, while the HARQ related information N_{HA} requires 2 bits, assuming synchronous HARQ. The UE ID information and duration assignment are identical for all cases, so they are excluded from the analysis. As for resource assignment, if we assume it is possible to use $\log_2$ based compression of joint resource assignment (with entropy coding), the number of bits required will be $ceil(N_{\text{FC}} \times \log_2(N_{\text{user}} + 1))$, where the N_{user} is the number of scheduled users over N_{FC} PRBs. The total number of bits needed for downlink signaling is then $(N_{\text{TF}} + N_{\text{HA}}) \times N_{\text{user}} + ceil(N_{\text{TF}} \times \log_2(N_{\text{user}} + 1)) =$

$(8+2)\times 10 + ceil(24\times\log_2(10+1)) = 184$ bits for the diversity MIMO FDPS cases. If SU-MIMO is used, and assuming that the extra MIMO mode selection information N_{MI} requires 2 bits per user, and that two instances of transport format and HARQ information are needed, the total number of bits becomes $(N_{\text{TF}}+N_{\text{HA}}+N_{\text{MI}})\times 5 + ((N_{\text{TF}}+N_{\text{HA}})\times 2 + N_{\text{MI}})\times 5 + ceil(N_{\text{FC}}\times\log_2(N_{\text{user}}+1)) = (8+2+2)\times 5+((8+2)\times 2+2)\times 5+ceil(24\times\log_2(11)) = 254$ bits. If the semi-adaptive approach is adopted, the signaling can be reduced to $(N_{\text{TF}}+N_{\text{HA}})\times 5 + ((N_{\text{TF}}+N_{\text{HA}})\times 2)\times 5+ceil(N_{\text{FC}}\times\log_2(N_{\text{user}}+1)) = (8+2)\times 5+((8+2)\times 2)\times 5+ceil(24\times\log_2(11)) = 234$ bits when the small overhead required to inform the UE of the MIMO mode to be used is not considered. The signaling can be further reduced to $(N_{\text{TF}}+N_{\text{HA}})\times 5+(N_{\text{TF}}+N_{\text{HA}})\times 5+ceil(N_{\text{FC}}\times\log_2(N_{\text{user}}+1)) = (8+2)\times 5+(8+2)\times 5+ceil(24\times\log_2(11)) = 184$ bits if SCW is used in transmission, i.e., in total a 30% reduction can be achieved in downlink control signalling for SU-MIMO. Similarly, we consider the control signalling for MU-MIMO whose allocation resolution is even smaller, *i.e.* , 48 RPBs per TTI. Thus the bits for joint resource assignment are increased to $ceil(2\times N_{\text{FC}}\times\log_2(N_{\text{user}}+1))$ with double number of resource blocks. The estimated signaling requirements are summarized in Table 8.1.

8.3 Performance Evaluation

In this section the signalling reduction methods discussed in Section 8.2 are performed incrementally, and the corresponding results are shown and explained. The simulator modeling and simulation assumptions are in Chapter 6.

We conduct the first signalling reduction approach by using semi-adaptive MIMO concept, but still with AB-CQI. As shown in Figure 8.4, for micro cell with UDO of 10, no significant difference is observed for two cases for different SDM-FDPS schemes. The MIMO selection for semi-adaptive is based on the G-factor threshold. The UEs with G-factor higher than the threshold utilize dual-stream transmission only, and vice versa. The thresholds used are chosen from the single-stream and double-stream selection probabilities cross point measured from the fast-adaptive simulations, similar to Figure 5.3. The practical thresholds depend on MIMO schemes used, antenna correlation, UE capabilities etc.

Further, we consider reduction of the codewords for SDM-FDPS by using SCW instead of MCW. Although not shown here, no noticeable difference is seen for MU-MIMO results. As shown in Figure 8.5 for SU-MIMO, only marginal loss is observed when SCW is used compared with MCW. The reason is that when the UDO is low, the number of PRBs scheduled per user is quite high, and the averaged SINR for each stream over so many PRBs is quite similar. On the other hand, when the UDO is high, the PRB per user is quite low, and SCW will be less efficient to

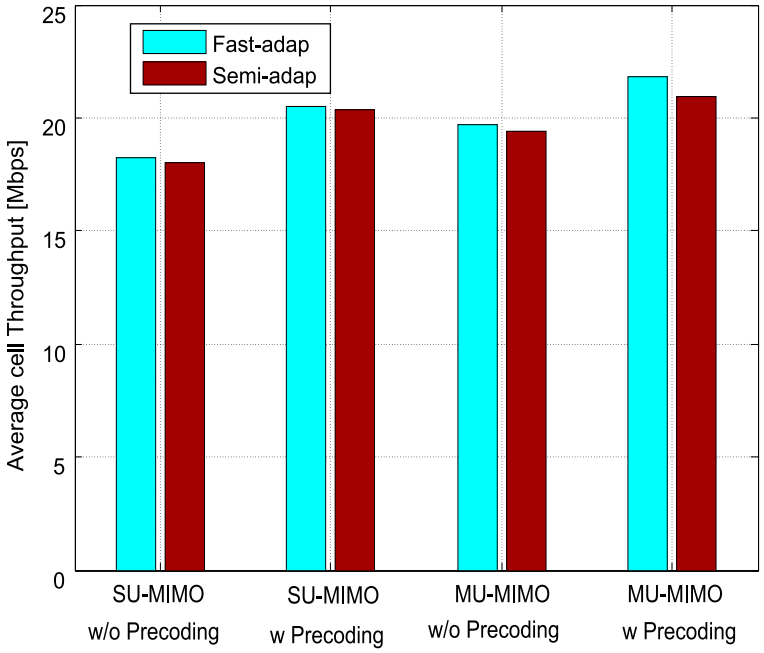

Figure 8.4: Comparison of fast-adaptive and semi-adaptive MIMO selection for Average Cell throughput in micro cell for SDM-FDPS at UDO of 10.

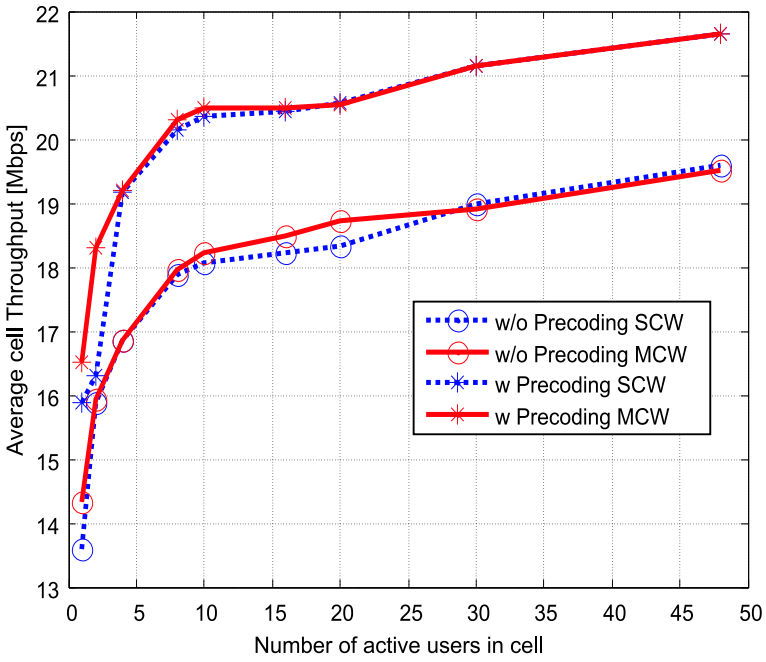

Figure 8.5: Comparison of Average Cell throughput in micro cell with one codeword and two codewords for SU-MIMO with FDPS.

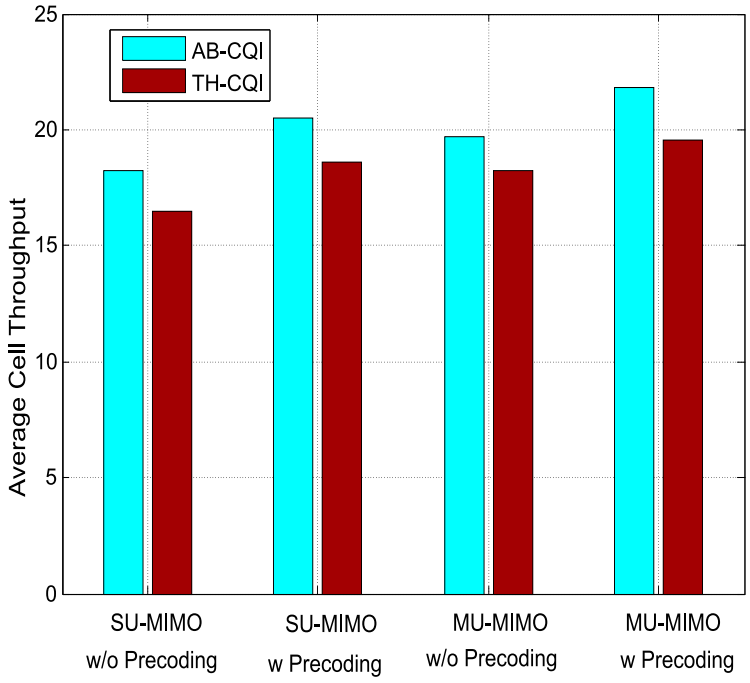

Figure 8.6: Comparison of AB-CQI and reduced TH-CQI on the Average Cell throughput in micro cell for SDM-FDPS at UDO of 10.

adapt to the imbalance between streams. The fact that the performance is already in the saturation range makes the loss quite small though.

Next, the extended TH-CQI scheme is used to reduce the CQI signalling for SDM-FDPS significantly. As we can see from the results in Figure 8.6 comparing AB-CQI and TH-CQI, the performance loss can be kept within 7-10%. However, as explained in the previous subsection, an uplink signalling reduction up to 91% and downlink signalling reduction up to 30% can be achieved.

8.4 Summary

In this chapter, the potential signaling reduction methods to realize the performance gain from SDM-FDPS are shown to be critical for practical system design. Due to the interaction between different gain mechanisms, the potential gain with some gain mechanisms reduces when FDPS presents. The understanding of this can help us safely reduce the signalling overhead while keeping most of the gain for SDM-FDPS. Therefore, various efficient ways to bring down the signalling requirements for SDM-FDPS are considered in the study. Specifically, semi-adaptive MIMO mode selection, single codeword transmission, and the threshold based CQI scheme have been investigated. Based on the 3GPP LTE framework, simulation

studies reveal that a significant reduction in signaling overhead (around 88% in uplink and 30% in downlink) can be achieved with only a marginal loss (within 7-10%) in cell throughput performance.

Chapter 9

Conclusion

9.1 Main Conclusions and Recommendations

One of the most important goals of the UTRA long term evolution cellular systems is to provide a significantly improved spectral efficiency compared to previous generation of systems, where it becomes necessary to investigate the efficient application of Multiple-Input Multiple-Output (MIMO) technology. One of the biggest challenges is to map the promised potential of MIMO effectively into attainable cell throughput gain in a practical system. To undertake this challenge, the design and analysis of the interoperation of MIMO, especially the multi-stream MIMO, with the other gain mechanisms in the system such as Link adaptation (LA), Hybrid ARQ (HARQ) L1 retransmission, packet scheduling, etc, becomes the essential task. Besides, practical issues with significant impact on the obtainable MIMO gain need to be carefully considered. Such issues include fairness between UEs, limited dynamic range of available SINR, amount of signaling overhead, adaptation uncertainties, CQI imperfections, etc. Therefore, in this Ph.D. study we have examined the efficient application of the MIMO technology concerning the tradeoffs between fairness, achievable gain and the signaling overhead and/or complexity. The conclusions and recommendations from this study can serve as a good guideline in system design of UTRA LTE concerning practical MIMO deployment.

To summarize, the main contributions of this dissertation are: (i) the development of a conceptual unified MIMO-OFDM framework, (ii) co-development of a link level simulator and benchmark link results for LTE downlink system with various baseline MIMO schemes, (iii) the analysis and design of closed-loop transmit diversity schemes with reduced weight feedback, (iv) the analysis and design of the adaptive MIMO solution through a unified SINR concept, (v) co-development of a network simulator, with the proposed MIMO aware FDPS algorithm, benchmark the system-level results for LTE downlink with spatial multiplexing MIMO and

FDPS (SDM-FDPS). (v) Various methods are suggested to reduce the signalling overhead to support SDM-FDPS. The main conclusions and recommendations are further outlined throughout as follows.

With the conceptual MIMO-OFDM framework, we understand that instantaneous optimal transmission strategy can be found with certain analytic constraints for each instantaneous time if we assume perfect channel knowledge. That is, symbols can be theoretically optimally dispersed over time, frequency and space resources with considerations such as capacity maximization, error probability target. However, considering other practical constraints such as complexity and signalling, in this study we preferred the simplified detached frequency and space-time processing which can achieve most of the gain.

From both the link and system level evaluation, we found that the multi-stream MIMO is a micro-cell feature only. In other words, there is no need to deploy mutli-stream MIMO for macro-cell scenario due to limited SNR dynamics available. This is well supported by results in Chapter 3 and Chapter 7. The results also show that for diversity MIMO schemes, 1x2 SIMO shows significant gain over SISO, while the gain from using extra transmit antenna as open loop scheme, *i.e.* , 2x2 SFC over 1x2 is rather small. The tradeoff between achievable gain and weight feedback for the closed-loop transmit diversity (CLTD) is identified in Chapter 4. From the study, we observe that the CLTD is still an important coverage improvement feature for low mobility users in the cell-edge, whereas the potential gain at cell level is rather limited. As for high mobility users, open-loop space time diversity schemes which stablise the link quality should be utilized instead. To analyze the fast adaptive MIMO selection gain, we introduced a unified SINR concept. This proves to be a very handy tool in the analysis of MIMO schemes with different number of streams. With the analysis in Chapter 5, we observe a good gain in single-user study with fast adaptive MIMO especially in correlated scenarios and/or with simple receiver. However, we would recommend the slow adaptive MIMO for uncorrelated scenarios and/or with advanced receivers. Moreover, the results in Chapter 8 show that the slow adaptive MIMO with a much reduced signaling requirements is as efficient as fast adaptive MIMO if FDPS gain presents.

To achieve the multi-user diversity gain, our study proposes practical yet efficient algorithms for SDM-FDPS. Depending on the scheduler flexibility, SU-MIMO and MU-MIMO are investigated. The analysis in the Chapter 7 reveals that the MU-MIMO can achieve higher gain with higher scheduling flexibility than SU-MIMO, and the precoding can further improve the performance. However, the gain is always at the price of higher signaling requirements. The traffic model is shown to be an important factor on cell performance gain. Up to 50-60% cell level gain is observed if infinite buffer model is used, while only 20-30% gain is observed with finite buffer model. Therefore, it makes more sense to make selection on SU-MIMO or MU-MIMO (precoding or not) depending on the specific

scenarios, such as the number of active users, the signaling resource available, UE capabilities, traffic property, etc. Practically, the eNode-B can gather some long-term statistics of the network, and make wise adaptation accordingly.

Due to the subtle interaction between different gain mechanisms, the potential gain for some gain mechanisms reduces in the presence of multi-user diversity. The understanding of this can help us safely reduce the signalling overhead while keeping most of the gain for SDM-FDPS, as shown in Chapter 8. For example, although multi-codeword is shown to be superior to single-codeword in link study, the gain is quite marginal when combined with SDM-FDPS. This is also true for fast adaptive MIMO. Since the scheduler always selects the best users, the chance of encounter low rank channel with multi-user diversity is quite low. Therefore, slow adaptive MIMO is recommended when FDPS is used. Besides, advanced CQI reduction schemes are further extended to support SDM-FDPS. With a careful design on the thresholds, it is shown to be very effective in reducing signaling requirements. The threshold value obtained from the simplified post-scheduling unified SINR analysis is shown to be very effective.

9.2 Future Work

At this very end point of thesis, we would like to address some proposals to continue the investigation performed in this Ph.D. study.

Since this thesis is constricted to FDD mode system only, the analysis and evaluation of MIMO in the TDD mode system is definitely needs further investigation and optimization. With the channel reciprocal property, the TDD mode provide better opportunity for some advanced MIMO solutions which need full information of the channel information. The signalling bottleneck from this study can be avoided. For example, concerning the MIMO-OFDM framework, when the full channel information is obtainable for the transmitter, further optimization of space-frequency-time processing will be of great interests. As for multi-user scheduling, we can perform advanced power loading, bit loading, and frequency-time-space resource allocation. Some other advanced interference avoidance techniques also become feasible. For example, the dirty paper coding (DPC) based on the interference presubtraction (or its sub-optimal variants) can be used to transmit an interference-free independent data stream to different users.

Furthermore, it is also interesting to explore the potential of MIMO combined with some new emerging technologies, such as cooperative communication, cognitive radio and mesh networks. For example, MIMO can be made beneficial to the cooperative communication technology. One cooperative MIMO scenario is with several idle UEs who can cooperate to work to help the nearby master UE. The UEs together can construct a bigger Virtual antenna array to improve the sys-

tem coverage (diversity type of MIMO) and data-transmission capability (spatial multiplexing type of MIMO). With bigger number of virtual antennas, we obtain higher flexibility in the utilization of the higher spatial freedom. Better tradeoff between spatial multiplexing gain and diversity gain can be exploited in this case. The connections among UEs can potentially be built through some shared spectrum communication technologies.

Appendix A

Formulation of Unified Framework for MIMO-OFDM

This appendix provides the detailed formulation of the unified framework for MIMO-OFDM as introduced in Chapter 2. Since the framework is based on linear dispersion code (LDC), the background information on LDC is first explained in Section A.1 and the derivation of the proposed framework is discussed in Section A.2.

A.1 Background information on Linear Dispersion Coding

Proposed by Hassibi in 2002 [Hass02], the Linear Dispersion Coding breaks the data stream into substreams that are dispersed in linear combinations over time and space, which is in principle a unified framework for most MIMO schemes. Basic concept of LDC is to write transmitted matrix S in this way:

$$S = \sum_{q=1}^{Q} (s_q C_q + s_q^* D_q) \ , \tag{A.1}$$

where $s_1, ..., s_Q$ are complex scalars (typically chosen from an r-PSK or r-QAM constellation) and where C_q the and D_q are fixed complex matrices with dimension (T,N_t). T is the number of symbols during which the propagation channel is constant and Q is the number of input modulated symbols on which the space-time processing is performed. The code is completely determined by the set of dispersion matrices $\{C_q, D_q\}$, whereas each individual codeword is determined by our choice of the scalars $s_1, ..., s_Q$. The LDC encoding can be depicted as in Figure A.1. Note that only 2 transmit antennas are illustrated here for simplicity.

The **Conj** block takes the complex conjugate of input symbols and the $\mathbf{C}$ and

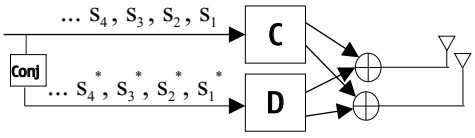

Figure A.1: Illustration of LDC Encoding

D code blocks consist of a series of dispersion matrices $\{C_1, ...C_q, ..., C_Q\}$ and $\{D_1, ...D_q, ..., D_Q\}$ respectively. The encoding procedure then proceeds as follows:

1. Each time instance q, one modulated symbol s_q and its complex conjugate s_q^* are mapped with the C_q and D_q matrices to corresponding space-time position.
2. After repeat this for Q modulated symbols, the output from **C** and **D** blocks are summed up to get the final coded space-time symbol.

Or equivalently, due to the linearity, we can decompose the s_q into real and imaginary parts

$$s_q = \alpha_q + j\beta_q \ , \tag{A.2}$$

and the transmitted matrix in Equation A.1 can be rewrite as

$$S = \sum_{q=1}^{Q} (\alpha_q A_q + j\beta_q B_q) \ , \tag{A.3}$$

where $A_q = C_q + D_q$ and $B_q = C_q - D_q$.

LDC subsumes as special case of V-BLAST, space-time code, orthogonal code, non-orthogonal code, etc. To give a example, we consider the LDC representation of STC, V-BLAST schemes as explained below.

a) Space-time coding (STC)

The dispersion matrices for STC are

$$C_1 = \begin{bmatrix} 1 & 0 \\ 0 & 0 \end{bmatrix}; \ D_1 = \begin{bmatrix} 0 & 0 \\ 0 & 1 \end{bmatrix}; \ C_2 = \begin{bmatrix} 0 & 1 \\ 0 & 0 \end{bmatrix}; \ D_2 = \begin{bmatrix} 0 & 0 \\ -1 & 0 \end{bmatrix}. \tag{A.4}$$

The output from block **C** is $C_1 \cdot s_1 + C_2 \cdot s_2 = \begin{bmatrix} s_1 & s_2 \\ 0 & 0 \end{bmatrix}$, and the output from block **D** is $D_1 \cdot s_1 + D_2 \cdot s_2 = \begin{bmatrix} 0 & 0 \\ -s_2^* & s_1^* \end{bmatrix}$. The sum of them is classic STC as $\begin{bmatrix} s_1 & s_2 \\ -s_2^* & s_1^* \end{bmatrix}$.

b) Vertical Bell Laboratories Layered Space-Time Architecture (V-BLAST)

The dispersion matrices for V-BLAST are

$$C_1 = \begin{bmatrix} 1 \\ 0 \end{bmatrix}; D_1 = \begin{bmatrix} 0 \\ 0 \end{bmatrix}; C_1 = \begin{bmatrix} 0 \\ 1 \end{bmatrix}; D_2 = \begin{bmatrix} 0 \\ 0 \end{bmatrix}. \tag{A.5}$$

The sum of block C and D is simply $\begin{bmatrix} s_1 \\ s_2 \end{bmatrix}$.

For STC, $T = Q = N_t = 2$. As for V-BLAST, $Q = T \times N_t$ and $T = 1$. If we define code rate as $R = \frac{Q}{T \times N_t}$, the STC has a rate of 1/2 and V-BLAST has a rate of 1. That is, the STC achieves half data rate, but with full diversity; the V-BLAST achieves full rate, but no diversity available. Other hybrid schemes make different level of tradeoff between rate and diversity.

A.2 Unified framework for MIMO-OFDM

In this subsection, we extend the idea of linear dispersion code to frequency domain as well and in principle gives a unified framework for many MIMO-OFDM schemes. Since the manipulation of three dimensions (frequency/time/space) is not very convenient, we reduced it back to two dimensions by the equivalence concept [Moli02] as introduced in Subsection 2.3.1. We assume the number of modulated symbols for each space-frequency-time processing is equal to Q. With each input symbol α_q, we have a dispersion matrix A_q with size of $(N_t \times N_c, T)$, where N_c is the number sub-carriers. The output of block $\mathbf{A}$ is

$$\sum_{q=1}^{Q} A_q \cdot \alpha_q \ . \tag{A.6}$$

Similarly, the output of block $\mathbf{B}$ is

$$\sum_{q=1}^{Q} B_q \cdot \beta_q \ , \tag{A.7}$$

where for each input symbol β_q we have dispersion matrix B_q with size of $(N_t \times N_c, T)$. Therefore the sum of the output from both blocks, the transmit matrix $\mathbf{S}$ is

$$\mathbf{S} = \sum_{q=1}^{Q} (A_q \cdot \alpha_q + jB_q \cdot \beta_q) \ . \tag{A.8}$$

The code rate is defined as $R = \frac{Q}{N_t \times N_c \times T}$.

To show that the framework is linear system, we reformulate the Equation A.8 into a more convenient format as follows. First, we stack the real and imaginary part of input modulated symbols as

$$[\alpha_1,\, \beta_1,\, \ldots,\, \alpha_Q,\, \beta_Q]^T \ . \tag{A.9}$$

We define

$$\widehat{A}_q = \begin{bmatrix} A_{R,q} & -A_{I,q} \\ A_{I,q} & A_{R,q} \end{bmatrix} \ , \tag{A.10}$$

$$\widehat{B}_q = \begin{bmatrix} -B_{R,q} & -B_{I,q} \\ B_{I,q} & -B_{R,q} \end{bmatrix} \ . \tag{A.11}$$

Therefore, we can rewrite the Equation A.8 into a matrix with dimension $(2 \times N_c \times N_t, T)$ as

$$\mathbf{S} = \begin{bmatrix} S^1_{1,1,R} & \cdots & S^T_{1,1,R} \\ S^1_{1,1,I} & \cdots & S^T_{1,1,I} \\ S^1_{1,2,R} & \cdots & S^T_{1,2,R} \\ S^1_{1,2,I} & \cdots & S^T_{1,2,I} \\ \vdots & \vdots & \vdots \\ S^1_{1,N_t,R} & \cdots & S^T_{1,Nt,R} \\ S^1_{1,N_t,I} & \cdots & S^T_{1,Nt,I} \\ S^1_{2,1,R} & \cdots & S^T_{2,1,R} \\ \vdots & \vdots & \vdots \\ S^1_{Nc,N_t,R} & \cdots & S^T_{Nc,Nt,R} \\ S^1_{Nc,N_t,I} & \cdots & S^T_{Nc,Nt,I} \end{bmatrix} = [\widehat{A}_1\, \widehat{B}_1\, \widehat{A}_2 \quad \ldots \widehat{A}_Q\, \widehat{B}_Q] \cdot \begin{bmatrix} \alpha_1 \\ \beta_1 \\ \vdots \\ \alpha_Q \\ \beta_Q \end{bmatrix} \ , \tag{A.12}$$

where $S_{i,j,R}$ represents the real part of the symbol at frequency i for transmit antenna j, and $S_{i,j,I}$ represents the corresponding imaginary part.

Assuming a MIMO channel in time domain at certain time instance as

$$H = \begin{bmatrix} \mathbf{h}_{11} & \ldots & \mathbf{h}_{1N_t} \\ \vdots & \ddots & \vdots \\ \mathbf{h}_{N_r 1} & \ldots & \mathbf{h}_{N_r N_t} \end{bmatrix} \ , \tag{A.13}$$

where each element $\mathbf{h}_{ij}$ is a vector with length of multipath taps N_{path} for transmit antenna j and receive antenna i. And the corresponding frequency domain channel response is given as

$$H(f) = \begin{bmatrix} \mathbf{h}(f)_{11} & \ldots & \mathbf{h}(f)_{1N_t} \\ \vdots & \ddots & \vdots \\ \mathbf{h}(f)_{N_r 1} & \ldots & \mathbf{h}(f)_{N_r N_t} \end{bmatrix} \ , \tag{A.14}$$

where each element is a vector $\mathbf{h}(f)_{ij} = [h(f_1)_{ij}, \ldots, h(f_{N_c})_{ij}]$ with the length of N_c.

For each subcarrier k, the channel matrix is given as

$$H(f_k) = \begin{bmatrix} h(f_k)_{11} & \ldots & h(f_k)_{1N_t} \\ \vdots & \ddots & \vdots \\ h(f_k)_{N_r1} & \ldots & h(f_k)_{N_rN_t} \end{bmatrix} , \tag{A.15}$$

and the corresponding transmit matrix and receive matrix with dimension of $(2 \times N_r, T)$ are expressed as

$$\mathbf{S}(f_k) = \begin{bmatrix} S^1_{k,1,R} & \cdots & S^T_{k,1,R} \\ S^1_{k,1,I} & \cdots & S^T_{k,1,I} \\ S^1_{k,2,R} & \cdots & S^T_{k,2,R} \\ S^1_{k,2,I} & \cdots & S^T_{k,2,I} \\ \vdots & \vdots & \vdots \\ S^1_{k,N_t,R} & \cdots & S^T_{k,N_t,R} \\ S^1_{k,N_t,I} & \cdots & S^T_{k,N_t,I} \end{bmatrix} , \tag{A.16}$$

$$\mathbf{Y}(f_k) = \begin{bmatrix} Y^1_{k,1,R} & \cdots & Y^T_{k,1,R} \\ Y^1_{k,1,I} & \cdots & Y^T_{k,1,I} \\ Y^1_{k,2,R} & \cdots & Y^T_{k,2,R} \\ Y^1_{k,2,I} & \cdots & Y^T_{k,2,I} \\ \vdots & \vdots & \vdots \\ Y^1_{k,N_r,R} & \cdots & Y^T_{k,N_r,R} \\ Y^1_{k,N_r,I} & \cdots & Y^T_{k,N_r,I} \end{bmatrix} . \tag{A.17}$$

Now if we reconstruct the channel matrix of Equation A.15 into a matrix with dimension of $(2 \times N_r, 2 \times N_t)$ to match the structure of transmit matrix,

$$\hat{H}(f_k) = \begin{bmatrix} \hat{h}(f_k)_{11} & \ldots & \hat{h}(f_k)_{1N_t} \\ \vdots & \ddots & \vdots \\ \hat{h}(f_k)_{N_r1} & \ldots & \hat{h}(f_k)_{N_rN_t} \end{bmatrix} , \tag{A.18}$$

where each element of it is defined as

$$\hat{h}(f_k)_{ij} = \begin{bmatrix} Re(h(f_k)_{ij}) & -Im(h(f_k)_{ij}) \\ Im(h(f_k)_{ij}) & Re(h(f_k)_{ij}) \end{bmatrix} . \tag{A.19}$$

Thus the linear relation between $\mathbf{S}(f_k)$ and $\mathbf{Y}(f_k)$ is formulated as

$$\mathbf{Y}(f_k) = \hat{H}(f_k) \cdot \mathbf{S}(f_k) + \mathbf{n}(\mathbf{f_k}) \ . \tag{A.20}$$

If we reshape the frequency domain channel matrix as

$$\mathsf{H}(f) = \begin{bmatrix} \hat{H}(f_1) & 0 & 0 \\ 0 & \ddots & 0 \\ 0 & 0 & \hat{H}(f_{N_c}) \end{bmatrix} , \tag{A.21}$$

a simple representation of the system can be given as:

$$\mathbf{Y} = \begin{bmatrix} Y^1_{1,1,R} & \cdots & Y^T_{1,1,R} \\ Y^1_{1,1,I} & \cdots & Y^T_{1,1,I} \\ Y^1_{1,2,R} & \cdots & Y^T_{1,2,R} \\ Y^1_{1,2,I} & \cdots & Y^T_{1,2,I} \\ \vdots & \vdots & \vdots \\ Y^1_{1,N_r,R} & \cdots & Y^T_{1,N_r,R} \\ Y^1_{1,N_r,I} & \cdots & Y^T_{1,N_r,I} \\ Y^1_{2,1,R} & \cdots & Y^T_{2,1,R} \\ \vdots & \vdots & \vdots \\ Y^1_{N_c,N_r,R} & \cdots & Y^T_{N_c,N_r,R} \\ Y^1_{N_c,N_r,I} & \cdots & Y^T_{N_c,N_r,I} \end{bmatrix} = \mathsf{H}(f) \cdot \mathbf{S} + \mathbf{n} \ . \tag{A.22}$$

With this very general representation, advanced processing techniques like precoding, spreading can be included with a careful design of the dispersion matrices. As seen, the system is still a linear function, therefore, we may use any decoding technique already in place for V-BLAST.

Appendix B

Soft Information Calculation for Turbo Decoder

This appendix provides an explanation on the calculation of soft information for turbo code in the link simulator as introduced in Chapter 3.

In order to improve the performance of turbo decoding, instead of hard demodulated bits, the M-ary QAM demodulator generates soft values as inputs to the turbo decoder reflecting the reliability on each bit. The Log-Likelihood Ratio (LLR) for turbo decoder concerning bit b_k is defined as

$$L(b_k) = \ln \frac{Pr(b_k = 1|x)}{Pr(b_k = 0|x)} \quad . \tag{B.1}$$

This is a ratio between the probability that this bit is 1 over the probability that this bit is 0 based on the knowledge of received bit x.

This equation could be taken equivalently in symbol space as [Zels04]

$$L(b_k) = \ln \frac{Pr(b_k = 1|\mathbf{s}_{est})}{Pr(b_k = 0|\mathbf{s}_{est})} = \ln \frac{\sum_{\mathbf{s}_i} Pr(\mathbf{s}_i|\mathbf{s}_{est})}{\sum_{\overline{\mathbf{s}_i}} Pr(\overline{\mathbf{s}_i}|\mathbf{s}_{est})} \quad , \tag{B.2}$$

where $\mathbf{s}_{est}$ is the estimated symbol and

$$\begin{aligned} \mathbf{s}_i &= \{\forall j : i^{th} \quad \textbf{component} \quad \textbf{of} \quad s_j \quad \textbf{is} \quad 0\} \ , \\ \overline{\mathbf{s}_i} &= \{\forall j : i^{th} \quad \textbf{component} \quad \textbf{of} \quad s_j \quad \textbf{is} \quad 1\} \ , \end{aligned} \tag{B.3}$$

and $i = 0, 1, 2, ..., \log_2 M - 1$, M is the modulation alphabet size, i.e., 8, 16, 32 or 64. With Bayes' rule, $Pr(A|B) = Pr(B|A) \cdot Pr(A)/Pr(B)$, the LLR becomes

$$L(b_k) = \ln \frac{\sum_{\mathbf{s}_i} Pr(\mathbf{s}_{est}|\mathbf{s}_i) Pr(\mathbf{s}_i)}{\sum_{\overline{\mathbf{s}_i}} Pr(\mathbf{s}_{est}|\overline{\mathbf{s}_i}) Pr(\overline{\mathbf{s}_i})} \quad . \tag{B.4}$$

Assuming the all symbols have equal probability to be transmitted, the $Pr(\mathbf{s}_i)$ and $Pr(\overline{\mathbf{s}_i})$can be omitted. Further, with the assumption of Gaussian receiver noise, the conditional probability density function can be found as [Zels04]

$$pr(\mathbf{s}_{est}|\mathbf{s}_i, H) = \det(\pi\mathbf{Q})^{-1} \exp(-(\mathbf{s}_{est} - \mathbf{s}_i)^H \mathbf{Q}^{-1}(\mathbf{s}_{est} - \mathbf{s}_i)) \ , \tag{B.5}$$

where the covariance matrix of the estimated error $(\mathbf{s}_{est} - \mathbf{s}_i)$, $\mathbf{Q}$, is defined as

$$\mathbf{Q} = E[(\mathbf{s}_{est} - \mathbf{s}_i).(\mathbf{s}_{est} - \mathbf{s}_i)^H] \ . \tag{B.6}$$

Take Equation B.5 into Equation B.4 yields

$$L(b_k) = \ln \frac{\sum_{\mathbf{s}_i} \exp(-(\mathbf{s}_{est} - \mathbf{s}_i)^H \mathbf{Q}^{-1}(\mathbf{s}_{est} - \mathbf{s}_i))}{\sum_{\overline{\mathbf{s}_i}} \exp(-(\mathbf{s}_{est} - \overline{\mathbf{s}_i})^H \mathbf{Q}^{-1}(\mathbf{s}_{est} - \overline{\mathbf{s}_i}))} \ . \tag{B.7}$$

The computation load for Equation B.7 is very high with the involvement of a lot of exponential calculations. In order to reduce the complexity, the equations can be simplified by transferring into the log arithmetic domain and then using the approximation

$$\ln\left(\sum_i e^{x_i}\right) \approx \max_i(x_i) \ , \tag{B.8}$$

where $\max_i(x_i)$ means the maximum value of x_i. Therefore if the max-log approximation is applied, Equation B.7 can be approximated as

$$\begin{aligned} L(b_k) &= \ln \frac{\exp(\max_{\mathbf{s}_i|b_k=1}(-(\mathbf{s}_{est} - \mathbf{s}_i)^H \mathbf{Q}^{-1}(\mathbf{s}_{est} - \mathbf{s}_i)))}{\exp(\max_{\mathbf{s}_i|b_k=0}(-(\mathbf{s}_{est} - \mathbf{s}_i)^H \mathbf{Q}^{-1}(\mathbf{s}_{est} - \mathbf{s}_i)))} \\ &= \min_{\mathbf{s}_i|b_k=0} (\mathbf{s}_{est} - \mathbf{s}_i)^H \mathbf{Q}^{-1}(\mathbf{s}_{est} - \mathbf{s}_i) - \min_{\mathbf{s}_i|b_k=1} (\mathbf{s}_{est} - \mathbf{s}_i)^H \mathbf{Q}^{-1}(\mathbf{s}_{est} - \mathbf{s}_i) \ . \end{aligned} \tag{B.9}$$

A baseline method for SISO and diversity MIMO schemes is mentioned in [3GPP01], where the covariance matrix $\mathbf{Q}$ is simply reduced to be a constant as

$$\mathbf{Q} = E[(\mathbf{s}_{est} - \mathbf{s}).(\mathbf{s}_{est} - \mathbf{s})^H] = \sigma_n^2 \ . \tag{B.10}$$

where σ_n^2 is the noise covariance. If we further define the parameter d_j as the Euclidean distance of the received symbol $\mathbf{s}_{est}$ from the points on the QAM constellation is $\mathbf{s}_i$ or its complement. Then Equation B.9 for diversity MIMO schemes can be simplified as

$$L(b_k) = \frac{1}{\sigma_n^2}[\min_{j \in S_i}\{d_j^2\} - \min_{j \in \overline{S_i}}\{d_j^2\}] \ . \tag{B.11}$$

As a example, we consider the soft-information calculation for JC with MMSE receiver. By following the signal model as in Chapter 2 Equation 2.35, the calculation of the covariance matrix $\mathbf{Q}$ for JC with MMSE receiver is given as [Zels04]:

$$\begin{aligned} \mathbf{Q} &= E[(\mathbf{s}_{est} - \mathbf{s}).(\mathbf{s}_{est} - \mathbf{s})^H] \\ &= E[(\mathbf{W}(\mathbf{Hs} + \mathbf{n}) - \mathbf{s}).(\mathbf{W}(\mathbf{Hs} + \mathbf{n}) - \mathbf{s})^H] \\ &= \sigma_n^2(\alpha\mathbf{I} + \mathbf{H}^H\mathbf{H})^{-1} \ , \end{aligned} \tag{B.12}$$

where α is equal to N_t/σ_n^2, in which N_t is the number of transmit antennas.

By using Equation B.12 and Equation B.9, the LLR for JC with MMSE receiver can be shown as

$$L(b_k) = \frac{1}{[\sigma_n^2(\alpha I + \hat{H}^H\hat{H})^{-1}]_{kk}}[\min_{j\in S_i}\{d_j^2\} - \min_{j\in \overline{S_i}}\{d_j^2\}] \ , \tag{B.13}$$

where $[\quad]_{kk}$ means that the diagonal element of that matrix is taken assuming the non-diagonal element is negligible.

Appendix C

Validation of Link simulator

The link simulator is a team work project, which is developed with other colleges in Aalborg University [1] as well as Nokia Siemens Networks [2] . Most of the code is written in MATLAB, but some bottleneck computations that do not run fast enough in MATLAB is recoded in C for higher efficiency and interface with MATLAB using MEX files. The validations of the link simulator from different aspects are provided in this appendix. The MIMO multipath channel and turbo code validation is shown in Section C.1 and Section C.2. Moreover, HARQ and MIMO schemes implementation validation are discussed in Section C.3 and Section C.4, respectively. After that, the statistic significance of is analyzed for all link simulation results in Section C.5.

C.1 MIMO Channel Validation

The MIMO channel model is based on the implementation in [Schu01] from I-METRA project. This implementation is also intensively utilized and validated in previous PhD project (Appendix C and D in [Berg05]). The 20-ray typical urban MIMO channel multipath fading statistics is compared with theoretical Rayleigh fading with appropriate power scaling as shown in Figure C.1. As shown, the MIMO channel fading statistics approximately matches with the Rayleigh fading on a per path basis.

[1] Phd students Akhilesh Pokhariyal, Christian Rom and Basuki E. Priyanto from the Department of Electronic Systems, Aalborg University, Denmark.

[2] Frank Frederiksen and Claudio Rosa from Nokia Siemens Networks Aalborg R&D, Denmark.

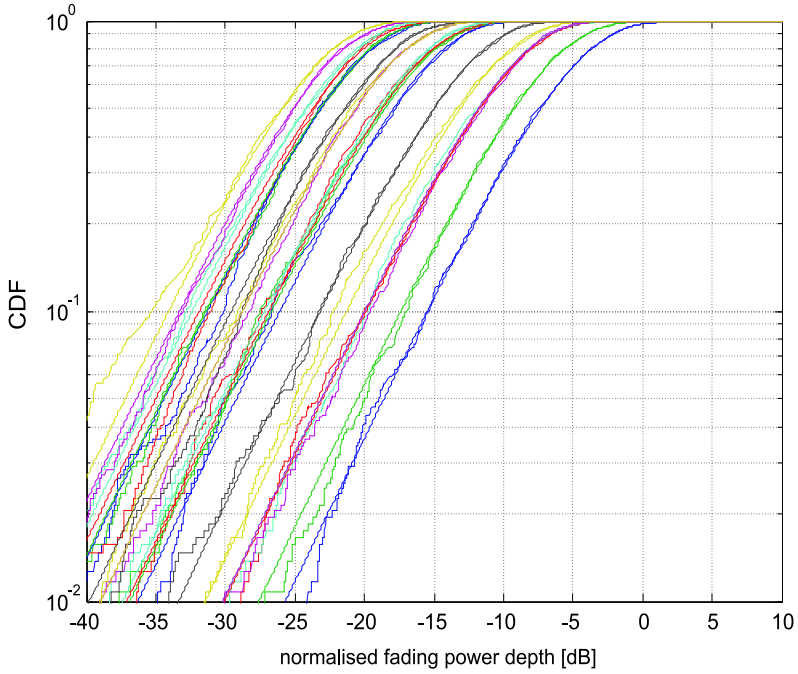

Figure C.1: Fading statistics verification.

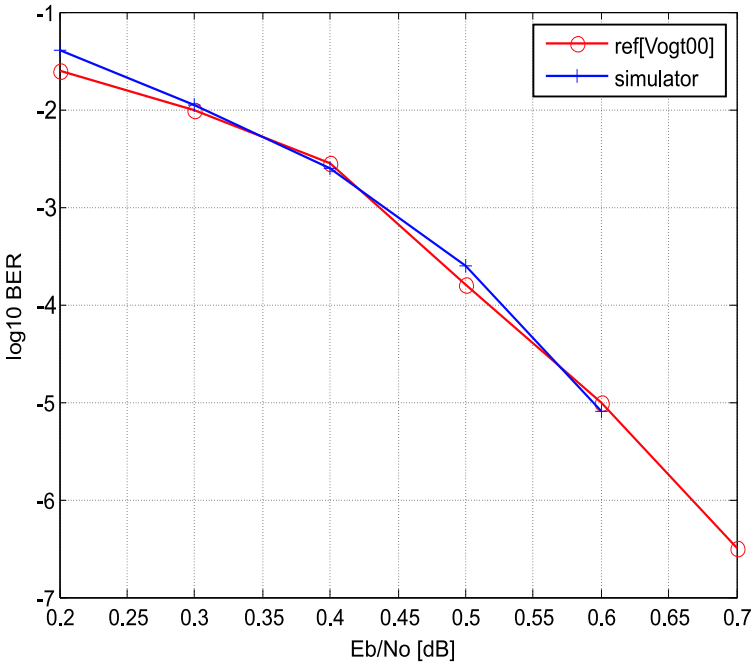

Figure C.2: Turbo coder performance verification with code rate 1/3 in AWGN channel with BPSK.

C.2 Turbo Code Implementation Validation

The turbo code implementation is carried out by following strictly the specification in UTRA release 6. As for the decoding algorithm, we select the "max-log-MAP" [Vogt00] sub-optimal algorithm since it requires a much reduced complexity with a only a marginal loss compared to optimal "MAP" algorithm. The basic BER performance in AWGN channel has been verified against results in [Vogt00] as shown in Figure C.2.

C.3 HARQ implementation validation

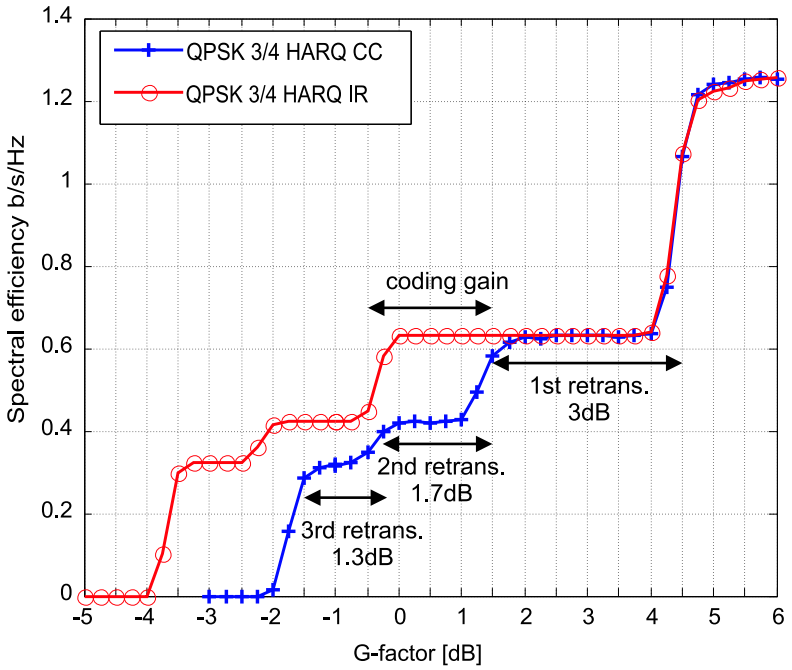

Figure C.3: spectral efficiency of HARQ retransmission gain

The HARQ validation is shown with spectral efficiency curves versus G-factor (*i.e.* average SNR) as shown in Figure C.3 for QPSK 3/4 SISO. With chase combining, since an identical copy of signal is sent for each retransmission, the total combining gain is correspondingly 3dB, 4.7dB and 6dB with retransmission number 1, 2 and 3. And according to the Equation 6.2 in Chapter 7, the effective throughput will be divided by the number of transmission performed, which forms a stair-case pattern as shown in Figure C.3. As shown, the spectral efficiency curve with CC forms a staircase with the width of each steps are around 3dB, 1.7dB and 1.3dB, which verified the HARQ implementation.

If the Incremental Redundancy HARQ is utilized, besides the combining gain, there is extra coding gain by retransmitting some of the punctured parity bits. For this case, the effective code rate after one IR retransmission will be around 3/8, quite close to its mother 1/3 code rate. After that, since the basic rate of turbo code is almost reached, no extra coding gain for further retransmissions.

C.4 Modulation and MIMO schemes implementation validation

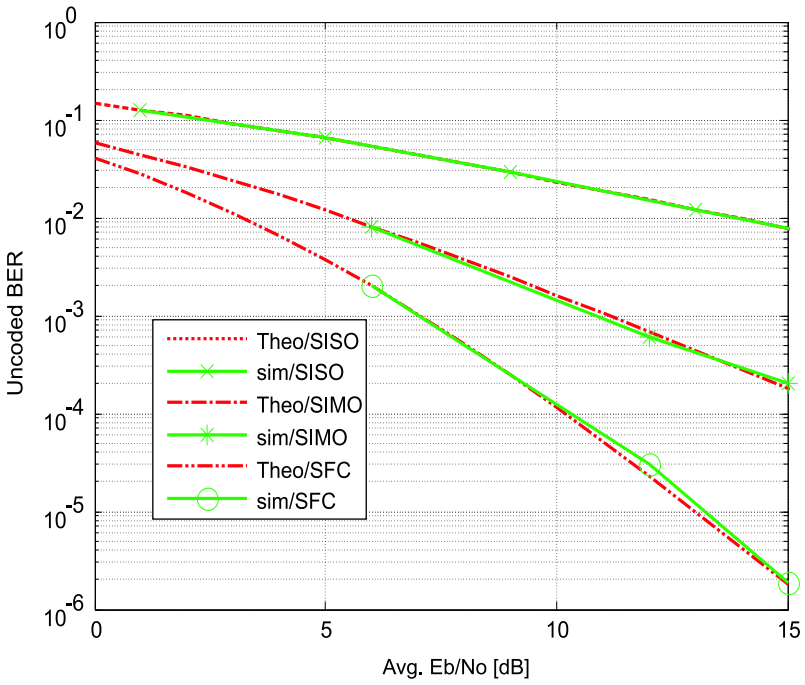

Figure C.4: Uncoded BER comparison from simulator and reference literature

The simulated uncoded BER for QPSK for SISO, 1x2 SIMO and 2x2 SFC is shown together with the theoretical bound in Figure C.4. The theoretical bound of bit error probability for QPSK with a diversity order of P can be found in [Proa95] as

$$P_b, QPSK = \frac{1}{2}[1 - \frac{\mu}{\sqrt{2-\mu^2}}\Sigma_{p=0}^{P-1}\binom{2p}{p}(\frac{1-\mu^2}{4-2\mu^2})^p] \quad , \tag{C.1}$$

where

$$\mu = \sqrt{\frac{\gamma_c}{1+\gamma_c}} \quad . \tag{C.2}$$

and received SNR per channel is $\gamma_c = \frac{2\gamma_b}{P}$ which is assumed to be identical for all the channels. γ_b is the average Eb/No. Quite good agreement is observed for

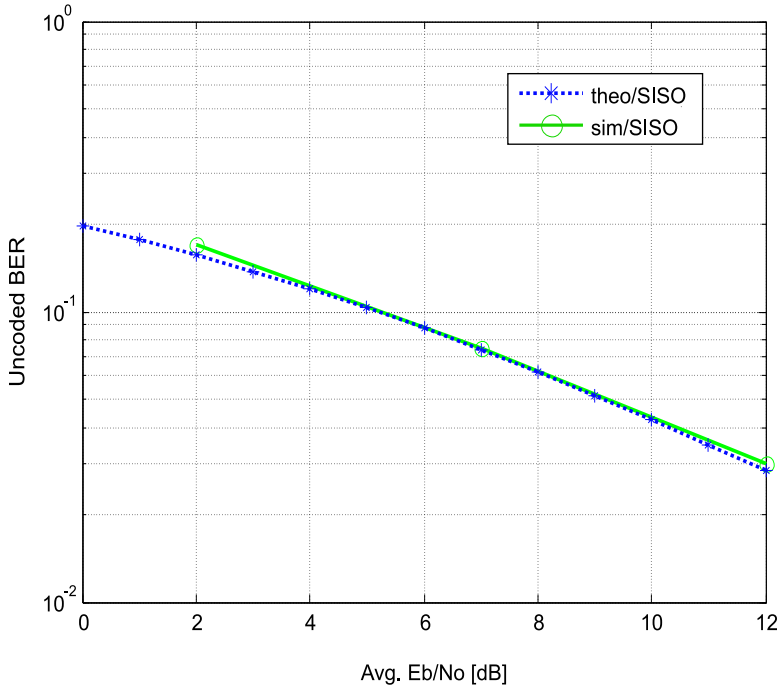

Figure C.5: Uncoded BER comparison for 16QAM with SISO.

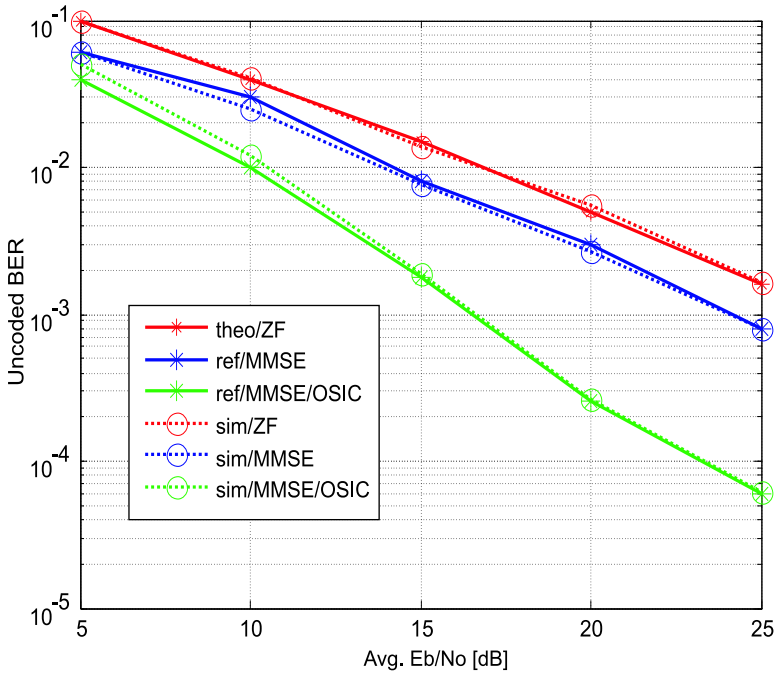

Figure C.6: Uncoded BER for JC with ZF, MMSE and OSIC receiver with BPSK in flat Rayleigh channel.

the simulation results and the theoretical bounds, which validates the MIMO implementation with QPSK modulation. The uncoded BER for 16QAM SISO is also shown against theoretical bound in Figure C.5. The average theoretical BER for 16QAM is given by as [Adac92]

$$P_b, 16QAM = \frac{1}{2} - \frac{3/8}{\sqrt{1+\frac{5}{2\gamma_b}}} - \frac{1/4}{\sqrt{1+\frac{5}{18\gamma_b}}} + \frac{1/8}{\sqrt{1+\frac{1}{10\gamma_b}}} \quad . \tag{C.3}$$

Again quite good agreement is seen between the simulation results and the theoretical bounds, which validates the implementation of 16QAM modulation.

The uncoded BER for JC with BPSK with different receiver is compared with reference curves from PhD thesis [Zels04] in Figure C.6. For ZF, MMSE and OSIC receiver, a good agreement is observed between the simulation results from the developed simulator and the reference ones, which validates the implementation of the JC.

C.5 Statistical Significance Analysis For Link Simulator

To gain confidence on the link-level results obtained, the statistical significance analysis is performed for the link simulator developed in this section. More specifically, the link simulator results are analyzed with mean multipath channel power as well mean SINR as follows.

C.5.1 Statistical Significance Analysis For Fading Channel Means

To assess which effect channel simulation inaccuracies have on link performance the statistics of the obtained multipath fading channel means are analyzed. Since the channel trace is normalized to 1 over 120λ, we stored a long trace of multipath channel power samples, *i.e.* , $\mathbf{h}^H\mathbf{h}$, over 21600TTI with a mobile speed of 3kmph. From this original set, 1000 sampled sets with 3600 continuous samples each, are drawn. This corresponds to a length of 20λ with which most of the link simulation actually runs for. The start point for each set is randomly chosen and the continuous samples are drawn into a set. Each re-sampled set is denoted $sub\{\mathbf{h}^H\mathbf{h}\}$. The ensemble average over the 3600 elements in every set is written as

$$E\langle sub\{\mathbf{h}^H\mathbf{h}\}\rangle_{3600} \quad . \tag{C.4}$$

For every set the relative deviation from the true mean is then calculated as

$$\frac{E\langle sub\{\mathbf{h}^H\mathbf{h}\}\rangle_{3600} - E_m\{\mathbf{h}^H\mathbf{h}\}}{E_m\{\mathbf{h}^H\mathbf{h}\}} \tag{C.5}$$

where the true mean, $E_m\{\mathbf{h}^H\mathbf{h}\}$, is given as 1. The distribution of the encountered relative sample mean deviations is displayed in Figure C.7. The mean distributions can be well approximated by Gaussian reference distributions with a standard deviations of 1.35%. The 99% the 95% and the 90% confidence interval values are directly obtained from the 1000 set mean estimates. They are indicated through the vertical lines in Figure C.7, and their values are given in Table C.5.1. It can be seen that 99 out of 100 simulations will give mean multipath channel power values within 3.1% of the true mean.

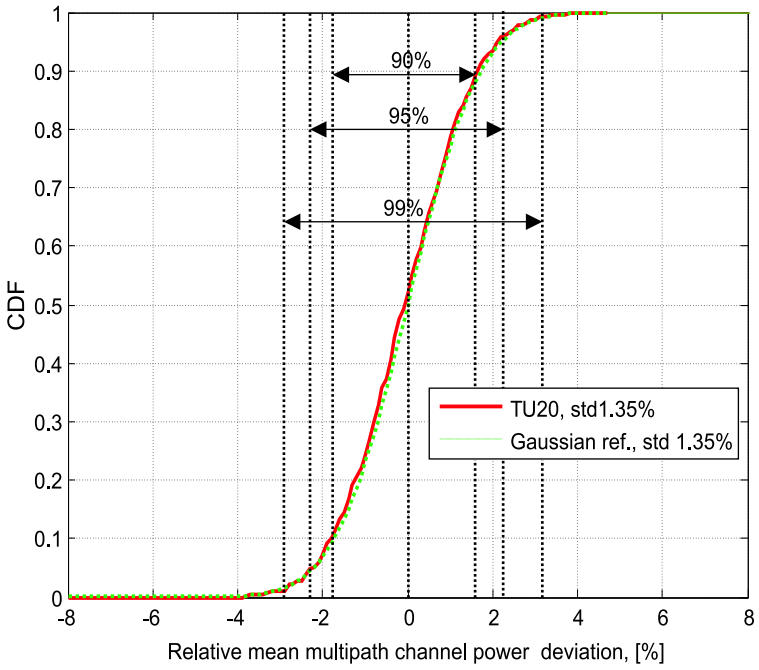

Figure C.7: Multipath standard deviation

Table C.1: Peak Data Rates For Example

Confidence level, [%]	Confidence Interval, [%]
99	[-3.10, 3.05]
95	[-2.27, 2.14]
90	[-1.82, 1.64]

C.5.2 Statistical Significance Analysis For Mean SINR

The statistical significance of the obtained link level results is further measured in terms of the reproducibility of the mean SINR over whole bandwidth. The 2x2 CLM1 case with grouping for Chapter 4 is considered. It is influenced by the random processes related to multipath fading, loss by imperfect weight due to quantization, grouping and delay. Using a similar re-sampling procedure as in previous subsection, 1000 re-sampled sets are produced from a 120λ long $SINR_{TTI}$ trace. The ensemble average over each re-sampled set is taken, and the relative deviation per trace is calculated as

$$\frac{E\langle sub\{SINR_{TTI}\}\rangle_{3600} - E\{SINR_{TTI}\}_{21600}}{E\{SINR_{TTI}\}_{21600}} \quad . \tag{C.6}$$

The relative sector mean SINR distribution is plotted in Figure C.8 together with a Gaussian reference distribution with a standard derivation of 1.10%. The 99%, the 95%, and the 90% confidence interval values are directly obtained from the 1000 set mean estimates. They are indicated through the vertical lines in Figure C.8. Their values are given in Table C.5.2. It is observed that 99 out of 100 simulations will give the cell mean SINR within 2.40% of the true mean.

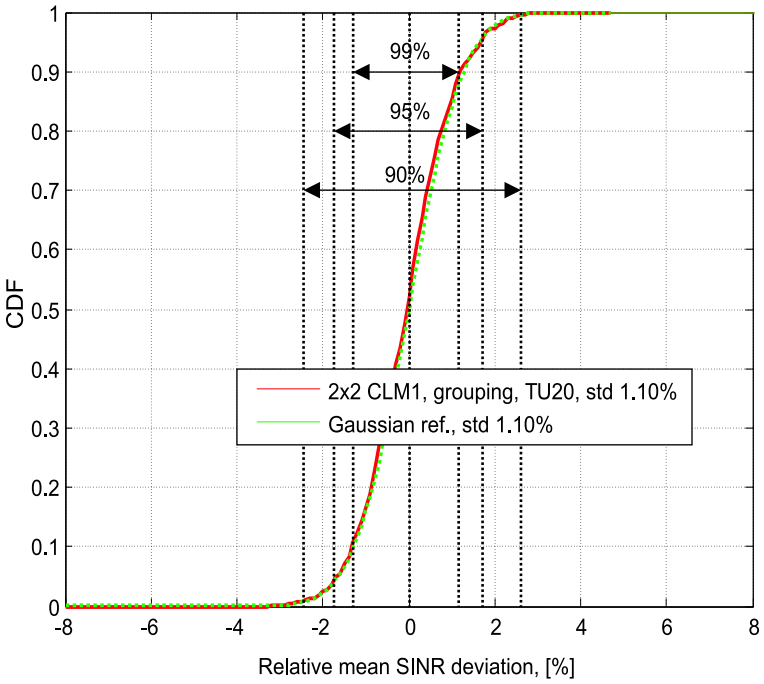

Figure C.8: Mean SNR standard deviation

Table C.2: Peak Data Rates For Example

Confidence level, [%]	Confidence interval, [%]
99	[-2.40, 2.30]
95	[-1.66, 1.60]
90	[-1.33, 1.19]

Appendix D

Issues of Channel profiles with the Space-Frequency Coding

During the results analysis, we found some issues concerning the Space-Frequency Coding (SFC) with different typical urban channel profiles in literatures. We further examined the results and explained the reason for this in this appendix.

At the time that most link study in this thesis is carried out, no channel model is specified in 3GPP. Therefore we choose to use the 20-taps typical urban channel (TU20) ([3GPP05], Section 5.1) since it exhibits reasonable frequency correlation over 20MHz. Afterwards, the 3GPP 25.814 recommended the usage of simpler 6-taps typical urban channel (TU06) for initial evaluation of LTE. In order to do a cross-check, we performed link level study with both channel profiles for selected cases.

Results show that for all the MIMO schemes that processing is performed over each sub-carrier, the performance is almost identical with both channel profiles with 10MHz bandwidth assumption. But since the SFC involves two neighboring sub-carriers, its performance with two channel profiles are slightly different. As shown in Figure D.1, the spectral efficiency of TU06 is worse compared to that of TU20, especially in high SNR range. The difference is smaller for 2x2 with one additional receive antenna, as in Figure D.2. Similar to the space-time coding (STC), the assumptions behind the SFC is that the neighboring sub-carriers experience the same channel condition. Due to frequency selectivity, this assumption is not perfectly satisfied and the frequency property of the channel profiles becomes important to investigate.

To look into this issue, we first compared the frequency correlation property of the two profiles in Figure D.3. As shown, the TU20 exhibits a more exponential decaying type of frequency correlation property, while TU06 has a strange fluctuation

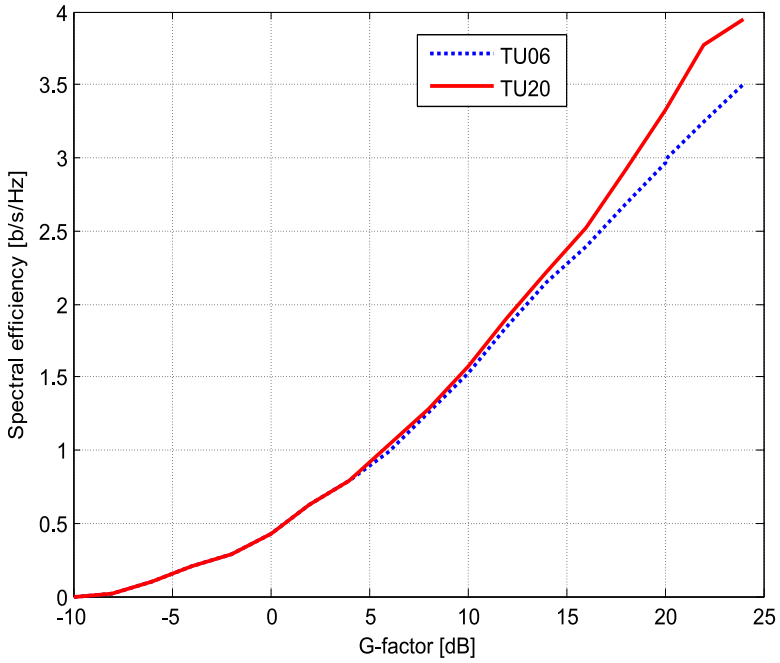

Figure D.1: The spectral efficiency loss of TU 06 with SFC 2x1.

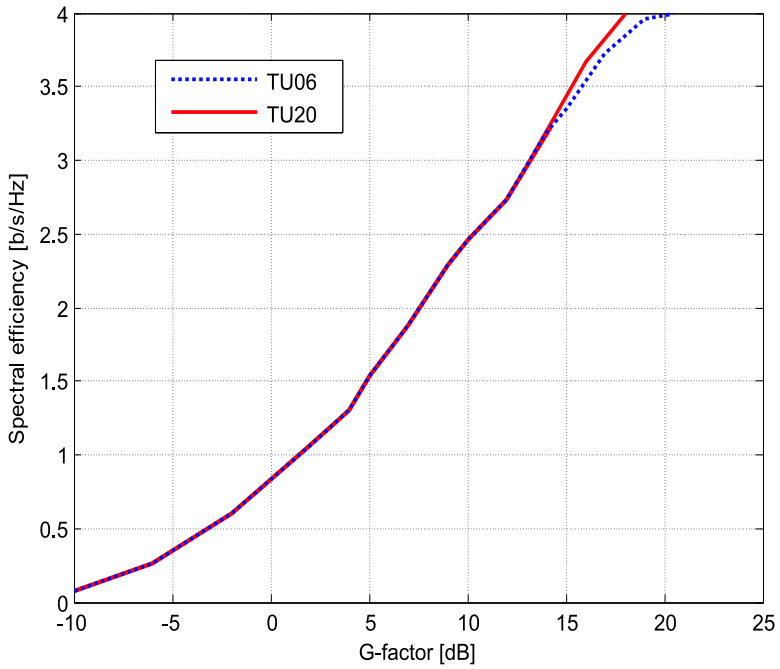

Figure D.2: The spectral efficiency loss of TU 06 with SFC 2x2.

of frequency correlation over bandwidth. If we define a coherence bandwidth as the frequency correlation of 0.9, the coherence bandwidth for TU06 is around one half of that for TU20. But if we define the coherence bandwidth as the frequency correlation of 0.5, it becomes difficult to compare them.

In addition, we stored the statistics from simulations with both channel profiles concerning the difference of channel coefficients between neighboring sub-carriers, as shown in Figure D.4. Since the amplitude is found to be quite similar, we choose to plot the phase information which changes faster than amplitude. As expected, the TU06 generates a bigger phase difference between neighboring sub-carriers than TU20, which results in higher performance loss specially in the high SNR range. The reason behind is that at high SNR range we usually utilize high order modulation such as 64QAM which is very sensitive to phase mismatch.

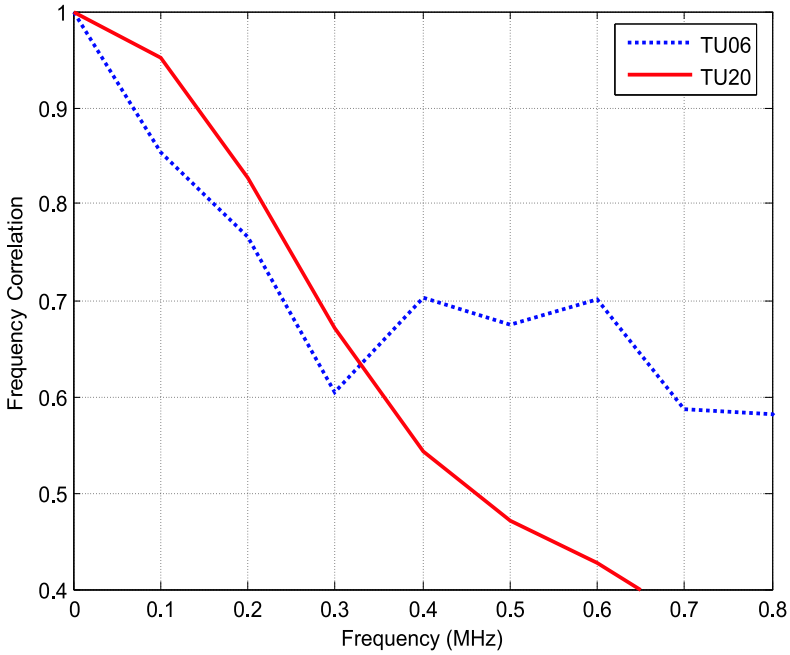

Figure D.3: The frequency correlation property of the two typical urban channel profiles.

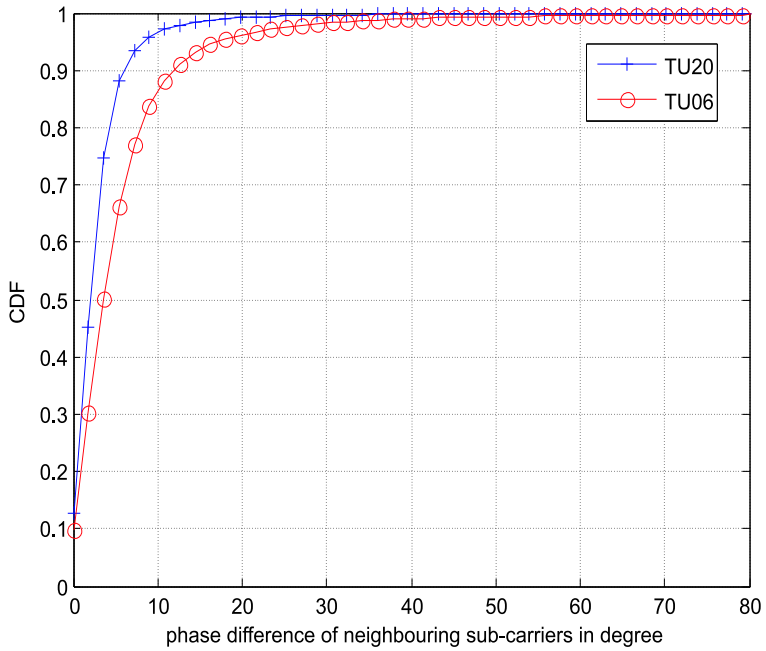

Figure D.4: The phase difference on neighboring sub-carriers of the two typical urban channel profiles.

Appendix E

Validation of network overlay modeling

Results with network overlay [1] is validated with various approaches in this appendix. The EESM link to system interface that all the system-level results based on is firstly verified in Section E.1 with the link simulator developed in Chapter 3. After that, the obtained network results are compared with some results in open literature in Section E.2. Then the statistical significance for the system results are analyzed in Section E.3.

E.1 EESM validation

The exponential effective SINR mapping (EESM) is recommended in Section A.4.3.2 in [3GPP04] to be used as the link to system interference for system-level performances evaluation of OFDM. The essential idea behind EESM is as follows. Firstly, one set of BLER curves for the selected MCS is obtained for an AWGN channel. Secondly, for frequency selective channels, it is necessary to map the current geometry and channel conditions (which will involve frequency-selective fading for a multi-path channel, for example) to an effective SINR value that may then be used directly with the AWGN curves to determine the appropriate block error rate.

[1] The simulator is developed together with Phd students Akhilesh Pokhariyal in Aalborg University.

As introduced in Section 3.3.1 of Chapter 3, the key EESM expression is

$$\text{SINR}_{eff} = -\beta \cdot \ln(\frac{1}{N_u}\sum_{k=1}^{N_u} e^{-\frac{\gamma_k}{\beta}}) \ . \tag{E.1}$$

In this section we presents the link-level simulation results that have been used to estimate appropriate values for β for each of the relevant QPSK, 16QAM and 64QAM MCS that are used in network evaluation of FDPS. The BLER points used for the β estimation process are also shown after the EESM mapping has been applied to demonstrate good agreement with the AWGN BLER curves, thus serving to further validate this effective SINR calculation process. The process can be illustrated as in Figure E.1.

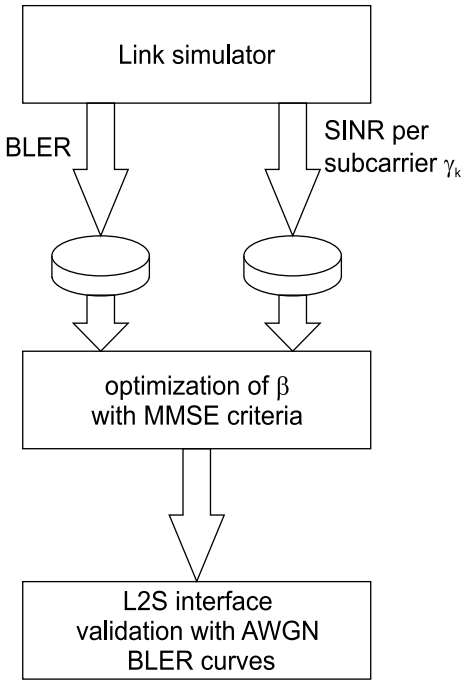

Figure E.1: The diagram of the EESM validation process

We followed the simulation methodology in [Eric04b] and [Eric04a]. For each of the MCS being considered, a number of link-level simulations were performed. For each of these individual simulations, a channel realization with random fading components for either the extended Pedestrian A [2] or the 20 taps Typical Urban models was generated and then held fixed over the duration of the simulation. That is, the frequency response of each channel realization remained constant over the length of the corresponding simulation, although the specific AWGN noise applied

[2]The extended channel profile of Pedestrian A is made with the methods in [Sore05]. The PDP is given in Table E.1.

Table E.1: The Power Delay Profile for the extended Pedestrian A

Relative Path Power (dB)	**Delay (ns)**
0.0	0
-1.8	32.55
-3.7	65.10
-2.5	97.65
-3.2	162.75
-8.0	195.30
-16.5	292.95

to the transmitted signal varied between different TTIs. The average power of the AWGN noise was kept constant. And this procedure was repeated for 100 random fading realizations and 5 different AWGN average noise power. All other relevant simulation assumptions were aligned with [3GPP06a]. Each simulation lasted for 10000 TTIs or until 200 TTI block errors had been observed, whichever came first. Simulation points with observed block error rates between 1% and 80% inclusive were used to estimate appropriate β values for each MCS. This BLER range represented the primary range of interest for further simulation work at the system-level. For each of the candidate BLER points within the desired range, the corresponding subcarrier SINR values were calculated from the channel frequency response profile and other relevant link-level parameters. Since the instantaneous noise samples on each sub-carriers vary over time, the actual effective SINR value for each TTI will be slightly different with the calculated SINR value. However, since the average noise power is kept constant throughout the simulation, we would expect the effective SINR over the whole bandwidth is almost constant over time with a rather small variation, *i.e.* , the actual whole bandwidth effective SINR for each TTI is statistically in a small bin around the calculated effective SINR. Therefore, with this approach we can obtain enough statistics with reasonable number of simulation runs.

To obtain the optimal β, we calculate the corresponding effective SINR for a range of candidate values of β. The appropriate value of β for each MCS was selected as the value that minimized the effective SINR estimation error defined as [Eric04a]

$$\text{ERROR}_{eff} = \frac{1}{N_{BLER}} \sum_{m} [(\text{SINR}_{eff})_m - (\text{SINR}_{AWGN})_m]^2 \qquad \text{(E.2)}$$

where the N_{BLER} is the number of useful simulated BLER points. For each MCS, at least 50 useful BLER points were obtained and then used to estimate β. $(\text{SINR}_{eff})_m$ is the effective SINR value for the m^{th} BLER point as calculated from Equation 3.1 of Chapter 3, and $(\text{SINR}_{AWGN})_m$ is the SINR value from the

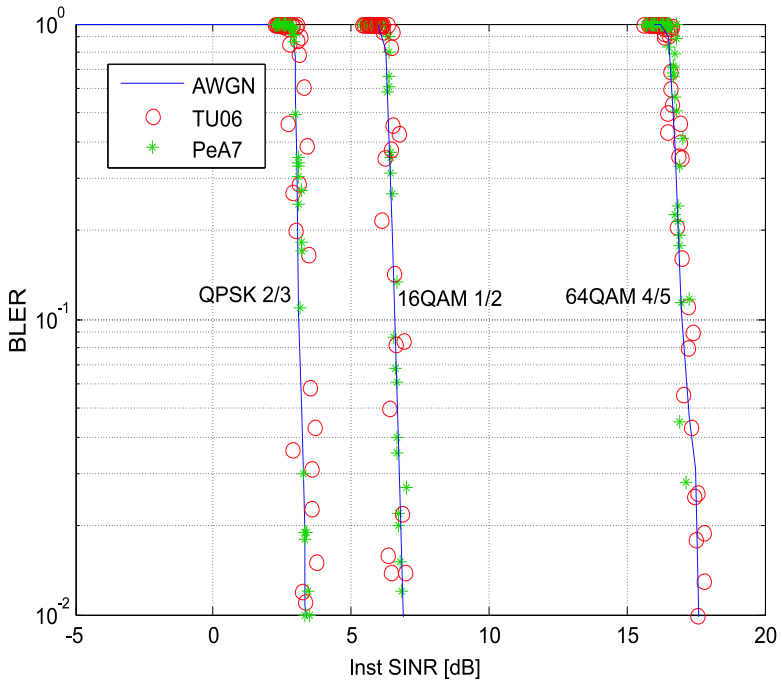

Figure E.2: Mapped EESM points for selected MCS

AWGN BLER curve for the MCS considered that yields the same block error rate as that observed from the link-level simulation for the m^{th} BLER point. Thus, it can be seen that Equation E.2 is optimized here according to an MMSE criterion. The obtained optimal β values are summarized in the Table E.2 which is further used for all system-level performance evaluations in this study.

Table E.2: Estimated β values for each MCS.

MCS	β value
QPSK 1/3	1.3798
QPSK 1/2	1.4457
QPSK 2/3	1.5895
16QAM 1/2	4.8263
16QAM 2/3	6.1017
16QAM 4/5	7.0974
64QAM 1/2	12.0908
64QAM 2/3	21.0007
64QAM 4/5	26.6427

Figure E.2 shows the individual BLER points after the EESM mapping has

been applied and compared these mapped points with the AWGN BLER curves for selected MCS cases. These results further validate the effectiveness of using the EESM approach for modeling OFDM block error performance in system-level simulations.

E.2 Comparison of Network Results with Literature

The comparison of the network performance is often quite difficult with different assumptions and cell structures. Here we pick three cases of results and compare with some published results.

Table E.3: Comparison of network results from simulation against references with FDPS.

scenario considered	1x2 macro Infinite buffer	2x2 SU-MIMO micro Infinite buffer	2x2 SU-MIMO macro Infinite buffer
reference	15.35 Mbps [Qual07]	32.5 Mbps [Noki06b]	15.8 Mbps [Eric07]
simulation	15.25 Mbps	33 Mbps	16 Mbps

The results of the 1x2 FDPS with infinite buffer is first compared with the results from Qualcomm Europe [Qual07], as shown in Table E.3. All results assume the macro case 1 with inter-cell distance 500 meters. Ten active users are dropped in the cell uniformly. Similar results are shown in other major contributor companies in [Alca07] [Huaw07] [Moto07] [NEC07] [Noki07b] [Sams07].

The 2x2 SU-MIMO results with infinite buffer is compared with the results in [Noki06b], also as shown in Table E.3. The reference results with PF scheduler are taken from Table V [Noki06b] for micro- cell scenarios. The assumption behind these results are 48 users in the cell among which 24 users are continuously served per sub-frame. The algorithm for these results are restricted in such way that one user can only use one RPB. Although we do not have such restriction in our simulation, we still expect similar results since the actual scheduled RPB per user from our simulation is also around 1 with such a high number of users.

The results of SU-MIMO is further checked in macro-cell scenarios with the Ericsson results in [Eric07]. Here 10 active users are simulated with infinite buffer best effort model. However, the results in [Eric07] is simulated in a time-dynamic multi-cell system tool, by which more realistic other cell interference is modeled. Quite good agreement is also made between results from other major contributor companies in [Huaw07] [Moto07] [Noki07b] .

One important thing to note is that the results from all reference cases are with real explicit HARQ retransmission scheduling. However, in our simulator we only

used a HARQ model to model the HARQ effect, therefore the effect of real HARQ retransmission is not included. This could also make small difference in the results. But as seen in the Table E.3, the obtained cell throughput from this simplified network simulator is in good agreement with other system level simulator in a quite diverse source.

E.3 Statistical Significance Analysis

Network performance is reflected mostly in the cell throughput. Its estimate depends on the random processes for user arrival, user-parameter assignment, channel quality metric model, and the underlying SINR trace statistics. To estimate the accuracy of obtained results, 100 network level simulations are performed for macro cell 1x2 with FDPS with finite buffer at UDO of 10.

We consider analyze the relative cell throughput distribution which is defined as

$$\frac{\text{cellTP}_i - E\{\text{cellTP}\}_{100}}{E\{\text{cellTP}\}_{100}}, \tag{E.3}$$

where cellTP_i is the cell throughput for each simulation run i and $E\{\text{cellTP}\}_{100}$ is the mean cell throughput over 100 simulation runs.

The relative cell throughput distribution from extensive simulation is plotted in Figure E.3. They can be approximated by Gaussian distributions with relative sector throughput standard deviation of 2.5%. The 99%, the 95%, and the 90% confidence interval values are directly estimated from the 100 simulation runs. They are indicated by the vertical lines in Figure E.3 and summarized in Table E.3. From that, it is estimated that 99 out of 100 simulations will give cell throughput values within 5.5% of the true mean.

Table E.4: Peak Data Rates For Example

Confidence level, [%]	Confidence interval, [%]
99	[-5.30, 5.20]
95	[-4.60, 3.90]
90	[-3.70, 3.70]

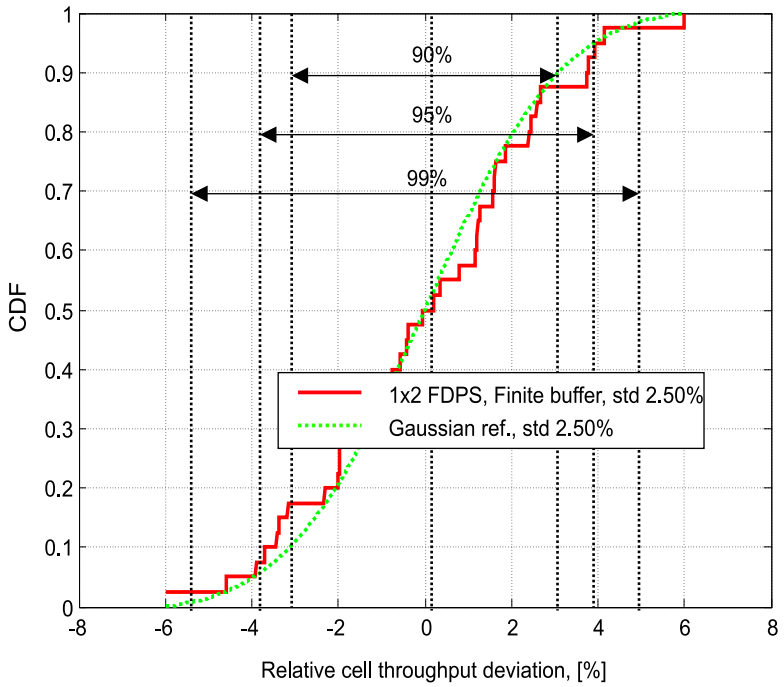

Figure E.3: Relative cell throughput standard deviation

Bibliography

[3GPP00a] 3GPP. Physical layer procedures (FDD) (Release 1999). Technical Specification TS 25.214 (V 3.3.0), Technical Specification Group Radio Access Network, Jun. 2000.

[3GPP00b] 3GPP. Proposed Study Item on Evolved UTRA and UTRAN. Technical Specification TD RP-040461, Technical Specification Group Radio Access Network, 2000.

[3GPP01] 3GPP. Physical Layer Aspects of UTRA High Speed Downlink Packet Access. Technical Specification TR 25.848 (V 4.0.0), Technical Specification Group Radio Access Network, Apr. 2001.

[3GPP03] 3GPP. Spatial channel model for Multiple Input Multiple Output (MIMO) simulations (Release 6). Technical Specification TR 25.996 (V 6.1.0), Technical Specification Group Radio Access Network, Sep. 2003.

[3GPP04] 3GPP. Feasibility study for OFDM for UTRAN enhancement. Technical Specifications TR 25.892 (V 6.0.0), Technical Specification Group Radio Access Network, Jun. 2004.

[3GPP05] 3GPP. Deployment aspects. Technical Specification TR 25.943 (V 6.0.0), Technical Specification Group Radio Access Network, Jan. 2005.

[3GPP06a] 3GPP. Physical Layer Aspects for Evolved UTRA. Technical Specification TR 25.814 (V 7.1.0), Technical Specification Group Radio Access Network, Oct. 2006.

[3GPP06b] 3GPP. Requirements for Evolved UTRA (E-UTRA) and Evolved UTRAN (E-UTRAN). Technical Specification TR 25.913 (V 7.3.0), Technical Specification Group Radio Access Network, Mar. 2006.

[Adac92] F. Adachi and M. Sawahashi. Performance analysis of various 16 level modulation schemes under rayleigh fading. *IEEE Electronic Letters*, 28(17):1579–1581, Aug. 1992.

[Alam98] S. M. Alamouti. A simple transmitter diversity scheme for wireless communications. *IEEE Journal on Selected Areas in Communications*, 16(8):1451–1458, Oct. 1998.

[Alca07] Alcatel-Lucent. DL E-UTRA Performance Checkpoint. TSGR1 AH R1-071967, 3GPP, Apr. 2007.

[Ande98] J. B. Andersen. High gain antennas in a random environment. In *The 9th IEEE International Symposium on Personal, Indoor and Mobile Radio Communications*, vol. 3, pp. 1275–1279, Sep. 1998.

[Barb04] S. Barbarossa. Trace-orthogonal design of mimo systems with simple scalar detectors, full diversity and (almost) full rate. In *IEEE workshop on signal processing advances in wireless communications (SPAWC 04)*, pp. 308–312, Jul. 2004.

[Baum05] D. S. Baum, J. Hansen, and J. Salo. An interim channel model for beyond-3G systems: extending the 3GPP spatial channel model (SCM). In *The 61th IEEE Vehicular Technology Conference*, vol. 5, pp. 3132– 3136, May 2005.

[Behr02] A. Behravan and T. Eriksson. PAPR and other measures for OFDM systems with nonlinearity. In *The 5th Wireless Personal Multimedia Communications Conference*, vol. 1, pp. 149–153, Oct. 2002.

[Berg03] L. T. Berger, T. E. Kolding, J. Ramiro-Moreno, P. Ameigeiras, L. Schumacher, and P. E. Mogensen. Interaction of transmit diversity and proportional fair scheduling. In *IEEE 57th Vehicular Technology Conference*, Apr. 2003.

[Berg05] L. T. Berger. *Performance of Multi-Antenna Enhanced HSDPA*. Dissertation, Aalborg University, April 2005.

[Bing90] J. A. Bingham. Multicarrier modulation for data transmission: An idea whose time has come. *IEEE Communications Magazine*, pp. 5–14, May 1990.

[Blcs02] H. Bölcskei, D. Gesbert, and A. J. Paulraj. On the capacity of ofdm-based spatial multiplexing systems. *IEEE Transactions on Communications*, 50(2):225–, Feb 2002.

[Bolc00] H. Bolcskei and A. Paulraj. Space-frequency coded broadband OFDM systems. In *IEEE Wireless Communications and Networking Conference*, vol. 1, pp. 1–6, Sep. 2000.

[Bolc03] H. Bolcskei, M. Borgmann, and A. Paulraj. Space-frequency coded MIMO-OFDM with variable multiplexing-diversity tradeoff. In *The IEEE International Conference on Communications*, vol. 4, pp. 2837– 2841, May 2003.

[Brue05] K. Brueninghaus, D. Astely, T. Salzer, S. Visuri, A. Alexiou, S. Karger, and G. A. Seraji. Link performance models for system level simulations of broadband radio access systems. In *The 16th IEEE Personal, Indoor and Mobile Radio Communications*, Sep. 2005.

[Catr02] S. Catreux, V. Erceg, D. Gesbert, and R. W. Heath Jr. Adaptive modulation and MIMO coding for broadband wireless data networks. *IEEE Communications Magazine*, 40(6): 108–115, June 2002.

[Chae04] C. B. Chae, M. Katz, C. Suh, and H. Jeong. Adaptive spatial modulation for MIMO-OFDM. In *IEEE Wireless Communications and Networking Conference*, vol. 1, pp. 87–92, Mar. 2004.

[Choi05] J. Choi and R. W. Heath Jr. Interpolation based transmit beamforming for MIMO-OFDM with limited feedback. *IEEE Transactions on Signal Processing*, 53(11):4125–4135, Nov 2005.

[Chun01] S. T. Chung, A. Lozano, and H. Huang. Approaching eigenmode BLAST channel capacity using V-BLAST with rate and power feedback. In *The 54th IEEE Vehicular Technology Conference*, vol. 2, pp. 915–919, Oct. 2001.

[Daba99] A. Dabak, S. Hosur, and R. Negi. Space time block coded transmit antenna diversity scheme for WCDMA. In *The IEEE Wireless Communications and Networking Conference*, vol. 3, pp. 1466–1469, Sep. 1999.

[Digh03] F. F. Digham and M. O. Hasna. Performance of ofdm with mqam modulation and optimal loading over rayleigh fading channels. In *IEEE 60th Vehicular Technology Conference*, Oct. 2003.

[DMB] DMB. The world DMB forum. http://www.worlddab.org.

[Dupl05] J. Duplicy, M. Louveaux, and L. Vandendorpe. Interference-free multi-user MIMO-OFDM. In *IEEE International Conference on Acoustics, Speech, and Signal Processing*, vol. 3, pp. iii/1149–iii/1152, March 2005.

[DVB] DVB. The global standard for digital television. http://www.dvb.org.

[Edfo96] O. Edfors, M. Sandell, J.-J. v. d. Beek, D. Landström, and F. Sjöberg. An introduction to orthogonal frequency-division multiplexing. Technical report, Luleå University of Technology, Sep. 1996.

[Elek03] Elektrobit, Nokia, Siemens, Philips, Alcatel, Telefonica, Lucent, Ericsson. Spatial radio channel models for systems beyond 3G. Technical Report R4-050854, Technical Specification Group Radio Access Network, 2003.

[Eric03] Ericsson. Effective SNR mapping for modelling frame error rates in multiple-state channels. Technical Report C30-20030429-010, 3GPP2, 2003.

[Eric04a] Ericsson. OFDM exponential effective SIR mapping validation. Technical Report R1-04-0089, Technical Specification Group Radio Access Network, 2004.

[Eric04b] Ericsson. System-level evaluation of OFDM - further considerations. Technical Report R1-03-1303, Technical Specification Group Radio Access Network, 2004.

[Eric07] Ericsson. E-UTRA Performance Checkpoint: Downlink. TSGR1 AH R1-071956, 3GPP, Apr. 2007.

[Fern04] P. Fernandes, P. Kyritsi, L. T. Berger, and J. Mártires. Effects of multi user MIMO scheduling freedom on cellular downlink system throughput. In *IEEE 60th Vehicular Technology Conference*, vol. 2, pp. 1148–1152, Oct. 2004.

[Fore05] A. Forenza, A. Pandharipande, H. Kim, and R. W. Heath Jr. Adaptive MIMO transmission scheme: exploiting the spatial selectivity of wireless channels. In *The 61th IEEE Vehicular Technology Conference*, vol. 5, pp. 3188 – 3192, May 2005.

[Fosc96] G. J. Foschini. Layered space-time architecture for wireless communication in a fading environment when using multi-element antennas. *Bell Labs Technical Journal*, 1996.

[Fred02] F. Frederiksen and T. E. Kolding. Performance and modeling of WCDMA/HSDPA transmission/H-ARQ schemes. In *IEEE 56th Vehicular Technology Conference*, Sep. 2002.

[Gerl02] H. Gerlach. Snr loss due to feedback quantization and errors in closed loop transmit diversity systems. In *The 13th IEEE Personal, Indoor and Mobile Radio Communications*, vol. 5, pp. 2117– 2120, Sep. 2002.

[Gesb03] D. Gesbert, M. Shafi, D. Shiu, P. J. Smith, and A. Naguib. From theory to practice: an overview of MIMO space-time coded wireless systems. *IEEE Journal on Selected Areas in Communications*, 21(3):281–302, Apr. 2003.

[Gesb04] D. Gesbert and M. S. Alouini. How much feedback is multi-user diversity really worth? In *IEEE International Conference On Communications*, pp. 234– 238, Sep. 2004.

[Golu96] G. H. Golub and C. F. V. Loan. *Matrix computations (3rd ed.)*. Johns Hopkins University Press, Baltimore, MD, USA, 1996. ISBN 0-8018-5414-8.

[Gore02] D. Gore, R. W. Heath Jr., and A. Paulraj. On performance of the zero forcing receiver in presence of transmit correlation. In *ISIT*, p. 159, July 2002.

[Hama00] J. Hämäläinen and R. Wichman. Closed-loop transmit diversity for FDD WCDMA systems. In *The 34th Asilomar Conference on Signals, Systems and Computers*, vol. 1, pp. 111–115, Oct. 2000.

[Hama01] J. Hamalainen and R. Wichman. Feedback schemes for FDD WCDMA systems in multipath environments. In *The 53rd Vehicular Technology Conference*, vol. 1, pp. 238–242, May 2001.

[Hass02] B. Hassibi and B. M. Hochwald. High-rate codes that are linear in space and time. *IEEE Transactions on Information Theory*, 48(7):1804–1824, Jul. 2002.

[Heat01a] R. W. Heath Jr., M. Airy, and A. J. Paulraj. Multiuser diversity for MIMO wireless systems with linear receivers. In *The 35th Asilomar Conference, Signals, Systems, and Computers*, vol. 2, pp. 1194–1199, Nov. 2001.

[Heat01b] R. W. Heath Jr., S. Sandhu, and A. Paulraj. Antenna selection for spatial multiplexing systems with linear receivers. *IEEE Communication Letters*, 5(4):142–144, April 2001.

[Heat05] R. W. Heath Jr. and A. J. Paulraj. Switching between diversity and multiplexing in MIMO systems. *IEEE Transactions on Communications*, 53(6):962–968, June 2005.

[Hoch04] B. M. Hochwald, T. L. Marzetta, and V. Tarokh. Multi-antenna channel hardening and its implications for rate feedback and scheduling. *IEEE Transactions on Information Theory*, 50:1893– 1909, Sep. 2004.

[Holm01] H. Holma and A. Toskala. *WCDMA for UMTS*. Wiley, Chichester, UK, revised edition edition, 2001.

[Holm06] H. Holma and A. Toskala, editors. *HSDPA/HSUPA For UMTS, High Speed Radio Access for Mobile Communications*. Wiley, Chichester, UK, 2006. ISBN 0-470-01884-4.

[Holt00] J. M. Holtzman. CDMA forward link waterfilling power control. In *IEEE 51st Vehicular Technology Conference*, pp. 1636–1667. Tokyo, Japan, May 2000.

[Hott03a] A. Hottinen. Multiuser scheduling with matrix modulation. In *the 3rd IEEE International Symposium on Signal Processing and Information Technology*, pp. 5–8, Dec. 2003.

[Hott03b] A. Hottinen and O. Tirkkonen. Matrix modulation and adaptive retransmission. In *the Seventh IEEE International Symposium on Signal Processing and Its Applications*, vol. 1, pp. 221–224, Jul. 2003.

[Huaw07] Huawei. LTE Downlink Performance Evaluation Results. TSGR1 AH R1-071961, 3GPP, Apr. 2007.

[IEEE99] IEEE. Part 11: Wireless LAN medium access control (MAC) and physical layer (PHY) specifications: High-speed physical layer in the 5 ghz band. Technical specifications, IEEE 802.11a, 1999.

[IEEE01] IEEE. Local and metropolitan area networks: Part 16, air interface for fixed broadband wireless access systems. Technical specifications, IEEE 802.16a, 2001.

[Inte06] Intel Corporation. Codebook design for precoded MIMO. TSG1#42 R1-06-0672, 3GPP, Denver, USA, February 2006.

[ITU 03] ITU-R. Recommendation m.1645: Framework and overall objectives of the future development of IMT-2000 and systems beyond IMT-2000. Technical report, 2003.

[Jake94] W. C. Jakes. *Microwave Mobile Communication*. IEEE Press, New Jersey, USA, IEEE reprinted edition, 1994. ISBN 0-7803-1069-1.

[Jors04] E. A. Jorswieck and A. Sezgin. Impact of spatial correlation on the performance of orthogonal space-time block codes. *IEEE Communications Letters*, 8(1):21 – 23, Jan. 2004.

[Jung04] K. Jung, C. S. Park, and K. B. Lee. Bit and power allocation for MIMO-OFDM systems with spatial mode selection over frequency-space-time-selective channels. In *The 60th IEEE Vehicular Technology Conference*, vol. 5, pp. 3404–3408, Sep. 2004.

[Kavc00] A. Kavcic and J. M. F. Moura. Matrices with banded inverses: inversion algorithms and factorization of Gauss-Markov processes. *IEEE Transactions on Information Theory*, 46(4):1495–1509, July 2000.

[Kish03] Y. Kishiyama, N. Maeda, K. Higuchi, H. Atarashi, and M. Sawahashi. Experiments on throughput performance above 100-Mbps in forward link for VSF-OFCDM broadband wireless access. In *The 58th IEEE Vehicular Technology Conference*, vol. 3, pp. 1863–1868, Oct. 2003.

[Kold02] T. E. Kolding, F. Frederiksen, and P. E. Mogensen. Performance aspects of WCDMA systems with high speed downlink packet access (HSDPA). In *IEEE 56th Vehicular Technology Conference*, vol. 1, pp. 477–481, Sep. 2002.

[Kold03] T. E. Kolding, K. I. Pedersen, J. Wigard, F. Frederiksen, and P. E. Mogensen. High speed downlink packet access: WCDMA evolution. *IEEE Vehicular Technology Soceity (VTS) News*, 50(1):4–10, Feb. 2003.

[Kold05] T. E. Kolding, A. Pokhariyal, N. Wei, and P. E. Mogensen. Impact of Channel Quality Signaling on Frequency Domain Link Adaptation Performance. In *Wireless Personal Mobile Communications*, Sep. 2005.

[Kold06] T. E. Kolding, F. Frederiksen, and P. A. Low-bandwidth channel quality indication for ofdma frequency domain packet scheduling. In *The IEEE International Symposium on Wireless Communication Systems*, Sep. 2006.

[Kova06] I. Z. Kovács, K. I. Pedersen, J. Wigard, F. Frederiksen, and T. E. Kolding. Hsdpa performance in mixed outdoor-indoor micro cell scenarios. In *The 17th IEEE Personal, Indoor and Mobile Radio Communications*, Sep. 2006.

[Li00] Y. Li, C. N. Georghiades, and G. Huang. Performance of downlink multicarrier CDMA with space diversity. In *IEEE Global Telecommunications Conference*, vol. 2, pp. 887–889, Nov. 2000.

[Liu04] S. Liu and J.-W. Chong. Improved design criterion for space-frequency trellis codes in mimo-ofdm systems. In *60th Vehicular Technology Conference*, vol. 2, pp. 1391–1395, Sep. 2004.

[Lo99] T. K. Y. Lo. Maximum ratio transmission. *IEEE Transactions on Communications*, 47 (10):1458–1461, Oct 1999.

[Love03] D. J. Love, R. W. Heath Jr., and T. Strohmer. Grassmannian beamforming for multiple-input multiple-output wireless systems. *IEEE Transactions on Information Theory*, 49 (10):2735–2747, Oct. 2003.

[Love04] D. J. Love and R. W. Heath Jr. Grassmannian beamforming on correlated MIMO channels. In *IEEE Global Telecommunications Conference*, vol. 1, pp. 106–110, Nov. 2004.

[Luce02] Lucent Technologies. PARC with APP decoding for HSDPA. TSG1#24 R1-02-0325, 3GPP, Orlando, USA, Feb. 2002.

[Moge07a] P. E. Mogensen. Trends in mobile communication systems beyond 3G. Professor Inauguration Lectures, Aalborg University, Denmark., Jan. 2007.

[Moge07b] P. E. Mogensen, N. Wei, A. Pokhariyal, I. Kovacs, F. Frederiksen, K. Pedersen, K. Hugl, T. E. Kolding, and M. Kuusela. LTE capacity versus Shannon. In *IEEE 65th Vehicular Technology Conference*, Apr. 2007.

[Moli02] A. Molisch, M. Win, and J. Winters. Space-time-frequency (STF) coding for MIMO-OFDM systems. *IEEE Communication Letters*, 6(9):370– 372, Sep. 2002.

[More03] J. R. Moreno. *System Level Performance Analysis of Advanced Antenna Concepts in WCDMA*. Dissertation, Aalborg University, July 2003.

[Moto05] Motorola. Summary of MIMO schemes for EUTRA. TSG RAN WG1 #42 R1-05-1238, 3GPP, San Diego, USA, Oct. 2005.

[Moto06] Motorola. MIMO evaluation proposal. TSGR1#44 R1-060615, 3GPP, Denver, USA, Feb. 2006.

[Moto07] Motorola. LTE Downlink System Performance Verification Results. TSGR1 AH R1-071976, 3GPP, Apr. 2007.

[Naka02] M. Nakamura, Y. Awad, and S. Vadgama. Adaptive control of link adaptation for high speed downlink packet access (HSDPA) in W-CDMA. In *The 5th Wireless Personal Multimedia Communications Conference*, vol. 2, pp. 382–386, Oct. 2002.

[Naru97] A. Narula. *Information Theoretic Analysis of Multiple-Antenna Transmission Diversity*. PhD thesis, Massachusetts Institute of Technology, June 1997.

[Naru98] A. Narula, M. J. Lopez, M. D. Trott, and G. W. Wornell. Efficient use of side information in multiple-antenna data transmission over fading channels. *IEEE Journal on Selected Areas in Communications*, 16(8):1423–1436, Oct. 1998.

[NEC07] NEC. LTE Downlink Performance. TSGR1 AH R1-071978, 3GPP, Apr. 2007.

[Noki06a] Nokia. Single vs. multiple codewords for DL MIMO. Technical Report R1-06-0283, Technical Specification Group Radio Access Network, Feb. 2006.

[Noki06b] Nokia. Updated downlink LTE evaluation results. Technical Report R1-06-2358, Technical Specification Group Radio Access Network, Sep. 2006.

[Noki07a] Nokia. Reduced CQI design for DL SU-MIMO. Technical Report R1-07-0388, Technical Specification Group Radio Access Network, 2007.

[Noki07b] Nokia Nokia-Siemens-Networks. LTE Performance Benchmarking. TSGR1 AH R1-071960, 3GPP, Apr. 2007.

[Nort03] Nortel Networks. Complexity comparison of OFDM HS-DSCH receivers and advanced receivers for HSDPA. Technical report, 3GPP, TSG-RAN Working Group 1, Marne La Vallée, France, May 2003.

[Ogaw03] K. Ogawa, Y.and Nishio, T. Nishimura, and T. Ohgane. A mimo-ofdm system for high-speed transmission. In *IEEE 58th Vehicular Technology Conference*, vol. 1, pp. 493–497, 2003.

[Pan04] Y.-H. Pan, K. Letaief, and Z. Cao. Dynamic resource allocation with adaptive beamforming for MIMO/OFDM systems under perfect and imperfect CSI. In *The IEEE Wireless Communications and Networking Conference*, vol. 1, pp. 93–97, Mar. 2004.

[Park05] K. W. Park and Y. S. Cho. An mimo-ofdm technique for high-speed mobile channels. *IEEE Communications Letters*, 9(7):604–606, July 2005.

[Pasc04] A. Pascual-Iserte, A. I. Pérez-Neira, and M. A. Lagunas. On power allocation strategies for maximum signal to noise and interference ratio in an ofdm-mimo system. *IEEE Transactions on Wireless Communications*, 3(3):808–820, May 2004.

[Paul03] A. Paulraj, R. Nabar, and D. Gore. *Introduction to Space-Time Wireless Communications*. Cambridge University Press, 2003. ISBN 0-521-82615-2.

[Paul04] A. Paulraj, D. Gore, R. Nabar, and H. Bolcskei. An overview of MIMO communications - a key to gigabit wireless. In *Proceedings of the IEEE*, vol. 92, pp. 198–218, Feb. 2004.

[Paut01] J. Pautler, M. Ahmed, and K. Rohani. On application of multiple-input multiple-output antennas to CDMA cellular systems. In *The 54th IEEE Vehicular Technology Conference*, vol. 3, pp. 1508–1512, Oct. 2001.

[Pokh06] A. Pokhariyal, T. E. Kolding, and P. E. Mogensen. Performance of downlink frequency domain packet scheduling for the UTRAN Long Term Evolution. In *The 17th IEEE Personal, Indoor and Mobile Radio Communications*, pp. 1–5, Sep. 2006.

[Pokh07] A. Pokhariyal. *Downlink Frequency domain Adaptation and Scheduling - A case study based on the UTRA long term evolution*. Dissertation, Aalborg University, Aug. 2007.

[Proa95] J. G. Proakis. *Digital Communications*. McGraw-Hill International series in electrical engineering. Communications and signal processing. McGraw-Hill, Inc., 3rd edition, 1995. ISBN 0-07-113814-5.

[Qual05] QualComm Europe. Description of link simulations of MIMO schemes for OFDMA based E-UTRA downlink evaluation. TSG-RAN WG1 #42 R1-05-0903, 3GPP, London, UK, Aug-Sep 2005.

[Qual06a] QualComm Europe. Description of single and multi codeword schemes with precoding. TSGR1#44 R1-060457, 3GPP, Denver, USA, Feb. 2006.

[Qual06b] QualComm Europe. Switching between SDMA and SU-MIMO. Technical Report R1-063437, Technical Specification Group Radio Access Network, 2006.

[Qual07] QualComm Europe. Downlink best effort performance. TSGR1 AH R1-071990, 3GPP, Apr. 2007.

[Rao85] C. Rao. Weighted distributions arising out of methods of ascertainment, in a celebration of statistics. *A.C. Atkinson &S.E. Fienberg, eds, Springer-Verlag*, 24:543–569, 1985.

[Rhee00] W. Rhee and J. M. Cioffi. Increase in capacity of multiuser OFDM system using dynamic subchannel allocation. In *The 51th IEEE Vehicular Technology Conference*, vol. 2, pp. 1085–1089, May 2000.

[Samp97] A. Sampath, P. S. Kumar, and J. M. Holtzman. On Setting Reverse Link Target SIR in a CDMA System. In *The 47th IEEE Vehicular Technology Conference*, vol. 2, pp. 929 – 933, May 1997.

[Samp02] H. Sampath, S. Talwar, J. Tellado, V. Erceg, and A. Paulraj. A fourth-generation MIMO-OFDM broadband wireless system: design, performance, and field trial results. *IEEE Communications Magazine*, 40(9):143–149, Sep. 2002.

[Sams07] Samsung. E-UTRA Performance Verification: DL Throughput. TSGR1 AH R1-071969, 3GPP, Apr. 2007.

[Sand01] S. Sandhu and A. Paulraj. Unified design of linear space-time block codes. In *IEEE Global Telecommunications Conference*, vol. 2, pp. 1073–1077, Nov. 2001.

[Schu01] L. Schumacher, J. P. Kermoal, F. Frederiksen, K. I. Pedersen, A. Algans, and P. E. Mogensen. MIMO channel characterisation. In *IST Project IST-1999-11729 METRA Deliverable 2*, February 2001.

[Shan48] C. E. Shannon. A mathematical theory of communications. *Bell Sys. Tech. Journal*, 27: 379–423, 623–656, 1948.

[Shar05] M. Sharif and B. Hassibi. On the capacity of mimo broadcast channels with partial side information. *IEEE Transactions on Information Theory*, 51(2):506–522, Feb. 2005.

[Sore05] T. B. Sørensen, P. E. Mogensen, and F. Frederiksen. Extension of the ITU channel models for wideband (OFDM) systems. In *The 62th IEEE Vehicular Technology Conference*, vol. 5, pp. 392– 396, Sep. 2005.

[Spen04] Q. Spencer, C. Peel, A. Swindlehurst, and M. Haardt. An introduction to the multi-user mimo downlink. *IEEE Communications Magazine*, 42(10):60–67, Oct. 2004.

[Stam02] A. Stamoulis, S. N. Diggavi, and N. Al-Dhahir. Intercarrier interference in MIMO OFDM. *IEEE Transactions on Signal Processing*, 50(10):2451–2464, Oct. 2002.

[Stub04] G. L. Stuber, J. R. Barry, S. W. McLaughlin, Y. Li, M. A. Ingram, and T. G. Pratt. Broadband MIMO-OFDM wireless communications. In *Proceedings of the IEEE*, vol. 92, pp. 271– 294, Feb. 2004.

[Sung03] J. H. Sung and J. R. Barry. Bit-allocation strategies for MIMO fading channels with channel knowledge at transmitter. In *IEEE 57th Vehicular Technology Conference*, vol. 2, pp. 813– 817, Apr. 2003.

[Tang05] J. Tang and X. Zhang. Link-adaptation-enhanced dynamic channel allocation for MIMO-OFDM wireless networks. In *The IEEE Wireless Communications and Networking Conference*, vol. 2, pp. 1126–1131, Mar. 2005.

[Tela95] I. E. Telatar. Capacity of multi-antenna Gaussian channels. Technical Memorandum BL011217-950615-07TM, AT&T Bell Labs, June 1995.

[Texa01] Texas Instrumets. Double-STTD scheme for HSDPA systems with four transmit antennas: Link level simulation results. TSG1#20 R1-01-0458, 3GPP, Busan, Korea, 2001.

[Texa05] Texas Instruments. Comparison of 2x2 mimo sic complexity to 1x2 lmmse complexity. TSGR1#43 R1-060457, 3GPP, Seoul, Korea, Nov. 2005.

[Thom05] T. A. Thomas, K. L. Baum, and P. Sartori. Obtaining channel knowledge for closed-loop multi-stream broadband MIMO-OFDM communications using direct channel feedback. In *IEEE Global Telecommunications Conference*, vol. 6, Nov. 2005.

[Vese06] N. Veselinovic and M. Juntti. Comparison of adaptive mimo ofdm schemes for 3g lte. In *The 17th IEEE International Symposium on Personal, Indoor and Mobile Radio Communications*, pp. 1–5, Sep. 2006.

[Vish02] S. Vishwanath, N. Jindal, and A. Goldsmith. On the capacity of multiple input multiple output broadcast channels. In *The IEEE International Conference on Communications*, vol. 3, pp. 1444–1450, Sep. 2002.

[Vogt00] J. Vogt and A. Finger. Improving the Max-log-MAP turbo decoder. *IEEE Electronics Letters*, 36(23):1937–1939, Nov. 2000.

[Wei06a] N. Wei, L. T. Berger, T. B. Sørensen, T. E. Kolding, and P. E. Mogensen. Tackling MIMO-OFDMA feedback load through feedback encoding. In *The International Symposium on Wireless Communication System*, Sep. 2006.

[Wei06b] N. Wei, A. Pokhariyal, C. Rom, B. E. Priyanto, F. Frederiksen, C. Rosa, T. B. Sørensen, T. E. Kolding, and P. E. Mogensen. Baseline E-UTRA downlink spectral efficiency evaluation. In *The 64th IEEE Vehicular Technology Conference*, Sep. 2006.

[Wei06c] N. Wei, T. B. Sørensen, T. E. Kolding, and P. E. Mogensen. Analysis and evaluation of link adaptation including MIMO adaptation. In *The 64th IEEE Vehicular Technology Conference*, Sep. 2006.

[Wei06d] N. Wei, B. Talha, T. B. Sørensen, T. E. Kolding, and P. E. Mogensen. Spectral efficiency of closed-loop transmit diversity with limited feedback for UTRA Long Term Evolution. In *The 17th IEEE Personal, Indoor and Mobile Radio Communications*, Sep. 2006.

[Wei07a] N. Wei, A. Pokhariyal, T. B. Sørensen, T. E. Kolding, and P. E. Mogensen. Mitigating signalling requirement for MIMO with frequency domain packet scheduling. In *IEEE 65th Vehicular Technology Conference*, Apr. 2007.

[Wei07b] N. Wei, A. Pokhariyal, T. B. Sørensen, T. E. Kolding, and P. E. Mogensen. Performance of MIMO with Frequency Domain Packet Scheduling in UTRAN LTE downlink. In *IEEE 65th Vehicular Technology Conference*, Apr. 2007.

[Weng05] C. Wengerter, J. Ohlhorst, and A. G. E. v. Elbwart. Fairness and throughput analysis for generalized proportional fair frequency scheduling in ofdma. In *IEEE 61th Vehicular Technology Conference*, May. 2005.

[Wint87] J. H. Winters. On the capacity of radio communication systems with diversity in a rayleigh fading environment. *IEEE Journal on Selected Areas in Communications*, 5 (5):871–878, June 1987.

[Wint94] J. H. Winters, J. Salz, and R. D. Gitlin. The impact of antenna diversity on the capacity of wireless communication systems. *IEEE Transactions on Communications*, 42:1740 – 1751, FEBRUARY/MARCH/APRIL 1994.

[Woln98] P. W. Wolniansky, G. J. Foschini, G. D. Golden, and R. A. Velenzuela. V-BLAST: An architecture for realizing very high data rates over the rich scattering wireless channel. In *URSI International Symposium on Signals, Systems, and Electronics*, pp. 295–300, Sep. 1998.

[Woo06] S. Woo, H. Yu, J. Lee, C. H. Lee, and J. Laskar. Effects of RF impairments in transmitter for the future beyond-3G communications systems. In *IEEE International Symposium on Circuits and Systems*, vol. 4, pp. 21–24, May 2006.

[Xia04] P. F. Xia, S. L. Zhou, and G. Giannakis. Adaptive MIMO-OFDM based on partial channel state information. *IEEE Transactions on Signal Processing*, 52(1):202–213, Jan 2004.

[Zels04] A. V. Zelst. *MIMO OFDM for Wireless LANs*. Phd thesis, Eindhoven University of Technology (TU/e), Apr. 2004.

[Zhen03] L. Zheng and D. N. C. Tse. Diversity and multiplexing: A fundamental tradeoff in multiple antenna channels. *IEEE Transactions on Information Theory*, 49:1073–1096, May 2003.

[Zhou02] S. Zhou and G. B. Giannakis. Adaptive modulation for multiantenna transmissions with channel mean feedback. *IEEE Transactions on Wireless Communications*, 3(5):1626–1636, Septermber 2002.